CONSIDERING FLOOD HAZARD AND RISK IN SPATIAL PLANNING

A SPATIALLY EXPLICIT OPTIMIZATION APPROACH

Karen GABRIELS

Supervisors:
Prof. Dr. Ir. Jos Van Orshoven, KU Leuven
Prof. Dr. Ir. Patrick Willems, KU Leuven

Members of the Examination Committee:
Prof. Dr. Ir. Ann Van Loey (chair), KU Leuven
Prof. Dr. Ir. Jan Diels, KU Leuven
Prof. Dr. Gert Verstraeten, KU Leuven
Prof. Dr. Ir. Dirk Cattrysse, KU Leuven
Prof. Dr. Ir. Marnik Vanclooster, UCLouvain

Dissertation presented in partial fulfilment of the requirements for the degree of Doctor of Bioscience Engineering

May 2021

Doctoraatsproefschrift nr. 1696 aan de faculteit Bio-ingenieurswetenschappen van de KU Leuven

© 2021 Karen Gabriels
Uitgegeven in eigen beheer, Karen Gabriels, Leuven

Alle rechten voorbehouden. Niets uit deze uitgave mag worden vermenigvuldigd en/of openbaar gemaakt worden door middel van druk, fotokopie, microfilm, elektronisch of op welke andere wijze ook zonder voorafgaandelijke schriftelijke toestemming van de uitgever.

All rights reserved. No part of the publication may be reproduced in any form by print, photoprint, microfilm, electronic or any other means without written permission from the publisher.

Acknowledgements

This PhD has been quite a journey, and I would not have been able to see it through without all the support, help and guidance of a number of people along the way. I would therefore like to take this opportunity to thank all those people who helped make this PhD research a reality. First of all, I am very grateful to FWO (Fonds Wetenschappelijk Onderzoek) for granting me a PhD fellowship, thereby making this research and personal journey possible.

I would like to express my utmost gratitude to Jos and Patrick, my supervisors, for their patient guidance all these years. I could always rely on your unrelenting support, kind advice and extensive expertise. I would like to thank both of you for the considerable time and effort you put into supervising my PhD. I enjoyed the inspiring discussions we had during our monthly meetings, which were like stepping stones for me, providing me with direction and motivation throughout this process. Jos, you gave me the opportunity to work as a researcher during my grant applications, spurring me onwards as the first one was denied. I highly appreciated, and often depended on, your creative ideas and suggestions. Thank you for your enthusiasm and trust. Patrick, it was a big help to me that I could rely on your wide-ranging expertise in all water-related matters. Thank you for believing in me, and for your clear and constructive feedback throughout this PhD.

I wish to thank the members of my supervisory committee, Jan Diels and Gert Verstraeten. The meetings we had, together with Jos and Patrick, are aptly called 'milestones', as they provided me with the opportunity to both look back and plan ahead. Your fresh insights thereby inspired thought-provoking discussions, and I much appreciate your feedback and suggestions, which helped to improve this research along the way. I would also like to extend my appreciation to the remaining members of the jury, Marnik Vanclooster, Dirk Cattrysse and Ann Van Loey as chair, for the commitment, time and effort they put into this research as well. Thank you all for taking the time and interest to read and extensively comment on my preliminary manuscript. Your constructive feedback helped me to gain additional insights and allowed me to make substantial improvements to this final PhD manuscript.

For the past years, I spent most of my time at tower 2, floor 3 (room 03.236) of the Geo-institute, home to the inspirational and international work environment of the Division of Forest, Nature and Landscape. I would like to thank all the colleagues I had the pleasure of working with over the past few years, not only for sharing their academic knowledge, but also for the interesting (and sometimes intense) discussions during coffee breaks, and the fun and relaxing labtrips.

Finally, I should like to take this opportunity to thank the home base, my family. Kathleen, zus, bedankt voor al die random kaartjes vol motivatie. Mama en papa, jullie staan altijd klaar met raad en daad, met logistieke, maar vooral ook met mentale steun. Jullie hebben ook vaak een duwtje in de rug gegeven, als ik het even niet meer zag zitten. Ik weet dat ik altijd bij jullie terecht kan voor wat dan ook. Bedankt voor die onvoorwaardelijke steun! Mijn grootouders en mijn ouders hebben me geleerd om altijd mijn best te doen en nooit op te geven. Zonder deze levenslessen en hun voorbeeld had ik dit doctoraat nooit kunnen voltooien. Dit werk wordt dan ook met veel liefde aan hen opgedragen.

Bedankt! Thank you all for everything!

The Floods – Rudyard Kipling

The rain it rains without a stay
In the hills above us, in the hills;
And presently the floods break way
Whose strength is in the hills.
The trees they suck from every cloud,
The valley brooks they roar aloud–
Bank-high for the lowlands, lowlands,
Lowlands under the hills!

The first wood down is sere and small,
From the hills–the brishings off the hills;
And then come by the bats and all
We cut last year in the hills;
And then the roots we tried to cleave
But found too tough and had to leave–
Polting through the lowlands, lowlands,
Lowlands under the hills!

The eye shall look, the ear shall hark
To the hills, the doings in the hills,
And rivers mating in the dark
With tokens from the hills.
Now what is weak will surely go,
And what is strong must prove it so–
Stand Fast in the lowlands, lowlands,
Lowlands under the hills!

The floods they shall not be afraid–
Nor the hills above 'em, nor the hills–
Of any fence which man has made
Betwixt him and the hills.
The waters shall not reckon twice
For any work of man's device,
But bid it down to the lowlands, lowlands,
Lowlands under the hills!

The floods shall sweep corruption clean–
By the hills, the blessing of the hills–
That more the meadows may be green
New-mended from the hills.
The crops and cattle shall increase,
Nor little children shall not cease.
Go–plough the lowlands, lowlands,
Lowlands under the hills!

Abstract

Floods are among the most frequently occurring and most damaging natural hazards in Europe, impacting heavily on economies and communities through a loss of life, property and livelihood. Moreover, an increasing trend in economic flood damages has been observed in the past decades, mainly driven by socioeconomic developments, such as a rising standard of living and urbanization in flood-prone areas. This trend prompted a shift in flood management from flood prevention, relying on structural defense measures, to a more integrated, system-wide approach focused on managing flood risk, which is defined as a combination of the flood hazard or probability and its potential damages. As such, sustainable flood risk management aims to efficiently reduce the societal, environmental and economic impacts of floods, for instance by looking for synergies with land use systems mitigating downstream flood risk. Land use systems, and their spatial configuration in the catchment, can impact flood risk by influencing the hydrological processes. Vegetated surfaces, such as forest and arable cover crops, have the capacity to mitigate flood hazard by increasing water retention and infiltration, thereby reducing the fraction of rapid surface runoff downstream. Conversely, sealing pervious soil surfaces exacerbates flood risk by inhibiting retention and infiltration, thereby increasing surface runoff. This capacity of land use systems to reduce or increase flood risk can be interpreted as a positive or negative flood insurance value.

This research project aimed to support nature-based flood risk management. For this purpose, a spatial optimization and comparative flood risk assessment framework were developed to identify the most suitable locations in a catchment for land use changes mitigating flood hazards downstream, and to quantify the flood insurance value of these land use changes. The developed frameworks were illustrated for study areas in Flanders, the northern region of Belgium, which has a high flood risk across its entire territory, as it is both flood-prone and characterized by a high degree of urbanization.

First, the impact of soil sealing on flood severity was assessed in data-driven analyses based on the Flemish spatial flood archive, containing records of flood extents dating back to 1988. Flooded area extents and corresponding flood volumes from this archive were analyzed along with time series of rainfall and land use for three middle-sized river subcatchments using linear regression and two machine learning methods, Support Vector Regression and Boosted Regression Trees. The machine learning methods were found suitable for this type of study, since their flexibility allows for spatially explicit models with larger sample sizes. However, the relationship between soil sealing and flood volume and extent could not be confirmed by the empirical analyses. The analyses were mainly limited by the length of the time series, limiting the number of observations. Additionally, uncertainties and possible inaccuracies associated with the recorded historical flood extents and inconsistencies in the land use classifications also impeded the data-driven analyses. It is therefore stressed that continued consistent monitoring of floods and land use changes is required.

As land use changes impact rainfall-runoff (RR) interactions in the catchment, spatially distributed hydrological models are needed to assess the hydrological impact of land use changes. However, due to their large computational burden, such hydrological models are typically applied in scenario-analyses, assessing ‘what-if’ problems requiring a limited number of model simulations. To address ‘where should’ questions, iterative spatial optimization analyses are required with a high number of model simulations to identify the spatial configuration of certain land use interventions promoting water retention and infiltration. The computational demand of such analyses can be reduced by implementing heuristic algorithms, limiting the solution space and approximating the optimal solution or by integrating a more computationally efficient and sufficiently accurate hydrological model. The latter approach was adhered to in this research whereby a computationally efficient and spatially-

explicit RR-model was developed, taking into account the spatial interactions between surface runoff generation, propagation and re-infiltration along the flow paths. The widely used Soil Conservation Service Curve Number (SCS-CN) method was used as a basis to formulate eighteen raster-based model configurations, testing different values for three model parameters in combination with two methods considering antecedent soil moisture conditions (AMC) and three re-infiltration algorithms. These model configurations were evaluated for three catchments, resulting in Nash-Sutcliffe Efficiency (NSE) values of 0.57, 0.56 and 0.64 for the most performant model configuration, implementing a λ parameter value of 0.05, the AMC correction method of the Soil and Water Assessment Tool (SWAT) and the re-infiltration algorithm devised by Van Loo (2018) with a hydraulic radius of 3 mm and a seasonally adjusted Manning's roughness coefficient. This model was judged sufficiently accurate to assess and compare the off-site hydrological impacts of land use alternatives.

Consequently, the developed rainfall-runoff model was integrated in an iterative optimization framework to address the question of where to implement certain land use interventions in order to most effectively minimize runoff accumulation, and thus flood hazard, in a downstream point of interest. This optimization framework iteratively ranks the performance of all alternative locations, while taking into account spatial interactions. The framework was tested for two medium-sized catchments for three land use change scenarios: afforestation, soil sealing and the implementation of winter cover crops. Results show the considerable impact of these land use changes and their locations on runoff accumulation at the downstream point of interest, with the priority locations having the greatest impact on downstream runoff volume and providing an indication on how to achieve a maximum impact on flood hazard with a minimum extent of the land use change under consideration. The priority locations for afforestation are characterized by high flow accumulation, highlighting the importance of enhancing the infiltration capacity in river valleys. Conversely, soil sealing is to be avoided in these locations and confined to locations upstream in the catchments.

Finally, the impact of land use changes at locations determined by the optimization framework were evaluated in a comparative flood risk assessment framework. In this framework, the relative economic impact of land use changes on flood damages and corresponding flood risk is determined, thus allowing for an explorative assessment of the efficiency of the proposed land use changes as flood mitigation measures. This flood risk assessment was illustrated for one study area, with the results showing that afforestation in river valleys corresponds to a large flood insurance value, while soil sealing in the upstream areas only results in a limited increase of flood risk.

In conclusion, the iterative optimization framework allows for the identification of the most effective locations for flood hazard mitigation through a particular land use change in catchments, while the comparative flood risk assessment allows for the calculation of the flood insurance value associated with land use changes mitigating flood risk. The generic frameworks can be applied to small to medium-sized, hilly catchments; and was illustrated for such catchments in Flanders, Belgium. The results consistently show the importance of river valleys in mitigating downstream flood hazards, as these areas are to be avoided for soil sealing and prioritized for afforestation, leading to a high potential flood insurance value. Consequently, the developed frameworks can be applied to build support for spatial planning initiatives integrating sustainable flood risk management, a pertinent policy topic, both in Flanders, Belgium and in wider Europe.

Samenvatting

In Europa zijn overstromingen één van de meest voorkomende natuurrampen, die gepaard gaan met zware maatschappelijke en economische gevolgen. Bovendien is de economische schade van overstromingen toegenomen in de laatste decennia omwille van socio-economische ontwikkelingen, zoals een stijgend welvaartsniveau en verstedelijking in overstromingsgevoelige gebieden. Deze trend was dan ook de aanleiding om het overstromingsbeheer, gericht op de controle van overstromingen door middel van infrastructuren, bv. sluizen en dijken, aan te passen naar een geïntegreerd overstromingsrisicobeheer, waarbij overstromingsrisico gedefinieerd wordt als het product van de kans op overstromingen met de resulterende schade. Een duurzaam overstromingsrisicobeheer is er dus op gericht om zo efficiënt mogelijk de sociale, ecologische en economische impact van overstromingen te beperken, onder andere door landgebruik, dat de capaciteit heeft om het overstromingsrisico stroomafwaarts te verminderen, te vrijwaren of nieuw te realiseren. Landgebruik, en de ruimtelijke verdeling ervan in het landschap, beïnvloedt het overstromingsrisico via hydrologische processen. Zo kan vegetatie, bv. bos en winterse bodembedekkers van landbouwpercelen, de snelle oppervlakkige afstroming van water vertragen en reduceren, waarbij de waterretentie en infiltratie in de bodem toenemen. Verharding van de bodem daarentegen verhoogt het overstromingsrisico door infiltratie en waterretentie te verhinderen, waardoor de snelle oppervlakkige afstroming toeneemt. Het vermogen van stroomopwaarts landgebruik om overstromingsrisico te beïnvloeden kan dus geïnterpreteerd worden als een verzekeringswaarde.

Het doel van deze doctoraatsthesis was om overstromingsrisicobeheer wetenschappelijk te onderbouwen aan de hand van doelgerichte landgebruiksveranderingen, met toepassing op Vlaanderen. Vlaanderen heeft een hoog overstromingsrisico, aangezien het zowel een grotendeels van nature overstromingsgevoelig gebied is en gekenmerkt wordt door een hoge graad van urbanisatie met een verspreid patroon. Daarom worden in deze thesis procedures ontwikkeld en geëvalueerd voor een ruimtelijke optimalisatie- en overstromingsrisico-analyse, met als doel enerzijds de meest geschikte locaties in het landschap te vinden voor landgebruiksveranderingen om het overstromingsrisico stroomafwaarts te verlagen, en anderzijds de reductie van het risico t.g.v. deze landgebruiksveranderingen, ofwel de verzekeringswaarde, te kwantificeren.

Eerst werd de impact van verharding op de ernst van overstromingen onderzocht in een empirische analyse op basis van de Vlaamse dataset met de contouren van overstromingen sinds 1988. De overstromingsoppervlakten en –volumes afgeleid van deze dataset en het historisch landgebruik werden samen geanalyseerd aan de hand van multivariate regressieanalyse en machine learning methoden. Deze machine learning technieken zijn geschikt voor empirische analyses, aangezien hun flexibiliteit ruimtelijk expliciete modellen met een hoger aantal observaties mogelijk maakt. Echter, de impact van verharding op overstromingsvolume en –oppervlakte kon niet worden aangetoond met de empirische analyses, die vooral werden gehinderd door de beperkte tijdsperiode waarvoor overstromingscontouren beschikbaar zijn. Bovendien kunnen de analyses ook beïnvloed worden door de onzekerheden verbonden aan de geregistreerde overstromingscontouren en de inconsistenties in landgebruiksclassificatie. Het is daarom van belang dat de registratie van overstromingen en landgebruik voortgezet wordt op een meer consistente manier.

Ruimtelijk expliciete, hydrologische modellen zijn nodig om het effect van landgebruiksveranderingen op de oppervlakkige afstroming in te schatten. Deze modellen hebben echter een lange rekentijd, waardoor ze eerder geschikt zijn om landgebruiksscenario's ('wat als?') met een beperkt aantal modelsimulaties te analyseren. Optimalisatie-analyses met de vraag waar landgebruiksveranderingen het grootste effect hebben op overstromingsgevaar, hebben een hoog aantal modelsimulaties nodig,

waardoor het nodig is om zeer rekenefficiënte modellen te gebruiken. Een rekenefficiënt en ruimtelijk expliciet afstromingsmodel werd ontwikkeld, dat ook rekening houdt met stroomafwaartse interacties tussen afstroming en herinfiltratie. Op basis van de populaire Soil Conservation Service Curve Number (SCS–CN) methode werden achttien modelconfiguraties ontwikkeld en geëvalueerd voor drie studiegebieden, waarbij twee methoden om bodemvochtgehalte in rekening te brengen en drie herinfiltratie-methoden werden getest, en de waarden voor drie verschillende parameters werden gevarieerd. Het meest performante model, met een Nash-Sutcliffe Efficiency (NSE) van 0.57, 0.56 en 0.64 in de drie studiegebieden, werd als accuraat genoeg beschouwd om de hydrologische impact van landgebruik off-site te kunnen inschatten. Dit afstromingsmodel implementeert de SCS–CN-methode met de λ parameter gelijk aan 0.05 en integreert hiermee de SWAT-methode om de CN aan te passen aan bodemvochtgehalte en de re-infiltratie methode voorgesteld door Van Loo (2018), met een hydraulische radius van 3 mm en een seizoensgebonden ruwheidscoëfficient.

Vervolgens werd dit afstromingsmodel geïntegreerd in een iteratieve optimalisatieprocedure om te zoeken waar bepaalde landgebruiksinterventies het meest effectief zijn om de accumulatie van oppervlakkige afstroming, en dus het overstromingsgevaar, te minimaliseren in een afwaartse locatie. In deze optimalisatieprocedure worden de alternatieve locaties gerangschikt op basis van de reductie in volume afgestroomd water ten gevolge van de landgebruiksinterventie, daarbij rekening houdend met ruimtelijke interacties stroomafwaarts. Deze procedure werd getest in twee stroomgebieden voor drie landgebruiksinterventies: bebossing, verharding en het planten van winterse bodembedekkers op akkerbouwpercelen. De resultaten tonen het aanzienlijke effect aan van deze landgebruiksveranderingen en hun locaties op de afwaartse accumulatie van oppervlakkige afstroming. De locaties met de hoogste prioriteit hebben de grootste impact, waarbij een indicatie gegeven wordt waar in het bekken een maximaal effect op overstromingsgevaar kan bekomen worden met een minimum aan betrokken oppervlakte. Deze analyse toont aan voor bebossing dat de meest geschikte locaties zijn gelegen in de valleien, wat het belang aantoont van het verhogen van de infiltratie-capaciteit in de riviervalleien. Verharding wordt daarentegen beter vermeden in de valleien.

Uiteindelijk werd het effect van landgebruiksveranderingen, bepaald door de optimalisatieprocedure, nagegaan in een analyse van de overstromingsrisico's. In deze analyse werd de relatieve economische impact van landgebruiksverandering op overstromingsschade berekend, en vervolgens gecombineerd met de overstromingskans om de relatieve impact van de landgebruiksverandering op het overstromingsrisico te bepalen. Hierdoor wordt een indicatie gegeven van de efficiëntie van de landgebruiksinterventies om het overstromingsrisico te verlagen. Deze analyse werd geïllustreerd voor een studiegebied, waarvan de resultaten aangeven dat bebossing in valleigebieden resulteert in een grote vermindering van het overstromingsrisico, waaraan de interpretatie kan gekoppeld worden dat de aanleg van bos op deze locaties een hoge verzekeringswaarde heeft. Het verharden van stroomopwaarts gelegen gebieden, en dus het vermijden van verharding in valleien, leidt tot een eerder beperkte stijging van het overstromingsrisico.

De resultaten van deze doctoraatsthesis tonen consistent het belang aan van riviervalleien in overstromingsrisicobeheer, aangezien deze gebieden een zeer lage prioriteit kregen voor verharding en een hoge voor bebossing, wat gepaard gaat met een hoge verzekeringswaarde. Deze resultaten kunnen dienen om het draagvlak te vergroten voor ruimtelijke interventies in het kader van duurzaam waterbeheer.

List of Figures

Figure 1.1. The different components of the flood risk concept.....4
Figure 1.2. Location of Flanders, Belgium in Western Europe. 7
Figure 1.3. Distribution of soil sealing in Flanders, expressed as % sealed per pixel (5m resolution) ...8
Figure 1.4. Recently flooded areas in Flanders in the period 1988-2016, visualized with the eleven major river basins and the main rivers, i.e. the navigable and category 1 watercourses. 9
Figure 1.5. a) Flood hazard, represented by flood extent, in Flanders, aggregated for coastal, fluvial and pluvial floods and visualized for three probability scenarios, b) Economic flood risk (€/m²/year), combining the economic damages of the three probability scenarios for coastal, fluvial and pluvial floods 12
Figure 1.6. Schematic outline of the PhD thesis.....16
Figure 1.7. Location of the study catchments in Flanders, Belgium.....16
Figure 1.8. General land use, based on the land use dataset of 2012, in the three study catchments: the Maarkebeek (a), Bellebeek (b) and Demer (c) catchments.....17
Figure 1.9. General soil type of the three study catchments: the Maarkebeek (a), Bellebeek (b) and Demer (c) catchments.....17
Figure 2.1. Location of the three studied subbasins in Flanders, Belgium: subbasins of the Maarkebeek (52 km²), Bellebeek (87 km²) and Demer (243 km²).....19
Figure 2.2. The spatial occurrence of flood events considered in the data-driven analyses between 1988 and 2016 21
Figure 2.3. Percentage of urban area and flooded volume/mm rainfall.....23
Figure 2.4. Partial dependence plots for the BRT models of the three subbasins of the Maarkebeek, Bellebeek and Demer.....33
Figure 2.5. Results of the sensitivity analysis for the linear regression models (a), Support Vector Regression models (b) and Boosted Regression Trees (c). 34
Figure 2.6. Assessment of the relationship between flood volume and measured peak discharge....38
Figure 3.1. Overview of the 18 configurations of the CN-based Rainfall-Runoff model. 44
Figure 3.2. Outline of the soil water balance model implemented in ArcNEMO.....45
Figure 3.3. Comparison of CN values adjusted to antecedent soil moisture conditions according to the NEMO method (Chow et al., 1988; Raes et al., 2006) and the method implemented in SWAT (Neitsch et al., 2011) 47
Figure 3.4. Schematic overview of the re-infiltration method based on SCS-CN method parameters. 48
Figure 3.5. Schematic overview of the re-infiltration method proposed by Van Loo (2018).....49
Figure 3.6. Schematic overview of the KSAT re-infiltration method.....49
Figure 3.7. Location of the Maarkebeek catchment in the Upper Scheldt basin and the Bellebeek catchment, with its subcatchment of the Hunselbeek, in the Dender basin in Flanders, Belgium.....50
Figure 3.8. a) Digital Elevation Model (DEM) (m) and b) its derived slope (m/m) of the Maarkebeek and Bellebeek catchments. 51
Figure 3.9. a) CN values (λ = 0.2), b) Manning's roughness coefficient *n* and c) saturated hydraulic conductivity (K_{SAT}, mm/hr) for the three studied catchments of the Maarkebeek, Bellebeek and Hunselbeek. 54
Figure 3.10. Histograms of the observed runoff volumes in the Maarkebeek (a), Bellebeek (b) and Hunselbeek (c) catchments.....56

Figure 3.11. Plots of the modeled and measured (meas.) discharge volumes (vol.) in mm at the outlet of the Bellebeek catchment for the RR-models implementing the re-infiltration method using SCS-CN parameters (P-I_a). 64
Figure 3.12. Log-log plots of the modeled and measured (meas.) discharge volumes (vol.) in mm at the outlet of the Bellebeek catchment for the RR-models implementing the re-infiltration method of Van Loo (2018) with SWAT AMC correction and a λ of 0.05 65
Figure 3.13. Log-log plots of the modeled and measured (meas.) discharge volumes (vol.) in mm at the outlet of the Bellebeek catchment for the RR-models implementing the re-infiltration method using the saturated hydraulic conductivity KSAT with SWAT AMC correction and a λ of 0.05 66
Figure 3.14. Log-log plot of modeled and measured (meas.) discharge volumes (vol.) at the outlets of the (a) Maarkebeek, (b) Bellebeek, and (c) Hunselbeek catchments for the model configuration implementing the Van Loo re-infiltration method with a hydraulic radius R_h of 3 mm and Manning's coefficient n with a seasonal adjustment, a λ of 0.05 and SWAT AMC correction 67
Figure 3.15. Visualization of the impact of implementing a seasonally variable Manning's roughness coefficient n in the re-infiltration method of Van Loo (2018) on the value of NSE, and its components α (alpha) and β (beta). 70
Figure 4.1. Flowchart of the iterative optimization framework, iteratively assessing pixels in the candidate set based on the change in accumulated runoff volume (Q_{accum}) at the downstream Point Of Interest (POI) resulting from a change in LU tye. 75
Figure 4.2. Digital Elevation Model (DEM), derived slope (m/m) map, conjugated Curve Number (CN) values (λ = 0.05) and Manning's n of the (a) Maarkebeek and (b) Bellebeek catchments. 76
Figure 4.3. (a) Relative frequency (%) of the conjugated Curve Numbers and (b) infiltration capacity (%) of the Maarkebeek and Bellebeek catchments 76
Figure 4.4. The rainfall distribution of selected winter (high AMC) and summer (low AMC) events in the Maarkebeek (a) and Bellebeek (b) catchments. 78
Figure 4.5. Conjugated CN values corrected for the high and low AMC events in the Maarkebeek (a) and Bellebeek (b) catchments. 78
Figure 4.6. The afforestation ranking results, expressed as accumulated runoff reduction at the outlet [mm], for the (a) Maarkebeek and (b) Bellebeek catchments, for two rainfall events with high AMC and low AMC. 81
Figure 4.7. The afforestation ranking results, expressed as accumulated runoff reduction at the outlet [mm], for the (a) Maarkebeek and (b) Bellebeek catchments, under three rainfall (P) events: 30 mm, 50 mm and 100 mm. 82
Figure 4.8. Standardized ranking of pixels considering their sealing in the (a) Maarkebeek and (b) Bellebeek catchments for the high and low AMC rainfall events. In the Bellebeek catchment, isolated patches of land, bordered by rivers, were excluded for sealing. 83
Figure 4.9. Standardized ranking of pixels considering their sealing in the (a) Maarkebeek and (b) Bellebeek catchments for three rainfall amounts (P) of 30, 50 and 100 mm 84
Figure 4.10. The ranking results for winter cover crop implementation, expressed as the accumulated runoff reduction [mm] at the outlet of the (a) Maarkebeek and (b) Bellebeek catchments, for the high AMC rainfall event and 30 mm, 50 mm and 100 mm rainfall (P) events. 85
Figure 4.11. The accumulated runoff (%) at the catchment outlets after (a) afforestation, (b) sealing and (c) winter cover crop implementation for three rainfall events 86
Figure 4.12. The average standardized ranks and its standard deviations for the Maarkebeek (a) and Bellebeek (b) watersheds, averaged for 30, 50 and 100 mm rainfall events and for three LU type changes 88

Figure 4.13. Boxplots of the standardized ranks' standard deviations (a) and flow accumulation (b) according to the average rank of afforestation, sealing and cover crop implementation in the Bellebeek and Maarkebeek catchments. 89
Figure 5.1. Framework determining relative flood damage and risk impact of land use changes. 95
Figure 5.2. The flood damage curves depicting the relationship between the inundation depth (cm) and the damage factor. 96
Figure 5.3. Extents of flooded areas in the Maarkebeek basin as recorded in the geospatial flood archive for the 2000–2016 period 98
Figure 5.4. Scatterplot of the flood volumes derived from the observed flood extents (Observed flood volume, m^3) and the flood volumes 101
Figure 5.5. (a) The inundation depth (m) and (b) the corresponding flood damage (€) per pixel (5m X 5m resolution) derived from the flood damage model in the Maarkebeek catchment resulting from the observed flood events 102
Figure 5.6. Flood risk, expressed as expected annual damages (€/year) in each pixel (5m X 5m resolution), in the Maarkebeek catchment based on the four observed flood events 102
Figure 5.7. Standardized afforestation ranks of pixels in the Maarkebeek catchment for the four flood events. 103
Figure 5.8. The standardized ranks for the soil sealing scenario for the four flood events in the Maarkebeek catchment. 104
Figure 5.9. Locations of the pixels selected for land use change implementation, i.e. the 750 highest ranked pixels (187.5 ha) in the ranking combined over the four flood events, for both the afforestation and soil sealing scenarios. 104
Figure 5.10. The relative impact in flood damages (%) after (a) implementing the afforestation scenario, resulting in a relative damage mitigation, and after (b) implementing the soil sealing scenario, resulting in a relative flood damage increment. 105
Figure 5.11. Relative flood risk mitigation (%) in the Maarkebeek catchment after afforesting the 750 highest ranked pixels in this land use change scenario. 107
Figure 5.12. Relative flood risk increment (%) in the flooded areas in the Maarkebeek catchment after sealing the 750 highest ranked pixels in this land use change scenario. 107
Figure 5.13. Flood risk (€/year per pixel of 25 m^2) in the Maarkebeek catchment as calculated by the LATIS tool based on the flood damages determined for flood events with a return period of 10, 100 and 1000 years. 110
Figure 6.1. Schematic depiction of the workflow followed in this thesis 112

List of Tables

Table 1.1. Key figures on the number of insurance claims, the corresponding total insured losses (million €) and the average loss per claim (€), as reported by Assuralia between 2006 and 2019 10
Table 2.1. Land use distribution (%) in the Maarkebeek, Bellebeek and Demer subbasins according to the reclassified and resampled (20 m resolution) land use datasets of 1995, 2001 and 2012, corrected using a land use change trajectory analysis 22
Table 2.2. Overview of flood events in the study areas, their meteorological characteristics and corresponding interpolated urban fractions. 24
Table 2.3. Results of the parameter tuning of the BRT for each of the study areas 27
Table 2.4. Adjusted R^2 and P-values of the Multiple Linear Regression models 29
Table 2.5. Coefficients (β) and their P-values of the Multiple Linear Regression (MLR) 29
Table 2.6. Adjusted R^2 and P-values of the Multiple Linear Regression models of the pooled sample (22 observations) 30
Table 2.7. RMSE and relative RMSE (rRMSE, %) of the Support Vector Regressions for the three subbasins testing different meteorological predictors 30
Table 2.8. Results of the recursive feature elimination (RFE) of the Support Vector Regression with as dependent variable the volume in a flood extent (m^3). 31
Table 2.9. RMSE and relative RMSE (rRMSE, %) of the Boosted Regression Trees for the three study areas predicting flood volume (m^3) and area (m^2).. 31
Table 3.1. Overview of the CN cover descriptions assigned to the land use classes for each Hydrological Soil Group (HSG), determined by soil texture and drainage information. 52
Table 3.2. Base value for the Manning's roughness coefficient n (n_b) according to the land use classes from the 2012 land use dataset 53
Table 3.3. Seasonal adjustment of the Manning's roughness coefficient n for vegetated land use classes from the tabulated, base values n_b used in fall conditions 53
Table 3.4. Characteristics of the selected rainfall events in the Maarkebeek, Bellebeek and Hunselbeek catchments for total rainfall (mm), peak discharges (m^3/s) and runoff volumes (mm) 56
Table 3.5. The NSE values of the different RR-models for the Maarkebeek, Bellebeek and Hunselbeek catchments for respectively 165, 164 and 124 rainfall events 59
Table 3.6. The relative RMSE (%) values of the different RR-models for the Maarkebeek, Bellebeek and Hunselbeek catchments for respectively 165, 164 and 124 rainfall events 60
Table 3.7. The linear correlation r of the different RR-models for the Maarkebeek, Bellebeek and Hunselbeek catchments for respectively 165, 164 and 124 rainfall events 61
Table 3.8. The error in variability α of the different RR-models for the Maarkebeek, Bellebeek and Hunselbeek catchments for respectively 165, 164 and 124 rainfall events 62
Table 3.9. The bias term β of the different RR-models for the Maarkebeek, Bellebeek and Hunselbeek catchments for respectively 165, 164 and 124 rainfall events 63
Table 3.10. The average sensitivity index S for changes in the hydraulic radius R_h in Manning's equation, implemented in the re-infiltration methods of Van Loo (2018) and its variant using K_{SAT} with standard Manning's roughness coefficients n and seasonally adjusted Manning's n 63
Table 4.1. Adjustments of Manning's n for the vegetated LU classes to winter (high AMC) and summer conditions (low AMC) 74
Table 4.2. Catchment-averaged runoff volumes (RO vol.; m^3) at the outlet of the Maarkebeek and Bellebeek catchments, following the different rainfall events with high AMC (winter), low AMC (summer) and 30, 50 and 100 mm uniform rainfall distributions. 80
Table 5.1. The maximum damage values as implemented in the flood damage model 97

Table 5.2. Overview of the flooded area (ha), total observed flood volume (m³), resulting flood damages (€), runoff volume accumulation at the flood extents' outlet (m³) and total modeled flood volume (m³) for each of the four observed flood events and their corresponding flood extents 100
Table 5.3. Relative flood damage mitigation and increment (%) after respectively afforesting and sealing the 750 highest ranked pixels in each land use change scenario 106

List of Abbreviations

ACO	Ant Colony Optimization
AMC	Antecedent Moisture Content
BI	Blue Infrastructure
BRT	Boosted Regression Trees
CN	Curve Number
CRED	Centre for Research on the Epidemiology of Disasters
DD	Drainage Density
DEM	Digital Elevation Model
EAD	Expected Annual Damages
ED	Edge Density
EM-DAT	Emergency Events Database
EMO	Evolutionary Multi-objective Optimization
ES	Ecosystem Services
EU	European Union
FA	Flow Accumulation
FC	Field Capacity
GA	Genetic Algorithm
GI	Green Infrastructure
GIS	Geographical Information System
KSAT	re-infiltration method based on the saturated hydraulic conductivity
L-CV	*L*-Coefficient of Variation
LU	Land use
LULC	Land use/land cover
MA	Mean Area
MLR	Multiple Linear Regression
NBS	Nature-Based Solutions
NEMO	Nutrient Emission MOdel
NFM	Natural Flood Management
NSE	Nash-Sutcliffe Efficiency
NSGAII	Nondominated Sorting Genetic Algorithm II
NWRM	Natural Water Retention Measures
OAT	One-At-a-Time
$P\text{-}I_a$	re-infiltration method based on the SCS-CN parameters
PP	Peak Precipitation
POI	Point Of Interest
PS	precipitation accumulated prior to the flood event
Psum	sum of the flood inducing precipitation
R^2	Coefficient of determination
RCP8.5	high-emissions Representative Concentration Pathway
RFE	Recursive Feature Elimination
RMI	Royal Meteorological Institute
RMSE	Root Mean Square Error
RR	Rainfall-Runoff
rRMSE	relative Root Mean Square Error
SA	Simulated Annealing
SAT	Saturated soil moisture content
SCS	Soil Conservation Service of the USDA
SD	Standard Deviation
SVR	Support Vector Regression

SW	Soil Moisture
SWAT	Soil & Water Assessment Tool
USDA	United States Department of Agriculture
VL	Van Loo
WP	Wilting Point

List of Symbols

α	ratio of the standard deviation of observations and simulations
β	Regression coefficient (Ch. 2), ratio of the means of observations and simulations (Ch. 3)
D	Flood damage (€)
H	Heterogeneity measure of Hosking and Wallis
I	Infiltration [mm]
I_a	Initial abstraction parameter of SCS-CN method [mm]
K_{SAT}	Saturated hydraulic conductivity [mm/hr]
n	Manning's roughness coefficient [$s/m^{1/3}$]
P	Precipitation [mm]
Q	Accumulated runoff volume [mm or m^3]
R	Flood risk (€/year)
R_h	Hydraulic radius [m]
s	slope [m/m]
S	Retention parameter of SCS-CN method [mm]
$\overline{S}$	Sensitivity index
ϑ	Soil water content
V	Surface flow velocity [m/s]
Vol	Volume [mm or m^3]

Table of Contents

Acknowledgements I
Abstract III
Samenvatting V
List of Figures VII
List of Tables X
List of Abbreviations XII
List of Symbols XIV
Table of Contents XV
Chapter 1 Introduction 1
1.1. General background 1
1.1.1. Floods: damages and trends in a changing environment 1
1.1.2. Towards nature-based flood risk management 2
1.1.3. Nature-based flood risk management and optimization 5
1.2. Flood hazard and management in Flanders, Belgium 7
1.3. Research objectives, research questions and thesis outline 14
Chapter 2 A data-driven analysis of the spatial flood archive to assess the impact of soil sealing on flood severity 18
2.1. Introduction 18
2.2. Material and Methods 19
2.2.1. Geospatial Data 19
2.2.2. Multiple Linear Regression 25
2.2.3. Machine Learning 26
2.2.4. Sensitivity Analysis 28
2.3. Results 28
2.3.1. Multiple Linear Regression 28
2.3.2. Support Vector Regression 30
2.3.3. Boosted Regression Trees 31
2.3.4. Sensitivity Analysis 34
2.4. Discussion 34
2.5. Conclusion 39
Chapter 3 A distributed and efficient CN-based rainfall-runoff model for land use optimization 41
3.1. Introduction 41
3.2. Material and Methods 43

3.2.1. Default SCS-CN method 43
3.2.2. Alternative model configurations 43
3.2.3. Study areas 50
3.3. Results 56
3.4. Discussion 67
3.5. Conclusion 71
Chapter 4 An iterative optimization approach identifying priority locations for land use change mitigating downstream river flood hazard 72
4.1. Introduction 72
4.2. Material and Methods 73
4.2.1. Rainfall-Runoff Model 73
4.2.2. Iteration framework 74
4.2.3. Study areas 75
4.2.4. Rainfall events and types of LU changes 76
4.3. Results 80
4.3.1. Afforestation 80
4.3.2. Soil Sealing 82
4.3.3. Winter Cover Crops 84
4.4. Discussion 86
4.5. Conclusion 90
Chapter 5 A comparative flood risk assessment evaluating the flood insurance value of land use changes 92
5.1. Introduction 92
5.1.1. Comparative flood risk assessment of land use changes 94
5.2. Material and Methods 94
5.2.1. Comparative flood damage and risk assessment 94
5.2.2. Case Study 98
5.3. Results 100
5.3.1. Flood damage and risk assessment of observed flood events 100
5.3.2. Comparative flood damage and risk assessment 102
5.4. Discussion 107
5.5. Conclusion 111
Chapter 6 General Discussion and Conclusions 112
6.1. General discussion 112
6.1.1. Upstream land use and downstream flood severity 113
6.1.2. Where to implement land use changes? An iterative optimization framework 116

6.1.3. Quantitative, economic impact of land use changes: the comparative flood damage and risk assessment 117
6.2. General conclusion 118
6.2.1. Policy implications 118
6.2.2. Perspectives for future research 119
References 121
Curriculum Vitae 139
List of publications 140

Chapter 1
Introduction

1.1. General background

1.1.1. Floods: damages and trends in a changing environment

Floods are one of the most devastating natural hazards worldwide with profound social and economic impacts. The long-term, global Emergency Events Database EM-DAT of the Centre for Research on the Epidemiology of Disasters (CRED) of UCLouvain records disasters worldwide based on four criteria: (i) disasters with ten or more fatalities, (ii) disasters affecting at least 100 people, (iii) disasters declared a national emergency, (iv) international aid requested as a result of the disasters. According to this database, floods were the most frequently occurring natural disasters between 1980 and 2017, constituting approximately 40% of all recorded natural disasters, thereby killing 250 000 people and causing an estimated US$ 800 billion or € 675 billion in economic losses (Guha-Sapir, 2020). Three main types of floods are commonly distinguished according to the cause of flooding (CRED & UNISDR, 2018; Munich Re, 2019):

- Fluvial floods: riverine floods, occurring when the discharge capacity of the river is exceeded;
- Pluvial floods: floods occurring when the infiltration capacity of the soil is exceeded by torrential rainfalls, e.g. flash floods and urban flooding due to an exceedance of the urban drainage capacity. These floods can occur independent of the river system, both in rural and urban areas;
- Coastal floods and storm surges: flooding of coastal areas from the sea

This distinction is also made in the EM-DAT database, with riverine floods occurring most frequently in the database, thereby inflicting the most damages and affecting the largest number of people (Guha-Sapir, 2020). In the European Economic Area, flood events caused 4300 fatalities and inflicted € 170 billion (US$ 200 billion) in direct economic damages between 1980 and 2017, constituting one-third of the direct economic damages caused by natural disasters in this period, with less than a quarter of these losses covered by a flood insurance scheme (EEA, 2019).

In the last decades, an increasing trend in the number of recorded flood events and associated economic losses has been observed. Barredo (2009) and Bouwer (2011) demonstrated that the main driver of the increasing economic flood losses, observed in Europe since 1970, are socioeconomic developments, including population growth, increasing wealth and ongoing urbanization in flood-prone areas. Increases in the frequency and severity of extreme flood events have been noted in the United States and in Europe between 1980 and 2009 (Berghuijs et al., 2017), though these trends also show strong temporal variability (Hodgkins et al., 2017; Kundzewicz et al., 2018). Blöschl et al. (2019) discerned regional patterns in European river flood discharge trends from 1960 to 2010: flood events increased in northwestern Europe due to increasing winter rainfall, while a decrease in floods was observed in southern and northeastern Europe; in the former due to decreasing precipitation and increasing evapotranspiration and in the latter due to decreasing snowmelt. These observations are largely consistent with climate change projections for Europe (IPCC, 2014), indicating that climate change is a driver of regional changes in flood hazard, though other studies have found it more difficult to discern the impact of climate change from natural variability and human impact on large-scale trends observed in flood datasets (Berghuijs et al., 2017; Hodgkins et al., 2017; Kundzewicz et al.,

2018). In small to medium-sized catchments, changes in landscape configuration and land use influence trends in flood hazard (Blöschl et al., 2007; Chang et al., 2009; Wheater & Evans, 2009). Vegetation plays an important role in the hydrology of these catchments (Bronstert et al., 2002; Peel, 2009), both through evapotranspiration, and through its contribution to surface roughness, thereby decelerating rapid surface runoff and increasing rainfall infiltration into the soil. Conversely, the process of sealing soil surfaces in urbanization, e.g. with concrete surfaces, makes these surfaces impermeable to infiltration of water into the soil, thus decreasing the potential for water storage and increasing the fraction of rapid surface runoff accumulating in downstream areas and discharged in the river system (Lin et al., 2007; Miller et al., 2014; Poelmans et al., 2011).

1.1.2. Towards nature-based flood risk management

Apart from climate change, land use changes and socioeconomic developments are increasingly recognized as the main drivers influencing flood hazard. Consequently, flood policy in Europe is moving away from a policy focused on traditional flood prevention to a policy aiming at flood risk management (Merz, Hall, et al., 2010; Sayers et al., 2015). Traditional flood prevention aims to provide protection against predefined design floods, through the implementation of technical defense measures, such as embankments and retention reservoirs. In contrast, flood risk management focuses on reducing the overall flood risk (Merz, Hall, et al., 2010; Meyer et al., 2009).

Though a wide variety of representations of the concepts of risk are implemented in risk assessment frameworks, **risk** is generally determined by a combination of hazard and the vulnerability of the elements exposed to this hazard. As such, three main factors constitute the concept of risk: hazard, exposure and vulnerability (IPCC, 2012; Merz, Hall, et al., 2010). **Hazards** can be defined as 'chance phenomena causing harm' (Merz, Hall, et al., 2010) or, more generally, as 'a potential occurrence of a natural or human-induced physical event that may cause loss of life, injury, or other health impacts, as well as damage and loss to property, infrastructure, livelihoods, service provision, and environmental resources' (IPCC, 2012). The concept of hazard thus entails the potential for adverse effects or consequences. These adverse consequences can be described by the concepts of exposure and vulnerability related to the hazard. **Exposure** refers to the elements, i.e. the people, livelihoods, ecosystems, and economic, social and cultural assets, exposed to the potential adverse effects of the hazard. **Vulnerability** describes the proneness of these exposed elements to the potential adverse consequences of hazardous events. The concept of vulnerability represents the role of social factors in disaster risk management, and is closely related to and often complimented with the concepts of adaptive capacity and resilience. These concepts are used to describe the characteristics of a system that help mitigate hazards' adverse consequences. Adaptive capacity refers to the ability of a system to adjust to changes in the environment; resilience, in disaster risk management, is subject to a wide range of interpretations, but can be generally defined as a system's ability to efficiently anticipate, absorb and recover from the adverse impacts of hazards. A lack of resilience or adaptive capacity will thus increase the system's vulnerability to the adverse impact of hazard events. In disaster risk management, risk is often qualitatively assessed in a probabilistic risk analysis, which calculates risk as the product of the probability of occurrence of a hazard event and its adverse consequences, determined by the hazard, exposure and vulnerability. Probabilistic risk analysis is often used to evaluate risk mitigation actions, however, other methods of risk analysis are implemented when probability estimates are too imprecise or when a full assessment of the social construct of risk is required, including a qualitative analysis of vulnerability, resilience and adaptive capacity of communities at risk (IPCC, 2012).

A schematic depiction of the interpretation in this PhD-research of the three components of risk with regards to flood events is provided in Figure 1.1. **Flood risk** is often determined in a probabilistic risk

analysis by multiplying the probability of occurrence of flood events with their expected consequences or flood damages (Grossi & Kunreuther, 2005; Merz, Hall, et al., 2010). When losses due to several flood events with different probabilities are combined, flood risk can be expressed as a monetary risk per year or as the expected annual damage (EAD, €/year), representing the integral of the damage-probability curve. Probabilistic flood risk analysis and damage-probability curves are used by insurance companies to assess their portfolios' potential losses and to determine insurance premiums and the type of coverage offered (de Moel et al., 2015; Grossi & Kunreuther, 2005; Ward, de Moel, et al., 2011). **Flood hazard** is characterized by its annual exceedance probability and corresponding flood severity. The *severity* or magnitude of flood events can be expressed by flood characteristics, such as the flood peak discharge, the resulting flood extent, flood volume, and the water depth and flow rate in the floodplain (Merz, Hall, et al., 2010). The *annual exceedance probability* of a flood event with a certain magnitude is then defined as the probability of occurrence in any year of a flood event with at least this magnitude. The probability of flood events is determined using a frequency analysis of hydrological extremes, either based on long-term time series of hydrological data or on long-term hydrodynamic model simulations. Consequently, the exceedance probability of a flood event is inversely related to its severity: severe events occur less frequently than moderate events. Alternatively, the probability of a flood event is also referred to by its return period, which is the reciprocal of the exceedance probability and denotes the average recurrence interval between flood events of a given magnitude. For instance, a flood event with an annual exceedance probability of 1% has a return period of 100 years (Chow et al., 1988; Grossi & Kunreuther, 2005).

In the case of flood risk, **exposure to floods** thus refers to the elements, i.e. the ecosystems, people and property, exposed to flooding and includes an appraisal of their value. Flood damage entails all negative, harmful impacts of floods on society, economy and the environment, which are generally classified into direct and indirect damages. Direct flood damage is defined as the damages occurring at the time of flooding through the physical contact of the exposed elements with flood waters, while indirect flood damage relates to the induced losses as a result of flooding. These indirect damages are removed from the flood event, either in space or time (Merz, Kreibich, et al., 2010). If indirect damages occur outside the flooded area, they are referred to as external damages, whereas internal damages occur within the flooded area (Kellens et al., 2013). A second distinction is made between tangible and intangible damages; the tangible damages can easily be expressed in monetary values, whereas intangible damages encompasses damage inflicted on elements of which the financial value is more difficult to assess. Examples of direct, tangible flood damage include damage to buildings, household effects and roads, whereas direct, intangible damages encompass loss of life, damage to cultural heritage and the impact on ecosystems vulnerable to flooding. Indirect, tangible flood damages are, for instance, costs related to traffic disruptions or induced production losses of companies situated outside the flooded area due to the interruption of their supply chains. Indirect and intangible damage entails the psychological impact of exposure to flooding (Merz, Kreibich, et al., 2010; Messner & Meyer, 2006). Flood risk analyses often only comprise an assessment of tangible flood damages, which are easier and more reliable to estimate than intangible flood damages (Merz, Kreibich, et al., 2010). Moreover, the assessment of external, tangible damages is often neglected due to limited data availability and the complexity of economic networks (Kellens et al., 2013).

The **vulnerability of elements to flooding** is commonly described by damage functions, providing a link between the valuation of the elements exposed to the flood and the corresponding flood hazard characteristics, established in the flood maps. Most often, damage functions are included in flood damage models in the form of depth-damage curves, detailing the impact of water depth on the value of the exposed elements (Gerl et al., 2016). A distinction can be made between empirical functions, based on historical data from flood damage databases, and expert damage functions, based on expert

knowledge (Kellens et al., 2013). Actual damage information possesses a higher accuracy than expert estimates and allows for an assessment of the variability and uncertainty of the damage estimates. However, damage surveys after flood events are rare and limited, providing a limited underlying database for damage functions. Though expert based damage functions are more subjective, they can be applied in any region, since they are not connected to a single flood event (Merz, Kreibich, et al., 2010).

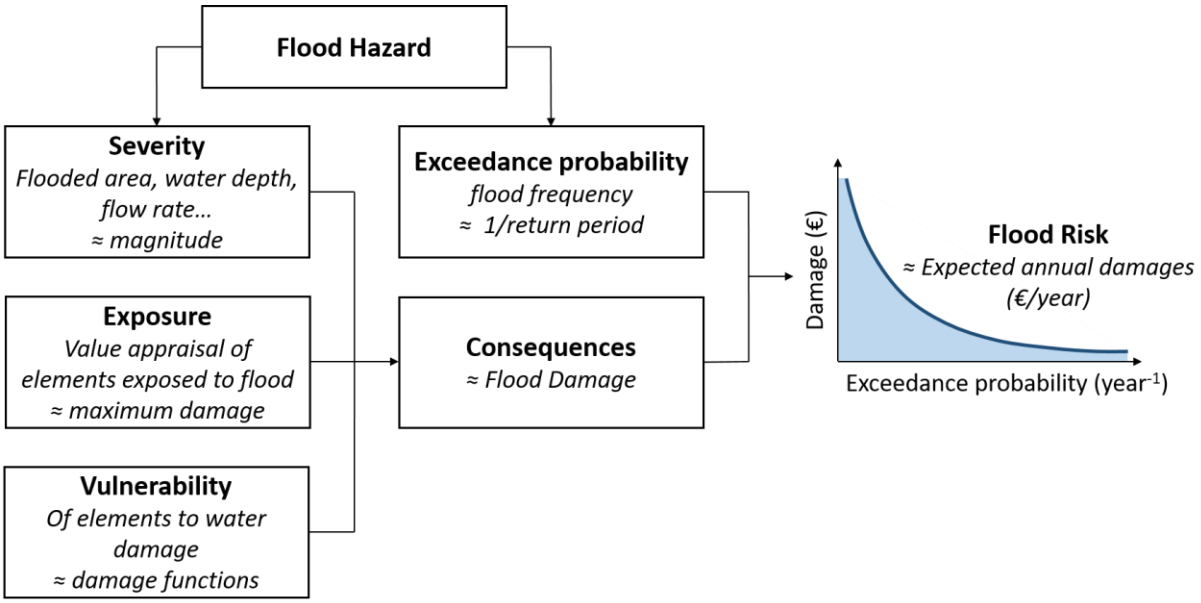

Figure 1.1. The different components of the flood risk concept (adapted from (de Moel et al., 2015; EEA, 2016; Messner & Meyer, 2006; Ward, de Moel, et al., 2011)).

Flood risk management strategies aim at reducing both flood hazard and its consequences, thereby complementing measures for flood prevention and mitigation with adaptation measures. For this purpose, flood risk management also relies on non-structural measures, such as setting up early warning systems, maintaining the existing flood protection infrastructure, providing flood insurance schemes, and promoting flood resilience through spatial planning guidelines and adapted building codes in flood-prone areas (Merz, Hall, et al., 2010; Sayers et al., 2015).

In the European Union (EU), flood risk management is the subject of the European Floods Directive (Directive 2007/60/EC), which builds on the Water Framework Directive (Directive 2000/60/EC), aiming to regulate water quality and quantity through river basin management plans (Directive 2000/60/EC, 2000). The Floods Directive requires member states to assess and map flood risk and to prepare flood risk management plans focused on prevention, protection and preparedness (Directive 2007/60/EC, 2007). Under this Flood Directive, the concept of flood risk management has continued to evolve into an integrated, system-wide approach combining societal, environmental and economic impacts of flooding, thereby seeking opportunities to promoting efficient flood risk management, maximizing the utility of investments, while taking into account social well-being, and promoting ecosystem services (EEA, 2016; Sayers et al., 2015). Synergies between flood risk management and ecosystem services are in particular aimed at by sustainable flood risk management approaches, which thus focus on nature-based measures such as the restoration of floodplains, unsealing of land, afforestation, the adjustment of land management practices (e.g. cover crop implementation) and the promotion of small, landscape structures delaying runoff (EEA, 2016; Thieken et al., 2016). Various

terms are used to refer to these measures, including Natural Water Retention Measures (NWRM), Natural Flood Management (NFM) or Nature-Based Solutions (NBS) (EEA, 2016; Hartmann et al., 2019; SEPA, 2016).

The concept of Ecosystem Services (ES) is therefore a key principle underlying sustainable flood risk management. Ecosystem services are defined as "the benefits people obtain from ecosystems" and are grouped into four types: (i) provisioning ES, e.g. food production through crops, (ii) regulating ES, e.g. flood regulation, (iii) cultural ES, e.g. recreation, and (iv) supporting ES, e.g. nutrient cycling (Millennium Ecosystem Assessment, 2005). Ecosystem services are often delivered off-site, i.e. the areas providing these ES are not the same as the areas benefiting from the services (Fisher et al., 2009). Therefore, the delivery of ES is also dependent on the spatial connectivity between these service providing and benefiting areas. However, ES quantification is still often limited to an on-site assessment of service providing areas, thereby disregarding ecosystem service flows and its beneficiaries (Bagstad et al., 2013; Syrbe & Walz, 2012). The distinct spatial relationship between ES providing, connecting and benefiting areas is especially pronounced in the ES of flood regulation (Syrbe & Walz, 2012). Flood regulation, classified as a regulating ES, refers to the capacity of (semi-)natural ecosystems to retain water that will not immediately runoff, thus co-determining flood hazards in the wider river catchment. Therefore, certain land use changes, such as afforestation, increase the delivery of flood regulation to downstream benefiting areas, while other land use changes, e.g. deforestation or urbanization, decrease the delivery of this ES by reducing the retention and infiltration capacity and increasing rapid surface runoff generation (Millennium Ecosystem Assessment, 2005).

By reducing and delaying surface runoff, land use systems providing flood regulation have the capacity to mitigate flood hazards by reducing the magnitude of flood events. As such, this risk-mitigating capacity can be interpreted as a 'flood insurance value', which these land use systems possess for the downstream areas benefiting from the risk reduction (Dallimer et al., 2020; Soto-Montes-de-Oca et al., 2020). Whereas financial flood insurance schemes provide financial compensation for flood losses, but do not reduce the risk, this flood insurance value attributed to land use systems mitigates the risk, but does not compensate for the damages (Baumgärtner & Strunz, 2014). A monetary quantification of this flood insurance value can form an incentive for stakeholders, such as beneficiaries, government agencies and insurance companies, to direct and fund nature-based solutions in a sustainable flood risk management framework. This quantification should take into consideration the spatial interactions between the risk-mitigating land use systems and the downstream benefiting areas (Soto-Montes-de-Oca et al., 2020).

1.1.3. Nature-based flood risk management and optimization

Along with the increasing interest in sustainable flood risk management, some tools have been developed to identify the locations in the landscape where the greatest effect of NBS could be achieved, and to quantify the impact of NBS on flood risk using hydrological and hydraulic models. The former are also referred to as opportunity mapping tools; these tools identify the locations in the catchment where NBS, including land use changes, have the highest potential to influence hydrological processes, such as runoff generation, accumulation and discharge (SEPA, 2016). An example of opportunity mapping is the Woodland for Water-project of Forest Research in Scotland, which identifies areas where afforestation could be most effective at reducing diffuse pollution and flood risk, with the latter objective evaluated with spatial datasets on flood risk and soil characteristics (Broadmeadow et al., 2014). However, these opportunity mapping tools only consider the on-site delivery of the flood regulation ES, i.e. the intrinsic suitability of locations, but do not consider the

spatial interactions between locations influencing the flood risk reduction delivered off-site, i.c. in downstream areas (SEPA, 2016; Vanegas et al., 2012).

Therefore, the impact of NBS on flood risk in the wider catchment should be further assessed with hydrological models describing the effect of land use changes on hydrological processes, such as infiltration, surface runoff and evapotranspiration. This relationship should be modeled in a spatially distributed way to account for the spatial configuration of land use, topography and soils in a catchment. Moreover, surface runoff should be routed to the river outlet to account for spatial interactions along the flow path and assess the off-site impact of land use changes at locations further downstream. The outputs of these hydrological models can then be combined with hydraulic models to assess the corresponding changes in flood depth and extent (Chow et al., 1988; SEPA, 2016). Consequently, flood damage and risk can be derived from these flood depths to assess the risk reduction or increase corresponding to the land use changes (e.g. de Moel, van Vliet, & Aerts, 2014; Koks, De Moel, Aerts, & Bouwer, 2014).

Spatially (semi-)distributed hydrological models are characterized by high complexity and, consequently, by high computational requirements (Jakeman & Hornberger, 1993; Perrin et al., 2001; Sivakumar, 2008). As such, applications of these models to assess the efficiency of NBS have mostly been limited to analyses of predefined land use change scenarios, answering 'what if' questions (e.g. Kalantari et al., 2014; Yan, Fang, Zhang, & Shi, 2013). These scenario-analyses can be used to compare land use change scenarios based on an objective, such as flood hazard or risk reduction, and identify which one performs best. In order to address the more practical 'where should' questions, optimization analyses are required, identifying the optimal scenario, defined as the spatial configuration of certain land use interventions optimizing, i.e. minimizing/maximizing, the objective (Seppelt & Voinov, 2002). These analyses require an iterative performance assessment of all alternative locations for a land use intervention, while taking into account spatial interactions: as the top-performing locations are selected in each iteration, the performance of the remaining alternatives needs to be updated to the altered situation (Vanegas et al., 2012). Optimization analyses therefore cover a much larger search space, requiring a high number of model simulations (Volk et al., 2010). Consequently, optimization analyses have a high computational burden, especially when combined with computationally intensive hydrological models.

To alleviate this burden, heuristic algorithms are widely implemented, limiting the search space of optimization analyses (Seppelt & Voinov, 2002; Yeo & Guldmann, 2010). Common heuristic algorithms include the Genetic Algorithm (GA), which are based on genetics and natural selection. GA expresses the alternative solutions to the optimization problems as genomes, consisting of several genes representing the control variables of the solution. The 'fitness' of the genomes under consideration, i.e. the population in GA terminology, are determined by an objective function. Subsequently, the 'fittest' genomes are selected in each iteration and based on this selection, a new and fitter population is evolved through the mutation and cross-over of genes (Seppelt & Voinov, 2002; Srivastava et al., 2002). Another heuristic approach is Simulated Annealing (SA), iteratively evaluates the neighbors of a certain solution, or 'state' in SA terminology, as alternatives based on an objective function and a probabilistic acceptance function. This probabilistic function allows the SA algorithm to accept slightly worse solutions to avoid converging on a local optimum. The acceptance function is expressed as a temperature, which progressively decreases across iterations, thereby decreasing the probability of accepting worse solutions. As such, the search space of SA algorithms is larger at the start of the optimization, and converges on a solution as the temperature drops (Lin et al., 2009). Several heuristic methods have also been developed in the field of swarm intelligence, such as Ant Colony Optimization (ACO). The ACO algorithm is inspired by the foraging behavior of ants. This search is randomly initiated

by a number of ants, which evaluate encountered food sources, and provide a positive feedback loop through the deposition of a pheromone trail attracting other members of the colony. ACO thus relies on artificial ants to move through the search space, leaving pheromone depending on the performance of encountered solutions to the objective function, until all ants are attracted to the same solution (X. Liu et al., 2012). By assessing part of the search space and thus of the possible solutions, these algorithms trade off the accuracy of the solution with computation time. Accordingly, it is not guaranteed that the obtained solution equals the global optimum, as these algorithms may converge on a local optimum (Yeo & Guldmann, 2010). An alternative to heuristic algorithms is the use of less complex, computationally efficient models, which are sufficiently accurate to compare solutions and determine the best one (Volk et al., 2010).

1.2. Flood hazard and management in Flanders, Belgium

Flanders is the northern administrative region of Belgium, located in Western Europe (Figure 1.2): it is situated on the North Sea and borders the Netherlands in the north and east and the Wallonia region and France in the south. Its terrain is mostly smooth and flat, evolving to a more hilly terrain towards the border with Wallonia (Agentschap Informatie Vlaanderen et al., 2006). Flanders counts 6.6 million inhabitants and covers an area of 1 362 554 ha, resulting in an average population density of 487 inhabitants/km² (Statbel, 2020).

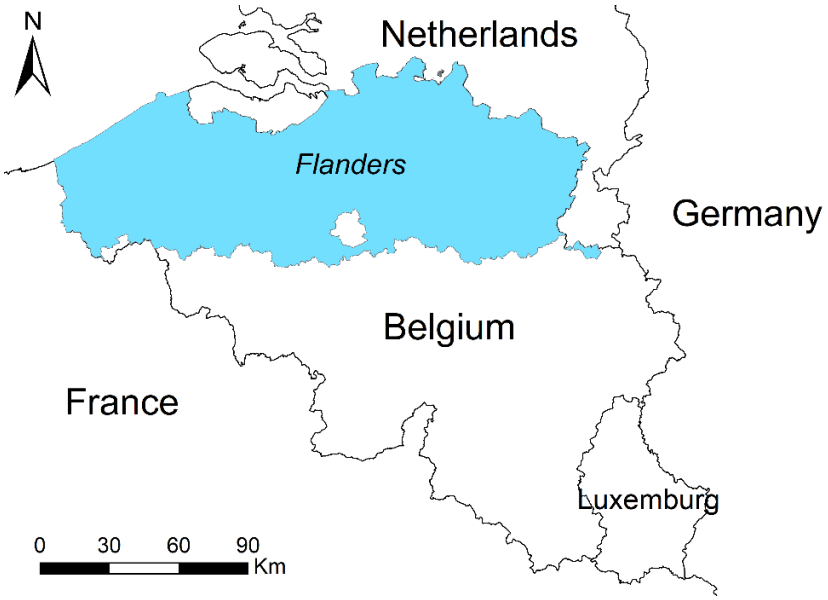

Figure 1.2. Location of Flanders, Belgium in Western Europe (Agentschap Informatie Vlaanderen, 2018; Eurostat, 2020).

Land use in Flanders is predominantly agricultural, with arable land and grassland, including natural grasslands, covering 52.1% of the area. Forest cover constitutes approximately 10% or 140 000 ha of land in Flanders (Pisman et al., 2018). However, Flanders is mostly known as one of the most urbanized regions in the EU, characterized by distinct urban sprawl (Poelmans & Van Rompaey, 2009). In 2013, 32.5% or 443 000 ha of Flanders was classified as settlement area (Departement Ruimte Vlaanderen, 2017), defined by the European Commission as 'the area of land used for housing, industrial and commercial purposes, health care, education, nursing infrastructure, roads and rail networks, recreation (parks and sports grounds)…' (European Commission, 2012). In 2016, the settlement area in Flanders had increased to 450 000 ha or 33%, corresponding to an increase of 6.4 ha/day (Departement Omgeving Vlaanderen, 2019a). The majority of this settlement area (38%) consists of residential buildings and gardens (Pisman et al., 2018). Part of these settlement areas can further be

categorized as 'with sealed soil', which is defined by the European Commission as 'the destruction or covering of soils by buildings, constructions and layers of completely or partly impermeable artificial material (e.g. asphalt, concrete…)' (Jones et al., 2012). In Flanders, soil sealing consists mostly of buildings, roads and parking lots, which constitute 14% of the total surface area (Pisman et al., 2018). The distribution and degree of soil sealing in Flanders is depicted in Figure 1.3, which also visualizes the fragmented nature of the urban systems (Agentschap Informatie Vlaanderen, 2016a). Correspondent to the increase in settlement area, soil sealing in Flanders has expanded with 1.5% between 2012 and 2018, hence increasing with 0.5% every three years (Departement Omgeving Vlaanderen, 2019b).

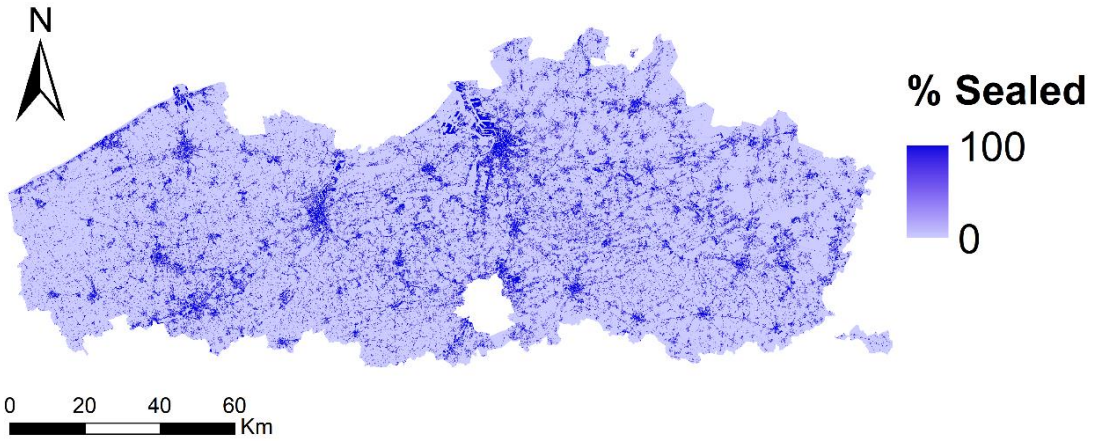

Figure 1.3. Distribution of soil sealing in Flanders, expressed as % sealed per pixel (5m resolution) (Agentschap Informatie Vlaanderen, 2016a).

Flanders is characterized by a dense river network with three main rivers: the Meuse, Scheldt and Yser. Most rivers in Flanders are tributaries of the Scheldt; Flanders is thus mostly situated in the international Scheldt river basin, which also includes the Yser basin and covers parts of Belgium, France and the Netherlands. The eastern part of Flanders, near the Dutch border, is part of the international river basin district of the Meuse, spanning Belgium, France, Germany, Luxembourg and the Netherlands (United Nations, 2009).

Flanders is prone to coastal, fluvial and pluvial floods, with 330 000 ha or 24.3% of its territory defined as naturally floodable (Van Orshoven, 2001). In order to monitor the effectively flooded areas, a geospatial archive is maintained by the Flemish Environment Agency since 1988, recording the contours of the areas flooded during a flood event from various different sources of information, including analogue maps for flood events predating 2000, and helicopter flights or reports from municipalities for current flood events. According to this archive, approximately 5% of Flanders has been flooded at least once between 1988 and 2016, as visualized in Figure 1.4 (Agentschap Informatie Vlaanderen & Vlaamse Milieumaatschappij, 2017). A large portion of settlement area is also at risk of flooding: one fifth of the built-up area is situated in natural flood-prone areas and 3% of the built-up area has been flooded at least once since 1988 (Poelmans & Van Rompaey, 2009). Consequently, floods may cause significant damage. In Belgium, private home insurance covers flood damage to buildings and household assets since March 1, 2006; and Assuralia, the professional association of insurance providers in Belgium, reports yearly on key figures of the insurance market in Flanders, which also include an indication of the number of claims and the insured losses as a result of flooding. An overview of these insured flood losses is provided in Table 1.1. The extreme flood event taking

place in the spring of 2016 caused the highest recorded loss since 2006, namely an insured loss of approximately € 144 million. As these losses represent key figures, the damage related to small-scale, pluvial flooding in Flanders is probably underrepresented by these figures, as the damage related to these frequent and widespread small-scale events also adds up to a significant amount. For instance, Verstraeten & Poesen (1999) found that in the municipality of Bertem eight small-scale floods, occurring between 1978 and 1992, resulted in a total damage of € 1.37 million, as actualized for 1999.

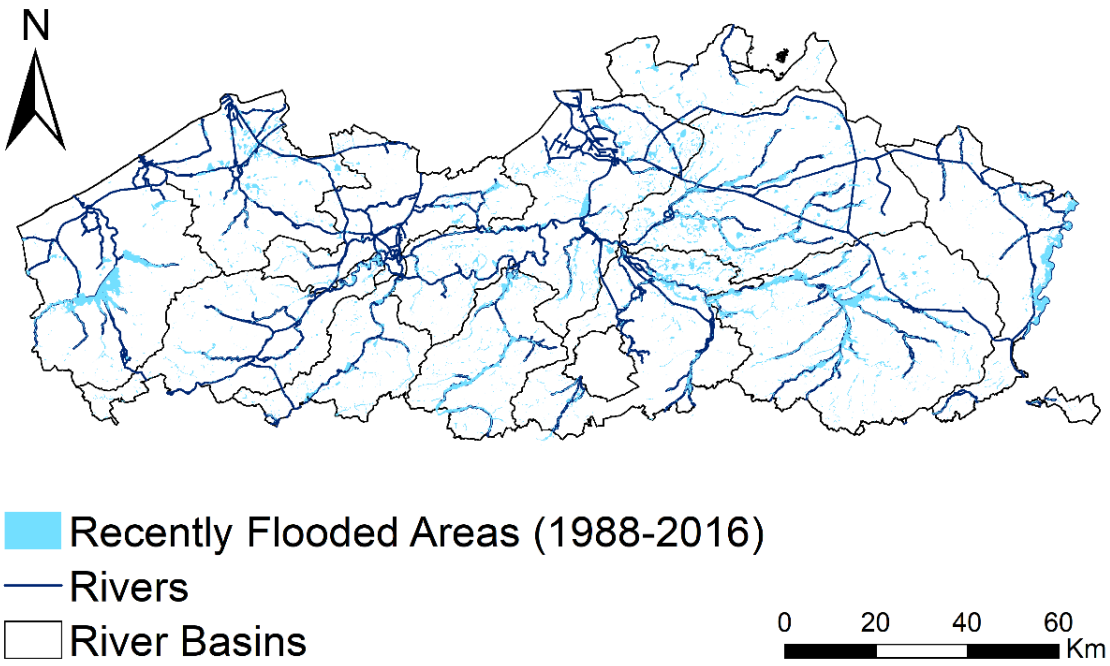

Figure 1.4. Recently flooded areas in Flanders in the period 1988-2016, visualized together with the eleven major river basins and the main rivers, i.e. the navigable and category 1 watercourses (Agentschap Informatie Vlaanderen & Vlaamse Milieumaatschappij, 2017, 2020; Vlaamse Milieumaatschappij & Agentschap Informatie Vlaanderen, 2020).

Table 1.1. Key figures on the number of insurance claims, the corresponding total insured losses (million €) and the average loss per claim (€), as reported by Assuralia between 2006 and 2019 (Assuralia, 2020).

Year	Nr. of claims	Insured loss (million €)	Average loss per claim (€)
2019	/	/	/
2018	5156	31.5	6109
2017	/	/	/
2016	26988	143.8	5328
2015	/	/	/
2014	9399	49.7	5293
2013	6455	16.9	2632
2012	7995	28.3	3534
2011	22114	86.1	3894
2010	9279	75.5	8135
2009	5300	25.3	4774
2008	16000	63	3938
2007	/	/	/
2006	/	/	/

Though official information on the reported flood damage specifically for Flanders is scarce, flood risk in the region has been assessed by means of a probabilistic risk analysis using the LATIS tool, a GIS-based flood risk assessment tool developed by Flanders Hydraulics Research and Ghent University (Beullens et al., 2017; Kellens et al., 2013). First, flood hazard, represented by flood extent (Figure 1.5), water depth and flow velocity in the floodplains, was modeled for coastal, fluvial and pluvial floods. Three different return periods were used in the probabilistic risk analysis: (i) a high probability scenario with a return period of 10 years, (ii) a medium probability scenario with a return period of 100 years, and (iii) a low probability scenario with a return period of 1000 years (Brouwers et al., 2015; VMM, 2015a). For each flood type, flood hazard maps were developed for each return period, with the exception of coastal floods, which do not occur with a high probability and were thus assessed for the medium and low probability scenario (VMM, 2018a). For each of the probability scenarios, representative hydrographs were derived from discharge-duration-frequency (QDF-) relationships, as determined in an extreme value analysis of long-term time series of rainfall-runoff discharges. These composite hydrographs were then combined with hydrological and hydrodynamic models, and with a Digital Elevation Model (DEM), to derive the corresponding flood extent, water depth and flow velocity for each return period (Deckers et al., 2009; Willems et al., 2002). The resulting flood extent, aggregated for the different flood types, is depicted in Figure 1.5. Respectively 7.5%, 4.21% and 2.35% of Flanders is affected by floods with a low, medium and high probability of occurrence. Noticeably large areas in the west of Flanders are affected in the medium and high probability scenarios, which is due to the impact of coastal floods. Flooded areas with a high probability of occurrence constitute for the most part grassland and natural areas, for 13% arable land and for 3% residential and industrial areas. As the probability of floods decreases, the proportion of residential and industrial areas affected by floods increases (Brouwers et al., 2015).

The latest version of LATIS, LATIS 4.0 (Beullens et al., 2017), determines the flood consequences corresponding to these probability scenarios. These consequences include possible casualties and the social, cultural, ecological and economic impacts. An estimate of the number of casualties is determined by LATIS through a function of flood depth and flow velocity. The social, cultural and

ecological risks are estimated based on impact scores. The social impacts provide a more general analysis of the people affected by floods, also taking into account their social vulnerability. Cultural impact of flooding is assessed based on a categorical valuation of the cultural heritage at risk, including its level of legal protection. The ecological impact of flooding on ecosystems is expressed a function of the ecosystems' ecological value and their vulnerability to flooding (VMM, 2018a). The economic valuation of flood damages, expressed as the monetary costs (€) resulting from the probability scenarios, are assessed by combining depth-damage curves with maximum damage values, which are derived from socio-economic and land use datasets. The maximum damage values are adjusted according to the 2015 ABEX-index, reflecting the evolution of the national average construction cost of buildings (Beullens et al., 2017). These economic flood damages correspond to respectively € 100 million, € 660 million and € 2.4 billion for floods with a high, medium and low probability (Brouwers et al., 2015). An overview of these different impacts according to flood type, as provided by the Flemish Environment Agency, indicates that most municipalities in Flanders suffer damages related to both fluvial and pluvial floods, though the impact related to pluvial floods is generally higher than the impact of fluvial floods (VMM, 2018a).

LATIS then combines the damage datasets for each probability scenario into flood risk maps, with the economic flood risk map for Flanders, aggregated for coastal, fluvial and pluvial floods, depicted in Figure 1.5 (VMM, 2015b). Based on this flood risk map, floods in Flanders cause overall a yearly, average economic damage of over € 50 million euros (Brouwers et al., 2015).

As a result of climate change, a shift in precipitation patterns has been observed in Flanders, with yearly precipitation significantly increasing since 1833 due to more precipitation in winter, and with periods of heavy precipitation becoming more frequent (Brouwers et al., 2015). The impact of climate change and soil sealing on river discharge and flood risk in Flanders was empirically assessed by the Flanders Environment Agency in a trend analysis of yearly surface runoff, baseflow and peak discharges at 48 gauging stations between 1990 and the summer of 2018. Since 1996, the return periods of peak discharges decreased, leading to an increasing likelihood of larger flood events. The trend line of surface runoff shows a small increase towards 2018, whereas a decreasing trend in baseflow was observed, which could be indicative of the impact of soil sealing, though these trends were not statistically significant. Overall, the time series under consideration were too short to distinguish the impacts of short-term climate variations from long-term climate change (VMM, 2020). Climate change scenarios also predict an increase in precipitation in winter and higher rainfall intensities in summer, leading to an increasing risk of riverine and urban floods. Future flood risk was modeled for the high-emissions scenario RCP8.5, leading to a temperature increase between 3.2°C and 5.4°C. Based on this scenario, flood probabilities will increase five- to tenfold by 2100, i.e. a flood with a current return period of 100 year is projected to occur once every 10 years in 2100. Consequently, double the amount of buildings and vulnerable infrastructure, such as health care facilities, child care centers and schools, will be at risk of severe flooding under the RCP8.5 scenario. Currently, 2.6% of main buildings are at risk of flood depths over 70 cm, which is set to increase under RCP8.5 to 6.9% by 2100, while the number of infrastructures related to vulnerable institutions at risk doubles from 7.3% to 15.7% (VMM, 2018b). Furthermore, ongoing urbanization could lead to an additional average increase of 3 to 10%, depending on the land use change scenario. Moreover, this increase could be as high as 100% in specific regions in Flanders, e.g. the Yser basin, due to urbanization in flood-prone areas (Brouwers et al., 2015). Poelmans et al. (2011) used a rainfall-runoff model to assess the impact of climate change and urban expansion on peak discharges in the Molenbeek catchment, situated in the greater Dijle catchment: climate change scenarios led to a broad range of impacts, and thus uncertainty, whereas urban expansion consistently increased peak discharges, i.e. 70-200% expansion in built-up areas increased peak discharges with 6-16%. Using a

lumped hydrological model, De Niel et al. (2020) found a comparable effect of urban development, with a 10% increase in built-up areas resulting in a 3% increase in peak discharges for the Grote Nete catchment.

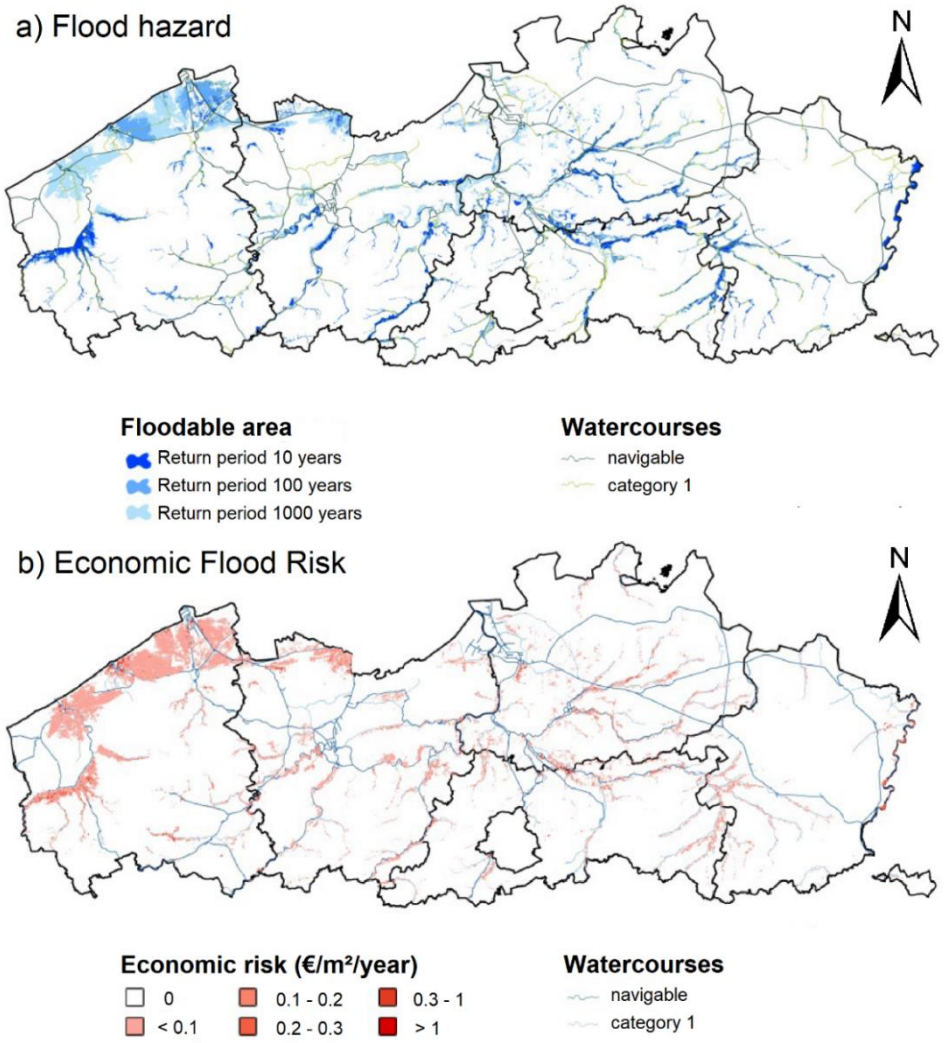

Figure 1.5. a) Flood hazard, represented by flood extent, in Flanders aggregated for coastal, fluvial and pluvial floods and visualized for three probability scenarios: a high probability flood event with a return period of 10 years, a medium probability with a return period of 100 years and a low probability with a return period of 1000 years (adapted from (VMM, 2015a)), b) Economic flood risk (€/m²/year), combining the economic damages of the three probability scenarios for coastal, fluvial and pluvial floods (adapted from (VMM, 2015b)). (source: Vlaamse Milieumaatschappij, Waterbouwkundig Laboratorium, Maritieme Dienstverlening & Kust, & De Vlaamse Waterweg nv, 2020).

The EU Flood Directive (Directive 2007/60/EC) and Water Framework Directive (Directive 2000/60/EC) have been implemented in Flanders' legislation through the Decree on Integrated Water Policy. In the context of this decree, river basin management plans, integrating the flood risk management plans, are established for the eleven subbasins in Flanders, visualized in Figure 1.4. These plans stipulate how, over a period of five years, water quality and groundwater quantity must be improved and how flood risk must be managed (Coördinatiecommissie Integraal Waterbeleid, 2018). In addition, the overarching Sigma-plan, initiated in 1977, aims to protect against floods and coastal storm surges of the main Scheldt river and its tributaries by constructing and reinforcing embankments, and by

creating natural flood control areas. This plan was updated in 2005 to include insights from flood risk management, including flood plain and wetland restoration, thereby also contributing to the nature conservation goals set within the framework of Natura 2000 (De Vlaamse Waterweg nv & Natuur en Bos, 2020). In general, flood risk management in Flanders is organized based on three levels: prevention, preparedness and protection. One of the most important policy instruments provided in the Integrated Water Policy Decree to prevent and reduce flood damage, is the so-called 'water check'. The water check precedes any planning permission for building or spatial planning projects and assesses the hydrological impact of these projects. If harmful consequences are to be expected, e.g. by building in flood risk areas, the permit may be denied or subjected to additional conditions, e.g. through structural adjustments reducing flood damage to buildings (Coördinatiecommissie Integraal Waterbeleid, 2015). To proactively prepare for floods, e.g. by alerting emergency services and the general public, an early-warning system was developed, combining hydrodynamic models with real-time measurements of precipitation, water level and river discharge, collected through an extensive network of gauging stations. This early-warning system can be consulted on www.waterinfo.be (Vlaamse Milieumaatschappij et al., 2020). Protection against floods in Flanders focuses in the first place on small-scale measures increasing the water retention capacity of the soil and landscape through establishing, for instance, Green and Blue Infrastructures (GI and BI) (VMM, 2019). GI and BI form networks of (semi-)natural areas delivering multiple ecosystem services, including flood regulation. These networks are also an integral concept of the regional strategic planning vision in Flanders, with the larger aim to increase the resilience and robustness of the landscape under future climatic and demographic changes. Green and blue networks increase the water retention and infiltration in the landscape, buffering against both flooding and droughts. To promote GI and BI, opportunities for afforestation in the vicinity of urban areas are explored, pilot projects supporting the unsealing of soils, i.e. the removal of concrete surfaces and buildings, are initiated and green roofs are subsidized (Departement Ruimte Vlaanderen, 2017; VMM, 2019). In addition to these measures, the increase of the water retaining and infiltrating capacity of the landscape by restoring wetlands natural flood plains in river valleys is high on the policy agenda. Recently, the regional government in Flanders presented the Blue Deal, a policy plan to combat drought after four consecutive years of rainfall deficits. This plan proposes an integrated approach to water resources management by increasing water retention and infiltration, and consequently allowing excess rainfall to recharge depleted groundwater supplies instead of accumulating downstream as rapid surface runoff (Vlaamse Regering, 2020). As a final level of protection, technical flood defense measures, such as dikes and retention basins, keep their importance for areas at risk of extreme flooding (Coördinatiecommissie Integraal Waterbeleid, 2015).

1.3. Research objectives, research questions and thesis outline

The main objective of this PhD research was to provide scientific support for the implementation of sustainable, nature-based flood risk management. This overall objective was materialized in three research questions:

1. *Do upstream land use changes, particularly soil sealing, affect downstream fluvial flood severity?* The generally accepted hypothesis that soil sealing exacerbates flood risk is evaluated for Flanders with a focus on fluvial flood risk.
2. *How can upstream locations be determined where land use change has the maximal resp. minimal impact on downstream fluvial flood hazard and severity?* Given the spatial interactions related to flood regulation and the computational burden associated with optimization analyses, this research question requires the integration of a computationally efficient and spatially explicit Rainfall-Runoff (RR)-model in an iterative prioritization framework.
3. *How can the mitigation or exacerbation of downstream fluvial flood hazard and severity exerted by upstream land use changes be characterized in terms of the monetary insurance value of the upstream land use system?* This assessment requires the determination and comparison of flood risk before land use changes, i.e. the reference flood risk, and after implementing upstream land use changes.

This PhD research as such focuses on larger-scale land use changes as nature-based solutions. The smaller-scale measures, e.g. the implementation of retention ponds or natural dams, were not taken into account. The relationship between upstream land use and downstream flood hazard is assessed with a view to provide an answer to the second and third research questions. Consequently, the impact of the land use changes on fluvial flood hazard and risk was investigated through the development of frameworks for spatial prioritization and flood risk assessment. These frameworks can inform decision-making and spatial planning of the most suitable locations in catchments for land use changes mitigating flood hazards and risks downstream, and provide the flood insurance value associated with these land use changes. The frameworks are developed and tested in the flood-prone and highly urbanized region of Flanders, however, their generic character allows implementation beyond Flanders, wherever similar input data are available.

First, approaches are needed to assess and quantify the impact of land use changes on flood severity. Hereby the focus is on the substantiation of the negative impact of soil sealing on flood hazards and risk, not only with hydrological modeling approaches (De Niel et al., 2020; Poelmans et al., 2011), but also with data-driven analyses (VMM, 2020). For Flanders, the latter was believed to be possible thanks to the availability of the spatial flood archive and associated datasets.

In line with the main objective, the overall problem statement and the research questions, the following specific research objectives were established:

1. To verify and assess in a data-driven analysis the hypothesis that increasing upstream soil sealing exacerbates the severity of downstream flood events;
2. To develop a modeling approach and tool for the relationship between land use, rainfall and soil saturation inputs and surface runoff that is spatially explicit and computationally efficient, in order to achieve the third specific objective;
3. To integrate the model developed in the second research objective in an iterative optimization framework capable of identifying the locations in watersheds where land use changes

associated with increased water retention, most effectively mitigate river flood hazard at a downstream point of interest;

4. To design and evaluate a methodology to quantitatively assess the flood risk impact of upstream land use changes, illustrated with land use changes at locations determined by the optimization framework of the third research objective.

Each of these research objectives correspond to a chapter of this thesis manuscript, schematically outlined in Figure 1.7. The analyses were performed and exemplified for different study areas, situated in three river basins in Flanders, as depicted in Figure 1.7. Three small- to medium-sized catchments were selected, since land use has been observed to influence the hydrological characteristics at this scale (Blöschl et al., 2007; Chang et al., 2009; Wheater & Evans, 2009). Additionally, catchments were selected where multiple flood extents, relating to several different flood events, were recorded in the geospatial flood archive. To limit the impact of urban drainage systems and complex river network structures, the catchments were selected to pertain to unnavigable river courses in mostly rural areas. The three study areas, selected based on these criteria, were the Maarkebeek, Bellebeek and Demer catchments, situated resp. in the primary river basins of the Upper Scheldt, Dender and Demer. The general land use in these catchments, based on the land use dataset from 2012, is depicted in Figure 1.8 (Agentschap Informatie Vlaanderen, 2016b). Figure 1.9 visualized the general soil types occurring in these catchments (Databank Ondergrond Vlaanderen, 2017). The relevant characteristics of these catchments are further introduced in the different chapters. In Chapter 2, the widely hypothesized, but poorly empirically supported relation between upstream soil sealing and downstream flood severity was analyzed in a data-driven approach for the Maarkebeek, Bellebeek and Demer catchments. In Chapter 3, a new, spatially distributed and computationally efficient rainfall-runoff model is developed and applied to the catchments of the Maarkebeek and the Bellebeek, and the latter's subcatchment of the Hunselbeek. In Chapter 4, this rainfall-runoff model is integrated in a novel iterative optimization framework to address the question of where to implement land use changes. This framework is illustrated for the catchments of the Maarkebeek and the Bellebeek, while the objective of the optimization is to minimize flood hazard downstream. In Chapter 5, an approach for the quantitative, economic assessment of the impacts on flood risk of the land use changes as determined in Chapter 4 was developed and illustrated for the Maarkebeek catchment. The general optimization and flood risk assessment frameworks, presented in resp. Chapter 4 and 5, are illustrated for medium-sized catchments in Flanders, however, these frameworks could be applied on other medium-sized catchment, either in Flanders or beyond its borders, provided the required input data is available.

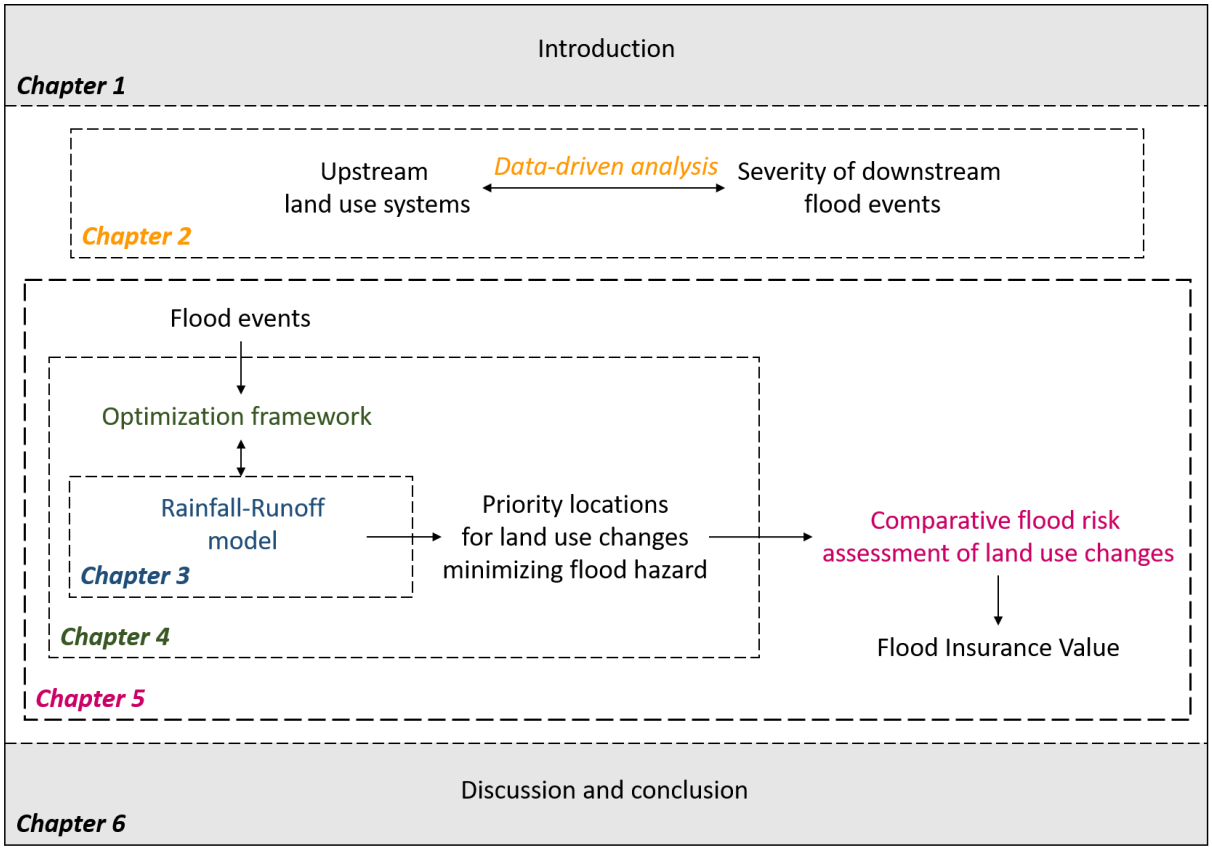

Figure 1.6. Schematic outline of the PhD thesis.

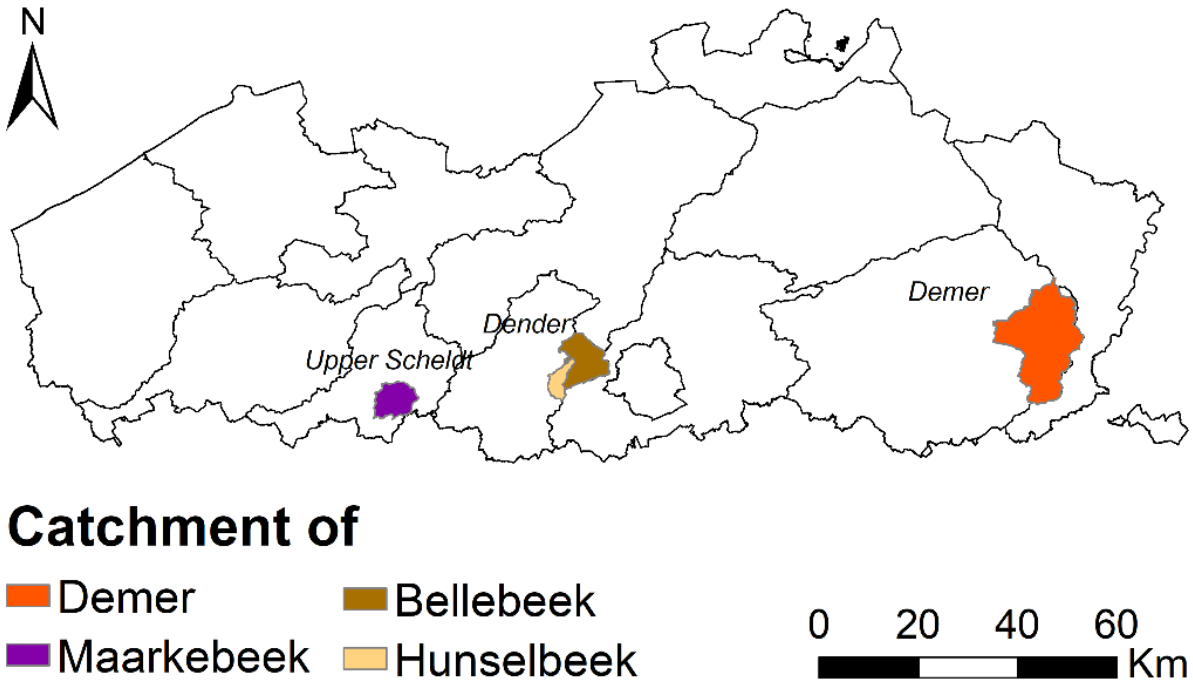

Figure 1.7. Location of the study catchments in Flanders, Belgium. The Demer subcatchment is located in the primary river basin of the Demer, the Maarkebeek catchment is situated in the Upper Scheldt basin, and the Bellebeek catchment and its subcatchment of the Hunselbeek are situated in the Dender basin (Agentschap Informatie Vlaanderen & Vlaamse Milieumaatschappij, 2020).

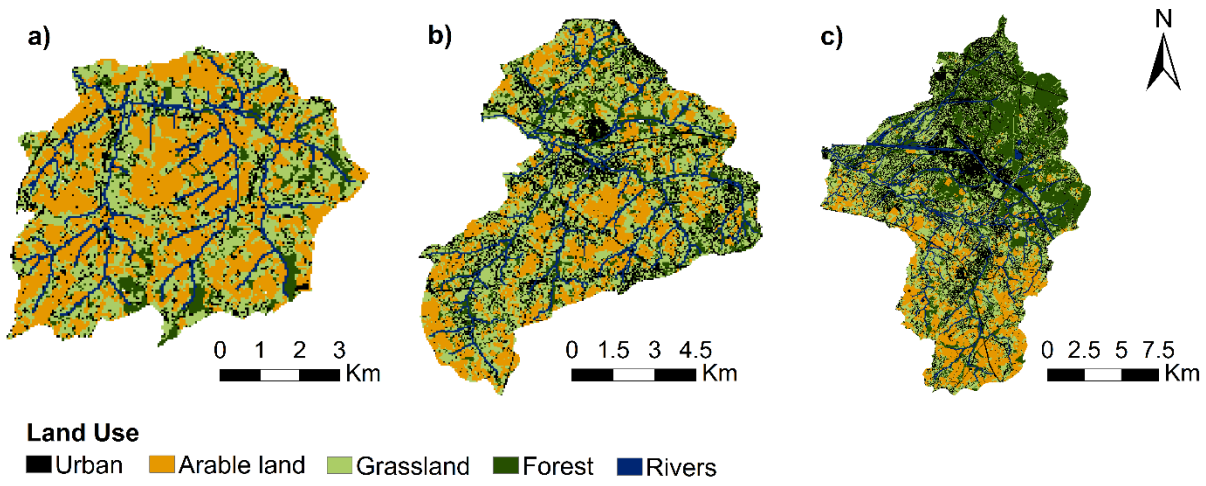

Figure 1.8. General land use, based on the land use dataset of 2012, in the three study catchments: (a) the Maarkebeek, (b) Bellebeek and (c) Demer catchments (Agentschap Informatie Vlaanderen, 2016b).

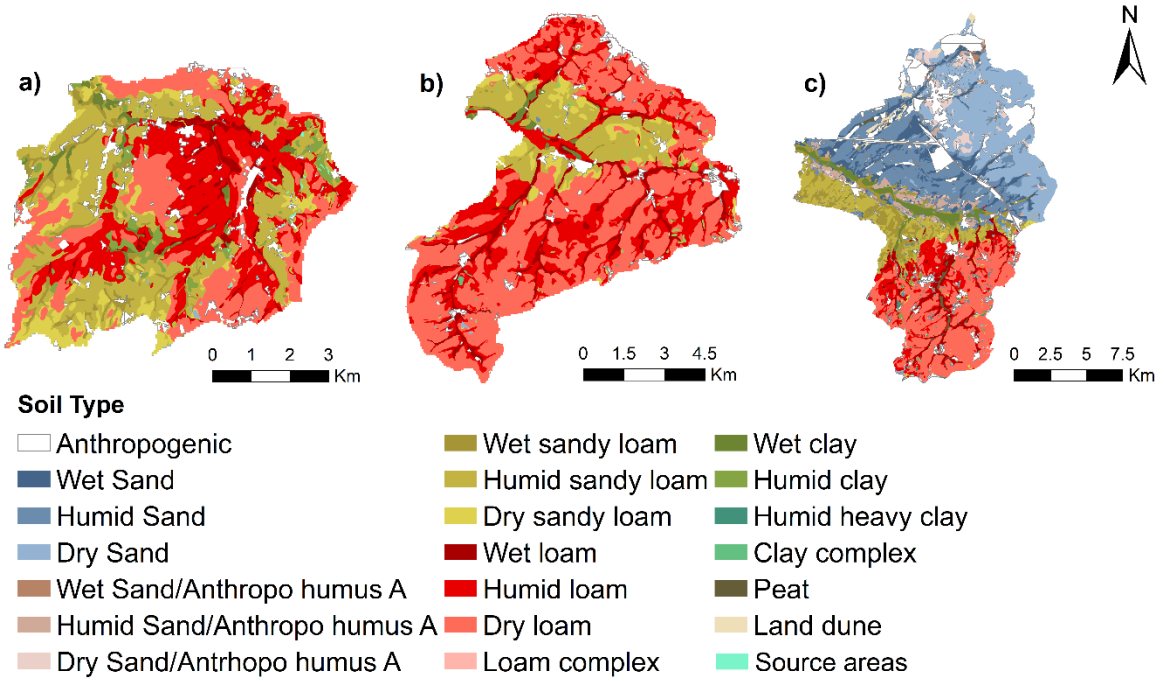

Figure 1.9. General soil type of the three study catchments: the (a) Maarkebeek, (b) Bellebeek and (c) Demer catchments (Databank Ondergrond Vlaanderen, 2017).

Chapter 2
A data-driven analysis of the spatial flood archive to assess the impact of soil sealing on flood severity

Results from this chapter have been published in:
Gabriels, K., Willems, P., & Van Orshoven, J. (2020). A data-driven analysis, and its limitations, of the spatial flood archive of Flanders, Belgium to assess the impact of soil sealing on flood volume and extent. *PLoS ONE*, *15*, 1–17. https://doi.org/10.1371/journal.pone.0239583

2.1. Introduction

Land use changes impact the hydrology of a watershed. Especially soil sealing caused by urbanization can affect the hydrological processes of a watershed by decreasing infiltration and water storage in the soil, thus increasing rapid infiltration-excess overland flow and decreasing slow subsurface flow. Consequently, urbanization poses a significant challenge for sustainable land management, especially regarding the process of soil sealing, defined here following the definition of the European Commission as the covering of soils by completely or partly impermeable artificial material (Jones et al., 2012). Soil sealing leads to faster runoff accumulation downstream, which affects the occurrence and severity of flood events (Bronstert et al., 2002; Lin et al., 2007; Miller & Hess, 2017). With urbanization increasing worldwide (United Nations, 2019) and climatic conditions becoming more erratic (IPCC, 2014), assessments of the hydrological impacts of land use changes are required in order to support future policy making regarding sustainable water resources management (Chu et al., 2017; Liu & Shi, 2017).

The impact of land-use dynamics on flow regimes is often assessed using (semi-)distributed hydrological models incorporating land use information (Braud et al., 2013; Kalantari et al., 2014; Lin et al., 2007; Miller & Hess, 2017; Sajikumar & Remya, 2015). Based on these flow regimes, hydrodynamic models can then be employed to simulate flood extents (Huang et al., 2017; Pappenberger et al., 2005; Yu & Lane, 2006). However, flood inundation modeling, and the attribution of changes in flood regimes based on such models, has limitations due to uncertainties in model structure, model parameters and model inputs (Bales & Wagner, 2009; Z. Liu & Merwade, 2018). Uncertainty in model structure arises from the type of hydraulic model, for instance one-dimensional or two-dimensional, and its underlying assumptions, e.g. regarding the river channel shape (Pappenberger et al., 2006; Teng et al., 2017). Issues related to parameter calibration, including overcalibration (Andréassian et al., 2012), and uncertainty regarding the input flow data from hydrological models (Merwade et al., 2008; Pappenberger et al., 2005) also add to the uncertainty of the modeled flood extents and inundation depths.

By continuously monitoring observed flooded areas, time series of ever-increasing length are obtained. With the availability of these longer time series, the opportunity arises to assess the relationship between soil sealing and flood volumes and extents in a data-driven approach, taking into account the meteorological conditions and landscape configuration. These data-driven approaches relate the input variables directly to the observed outputs, and thus do not explicitly consider the underlying physical process. Given the complexity and nonlinearity of the hydrological processes

involved, such as infiltration and evapotranspiration, the nonparametric and nonlinear data-driven methods are assumed suitable to assess the characteristics of flood phenomenon (V. K. Gupta et al., 2010; Merz et al., 2013).

Such empirical, data-driven analysis is tested in three study catchments, situated in three river basins in Flanders. As stipulated in Section 1.2, Flanders is both highly urbanized and prone to flooding, making it an interesting study case to assess the impact of sealing soil surfaces with artificial impermeable materials on flood events using the contours of the flooded areas, as recorded in a spatially explicit archive. Data from this archive, along with rainfall and land use data, were collected for three subbasins and analyzed using three statistical approaches, namely linear regression models and two Machine Learning (ML) methods: Support Vector Regression (SVR) and Boosted Regression Trees (BRT). A sensitivity analysis was performed to assess which factors impact the models most by alternately introducing variation into each of the factors.

2.2. Material and Methods

2.2.1. Geospatial Data

Study Areas

The data-driven analyses were carried out on three subbasins from different primary river basins in Flanders, Belgium (Figure 2.1). The boundaries of these subbasins were determined based on the hydrographical zones map of Flanders (Agentschap Informatie Vlaanderen & Vlaamse Milieumaatschappij, 2020). The first study area, the Maarkebeek subbasin, is situated in the Upper Scheldt river basin and has an area of approximately 52 km². The subbasin of the Bellebeek river (87 km²) is located in the Dender basin. Finally, a subbasin of the Demer river of 243 km² was selected as a third study area.

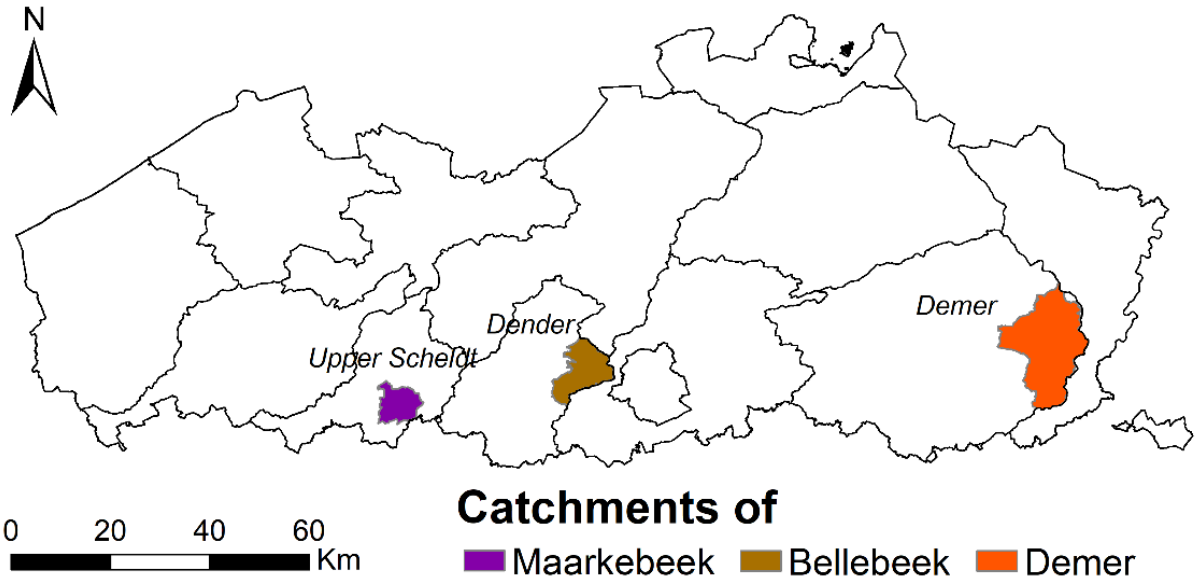

Figure 2.1. Location of the three studied subbasins in Flanders, Belgium: subbasins of the Maarkebeek (52 km²), Bellebeek (87 km²) and Demer (243 km²) (Agentschap Informatie Vlaanderen & Vlaamse Milieumaatschappij, 2020).

Meteorological Data

Hourly precipitation data from the closest weather station of the Royal Meteorological Institute and the Flemish Environment Agency, retrieved from www.waterinfo.be, were used to derive information

on accumulated precipitation prior to the flood events and the intensity of the flood-inducing rainfall. The rainfall datasets available for the Bellebeek was mostly complete, whereas for the Maarkebeek and Demer subbasins no hourly rainfall information was available in resp. 2002 and 2003. Four derived variables were tested in the statistical analyses: the precipitation accumulation over the 14 days and 30 days prior to the flood event and the hourly and 6-hourly peak precipitation intensity 24 hours before the flood. An overview of this data for each recorded flood event in the subbasins is provided in Table 2.2.

Geospatial Flood Archive

The flood data were derived from the geospatial archive of flooded areas in Flanders (Agentschap Informatie Vlaanderen & Vlaamse Milieumaatschappij, 2017). This archive is published and maintained as a geodataset by the Flemish Environment Agency. Its latest update contains the contours of significant flooded areas in Flanders between 1988 and 2016 (Figure 2.2). The flooded area associated with a flood event thus consists of one or more separate contours, which are further referred to as flood extents. The flood extents of each event are recorded in the spatial archive as polygon features. The dataset is compiled from a variety of sources. Prior to 2000, when the archive was first assembled, the flood extents in each event were digitized from analogue maps. Later, mainly information provided by municipalities and aerial orthophotographs were used to update the archive. An updated version is released approximately every four years.

In the Maarkebeek subbasin, flood events were recorded in seven years, namely 1993, 1995, 1998, 1999, 2002, 2003 and 2010. In 2002, two flood events occurred, resulting in one recorded flood extent in respectively February and August. As no hourly rainfall information was available for 2002 in the Maarkebeek, these flood events were not considered in the following analyses. In the Bellebeek subbasin, floods occurred in seven years (1988, 1993, 1999, 2002, 2003, 2010 and 2016), while in the Demer subbasin, nine flood events were taken into account: one event in 1988, 1998, 2004 and 2007, three in 2010 and two in 2016. These flood events were recorded in the spatial flood archive in respectively 48, 117 and 184 flood extents in the Maarkebeek, Bellebeek and Demer subbasins. Table 2.2 provides the number of flood extents associated with each flood event. The outlines of these flood extents were combined with a Digital Elevation Model (DEM) with a resolution of 5 m to derive the volume of water present in each extent (Agentschap Informatie Vlaanderen et al., 2006). This was done by fitting a linear, least-squares trend surface through the x, y and z-vertices of the flood extent boundary using a first-order polynomial regression (ESRI, 2016), assuming the elevation of the water level equals the surface elevation in the extents' borders. Subsequently, the DEM is subtracted from the water elevation trend to obtain water depth. If the elevation was higher than the trend surface, water depth was set to zero. Finally, the water depth is multiplied with the area of the extent to obtain the flood volume. The flood volume (m^3) and extent (m^2) were assessed in the statistical analyses as dependent variables.

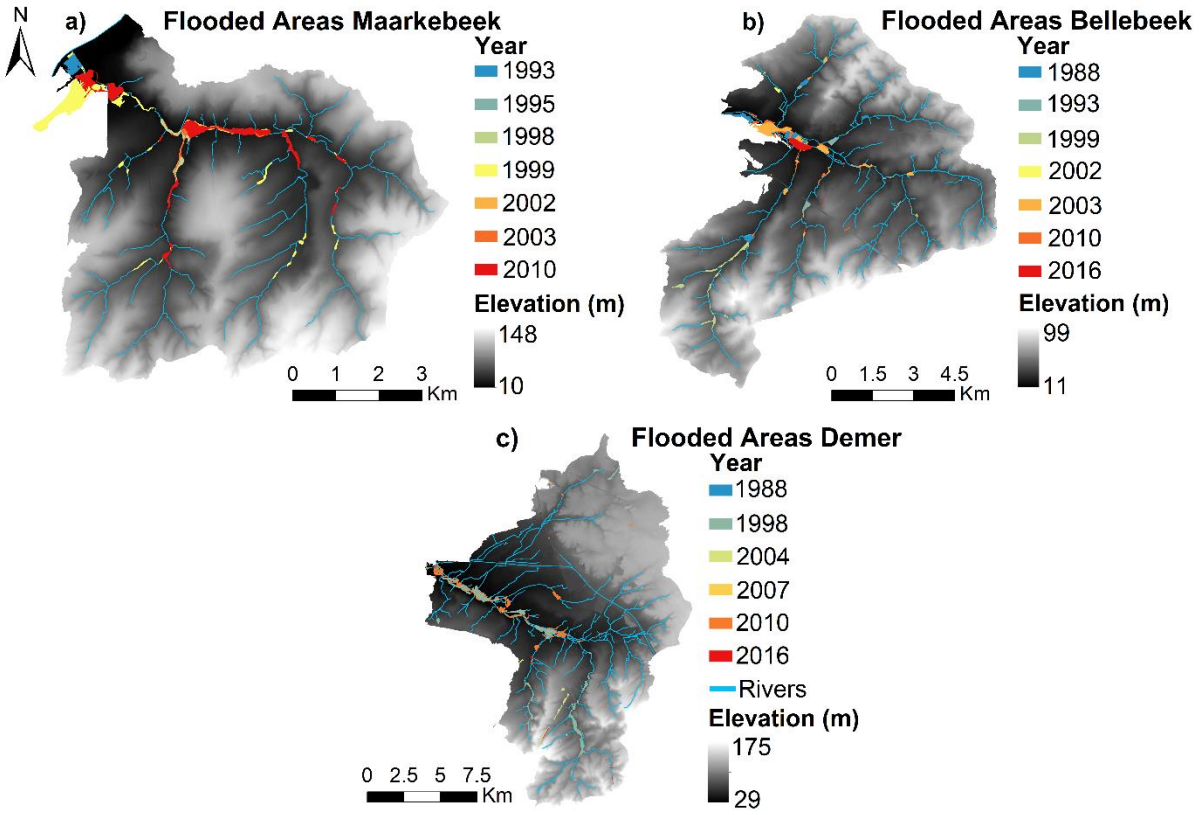

Figure 2.2. The spatial occurrence of flood events considered in the data-driven analyses between 1988 and 2016: (a) six flood events in the Maarkebeek subbasin, (b) seven flood events in the Bellebeek subbasin and (c) flood events in the Demer subbasin in nine years (Agentschap Informatie Vlaanderen et al., 2006; Agentschap Informatie Vlaanderen & Vlaamse Milieumaatschappij, 2017).

Land Use Data

The land use data were derived from three land use/land cover (LULC) maps valid for 1995, 2001 and 2012, covering the area of Flanders. The 1995 land use map was derived from multispectral LANDSAT imagery using a maximum likelihood classification and describes the land use in Flanders in 27 classes, of which 21 occur in the study areas, with a resolution of 20 m (Gulinck et al., 1996; Honnay et al., 2003). The land use map of 2001 was derived from LANDSAT images using semi-automatic classification. It has a resolution of 15 m and distinguishes nine classes, with eight occurring in the subbasin, with a mean squared positional error of 18 m (Agentschap Informatie Vlaanderen, 2002). The most recent land use map available is from 2012, which was constructed based on multispectral orthophotos and administrative parcel information using segment-based classification. It has a resolution of 5 m with 14 classes, all of which occur in the study areas, and a kappa-coefficient of 89.6%, which was derived by comparison with a sample of 1252 points using an orthophoto of 2012 as reference data (Agentschap Informatie Vlaanderen, 2016a).

In order to geometrically and thematically align these land use maps, they were first resampled using the nearest neighbor algorithm to stack them at the resolution of 20 m. A land use change trajectory analysis was then applied to identify and correct improbable or impossible land use changes (Carmona & Nahuelhual, 2012; Powell et al., 2008; Verbeiren et al., 2012; Wang et al., 2012). This analysis consisted in: (i) listing all LULC change combinations per pixel, (ii) expert-based evaluation of the likeliness of each combination and (iii) adjusting improbable changes when possible, e.g. changes from urban into another land use were reversed. This was done for every study area, after which the LULC maps were reclassified into the five classes of urban, arable land, forest, other green and water (Table

2.1), with the urban land use class used as a proxy for soil sealing. The percentages of adjusted urban area for the three land use maps are visualized in Figure 2.3, together with the volume of water in the flooded areas divided by the accumulated precipitation to obtain the flood volume per mm of rainfall. The Maarkebeek subbasin is the least urbanized, followed by the subbasins of the Bellebeek and the Demer. Urbanization takes place in all three study areas between 1995 and 2012, accelerating in the subbasins of the Maarkebeek and Bellebeek after 2001, and decelerating after 2001 in the Demer subbasin.

Table 2.1. Land use distribution (%) in the Maarkebeek, Bellebeek and Demer subbasins according to the reclassified and resampled (20 m resolution) land use datasets of 1995, 2001 and 2012, corrected using a land use change trajectory analysis (Agentschap Informatie Vlaanderen, 2002, 2016b; Gulinck et al., 1996).

	Maarkebeek			**Bellebeek**			**Demer**		
Land use class	**1995**	**2001**	**2012**	**1995**	**2001**	**2012**	**1995**	**2001**	**2012**
Urban	4	6	10	10	13	20	16	20	26
Arable land	57	68	42	40	58	26	31	31	16
Forest	6	5	11	10	7	15	27	27	28
Other green	32	21	36	40	22	40	24	20	29
Water	< 1	< 1	< 1	< 1	< 0.1	< 0.1	2	2	2

The Multiple Linear Regression uses the urban fraction of the subbasins as predictor variable to model respectively flood volume and area. In order to estimate this urban fraction for years when floods occurred but no land use data were available, a linear regression was performed for each of the study areas, visualized in Figure 2.3 together with the flood volume per mm rainfall. These regressed urban fractions, provided in Table 2.2, were used as independent variable for all flood events in the Multiple Linear Regression analysis. The machine learning methods, on the other hand, incorporate the urban fraction upstream from the flood extents as predictor. For flood events occurring before 1999, these upstream fractions were derived from the adjusted 1995 LULC data, for flood events occurring between 1999 and 2005, the land use dataset of 2001 was used, and for flood events after 2005, the land use dataset of 2012 was used to derive the urban fractions.

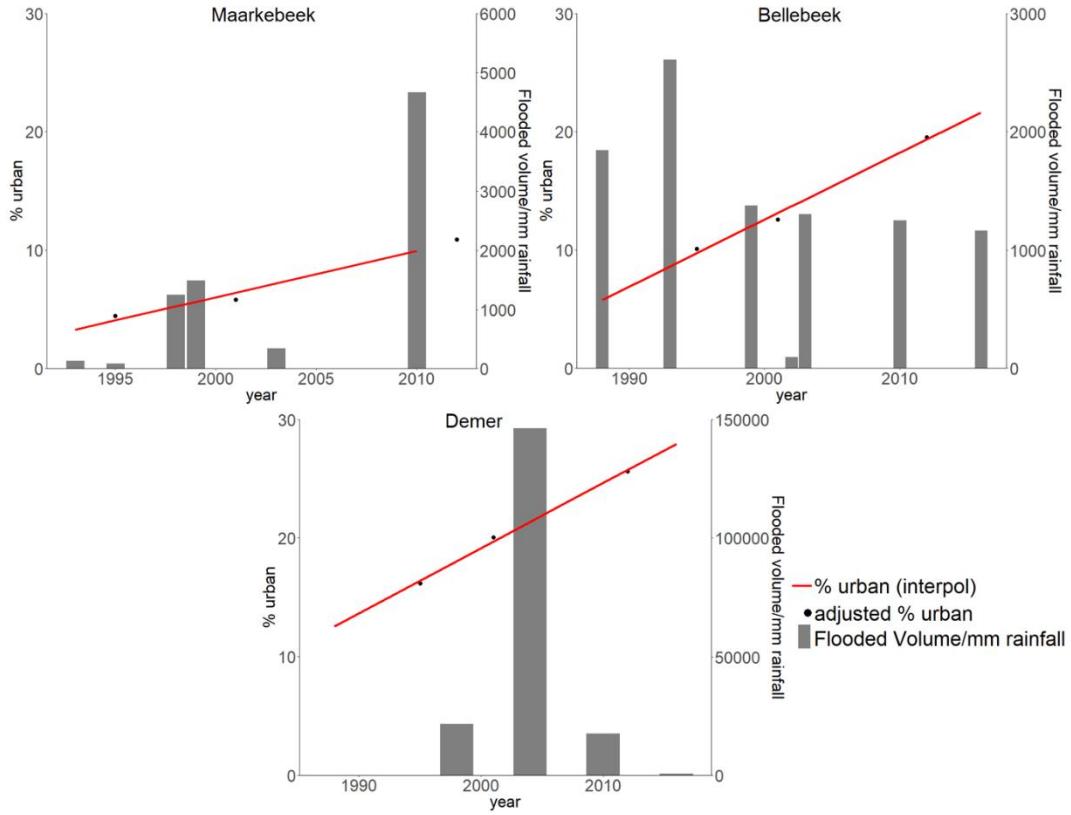

Figure 2.3. Percentage of urban area and flooded volume/mm rainfall. Corrected and interpolated percentages of urban areas and the flooded volumes (m^3) divided by the accumulated precipitation 14 days prior to the flood events (mm) to provide the flooded volume per mm rainfall.

Table 2.2. Overview of flood events in the study areas, their meteorological characteristics and corresponding interpolated urban fractions (# = number of flood extents associated with the flood event, Vol = volume of water in flooded area, PP = peak precipitation prior to the flood event, PS = accumulated precipitation prior to the flood event).

Subbasin	Date	#	Vol (m^3)	Area (ha)	PP (mm/hr)	PP (mm/6hr)	PS (mm/14d)	PS (mm/30d)	Urban (%)
Maarkebeek	30/12/1993	1	17 378	11.6	4.6	1.4	100	179	3.3
	25/01/1995	1	5126	5.5	3.3	1.9	62	169	4.1
	09/09/1998	1	45 485	14	9.3	1.6	45	103	5.2
	25/12/1999	30	366 155	106.3	4.3	2	102	114	5.6
	01/01/2003	3	15 088	6.1	3.2	1.5	53	113	7.2
	13/11/2010	12	347 663	84.2	8.3	3.4	67	117	9.9
Bellebeek	12/03/1988	15	86 874	33.4	3.1	1	47	62	5.8
	19/12/1993	15	191 590	19.3	2.4	1.6	74	84	8.6
	24/12/1999	11	106 184	28.2	9.1	4	77	105	12
	05/08/2002	2	7965	2.6	7.0	1.2	83	100	13.7
	01/01/2003	18	125 316	76.7	4.5	1.7	96	119	14.3
	12/11/2010	47	60 182	32.8	8.2	3.3	48	101	18.2
	01/07/2016	9	62 231	22.3	2.9	0.85	53	105	21.6
Demer	12/03/1988	4	3 246	1.1	2.7	1.4	60	73	12.5
	13/09/1998	41	1 424 014	344.5	9.1	6.4	66	118	18
	6/08/2004	7	226 598	35.8	0.4	0.1	2	64	21.3
	8/11/2007	2	2257	1.2	4.9	1.5	41	43	23
	14/08/2010	7	81 856	19.6	5.8	2.1	32	53	24.6
	12/11/2010	82	293 123	163	4.1	4.4	46	66	24.6
	13/12/2010	5	173 244	33.6	2.5	0.8	20	34	24.6
	26/05/2016	5	2939	2.4	13.6	4.3	28	83	27.9
	01/06/2016	31	78 476	19.9	4.6	3.4	134	121	27.9

2.2.2. Multiple Linear Regression

Multiple Linear Regression (MLR) models the relationship between a dependent response variable y and *n* independent explanatory variables x_1, $x_2 \ldots x_n$ by fitting a linear equation to the observations, which takes the general form: $y = \beta_0 + \beta_1 * x_1 + \cdots + \beta_n * x_n + \varepsilon$, with ε the error term and β the regression coefficients. This method was selected, since it provides a simple and straightforward way to explore the data allowing a comparison to the more sophisticated machine learning techniques.

MLR assumes a linear relationship between the dependent variable and each of the independent variables based on uncorrelated observations (Grégoire, 2014). Since spatial interactions occur between individual flood extents, the uncorrelated observations were linked directly with the flood events (6 for the Maarkebeek, 7 for the Bellebeek and 9 for the Demer). The dependent variables tested are the total area flooded during an event (m^2) and the corresponding volume of water (m^3). Considering the limited number of observations, the number of independent variables considered in the linear regression analysis is also restricted. The meteorological variables tested are the accumulated precipitation over 14 and 30 days, peak precipitation (hourly and 6-hourly) and the urban fraction (see Table 2.2):

$$Volume = \beta_0 + \beta_1 * Precipitation\ Sum + \beta_2 * Precipitation\ Peak + \beta_3 * Urban\ fraction \quad (2.1)$$

Given the small sample size in each of the study areas, a regional approach was also tested, implementing the MLR models on the pooled observations of the subbasins. In this approach, observations from similar sites are combined to enlarge the sample size aiming at a more representative and higher accuracy of statistical assessments (Mostofi Zadeh & Burn, 2019). The combined sites should form homogeneous groups, which was assessed with the Hosking and Wallis homogeneity test. This homogeneity test is based on L-moments ratios, which describe the shape of probability distributions of ordered data observations. The Hosking and Wallis homogeneity test compares the L-moments ratios variability of the observations with the variation expected in a homogeneous region (Hosking & Wallis, 1993). For this purpose, the weighted variance *V* of the L-coefficient of variation (*L-CV*) is derived:

$$V = \sqrt{\left(\frac{\sum_{i=1}^{N} n_i * (t^{(i)} - \bar{t})^2}{\sum_{i=1}^{N} n_i}\right)} \quad (2.2)$$

with *N* the number of sites, n_i and $t^{(i)}$ the number of observations and L-coefficient of variation at site *i*, and $\bar{t}$ the regional L-coefficient of variation. Sites are assumed homogeneous if *V* is similar to the variance of *L-CV* values derived from Monte Carlo simulations of a four-parameter kappa distribution. This is assessed using the heterogeneity measure *H*:

$$H = \frac{V - \mu_V}{\sigma_V} \quad (2.3)$$

with μ_V and σ_V respectively the mean and standard deviation of the simulated *V* values (Alila, 1999; Kachroo et al., 2000; Mostofi Zadeh & Burn, 2019). Site groups are considered homogeneous if $H<1$, possibly homogeneous if $1<H<2$, and definitely heterogeneous if $H>2$ (Hosking & Wallis, 1993).

Before pooling, the observed flood volume was expressed in mm relative to the subbasins' area and the flooded area was expressed as an area fraction of the subbasins. After pooling these observations of the three study sites, the heterogeneity measure *H* was calculated using 500 Monte Carlo simulations, resulting in *H* values of 0.23 and 0.58 for respectively flood volume (mm) and flooded area fraction. For all independent variables assessed in the linear regression analysis, *H* was smaller

than 1 after standardization, with *H* values for the 14-day and 30-day precipitation sum, hourly and 6-hourly peak precipitation, and urban fraction corresponding to resp. -0.09, 0.50, 0.25, -0.21 and 0.36. The three subbasins can thus be considered a homogeneous group for these flood characteristics. Since pooling the observations increases the sample size to 22 observations, two additional independent variables were included in the pooled MLR models. The total rainfall amount (mm) of the flood-inducing rainfall (*H* = 0.54) was included as an additional flood characteristic. The drainage density (m^{-1}) of the subbasins was added as a catchment characteristic, calculated by dividing the stream length by the catchment area.

2.2.3. Machine Learning

Machine learning aims to develop data-driven methods which improve with increasing experience or learning (Jordan & Mitchell, 2015). These data-driven learning methods provide a range of advantages, including a greater flexibility in data assumptions and less reliance on expert knowledge, which makes them also applicable in flood risk and susceptibility assessments (Gizaw & Gan, 2016; S. S. Lee et al., 2017; Y. Lee & Brody, 2018; Mojaddadi et al., 2017; Tehrany et al., 2014). A range of different methods have been developed, of which two were applied to our data: Support Vector Regression (SVR) and Boosted Regression Trees (BRT). The accuracy of each model was assessed with the Root Mean Square Error (RMSE), with *n* the number of flood extents, and Y_{obs} and Y_{pred} the observed and predicted flooded volume or area:

$$RMSE = \sqrt{\frac{\sum_{i=1}^{n}\left(Y_{obs,i} - Y_{pred,i}\right)^2}{n}} \quad (2.4)$$

The relative RMSE (rRMSE) was also calculated by dividing the RMSE by the mean volume of water or area of the flood extents in each study area, i.e. 11 588 m³ and 47 424 m² in the Maarkebeek subbasin, 5473 m³ and 18 397 m² in the Bellebeek subbasin and 12 423 m³ or 33 753 m² in the Demer subbasin. The error estimates were calculated based on an independent test-set.

The observations used in the SVR and BRT are the individual flood extents, since the absence of spatial correlation is not a prerequisite for these methods. This resulted in 48 observations in the Maarkebeek subbasin, 117 observations in the Bellebeek subbasin and 184 observations in the Demer subbasin. The response variables were the volume of water in these extents and their respective area. There were six predictors included in the models: accumulated precipitation, peak precipitation, upstream urban fraction, mean upstream urban area, edge density of the upstream urban area and the flood extents' respective flow accumulation. Two alternatives for the two meteorological predictors were tested, resulting in four possible combinations of peak precipitation (mm/hr; mm/6 hr) and accumulated precipitation (mm/14 days; mm/30 days). The urban fraction in the area upstream of the flood extent was also included as a predictor, as were two indices of urban fragmentation and connectivity: (i) the mean area of an urban, upstream flood extent (m²), and (ii) the edge density (m/m²) of the urban upstream area, defined as the total circumference of upstream urban areas divided by the total upstream urban area. A higher mean area indicates a more compacted urbanization, whereas a higher edge density indicates a more fragmented upstream urban area. The location of the individual flood extents in the subbasin was represented in the model by the flow accumulation variable (Tarboton et al., 1991). The flow accumulation was derived from the DEM and equals the number of upstream pixels that drain into an outlet. In this case, the most downstream pixel of each individual extent was taken as the outlet. A pixel with a higher flow accumulation value is located more downstream in the subbasin.

Support Vector Regression

The Support Vector algorithm constitutes a supervised, nonlinear learning method which can be applied for classification or regression, in the latter case it is referred to as Support Vector Regression (SVR) (Heremans & Van Orshoven, 2015; Jordan & Mitchell, 2015; Smola & Schölkopf, 2004). In SVR, the inputs are first mapped to a hyperplane using a kernel function, which can be linear or radial. Next, a linear regression function is constructed in this hyperplane, which minimizes an ε-insensitive loss function. A regularization parameter controls the trade-off between model complexity and the loss function (Gizaw & Gan, 2016; Heremans & Van Orshoven, 2015; Smola & Schölkopf, 2004). The models and their parameters were tuned and implemented using the 'caret' package in R-software, using repeated k-fold cross-validation (Kuhn, 2008), with ten repeats and five folds. The importance of the different predictors in the SVR was assessed using the feature selection procedure Recursive Feature Elimination (RFE), a well-known selection method for support vector algorithms. RFE first fits a model to all the predictors and ranks the features based on their importance in this model. Next, in an iterative process a model is trained while leaving out one feature based on its ranking, thus also determining the best feature subset size and composition (Guyon et al., 2002). The average adjusted R^2 and its standard deviation over the different resampling loops were used to assess the importance of each predictor (Kuhn, 2008).

Boosted Regression Trees

Tree-based models, like BRT, use binary splits to partition the predictor space into homogeneous regions. These hierarchical decision trees automatically take into account interactions between predictors and are insensitive to outliers. However, small changes in training data can give different results (Elith et al., 2008). Consequently, single tree models are unstable (Strobl et al., 2009). Boosting is a method to increase the model accuracy by combining a large number of single tree models to optimize the predictive performance. This is done in a stepwise, iterative way where a new tree is fitted on the residuals of the model (Elith et al., 2008). Three parameters need to be specified to fit a BRT: (i) the learning rate, i.e. the weight given to each tree as it is added to the model, (ii) the tree complexity or the number of nodes in a tree and (iii) the number of trees required, which is controlled by the learning rate and tree complexity (Elith et al., 2008; Heremans & Van Orshoven, 2015). The 'train' function in the 'caret' package of the R-software was used to set the optimal values of the learning rate and tree complexity for each of the study areas (Kuhn, 2008). Next, the package 'dismo' of R was used to determine their optimal tree sizes and to develop the BRT (Hijmans et al., 2016). Table 2.3 shows the results of this parameter tuning. The results of the BRT are visualized by partial dependence plots, which show the effect of a predictor on the response, while accounting for the average effect of all other predictors. Though not a perfect representation, especially when the predictors are correlated, these plots provide a useful basis for the interpretation of the model (Elith et al., 2008).

Table 2.3. Results of the parameter tuning of the BRT for each of the study areas.

Subbasin	Learning rate	Tree complexity	Number of trees
Maarkebeek	0.001	4	1450
Bellebeek	0.001	6	1600
Demer	0.001	4	1200

2.2.4. Sensitivity Analysis

A sensitivity analysis was performed to assess which of the candidate predictors influence the flood volume models' outputs most. In this analysis, the input values were perturbed One-At-a-Time (OAT). The impact of these perturbations was assessed by a sensitivity index, where M is the number of factors in the model, x_i is the nominal value of the i-th input factor, g is the model's response and Δ_i is the variation of the input factor (Francos et al., 2003; Pianosi et al., 2016):

$$\overline{S_i}(x) = abs\left(\frac{g(x_1, \dots, x_i + \Delta_i, \dots, x_M) - g(x_1, \dots, x_i, \dots, x_M)}{\Delta_i}\right) \quad (2.5)$$

This OAT approach was performed for several Δ_i and the mean $\overline{S_i}$ and its standard deviation were calculated to assess each factor's sensitivity: a higher $\overline{S_i}$ indicates a higher sensitivity (Pianosi et al., 2016). The perturbations were chosen so that the entire range of the factor was covered. The perturbed nominal values were randomly based on one of the observations for each study area: the flood event recorded on 30/12/1993 was selected for the Maarkebeek subbasin, for the Demer subbasin the recorded flood event on 12/11/2010 was selected, and for the Bellebeek subbasin the observation on 05/08/2002 was selected.

2.3. Results

2.3.1. Multiple Linear Regression

As measures of the model accuracy, Table 2.4 provides the adjusted R^2 and P-values of the MLR models, with resp. six, seven and nine observed flood events in the Maarkebeek, Bellebeek and Demer subbasins. Overall, the adjusted R^2 are low, signifying a low model accuracy, for any combination of meteorological variables. A higher adjusted R^2 is obtained for models predicting flood volume as opposed to flooded area, with the highest R^2 achieved in the Maarkebeek subbasin. The results of the Bellebeek subbasin are the weakest, with negative R^2 and high P-values for all models. The results are exemplified in Table 2.5, showing the coefficients of the linear regression models predicting flood volume with an accumulated precipitation over 14 days and peak precipitation intensity as meteorological variables. The most accurate model in this configuration, with an adjusted R^2 of 0.80 and a p-value of 0.12, was obtained for the subbasin of the Maarkebeek. The results for the Demer and Bellebeek are weaker with negative adjusted R^2, high p-values and a negative coefficient for the peak precipitation predictor in the model of the Bellebeek subbasin. Both models of the Demer and Bellebeek result in a negative coefficient for the urban fraction, i.e. more urbanization leads to less flood volume, while the more accurate model of the Maarkebeek confirms, with a positive coefficient, the hypothesis: a higher urban fraction leads to a larger flood volume.

Table 2.4. Adjusted R^2 and P-values of the Multiple Linear Regression models. The dependent variable are the volume of the flood events (Vol; m^3) and the flooded area (Area; m^2). The independent variables are the accumulated precipitation (PS14; mm/14 days and PS30; mm/30 days), hourly peak precipitation (PP; mm/hr and PP6; mm/6 hr) and the fraction of urban areas (Urban) in the subbasin.

	Maarkebeek		Demer		Bellebeek	
Vol	**adj. R^2**	**P-value**	**adj. R^2**	**P-value**	**adj. R^2**	**P-value**
PS14+PP+Urban	0.80	0.12	-0.22	0.68	-0.24	0.65
PS14+PP6+Urban	0.84	0.1	0.38	0.16	-0.49	0.80
PS30+PP+Urban	0.34	0.37	0.002	0.46	-0.01	0.51
PS30+PP6+Urban	0.80	0.12	0.34	0.19	-0.45	0.78
Area	**adj. R^2**	**P-value**	**adj. R^2**	**P-value**	**adj. R^2**	**P-value**
PS14+PP+Urban	0.38	0.35	-0.29	0.76	-0.74	0.92
PS14+PP6+Urban	0.37	0.35	0.53	0.09	-0.78	0.94
PS30+PP+Urban	-0.83	0.86	-0.10	0.57	-0.30	0.69
PS30+PP6+Urban	-0.002	0.54	0.49	0.10	-0.49	0.80

Table 2.5. Coefficients (β) and their P-values of the Multiple Linear Regression (MLR). The dependent variable is the flood volume (m^3) of the flood events (Maarkebeek: 6 obs., Bellebeek: 7 obs., Demer: 9 obs.). Coefficients are provided for the intercept (β_0; m^3), accumulated precipitation (β_1; mm/14 days), peak precipitation (β_2; mm/hr) and the fraction of urban areas (β_3) in the subbasin.

	Maarkebeek		Demer		Bellebeek	
	Coeff.	**P-value**	**Coeff.**	**P-value**	**Coeff.**	**P-value**
β_0	-429925	0.08	881981	0.34	132525	0.37
β_1	2553	0.14	1352	0.78	760	0.63
β_2	17604	0.23	42140	0.41	-8246	0.47
β_3	4128928	0.07	-4000000	0.33	-364897	0.52
adj R^2	0.80		-0.22		-0.24	
P-value	0.12		0.68		0.65	

Table 2.6 shows the results of the MLR fitted on the pooled sample, consisting of 22 observations. These analyses included the additional variables of the precipitation sum of the flood-inducing rainfall (mm) and the drainage density (m^{-1}) of the subbasins. The adjusted R^2 of these pooled MLR models are low, indicating that pooling the samples did not result in a better estimate of the flood volume or area compared to the results for the individual basins.

Table 2.6. Adjusted R^2 and P-values of the Multiple Linear Regression models of the pooled sample (22 observations). The dependent variable are the volume of the flood events (Vol; mm) and its area fractions (Areaf). The independent variables are the accumulated precipitation (PS14; mm/14 days and PS30; mm/30 days), the precipitation sum of the flood-inducing rainfall (Psum; mm), hourly peak precipitation of the flood-inducing rainfall (PP; mm/hr and PP6; mm/6 hr), the fraction of urban areas (Urban), and the drainage density of the basins (DD; m^{-1}).

	Pooled sample	
Vol	**adj. R^2**	**P-value**
PS14+Psum+PP+Urban+DD	0.0007	0.45
PS14+Psum+PP6+Urban+DD	0.17	0.16
PS30+Psum+PP+Urban+DD	-0.000035	0.45
PS30+Psum+PP6+Urban+DD	0.22	0.11
Areaf	**adj. R^2**	**P-value**
PS14+Psum+PP+Urban+DD	0.03	0.38
PS14+Psum+PP6+Urban+DD	0.10	0.25
PS30+Psum+PP+Urban+DD	0.02	0.41
PS30+Psum+PP6+Urban+DD	0.12	0.22

2.3.2. Support Vector Regression

Table 2.7 shows the RMSE and rRMSE for the different SVR model configurations predicting flood volume and area of flood extents in the three studied subbasins. These error estimates show little variation when different combinations of meteorological predictors are implemented in the models. The errors are high for all three study areas, but lowest for the SVR models predicting the area extent in the Maarkebeek subbasin.

Table 2.7. RMSE and relative RMSE (rRMSE, %) of the Support Vector Regressions for the three subbasins testing different meteorological predictors.

	Maarkebeek		**Demer**		**Bellebeek**	
Vol	**RMSE (m^3)**	**rRMSE (%)**	**RMSE (m^3)**	**rRMSE (%)**	**RMSE (m^3)**	**rRMSE (%)**
PS14 - PP	11 292	97	19 192	155	7 725	141
PS14 - PP6	11 993	103	19 255	155	7 595	139
PS30 - PP	11 449	99	19 329	156	7 899	144
PS30 - PP6	13 219	114	19 404	156	7 928	145
Area	**RMSE (m^2)**	**rRMSE (%)**	**RMSE (m^2)**	**rRMSE (%)**	**RMSE (m^2)**	**rRMSE (%)**
PS14 - PP	27 722	58	67 064	199	39 688	216
PS14 - PP6	27 756	59	64 360	191	39 006	212
PS30 - PP	27 821	59	71 790	213	39 648	216
PS30 - PP6	27 855	59	71 903	213	39 301	214

The results of the Recursive Feature Elimination, performed with an accumulated precipitation over 14 days and hourly peak precipitation, are given in Table 2.8. The predictors are ranked based on the mean R^2: a higher mean R^2 indicates a higher importance of the predictor in the SVR model. The standard deviation (SD) provides information on the variability of the mean R^2. The flow accumulation is ranked first by the RFE in each SVR, the accumulated precipitation is ranked low for all SVR models. The fraction of upstream urban area is ranked third out of six in the SVR of the Maarkebeek subbasin,

fourth in the Demer subbasin and fifth in the Bellebeek subbasin. The fragmentation indices, edge density and mean area of the upstream urban areas, are ranked low in the SVR of the Maarkebeek and higher in the SVR of the Demer and the Bellebeek.

Table 2.8. Results of the recursive feature elimination (RFE) of the Support Vector Regression with as dependent variable the volume in a flood extent (m^3). The independent variables are the accumulated precipitation (PrecSum; mm/14 days), peak precipitation (PeakP; mm/hr), flow accumulation (Flow Acc), fraction of the urban area upstream to each flood extent (Upstream Urban), mean area of upstream urban patches (Mean Area; m^2) and edge density of upstream urban patches (m/m^2). Each predictor's mean R^2 and its standard deviation (SD) over the different resampling loops together with its rank are provided.

	Maarkebeek			Demer			Bellebeek		
	mean R^2	SD	rank	Mean R^2	SD	rank	Mean R^2	SD	rank
Flow Acc	0.46	0.075	1	0.079	0.013	1	0.72	0.064	1
PeakP	0.31	0.063	2	0.042	0.015	5	0.022	0.013	4
PrecSum	0.20	0.051	5	0.006	0.005	6	0.004	0.018	6
Upstream Urban	0.31	0.101	3	0.032	0.008	4	0.022	0.021	5
Mean Area	0.28	0.066	4	0.055	0.017	2	0.036	0.038	2
Edge density	0.20	0.063	6	0.036	0.010	3	0.024	0.018	3

2.3.3. Boosted Regression Trees

Table 2.9 shows the RMSE and rRMSE of the Boosted Regression Trees for the three subbasins. The RMSE of the BRT models are high for both the flood volume and area, with the relatively lowest errors obtained in the Maarkebeek subbasin. The error estimates show little variation when different meteorological predictors are used in the models.

Table 2.9. RMSE and relative RMSE (rRMSE, %) of the Boosted Regression Trees for the three study areas predicting flood volume (m^3) and area (m^2) using different meteorological predictors for accumulated precipitation (PS14; mm/14 days, PS30; mm/30 days) and peak precipitation (PP; mm/hr, PP6; mm/6 hr).

	Maarkebeek		Demer		Bellebeek	
Vol	**RMSE (m^3)**	**rRMSE (%)**	**RMSE (m^3)**	**rRMSE (%)**	**RMSE (m^3)**	**rRMSE (%)**
PS14 - PP	18 410	159	46 095	371	15 343	280
PS14 - PP6	18 599	161	46 257	372	15 419	282
PS30 - PP	18 507	160	46 207	372	15 446	282
PS30 - PP6	18 996	164	46 086	371	15 423	282
Area	**RMSE (m^2)**	**rRMSE (%)**	**RMSE (m^2)**	**rRMSE (%)**	**RMSE (m^2)**	**rRMSE (%)**
PS14 - PP	92 495	195	87 984	261	38 474	209
PS14 - PP6	92 527	195	87 683	260	38 787	211
PS30 - PP	92 545	195	88 088	261	38 608	210
PS30 - PP6	92 964	196	87 917	260	38 634	210

Figure 2.4 shows the partial dependence plots for the Maarkebeek, Bellebeek and Demer subbasins for each predictor of the BRT models predicting flood volume, implementing 14-day accumulated precipitation and hourly peak precipitation as meteorological predictors. The flow accumulation is the most important predictor in the three BRT models with a relative importance of 54.2% in the Maarkebeek BRT model, 72.7% in the Bellebeek model and 64.1% in the Demer model. The fraction of urban area upstream of the flood extents is the second most important predictor in the BRT models,

with the highest importance in the Maarkebeek model (26%). The fragmentation indices, mean area and edge density of the upstream urban area, are of low importance (< 5%) in the BRT models, except for the edge density in the BRT model of the Maarkebeek basin (9.3%). The meteorological variables, accumulated precipitation and peak precipitation, are of relatively little importance in the models, which is also reflected by the results in Table 2.8, showing little variation with different meteorological predictors. These predictors are most important in the Demer model with an importance of 8.2% for the accumulated precipitation and 7.1% for the peak precipitation.

Overall, the partial dependence plots of flow accumulation in Figure 2.4 show that a higher value for flow accumulation results in a higher flood volume, indicating that zones close to the outlet are more prone to flooding. In the Maarkebeek model, the partial dependence plot indicates that higher upstream urban fractions contribute to flood volume, while this predictor has a negative effect in the Bellebeek and Demer models. Some of the partial dependence plots also indicate contra-intuitive and unlikely results. The partial dependence plot of the accumulated precipitation in the BRT model of the Maarkebeek basin indicates that a higher accumulated precipitation results in a lower volume of flood water. In the models of the Bellebeek basin and Demer subbasin, a higher peak precipitation or accumulated precipitation, resp., results in a lower flood volume.

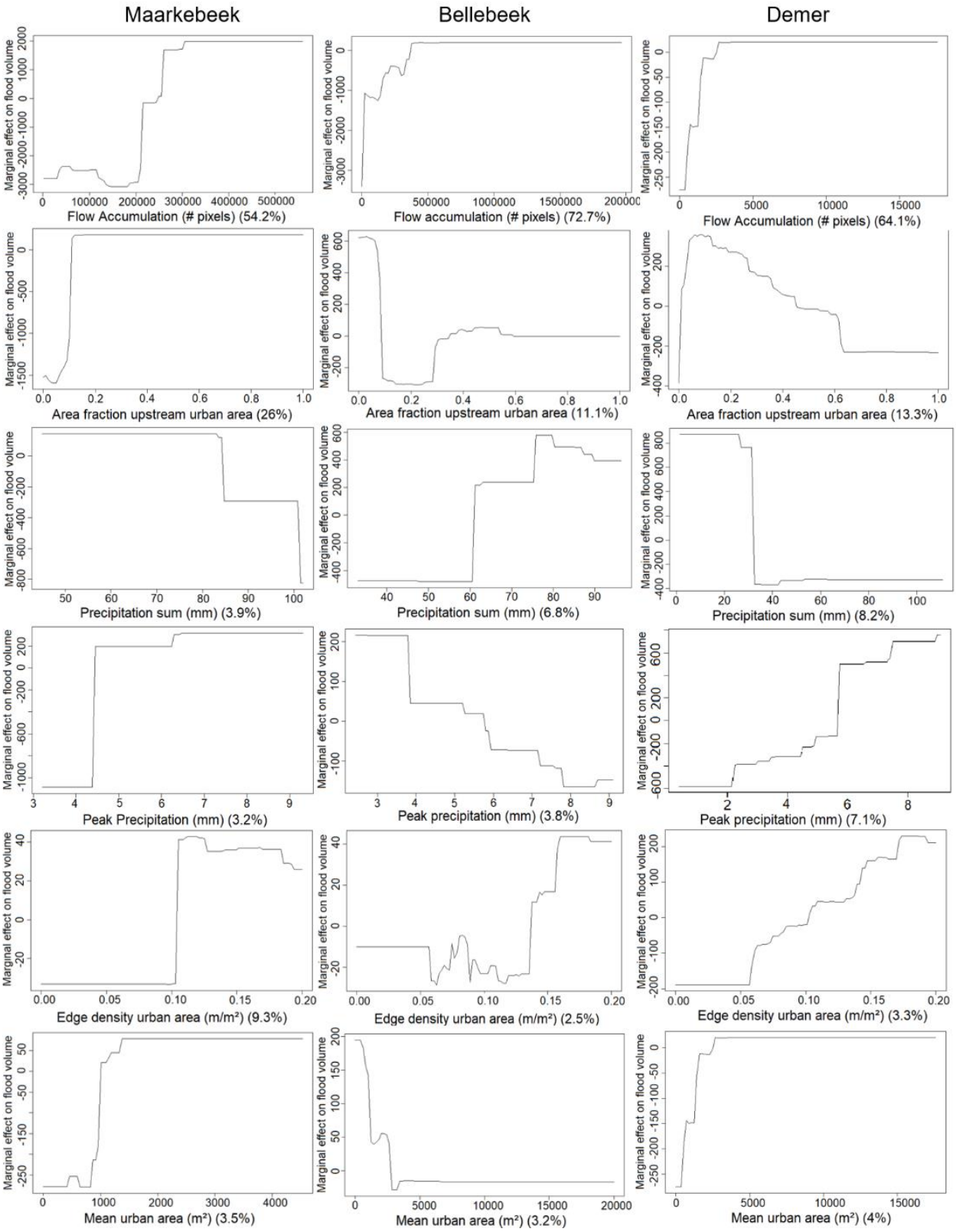

Figure 2.4. Partial dependence plots for the BRT models of the three subbasins of the Maarkebeek, Bellebeek and Demer. The importance of each predictor is given underneath the plots, expressed as a percentage.

2.3.4. Sensitivity Analysis

The sensitivity analysis was performed on one single flood volume model configuration for each of the statistical methods, namely the models implementing the 14-day accumulated precipitation and hourly peak precipitation, as the models implementing these meteorological factors have the lowest RMSE in predicting flood volume.

The results of the sensitivity analysis are given in Figure 2.5. These results show that, of the three statistical methods, the linear regression models are most sensitive to variations in the input data, followed by the SVR and BRT models, although the latter have the highest standard deviations of mean S_i. This is because the S_i of the BRT models follow the patterns shown in the partial dependence plots (see Figure 2.4): in some ranges of the factor values the S_i are zero, which means that a change in the factor does not result in a change of the flood volume; in other areas the sensitivity is higher, explaining the relatively high standard deviations of the S_i. Overall, the models show a relatively high sensitivity to variations in the urban fraction and the precipitation factors.

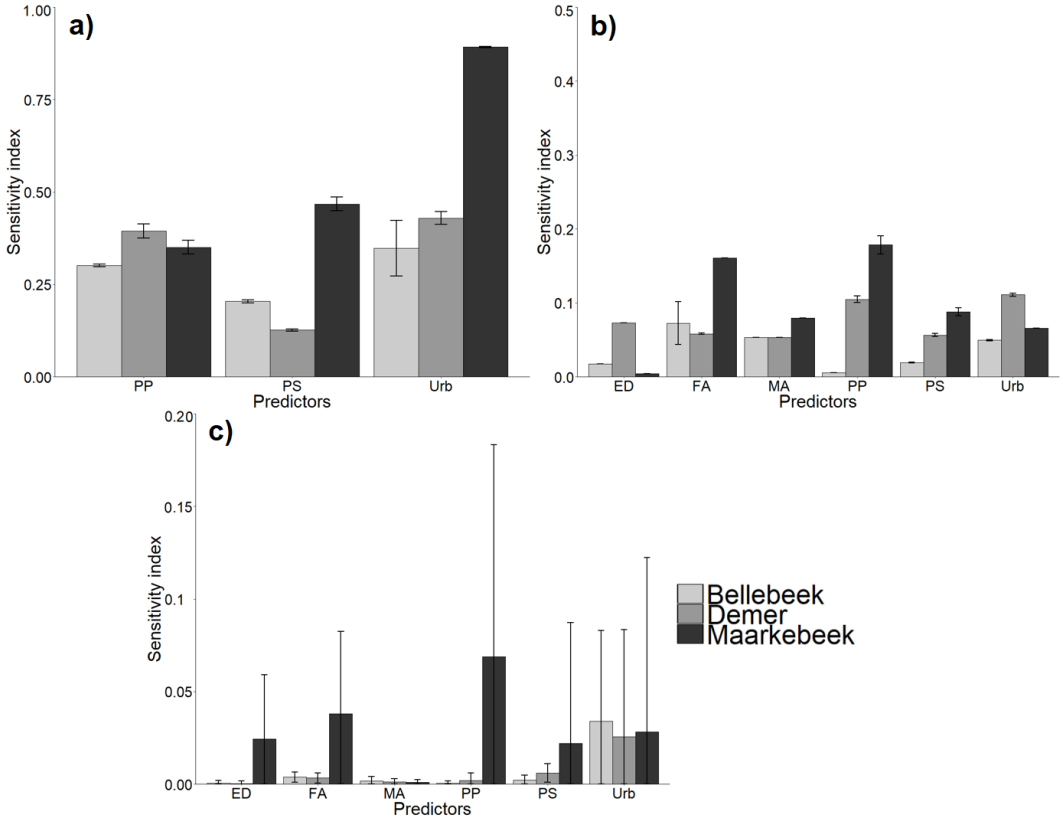

Figure 2.5. Results of the sensitivity analysis for the linear regression models (a), Support Vector Regression models (b) and Boosted Regression Trees (c). The sensitivity of the models for each factor is given: hourly precipitation peak (PP), 14-day accumulated precipitation (PS) and the area fraction of (upstream) urban areas (Urb), as well as edge density (ED), flow accumulation (FA) and mean urban area (MA).

2.4. Discussion

The relationship between soil sealing due to urbanization and flood severity, expressed by flood volume and area, derived from a spatial flood archive, was analyzed for three subbasins in Flanders using Multiple Linear Regression models and two machine learning methods, Support Vector Regressions and Boosted Regression Trees.

Since these statistical analyses derive the response variables from the spatial flood archive, the temporal dynamics of soil sealing on infiltration-excess surface runoff, resulting in higher and faster peak flows (Bronstert et al., 2002; Miller & Hess, 2017), were not considered in this study. Moreover, these analyses only included flood events recorded in the geospatial archive in the Maarkebeek, Bellebeek and Demer subbasins. A more extensive analysis could be performed including extreme rainfall events which did not result in a flood event, i.e. with no recorded flood extents. This analysis was not followed through, as it was found in a limited, unreported follow-up analysis that including such 'no flood' events in the currently implemented models lowers model performance even further. In addition, the SVR and BRT models implemented spatially explicit predictors pertaining directly to the recorded flood extents, which would complicate the inclusion of events without recorded flood extents. Alternatively, based on this 'flood'/'no flood' event database, the relationship between the susceptibility to floods, rather than flood volume and area, and soil sealing could be regarded using a logistic regression model, similar to the approach followed in Van Den Eeckhaut et al. (2006).

The MLR provides a simple and straightforward model, however, as it assumes observations to be uncorrelated, the aggregated flood extents were taken as observations in the models, omitting the spatial component and limiting the sample size. The small sample size reduces the statistical power of these models and limits the number of predictors that could be taken into account. Thus, a regional approach was also tested, pooling the observations of the three study areas into a larger sample of 22 observations. However, the adjusted R^2 values of MLR models of both the individual subbasins and the pooled sample were low, indicating a poor linear fit between the variables. The absence of a linear relationship is not surprising, given the complexity of the relationship between floods and land use changes, including urbanization (Bronstert et al., 2002). The linear regression models considered the urban fraction of each subbasin as a predictor variable for flood volume and area. A more detailed analysis could be undertaken to the role of urban areas on flood severity, making the distinction between the fraction of urban areas in valleys or on hillslopes. However, this analysis was not carried out, given the low model performance of the MLR models. The MLR models also allow for negative predictions of the dependent variables, i.e. flood volume and area. The issues of nonlinearity and negative predicted volumes, could be handled through a transformation of the dependent variable, e.g. by applying a logarithmic function, thereby establishing a log-linear relationship with the independent variables. In this regard, the flexible Generalized Linear Models (GLM) could also provide a promising and more extensive alternative to Multiple Linear Regression models. GLM allow for the dependent variable to be described by a wide range of distributions (e.g. exponential distribution) and model a linear relationship between the independent variables and the dependent variable through a link function, e.g. a logarithmic function.

Machine learning methods do not assume a linear relationship between variables and allow for observations to be spatially correlated, making them more promising to assess the complex relationship between soil sealing and flood severity. Both methods implemented in this study, SVR and BRT, have been applied in environmental research (Heremans & Van Orshoven, 2015; Ottoy et al., 2017; Sindayihebura et al., 2017), including flood susceptibility mapping and regional flood frequency analysis (Gizaw & Gan, 2016; S. S. Lee et al., 2017; Y. Lee & Brody, 2018; Mojaddadi et al., 2017; Tehrany et al., 2014). Due to the greater flexibility in data assumptions in SVR and BRT, individual flood extents could be implemented as observations and the locations of these extents were included through their flow accumulation, thus increasing the sample size in each subbasin and making the statistical analyses spatially explicit. Thus, the urban fraction upstream from each flood extent could be taken into account in the SVR and BRT. Moreover, the increased sample size also allowed additional predictors could be incorporated in the models compared to the MLR models. The edge density and mean area of the upstream urban areas were thus taken into account as measures of urban

fragmentation in the area upstream from the flood extent. However, though individual flood extents were taken as observations, these extents still pertain to the same number of flood events. Hence, the sample size of the machine learning analyses did not increase with regards to the meteorological predictors.

The empirical analysis of Putro, Kjeldsen, Hutchins, & Miller (2016) shows an upward trend in runoff totals between 1960 and 2010 in two urbanized catchments in the southern United Kingdom in a comparison with two nearby, rural catchments. The urban area of the two urbanized catchments increased from approximately 10% in 1960 to a little over 20% in 2010. This increase of approximately 10% is similar to the increase in urban areas observed in the Bellebeek and Demer subbasins (Table 2.1), however, as it was observed over a longer period of time, the urbanization rate in the UK catchments is lower than the urbanization rate in the Bellebeek and Demer subbasins. The hypothesis of an increasing trend in flood volume and area, similar to the trend in runoff totals, cannot be confirmed by our analyses, as no clear relationship with the urban area indicators is identified, model accuracy is low with both statistical methods and a number of unlikely associations, e.g. higher precipitation resulting in lower flood volumes, are present in all models. A possible explanation is the limited sample size, and consequently limited training set size, in our analyses, as only respectively 48, 117 and 184 flood extents were recorded in resp. six, seven and nine flood events between 1988 and 2016 in the Maarkebeek, Bellebeek and Demer subbasins. Pooling flood events did not improve accuracy in the linear regression models. An analogue pooling analysis was attempted for the SVR and BRT models, pooling the observed flood extents into a dataset of 349 extents, but here as well the error remained high. Predicting resp. flood volume and area fraction, the rRMSE was between 170 % and 270 % for the pooled SVR models with different meteorological variables and between 290 % and 300 % for the pooled BRT models. A more extensive regional analysis, pooling flood events from more subbasins than the three study areas included in this research, may improve model accuracy (Mostofi Zadeh & Burn, 2019).

Overall, a lower RMSE was achieved with the SVR models, which were also found to be more sensitive to variations in the input data. The better model performance of the SVR methods is contrary to the findings of Heremans et al. (2015), indicating that in sub-pixel land use classification, the accuracy of SVR models is more impacted by small training set sizes than BRT. The models with the lowest error were obtained for the Maarkebeek subbasin, which is the smallest, least urbanized study area. The urban fraction in the models of this subbasin also has a larger impact on flood volume compared to the other study areas (Table 2.8). This could be explained by the scale-effect (Blöschl et al., 2007): the impact of land use and vegetation decreases with catchment size. This may indicate that the studied subbasins are too large to assess the effect of urbanization on flood volume and extent.

As in process-based hydrological and hydraulic models, uncertainty in the input data of the models is also an important source of error in data driven models (Merwade et al., 2008; Pappenberger et al., 2005). The meteorological, flood and land use data were therefore studied for potential errors.

The meteorological data, used to derive the meteorological predictors, were retrieved from the weather station closest to the studied subbasins. However, convective, local storm events causing floods may be underestimated by these point observations. This could cause inaccuracies when the precipitation station data are applied to local flood extents. The precipitation indicators derived from these data showed a relatively high sensitivity in the models predicting flood volume, indicating that these inaccuracies may have a large impact. Integrating data from multiple weather stations or using spatially explicit rainfall maps derived from RADAR images may improve model results and reduce inaccuracies in the rainfall data. In addition, this would allow the incorporation of spatially explicit meteorological predictors in the SVR and BRT.

The flood volumes and areas, used as the dependent variable in the statistical analyses, were derived from a DEM with a resolution of 5 m and the geospatial archive of the contours of the flooded areas in Flanders as recorded between 1988 and 2016. To assess the accuracy of the derived volumes, a linear regression was performed for the three study areas between the volume of water in flood extents, summed per flood event, and the measured peak discharge during these flood events at the outlet of the basins (Vlaamse Milieumaatschappij et al., 2020). It was assumed that a monotone increasing relationship exists between these variables: a higher peak discharge would result in a higher volume of water in the flood plains. The results of these regressions are shown in Figure 2.6. The best relationship was obtained in the Maarkebeek basin with an adjusted R^2 of 0.56, the relationships in the Bellebeek and Demer basins resulted in negative adjusted R^2. Though some uncertainty is also related to the measured peak discharges, this exploratory analysis might indicate a poor relationship between the measured peak discharge and the derived flood volumes, which could indicate the presence of errors in the derivation of flood volume from the flood extents and DEM. The DEM has an error associated with it of approximately 7 cm on sealed surfaces and short grass; this error will be higher for other, more irregular surfaces (Agentschap Informatie Vlaanderen et al., 2006). However, this error is relatively small compared to the error associated with the recorded flood extents, estimated at several meters depending on the data source. The error associated with the recorded flood extents will thus contribute more to the error in the flood volume estimation than the error in the DEM. However, the error in flood volume estimation is larger than the error in flood area, due to the integration of the DEM and its associated uncertainty.

In addition, the recorded extents do not always represent the maximum extent of the flooded area, but an average or accidental extent. Especially flood contours recorded before the year 2000 may contain inaccuracies, since these extents were digitized from analogue recordings. Moreover, the recorded flood extents may be biased towards larger flood events, recorded in helicopter flights, or flood events causing damage, with extents reported by local municipalities. The extents of smaller-scale flood events may thus not be fully representative for the actual size of the flood. The consistent use of modern techniques, such as the use of drone technology or orthophotos to map the extent of flooded areas may help to reduce these errors.

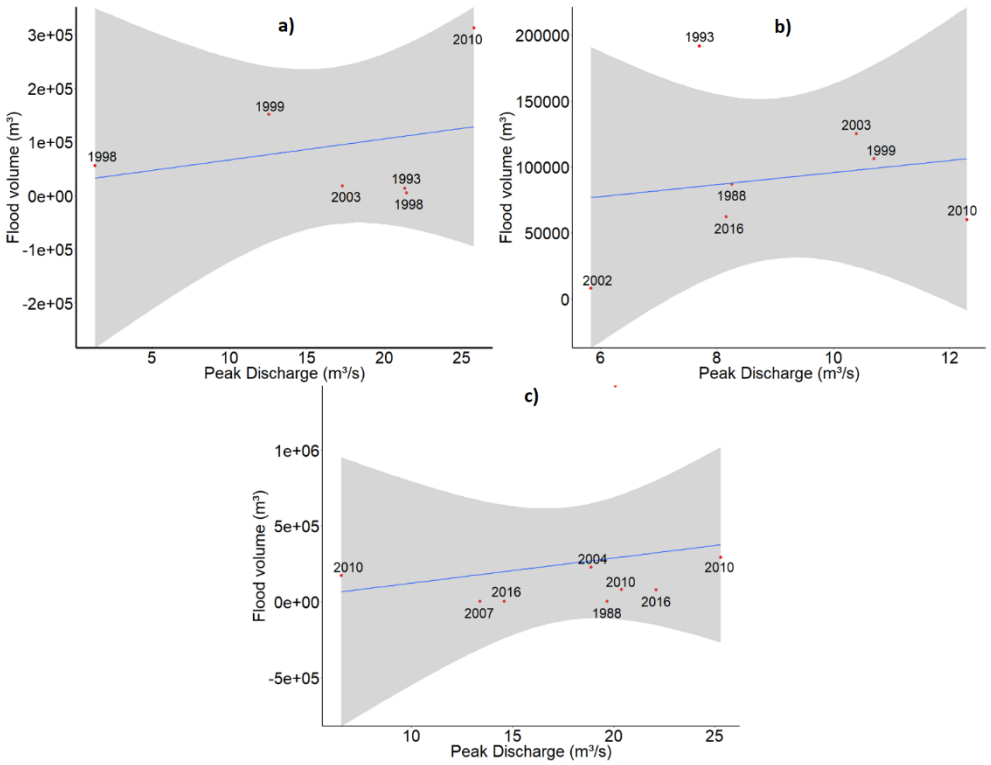

Figure 2.6. Assessment of the relationship between the flood volume and measured peak discharge: linear regression and confidence intervals of the volume of water in flooded areas (summed per event) versus the measured peak discharge during the flood events in the (a) Maarkebeek basin (adj. R^2 = 0.56, p-value = 0.055), (b) Bellebeek (adj. R^2 = -0.18, p-value = 0.803), (c) Demer (adj. R^2 = -0.095, p-value = 0.598).

The urban fraction is another important input factor in the statistical models, included in the machine learning methods as the fraction of upstream urban area from every flood extent. These fractions were derived from three land use maps spanning the 1995-2010 period, a low number considering the rate of urbanization in Flanders (Poelmans & Van Rompaey, 2009). The assumption was made that each land use map was representative for a number of years, linking several of the flood events to one land use dataset. These assumptions may have introduced errors in the estimated urban fractions, which can only be improved when more land use datasets become available. Another limitation for the land use datasets was the sparse or inadequate metadata, especially about the datasets' quality. The metadata was largely missing for the 1995 land use dataset, while for the 2001 dataset only the mean squared positional error was reported without further explanation (Agentschap Informatie Vlaanderen, 2002). However, the metadata information regarding accuracy for the 2012 land use dataset was complete and indicated a high positional accuracy with a kappa-coefficient of 89.6% (Agentschap Informatie Vlaanderen, 2016a). A land use trajectory analysis was performed to remove some of the inconsistencies in the classification between the land use datasets. However, inconsistencies remain, especially between the land use map of 2001 and those of 1995 and 2012: the area fraction of forest and arable land are both lower in 2001 than they are in 1995 and 2012 (Table 2.1), indicating that this is most likely an inconsistency in this land use map and possibly due to the more generalized classes in 2001 (9 classes) as compared to 1995 (27 classes) and 2012 (14 classes). This difference in classification impedes the statistical analyses, as the sensitivity analysis indicated that the statistical models were sensitive to variations in urban fractions.

Besides the limited number of observations and the uncertainty related to the input datasets, the low model performance could also be related to the predictors included in the model, as they only pertain

to meteorological conditions and urban land use. Additional factors are thus not included, though they may influence flood severity.

One such factor of influence is the occurrence of soil compaction, defined by the European Commission as 'the physical degradation of soil due to the reorganisation of soil micro and macro aggregates, which are deformed or even destroyed under pressure' (Jones et al., 2012). Similarly to sealing, soil compaction lowers the water infiltration capacity of the soil, thus increasing rapid surface runoff. Soil compaction occurs when pressure, for instance from heavy machinery, is exerted on soils, especially under wet conduction. In arable land, ploughing often leads to a compaction of the subsoil in the form of a plough pan layer. Besides soil erosion, compaction is one of the most important causes of soil degradation. The susceptibility of subsoils in Flanders to compaction as a result of agricultural management was assessed based on an analysis of the structural stability of the subsoil, which relates to soil texture, drainage and organic matter content. This analysis shows that large areas in Flanders, especially those areas with a loamy soil texture, are susceptible to compaction (Van De Vreken et al., 2009). The Bellebeek, Maarkebeek, and the southern part of the Demer subbasin are characterized by sandy and silt loam soil textures (see Figure 1.9) and correspond to areas indicated as susceptible to soil compaction. As the Bellebeek and Maarkebeek are both rural areas, with a high fraction of arable land, soil compaction in these subbasins may also influence the severity of floods, analogue to soil sealing.

Perhaps the most important factor not taken into account in these statistical analyses is the presence of flood control measures in the different subbasins. Several stakeholders, including the Flemish Environment Agency and local municipalities, implement flood control measures, which are described in the basin management plans of the Upper Scheldt, Dender and Demer basins for resp. the Maarkebeek, Bellebeek and Demer subbasins (Coördinatiecommissie Integraal Waterbeleid, 2016a, 2016c, 2016b). A review of these basin management plans shows that a focus on flood control is present in the Maarkebeek subbasin through the implementation of a river contract, drawn up between all involved governmental stakeholders. This contract includes measures such as the implementation of flood control reservoirs, the adjustment to river structures, including removing or increasing the height of bridges and widening culverts, and the use of early-warning systems to timely adjust flow control structures, such as weirs (Vlaamse Milieumaatschappij, 2015). A similar river contract initiative, with an additional participatory approach, has started in the Bellebeek in 2020. Flood severity in the Bellebeek has been successfully reduced through the implementation of water retention reservoirs (Vlaamse Milieumaatschappij, 2020). In the Demer subbasin, flood control is managed by allowing the Demer to meander in parts of the basin, thus increasing the buffer capacity in the valleys. However, these plans detail actions taken in the planning period 2010 –2015. As such, actions described will impact flood severity after 2010, though similar actions could have been taken before 2010. Aditionally, small-scale soil erosion control measures help to reduce rapid surface runoff and will thus influence flood severity. Such measures, including buffer strips, ditches, sediment retention ponds and check dams, have been implemented in all three subbasins (Databank Ondergrond Vlaanderen, 2021). These measures can thus exert an influence flood severity, as research by Maetens et al. (2012) shows that buffer strips reduce annual runoff from agricultural plots, though this impact will most likely be smaller than the effect of the flood control measures.

2.5. Conclusion

The generally accepted hypothesis, that the expansion of soil sealing leads to increased flood severity downstream, cannot conclusively be confirmed by the results of our analyses. Though the urban fraction is an important indicator in the machine learning models, the RMSE is high and the models

reveal inconsistencies, such as a negative associations between accumulated precipitation and flood volume.

This finding may be partly explained by errors in the datasets: the contours present in the geospatial flood archive may not be fully correct due to digitization errors, may not always show the maximum extent of the floods or contain bias towards larger flood events causing damage to urban areas; the land use data had different classification schemes, which could introduce errors in the derived urban fractions; and point observations from the meteorological stations may have missed local heavy precipitation intensities causing floods. The sensitivity analysis shows that the models, in particular the SVR models, are sensitive to these inaccuracies. Consistency in the monitoring of flood extents and in the classification of land use datasets is therefore important to allow data-driven analyses. A higher consistency in the monitoring of flood events can also contribute to a reduced bias. Long-term flood monitoring will also help increase the currently limited sample size. Another possible explanation for the high RMSE and model inconsistencies could be the scale-effect (Blöschl et al., 2007), which states that the impact of land use and vegetation on flood events decreases with catchment size. This could be reflected in the fact that the models with the lowest error were obtained in the smallest study area, namely the Maarkebeek subbasin.

The low model performance could also relate to the predictors in the model pertaining only to meteorological conditions at the time of flooding and urban land use in the subbasins. Other factors influencing flood severity include the implementation of flood and soil erosion control measures and the occurrence of soil compaction in the subbasins. These factors may counteract or exacerbate the impact of soil sealing on flood severity.

Despite these limitations, it was found that the machine learning methods applied in this study, Support Vector Regression and Boosted Regression Trees, were suitable for a data-driven analysis of the relationship between urbanization and flood volume and area. Due to the more flexible data assumptions in these machine learning methods, the individual flood extents could be considered as observations, thus increasing the observation sample size and allowing the location of these extents to be included in the models. Consequently, the presented machine learning analyses are spatially explicit. However, the spatial explicitness pertains only to the predictors associated with urban land use, not to the meteorological events, which are still derived from the same limited number of flood events.

In conclusion, we can state that SVM and BRT are promising approaches for the empirical, data-driven assessment of the relationship between soil sealing and flood volume and area. Clearly, there are data limitations to overcome, such as inconsistencies and inaccuracies as well as the limited length of the time series of flood extents. Of course, these limitations will also affect the performance of approaches based on mechanistic models. The data limitations indicate the need for a continued consistent monitoring of both flood events and land use changes in order to allow for more consistent outcomes of a data-driven analysis.

Chapter 3
A distributed and efficient CN-based rainfall-runoff model for land use optimization

Results from this chapter have been submitted for publication:
Gabriels, K., Willems, P., & Van Orshoven, J. A distributed CN-based rainfall-runoff model for land use optimization [Manuscript submitted for publication to Journal of Hydrology].

3.1. Introduction

The relationship between rainfall and runoff is an important driver of hydrological processes at the watershed scale. This relationship is influenced by meteorological and watershed variables, such as slope, soil, soil cover characteristics and surface roughness (McCuen, 1998). Human activities can significantly alter both types of variables: rainfall in many regions is becoming more erratic under anthropogenic climate change, going along with an increasing occurrence of extreme precipitation events (IPCC, 2014), while land use/land cover (LULC) changes, such as urbanization, affect infiltration capacity, vegetation cover and surface roughness (Braud et al., 2013; United Nations, 2019; Yan et al., 2013).

Consequently, adequate Rainfall-Runoff (RR-)models able to assess the impact of land use changes on hydrological processes and water resources are increasingly needed to support sustainable spatial planning policy (Breuer et al., 2009; Yan et al., 2013). Given the spatial variability of watershed characteristics and LULC changes, RR-models assessing the hydrological impacts of land use changes are typically process-based, spatially (semi-)distributed models, e.g. Soil and Water Assessment Tool (SWAT) (Neitsch et al., 2011), TOPMODEL (Beven & Kirkby, 1979; Gao et al., 2015), MIKE SHE (DHI Software, 2008). MIKE SHE, developed as a commercial package by the Danish Hydraulic Institute, is a fully distributed, physical model describing the main hydrological processes, including infiltration, surface runoff, and soil water and groundwater flow, using different time-steps. MIKE SHE is also integrated with a hydraulic module, MIKE Hydro River, to simulate flooding (DHI Software, 2008). Kalantari et al., 2014 used MIKE SHE to assess the hydrological response of different land use measures, including afforestation scenarios, which led to a decrease in peak discharge and total runoff. Results also indicated that the effect of land use measures depends on their spatial distribution and on storm characteristics. SWAT was developed by the Agricultural Research Service of the US Department of Agriculture (USDA) and the Texas AgriLife Research institute of the Texas A&M University. SWAT assesses the impact of management practices on water quality on a daily basis and thereby models the main hydrological processes in a semi-distributed way, lumping areas with the same land cover, soil and management in Hydrological Response Units (HRU) (Neitsch et al., 2011). Using SWAT, Yan et al. (2013) assessed the impact of historical land use changes on streamflow and sediment yield in a watershed in China, finding that mainly changes in urban land, forest and farmland affected streamflow. TOPMODEL, developed by Beven & Kirkby (1979), models hydrological processes using a set of conceptual tools. Gao et al. (2015) adjusted TOPMODEL into a distributed model accounting for overland flow routing to assess the impact of land management changes on peak discharges in peatland landscapes.

However, given their high computational times (Jakeman & Hornberger, 1993; Perrin et al., 2001; Sivakumar, 2008), these models are typically applied in scenario-analyses, assessing 'what-if' problems

with a limited number of simulations (Fang et al., 2013; Gao et al., 2015; Kalantari et al., 2014; Wu et al., 2015; Yu et al., 2018). Spatial optimization analyses, on the other hand, assess 'where-should' issues, identifying where land use interventions would have the largest impact. Combining these analyses with hydrological models thus allows the identification of land use patterns optimizing hydrological functions. Such optimization analyses thereby provide additional information to policy makers, river basin managers and spatial planners. However, given their bigger search space, these optimization analyses require a large number of model simulations and thus have a high computational burden (Volk et al., 2010). To reduce the computational requirements, optimization analyses often rely on heuristic algorithms, e.g. genetic algorithms, to limit the search space, thereby rather approximating the global optimal solution (Lin et al., 2009; Seppelt & Voinov, 2003; Yeo & Guldmann, 2010). Alternatively, to allow for a more complete assessment of the search space, the computational requirements of the model integrated in the optimization analysis can be lowered, for instance by reducing its complexity, while maintaining enough accuracy to compare and evaluate land use interventions (Volk et al., 2010).

This chapter therefore focuses on the development of a computationally efficient RR-model to be integrated in an iterative and spatially explicit optimization framework to identify spatial patterns minimizing flood hazard in a catchment (Chapter 4). This model should therefore be able to assess the hydrological response of rainfall events at a downstream point of interest, while taking into account the spatial variability in rainfall-land use interactions. The event-based, empirical Soil Conservation Service Curve Number (SCS-CN) method is suited for this purpose, as it is widely-used, conceptually straightforward and easy to implement, with the Curve Number (CN) model parameter, accessible through look-up tables, describing the impact of land use on surface runoff, and the total rainfall of the storm event as model input variable (Hawkins et al., 2009; USDA Natural Resource Conservation Service, 1986).

In order for the RR-model to be able to assess the impact of spatial distribution of land use changes, the default SCS-CN method was implemented in a raster-based approach. It is also critical to take into account the spatial interactions between runoff generation, propagation and re-infiltration in the catchment (Gao et al., 2015). The SCS-CN method was therefore combined with an overland flow routing algorithm, describing the lateral movement of overland flow to the outlet, and with a re-infiltration algorithm, allowing runoff to infiltrate along its flow path. Few hydrological models have been developed explicitly taking into account re-infiltration (Corradini et al., 2000; Gao et al., 2015; Niu et al., 2014), and only a limited number of re-infiltration algorithms have been developed based on the SCS-CN method (Her & Heatwole, 2016; Van Loo, 2018).

The tabulated CN values for average soil moisture conditions are adjusted in the RR-model to the initial soil moisture conditions prior to the specific rainfall event, referred to as the Antecedent Moisture Conditions (AMC) (Hawkins et al., 2009). The original formulation of the SCS-CN method adjusted the tabulated CN values based on 5-day antecedent precipitation (USDA Natural Resource Conservation Service, 1986). However, this method experiences three major flaws: it results in discrete jumps of CN values between AMC levels, the 5-day antecedent precipitation was implemented based on subjective judgement, and it does not consider effects of evapotranspiration and drainage. Therefore, alternative methods were proposed to adjust CN values to antecedent rainfall and subsequent soil moisture conditions (Hawkins et al., 2009; Mishra et al., 2008).

To find a performant, computationally efficient RR-model, several AMC correction and re-infiltration algorithms were implemented in different configurations of the RR-model. Two AMC correction methods were tested in the RR-model: the method proposed by Chow et al. (1988) as implemented by Raes et al. (2006), and the method proposed by Neitsch et al. (2011). These methods were also

compared to the performance of the tabulated CN values without AMC correction. Since only few SCS-CN based re-infiltration algorithms have been developed, two re-infiltration algorithms were proposed and tested in addition to the algorithm proposed by Van Loo (Van Loo, 2018). Several values for model parameters were also implemented and tested. The different model configurations were applied and evaluated in three catchments in the region of Flanders, Belgium for a number of storm events occurring between 2000 and 2012.

3.2. Material and Methods

3.2.1. Default SCS-CN method

The SCS CN-method calculates site specific runoff *Q* based on tabulated CN values characterized by land use and soil information. To determine runoff *Q*, the potential maximum retention *S* is calculated, from which the initial abstraction I_a is subsequently derived through a multiplication with the λ parameter:

$$S\ [mm] = \frac{25400\ -\ 254 * CN}{CN} \tag{3.1}$$

$$I_a\ [mm]\ =\ \lambda * S \tag{3.2}$$

Runoff *Q* occurs when the total volume of rainfall *P* during a storm event is larger than I_a (Hawkins et al., 2009; USDA Natural Resource Conservation Service, 1986):

$$P \geq I_a\text{: } Q\ [mm]\ =\ \frac{(P - I_a)^2}{P + I_a - S} \tag{3.3}$$

The default implementation of the SCS CN-method assumes λ=0.2 and implements the reference, tabulated CN values, without taking into account overland flow routing or corresponding re-infiltration.

3.2.2. Alternative model configurations

Different alternative model configurations based on the default implementation of SCS-CN method were evaluated to construct a computationally efficient, raster-based RR-model, able to propagate runoff through the catchment to the river courses, while taking into account re-infiltration along the overland flow paths. Once runoff has reached the river, no re-infiltration is taken into account and runoff is consecutively routed to the neighboring river pixel with the lowest elevation value until the outlet is reached.

Figure 3.1 shows the configurations of the tested, computationally efficient RR-models in which three Antecedent Moisture Conditions (AMC) correction methods, two λ parameter values and three re-infiltration algorithms were combined in order to find the most accurate one. Alternative to implementing the reference, tabulated CN values without AMC correction (CN_2), two AMC correction methods based on equations from Chow et al. (1988) and Neitsch et al. (2011) were assessed. Besides the default assumption of λ=0.2, a λ parameter value of 0.05 was also tested in the SCS-CN method, as research by Woodward et al. (2003) has shown that a value of 0.05 leads to a better approximation of I_a. Finally, three different re-infiltration algorithms were implemented: re-infiltration based on SCS-CN parameters (*P*-I_a), the re-infiltration scheme of Van Loo (2018) (VL) and an adjusted version of the latter method using the saturated hydraulic conductivity K_{SAT} (KSAT). In the latter VL- and KSAT-methods, Manning's equation was used to determine overland flow velocity. Different values for this equation's parameters of hydraulic radius R_h and Manning's roughness coefficient *n* were evaluated.

All model configurations were implemented in Python-code (version 2.7) using mostly NumPy functions. Model performance was assessed with the Nash-Sutcliffe Efficiency (NSE), its three components and the relative RMSE (rRMSE). These performance measures were calculated for runoff volumes resulting from rainfall events ranging between 1 and 80 mm.

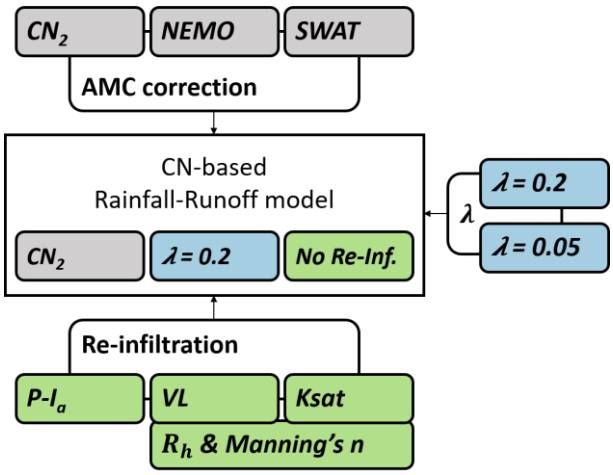

Figure 3.1. Overview of the 18 configurations of the CN-based Rainfall-Runoff model consisting of the combination of three AMC correction methods, two λ parameter values and three re-infiltration schemes.

Parameter λ

In the SCS-CN method, initial abstraction I_a is expressed as a fraction λ of the retention S. The reference value for λ is 0.2, such that $I_a = 0.2*S$. However, several authors have shown that this assumption leads to an overestimation of I_a, thus a lower, alternative λ of 0.05 was proposed (Hawkins et al., 2009; Woodward et al., 2003). The tabulated CN values for a λ of 0.2 need to be conjugated to fit a λ of 0.05 according to Equation 3.4 (Hawkins et al., 2009):

$$CN_{\lambda=0.05} = \frac{100}{1.879 * \left(\frac{100}{CN_{\lambda=0.2}} - 1\right)^{1.15} + 1} \qquad (3.4)$$

The performance of both λ values in the RR-model configurations were evaluated.

Antecedent Moisture Condition adjustments

Three AMC levels are defined by the SCS-CN method: dry conditions corresponding to wilting point (AMC I, CN_1), average conditions (AMC II, CN_2) and wet conditions corresponding to field capacity (AMC III, CN_3) (USDA Natural Resource Conservation Service, 1986). Two AMC correction methods, based on equations from Chow et al. (1988) and from Neitsch et al. (2011), were tested in the RR-model configurations, next to implementing the reference CN_2 values without AMC correction. The AMC correction method of Chow et al. (1988) was also implemented in the BUDGET-model of Raes et al. (2006), combining them with relationships derived from Smedema and Rycroft (1983). This BUDGET-model was implemented in the nutrient-emission model ArcNEMO (Van Opstal et al., 2013), originally commissioned by the Flemish Environment Agency and developed by the department of Earth and Environmental Sciences of the KU Leuven and the Soil Service of Belgium (Van Opstal et al., 2014). This corresponding AMC correction method will therefore be referred to as the NEMO method.

The ArcNEMO model is spatially distributed, raster-based model with a spatial resolution of 50 m, however, it does not account for spatial interactions through surface runoff routing. The soil water balance module of ArcNEMO, schematically depicted in Figure 3.2, first compartmentalizes the soil

based on the groundwater depth and consequently calculates the soil water content ϑ for each soil compartment *i* in a daily time step, thereby accounting for internal drainage, surface runoff, infiltration and evapotranspiration (Raes et al., 2006; Van Opstal et al., 2014). Surface runoff is determined by the SCS-CN method, adjusting the CN to the soil moisture conditions of the previous day following the procedure of Chow et al. (1988).

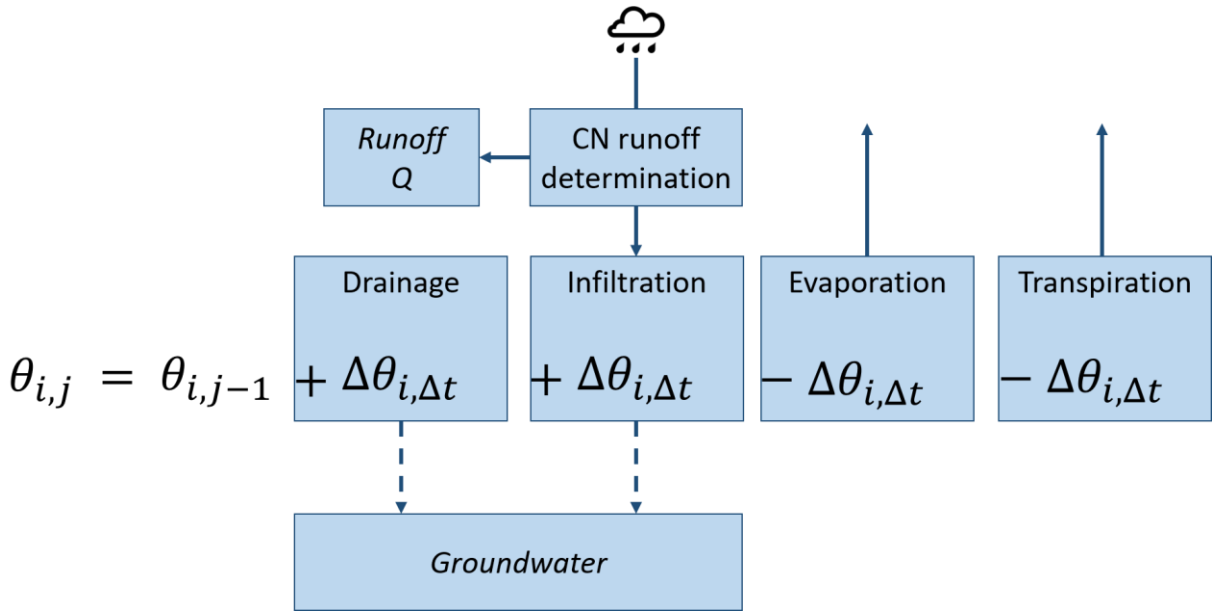

Figure 3.2. Outline of the soil water balance model implemented in ArcNEMO, based on Raes et al. (2006), calculating soil water content ϑ in soil compartment *i* for day *j* starting from the soil water content of the previous day (*j-1*). Excess drainage and infiltration is added to the groundwater compartment (adapted from Van Opstal et al. (2014)).

Chow et al. (1988) determined CN_1 and CN_3, corresponding to AMC I and AMC III, from CN_2 according to resp. Equation 3.5 and 3.6. The soil characteristics determining this soil water balance, namely soil moisture content at wilting point (ϑ_{WP}) and at field capacity (ϑ_{FC}), were derived by means of pedotransfer-functions from a legacy soil profile database (Beckers et al., 2011; Ottoy et al., 2015; Weynants et al., 2009). From the daily soil water balance, the antecedent moisture content (ϑ_{AMC}) in the top 30 cm of soil is determined (Raes et al., 2009; Van Opstal et al., 2013). Based on this ϑ_{AMC}, CN values are adjusted following Equations 3.7 to 3.10 (Raes et al., 2009; Smedema & Rycroft, 1983). If ϑ_{AMC} is smaller than ϑ_{WP}, the CN value is set equal to CN_1 (Equation 3.7). If ϑ_{AMC} is larger than ϑ_{WP} and smaller than the average of ϑ_{FC} and ϑ_{WP}, a linear interpolation between CN_1 and CN_2 is used to determine CN (Equation 3.8). If ϑ_{AMC} is larger than the average of ϑ_{FC} and ϑ_{WP} but smaller than ϑ_{FC}, a linear interpolation between CN_2 and CN_3 is implemented (Equation 3.9). Finally, if ϑ_{AMC} is larger than ϑ_{FC}, CN_3 is used to calculate runoff (Equation 3.10) (Chow et al., 1988).

$$CN_1 = \frac{4.2 * CN_2}{10 - 0.058 * CN_2} \quad (3.5)$$

$$CN_3 = \frac{23 * CN_2}{10 + 0.13 * CN_2} \quad (3.6)$$

$$if\ \theta_{AMC} < \theta_{WP}: CN = CN_1 \quad (3.7)$$

$$if\ \theta_{WP} \leq \theta_{AMC} < \frac{\theta_{WP} + \theta_{FC}}{2}: CN = CN_1 + \frac{(\theta_{AMC} - \theta_{WP}) * (CN_2 - CN_1)}{\frac{\theta_{FC} - \theta_{WP}}{2}} \quad (3.8)$$

$$if\ \frac{\theta_{WP}\ +\ \theta_{FC}}{2}\ \leq\ \theta_{AMC}\ <\ \theta_{FC}\colon CN\ =\ CN_2\ +\ \frac{\left(\theta_{AMC}\ -\ \frac{\theta_{FC}\ +\ \theta_{WP}}{2}\right)\ *\ (CN_3\ -\ CN_2)}{\frac{\theta_{FC}\ -\ \theta_{WP}}{2}} \quad (3.9)$$

$$if\ \theta_{FC}\ \leq\ \theta_{AMC}\colon CN\ =\ CN_3 \quad (3.10)$$

Neitsch et al. (2011) proposed a CN adjustment of a different form, provided in Equations 3.11 and 3.12, which were implemented in the semi-distributed hydrological model of the Soil and Water Assessment Tool (SWAT). This method will therefore be referred to as the SWAT method. SWAT includes the option to adjust the potential retention variable *S* (Equation 3.1) according to the water content in the soil profile. First, the potential maximum retentions S_1 and S_3 are derived from CN_1 and CN_3 (Equation 3.1). Shape coefficients w_1 and w_2 are then calculated from these retentions S_1 and S_3 and from soil moisture content at field capacity *FC* [mm] and saturated soil moisture content *SAT* [mm] (Equations 3.13 and 3.14). The AMC corrected retention *S* is then derived from S_1 according to Equation 3.15 using coefficients w_1 and w_2, and soil moisture *SW* [mm], which is the antecedent moisture in the soil profile subtracted with soil moisture at wilting point. The retention *S* is then used to determine the corresponding the AMC corrected abstraction I_a according to Equation 3.2, and consequently runoff *Q* is calculated using Equation 3.3.

$$CN_1\ =\ CN_2\ -\ \frac{20\ *\ (100\ -\ CN_2)}{100\ -\ CN_2\ +\ e^{\,2.533\ -\ 0.0636\ *\ (100\ -\ CN_2)}} \quad (3.11)$$

$$CN_3\ =\ CN_2\ *\ e^{0.00673\ *\ (100\ -\ CN_2)} \quad (3.12)$$

$$w_1\ =\ ln\left(\frac{FC}{1\ -\ S_3\ *\ S_1^{-1}}\ -\ FC\right)+\ w_2\ *\ FC \quad (3.13)$$

$$w_2\ =\ \frac{ln\left(\frac{FC}{1\ -\ S_3\ *\ S_1^{-1}}\ -\ FC\right)\ -\ ln\left(\frac{SAT}{1\ -\ 2.54\ *\ S_1^{-1}}\ -\ SAT\right)}{SAT\ -\ FC} \quad (3.14)$$

$$S\ =\ S_1 *\ \left(1\ -\ \frac{SW}{SW\ +\ e^{\,w_1\ -\ w_2\ *\ SW}}\right) \quad (3.15)$$

The adjustments to CN values implemented by both AMC correction methods are illustrated in Figure 3.3 for three CN_2 values of 55, 70 and 90 and a soil with ϑ_{WP}, ϑ_{FC} and ϑ_{SAT} equal to resp. 0.12, 0.36 and 0.46 and a soil thickness of 1 m.

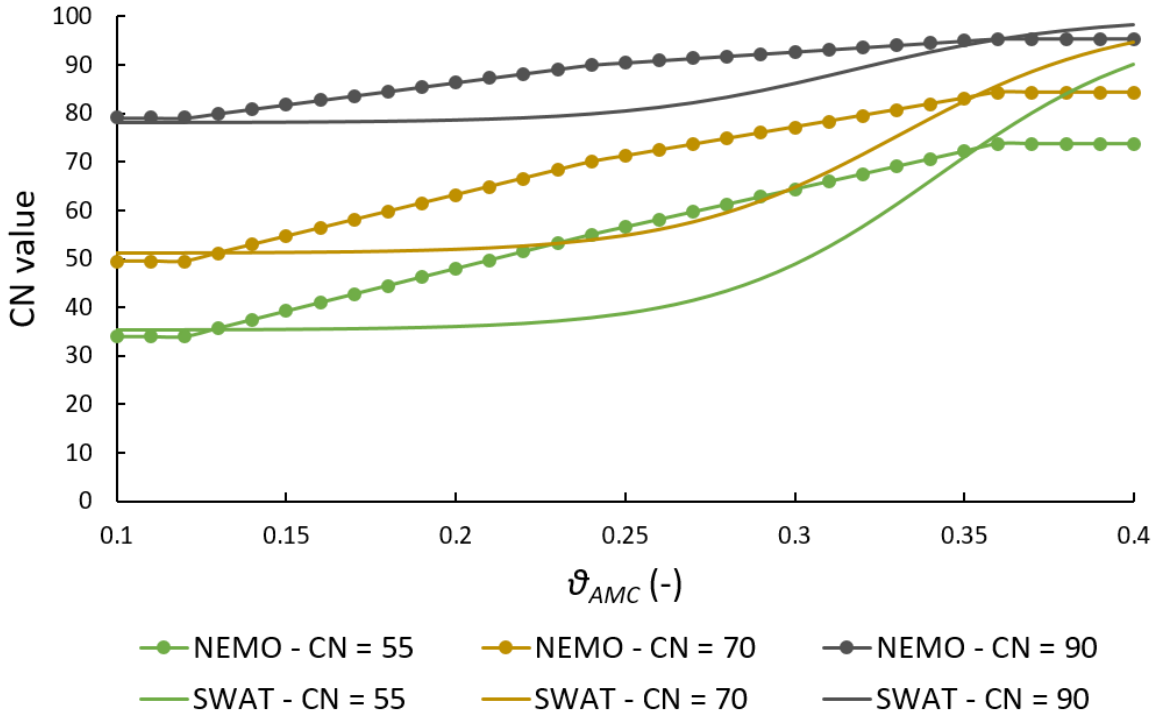

Figure 3.3. Comparison of CN values adjusted to antecedent soil moisture conditions according to the NEMO method (Chow et al., 1988; Raes et al., 2006) and the method implemented in SWAT (Neitsch et al., 2011) for a soil with ϑ_{WP}, ϑ_{FC} and ϑ_{SAT} equal to resp. 0.12, 0.36 and 0.46 and a soil thickness of 1 m.

Re-infiltration algorithms

Runoff Q was routed along the flow paths, determined by the single flow direction algorithm of Jenson & Domingue (1988) according to a DEM. To calculate re-infiltration along these flow paths, three re-infiltration algorithms were tested in the RR-model configurations: the method proposed by Van Loo (2018) and two new alternatives.

In the first re-infiltration method under consideration, each pixel's infiltration capacity is based on its initial abstraction I_a (Figure 3.4). When rainfall P is lower than I_a, no runoff is generated on the pixel and its infiltration capacity is assumed as the difference between P and I_a. This difference is subtracted from the incoming runoff Q_{input} of upstream pixels. If P is higher than I_a, runoff is generated under the assumption that the pixel's infiltration capacity is saturated and thus 0. This method was tested as it is straightforward, estimating infiltration based solely on total rainfall and the basic SCS-CN parameter I_a, which inherently contains information on the soil and land use types.

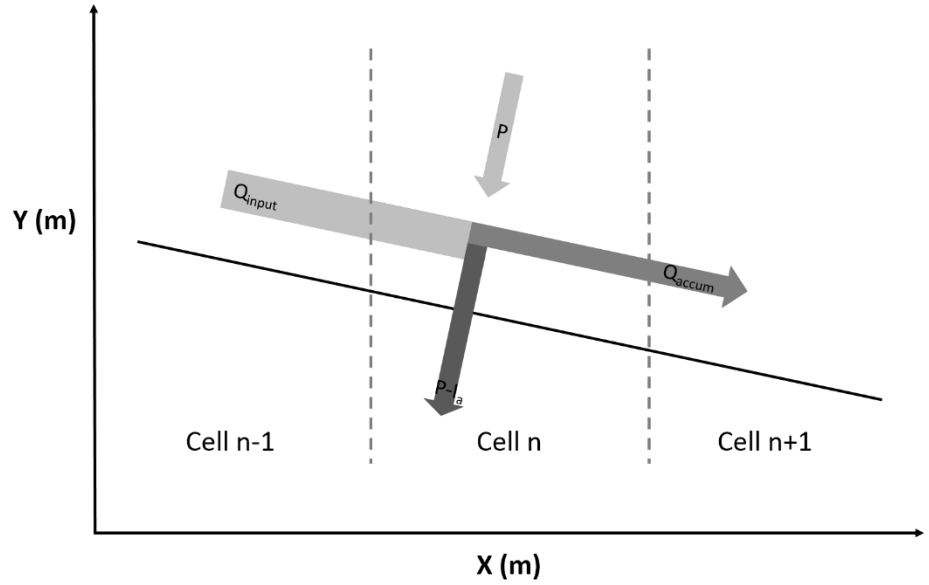

Figure 3.4. Schematic overview of the re-infiltration method based on SCS-CN method parameters.

The performance of the re-infiltration method of Van Loo (2018), schematically depicted in Figure 3.5, was also assessed. This method combines the SCS-CN method with Manning's equation to assess runoff and infiltration in each pixel. Since the SCS-CN method calculates runoff and infiltration using a daily time-step, the infiltration needs to be corrected to account for the runoff rate, and corresponding re-infiltration time, across the pixel, as determined using Manning's equation.

Incoming runoff Q_{input} is added to rainfall P to obtain P_{total}, which is used to calculate runoff Q as in Equation 3.3. The infiltration I_{ori}, defined as $P_{total} - Q$, is interpreted as an infiltration rate per hour. The actual infiltration I is then estimated by multiplying I_{ori} with the travel time of the overland flow over the pixel. This travel time is derived from the runoff flow velocity V as calculated by Manning's equation, with R_h [m] the hydraulic radius, s [m/m] the slope of the pixel and n [s/m$^{1/3}$] the Manning's roughness coefficient.

$$V = \frac{R_h^{\frac{2}{3}} * s^{\frac{1}{2}}}{n} \tag{3.16}$$

The Manning's coefficient n is an index of surface roughness, while the hydraulic radius R_h is defined as the cross-sectional area of the channel divided by its wetted perimeter, which will approximate flow depth for overland flow (McCuen, 1998). Flow velocity V is calculated using an assumed, constant value for R_h and multiplied with the pixel resolution to determine the corresponding travel time and actual infiltration I. Excess infiltration I_{red}, calculated as $I_{ori} - I$, is then added to runoff Q to obtain the accumulated runoff Q_{accum}, flowing to the downstream pixel (Van Loo, 2018).

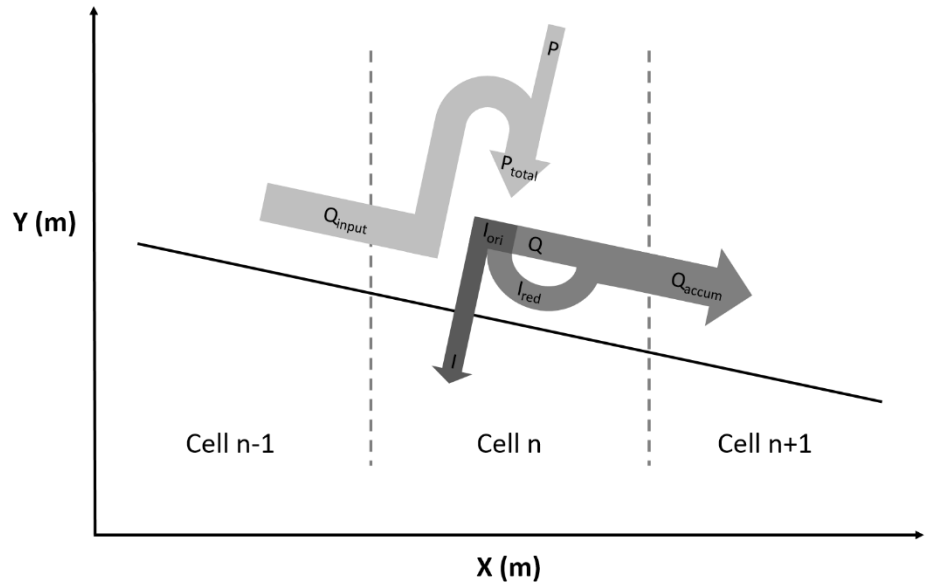

Figure 3.5. Schematic overview of the re-infiltration method proposed by Van Loo (2018).

The re-infiltration method of Van Loo (2018) derives runoff Q (Equation 3.3) from P_{total}, a combination of rainfall P and incoming runoff Q_{input}. Values of P_{total} can thus exceed the range of rainfall amounts used to determine this empirical equation. An adaptation of the Van Loo method was therefore also tested, assessing infiltration from rainfall P and re-infiltration from incoming runoff Q_{input} separately. Moreover, instead of assuming I_{ori} is the infiltration rate, the physical soil characteristic of saturated hydraulic conductivity K_{SAT} was implemented as infiltration rate, as displayed in Figure 3.6. Runoff Q is calculated according to Equation 3.3, using rainfall P and infiltration I_P equaling P-Q. Re-infiltration is determined based on the incoming runoff Q_{input}: to assess the infiltration I_Q from incoming runoff Q_{input}, K_{SAT} is multiplied with the travel time over pixels, calculated with Equation 3.16. Excess infiltration I_{red} is then added to runoff Q, resulting in the accumulated runoff Q_{accum}, flowing downstream.

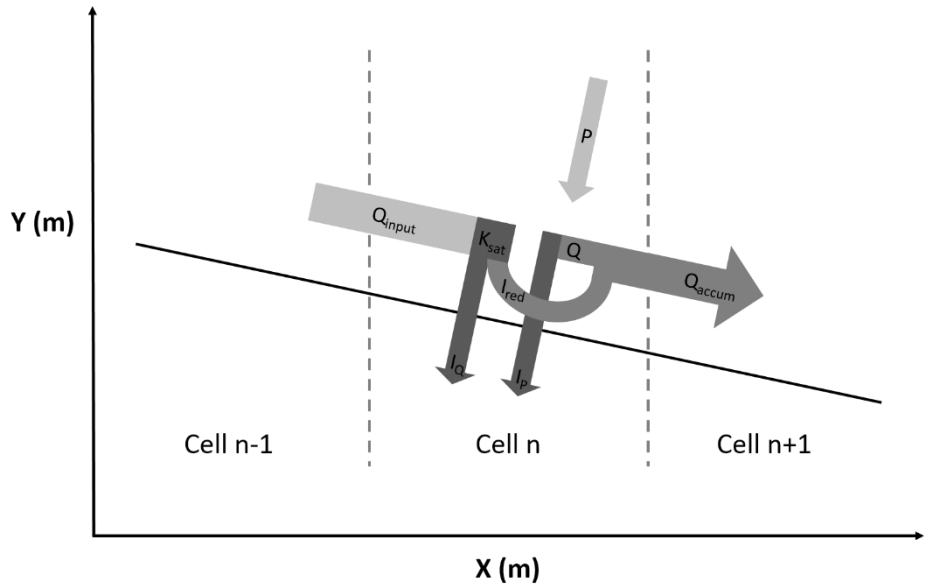

Figure 3.6. Schematic overview of the KSAT re-infiltration method, adjusted from Van Loo (2018) by assessing infiltration I_P from rainfall P and re-infiltration I_Q from incoming runoff Q_{input} separately, with the saturated hydraulic conductivity K_{sat} assumed as infiltration rate to determine I_Q.

3.2.3. Study areas

In this study, the RR-model configurations were implemented with a spatial resolution of 50 m X 50m. The RR-model configurations were tested for three catchments in Flanders: the Maarkebeek catchment, Bellebeek catchment and one of its subcatchments, i.c. the Hunselbeek (Figure 3.7). The boundaries of these catchmentes were delineated based on the location of the flow gauging stations at the outlets of the catchments and the filled DEMs of the basins. The general land use in both these catchments is depicted in Figure 1.8 according to the land use datase from 2012 (Agentschap Informatie Vlaanderen, 2016b). The Maarkebeek watershed, situated in the Upper Scheldt river basin, has an area of 48 km² and its land use is predominantly agricultural, with arable land and grasslands covering respectively over 40% and 35% of the watershed. Forest and urban areas cover approximately one tenth of the Maarkebeek catchment. The Bellebeek catchment, with an area of 88 km², is the more urbanized watershed, with urban land use types constituting one fifth of its area. The Bellebeek watershed is also more afforested (16%) than the Maarkebeek watershed. Its agricultural area is dominated by grasslands (40%) rather than arable land (25%). To assess the performance of the hydrological model over different spatial scales, the model performance was also assessed for the Hunselbeek catchment, a nested subcatchment of the Bellebeek (Amatya et al., 2016). The Hunselbeek subcatchment has an area of 21.5 km², thereby comprising nearly a quarter of the larger Bellebeek catchment. As in the Bellebeek catchment, 40% of the Hunselbeek watershed is covered by grassland, while approximately a third of this subcatchment consists of arable land. Urban areas and forests cover respectively 16% and 13% of the area (Agentschap Informatie Vlaanderen, 2016b). Top soil textures in the Maarkebeek and Bellebeek catchments are silt and silt-loam (see Figure 1.9) (Databank Ondergrond Vlaanderen, 2017; Dondeyne et al., 2013). The slopes in the study areas, applied in Manning's equation (Equation 3.16), were derived from the filled DEM (Figure 3.8) (Agentschap Informatie Vlaanderen et al., 2006). To avoid a flow velocity of zero, a minimum slope of 0.001 m/m was implemented. The Maarkebeek catchment has a more accidented terrain than the Bellebeek catchment, with an average slope of 6% versus 4% in resp. the Maarkebeek and Bellebeek catchment and a maximum slope of approx. 24% in both catchments.

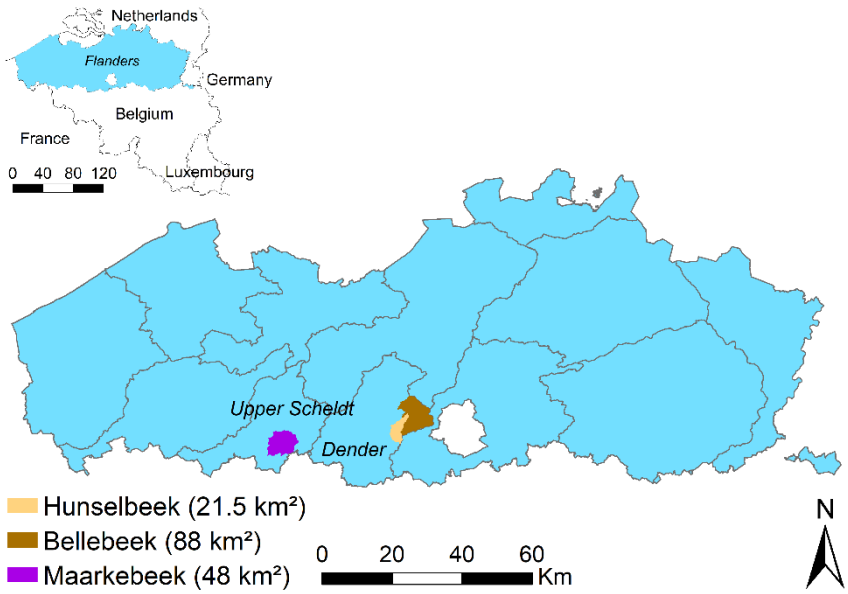

Figure 3.7. Location of the Maarkebeek catchment in the Upper Scheldt basin and the Bellebeek catchment, with its subcatchment of the Hunselbeek, in the Dender basin in Flanders, Belgium (Agentschap Informatie Vlaanderen, 2018; Agentschap Informatie Vlaanderen & Vlaamse Milieumaatschappij, 2020; Eurostat, 2020).

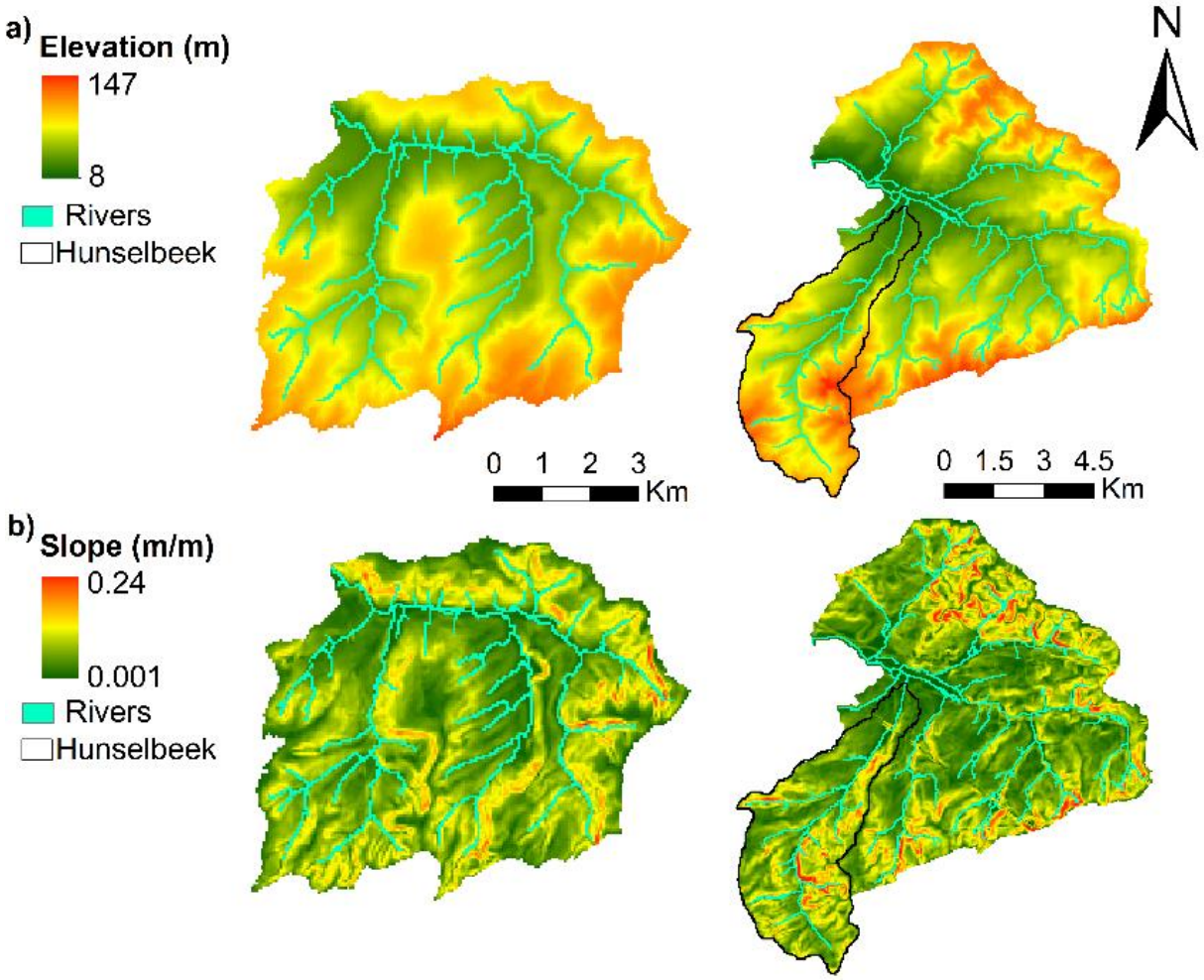

Figure 3.8. a) Digital Elevation Model (DEM) (m) (Agentschap Informatie Vlaanderen et al., 2006) and b) its derived slope (m/m) of the Maarkebeek and Bellebeek catchments.

Implementation of model configurations

The CN values for a λ of 0.2 were derived from the 2012 land use dataset with 5 m resolution (Figure 1.8) (Agentschap Informatie Vlaanderen, 2016b) and soil information on texture and drainage (Figure 1.9) using look-up tables (USDA Natural Resource Conservation Service, 1986). An overview of the implemented CN values can be found in Table 3.1. The resulting CN dataset was then resampled to a resolution of 50 m using bilinear interpolation (Figure 3.9).

Table 3.1. Overview of the CN cover descriptions (USDA Natural Resource Conservation Service, 1986) assigned to the land use classes (Agentschap Informatie Vlaanderen, 2016b) for each Hydrological Soil Group (HSG), determined by soil texture and drainage information (A = well drained, B = moderately drained, C = low infiltration rate, D = permanent high water).

		CN for each HSG			
Land use class	**CN cover**	*A*	*B*	*C*	*D*
Buildings	urban – impervious areas – roofs	*98*	*98*	*98*	*98*
Roads	Urban – streets – paved (ditches)	*83*	*89*	*92*	*93*
Other sealed surfaces	Urban – commercial and business	*89*	*92*	*94*	*95*
Railroads	Urban – streets – gravel	*76*	*85*	*89*	*91*
Other unsealed surfaces	Urban – open space (good)	*39*	*61*	*74*	*80*
Arable land	Row crops – straight rows (good)	*67*	*78*	*85*	*89*
Grassland – Meadows	Other agriculture – Meadow	*30*	*58*	*71*	*78*
Grassland – Pastures	Other agriculture – Pasture (fair)	*49*	*69*	*79*	*84*
Forest	Woods (good)	*30*	*55*	*70*	*77*

Consequently, these CN values were conjugated for a λ of 0.05 according to Equation 3.4. The antecedent soil moisture conditions implemented in Equations 3.7–3.10 and 3.13–3.15 of the AMC correction methods were derived from daily soil water balance simulations run by ArcNEMO from 2000 to 2012 for the three study areas. Manning's equation (Equation 3.16), applied in the re-infiltration methods of Van Loo (2018) and its variant KSAT, derives the travel time over pixels requires values for slope (Figure 3.8), the hydraulic radius R_h and Manning's roughness coefficient n. For overland flow, R_h is approximated by overland flow depth. For simplicity, a constant and uniform value for flow depth was assumed, whereby three values were assessed: 1 mm, 2 mm and 3 mm. An increase in R_h will increases overland flow velocity, thereby lowering the travel time over pixels, and thus reducing infiltration and increasing runoff volumes. The sensitivity of the Van Loo and KSAT re-infiltration methods to the R_h values was assessed using the sensitivity index $\bar{S}$, with M the model response variable under consideration (Pianosi et al., 2016):

$$\bar{S} = abs\left(\frac{M(x_1, \dots, R_h + \Delta, \dots, x_M) - M(x_1, \dots, R_h, \dots, x_M)}{\Delta R_h}\right) \quad (3.17)$$

Values for Manning's n (Table 3.2) were determined based on the 2012 land use dataset (Agentschap Informatie Vlaanderen, 2016b) using look-up tables (Engman & ASCE, 1986; Kalyanapu et al., 2009; Morgan et al., 1998; Vieux, 2016). Since seasonality may affect soil roughness for vegetated land cover classes, the performance of a Manning's n adjusted to the meteorological seasons was also assessed. The tabulated Manning's n values in Table 3.2 were taken as the base value n_b in fall and these were seasonally adjusted depending on the vegetation type (Table 3.3): n_b increased to account for increasing vegetation cover in spring and summer and lowered to account for sparser vegetation in winter (Arcement & Schneider, 1989), resulting in higher infiltration and lower runoff in spring and summer than in winter and fall. The saturated hydraulic conductivity K_{SAT} (mm/hr) implemented in the KSAT re-infiltration was collected from the ArcNEMO database (Van Opstal et al., 2013). This dataset, visualized in Figure 3.9, was initially derived using pedotransfer functions (Weynants et al., 2009) based on the database Aardewerk-Stat (Beckers et al., 2011; Ottoy et al., 2015).

Table 3.2. Base value for the Manning's roughness coefficient *n* (n_b) according to the land use classes from the 2012 land use dataset (Agentschap Informatie Vlaanderen, 2016) and look-up tables (Engman & ASCE, 1986; Kalyanapu et al., 2009; Morgan et al., 1998).

Land use class	**Manning's *n* (n_b)**
Buildings/ Other sealed	0.02
Roads	0.011
Railroads	0.012
Water	0.8
Other unsealed	0.04
Arable	0.09
Meadows/Pasture	0.15
Forest	0.4
Grass (side road/shore)	0.1

Table 3.3. Seasonal adjustment of the Manning's roughness coefficient *n* for vegetated land use classes from the tabulated, base values n_b used in fall conditions (Arcement & Schneider, 1989; Engman & ASCE, 1986; Kalyanapu et al., 2009; Morgan et al., 1998; Vieux, 2016).

	Manning's *n*		
Land use class	*Winter*	*Spring*	*Summer*
Arable land	n_b-0.04	n_b+0.03	n_b+0.09
Grass cover	n_b-0.03	n_b+0.02	n_b+0.05
Forest	n_b-0.05	n_b+0.05	n_b+0.1

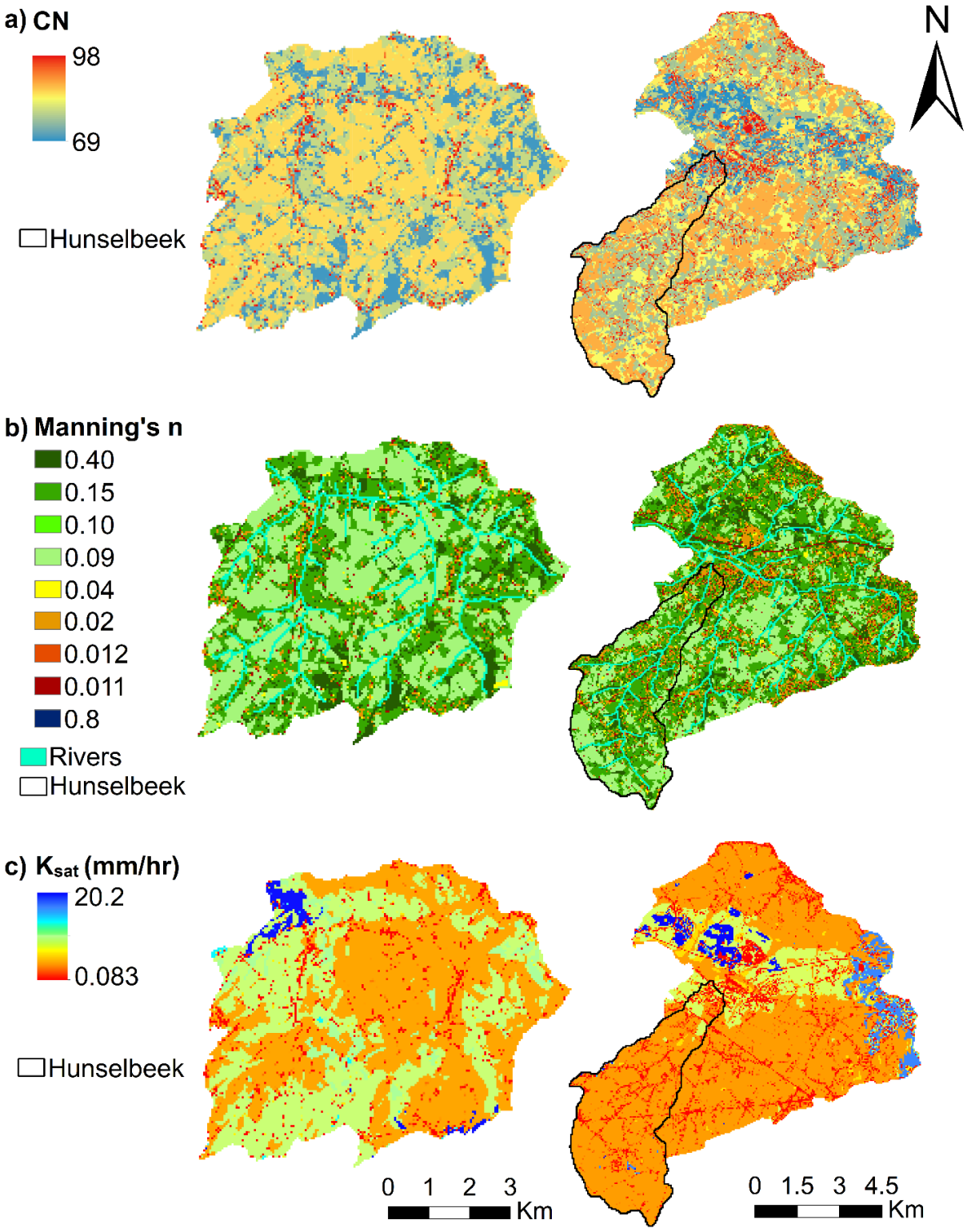

Figure 3.9. a) CN values (λ = 0.2), b) Manning's roughness coefficient *n* and c) saturated hydraulic conductivity (K_{SAT}, mm/hr) (Van Opstal et al., 2013) for the three studied catchments of the Maarkebeek, Bellebeek and Hunselbeek.

Evaluation of model configurations

Validation data were collected in the form of rainfall events resulting in peak discharges at least 1.5 times higher than the baseflow prior to the event. Accordingly, daily rainfall data were acquired from the rain gauge networks of the Royal Meteorological Institute (RMI) and the Flanders Environment Agency (VMM) (Van Opstal et al., 2014). Discharge data were derived from flow gauging stations at the watershed outlets (Vlaamse Milieumaatschappij et al., 2020). Based on these data, respectively 165, 164 and 124 rainfall events were selected for the Maarkebeek, Bellebeek and Hunselbeek watersheds (Table 3.4). From the events' hydrographs, runoff volumes were derived by separating direct runoff from baseflow using the constant-slope method, i.e. separating direct runoff and baseflow using the line between the lowest discharge before the rising limb of the hydrograph and the inflection point on its recession limb (McCuen, 1998). Histograms of the runoff volumes collected in each study catchment are provided in Figure 3.10. Based on this rainfall event information, the RR-models modeled the runoff volumes at the outlets. The model accuracy was then assessed with the RMSE (see Equation 2.4) relative to the mean of the observed runoff volumes (rRMSE), and the Nash-Sutcliffe Efficiency (NSE) with n the number of validation events, Y_{obs} and $\bar{Y}_{obs}$ the runoff volumes derived from the discharge data and their mean, and Y_{pred} the runoff volumes calculated by the RR-model (Nash & Sutcliffe, 1970):

$$NSE = 1 - \frac{\sum_{i=1}^{n}\left(Y_{obs,i} - Y_{pred,i}\right)^2}{\sum_{i=1}^{n}\left(Y_{obs,i} - \bar{Y}_{obs,i}\right)^2} \quad (3.18)$$

The NSE assesses model performance compared to the mean of the observed values, with negative NSEs indicating a model prediction worse than the mean, while a NSE of 1 representing a perfect prediction. Model performance is further described by its three components: the linear correlation r, the error in variability α and the bias term β. The variability error α is defined as the ratio of the standard deviations σ of predicted and observed values ($\sigma_{pred}/\sigma_{obs}$); bias term β equals the ratio of the means μ of predicted and observed values (μ_{pred}/μ_{obs}). For these three NSE components, r, α and β, a value of 1 represents a perfect model performance (Gupta et al., 2009; Knoben et al., 2019).

ArcNEMO was used to calculate daily discharge simulations between 2001 and 2010 for the studied catchments, which resulted in NSEs of respectively 0.42, 0.33 and 0.43 for the Maarkebeek, Bellebeek and Hunselbeek catchments. Based on ArcNEMO's performance and thresholds reported by Ladson (2008), the RR-model performance was deemed adequate if NSE values > 0.3 and good if NSE > 0.5 (Moriasi et al., 2007).

Table 3.4. Characteristics of the selected rainfall events in the Maarkebeek, Bellebeek and Hunselbeek catchments for total rainfall (mm), peak discharges (m^3/s) and runoff volumes (mm).

		Maarkebeek	Bellebeek	Hunselbeek
No. of events	*Winter*	70	54	42
	Spring	28	31	21
	Summer	25	43	30
	Fall	42	36	31
	Total	***165***	***164***	***124***
Rainfall depth [mm]	*Min.*	1	6.3	2.2
	Max.	61.3	74.6	80.2
	Mean	18.0	19.9	21.3
	Stdev.	11.1	10.8	12.0
Measured peak discharge [m^3/s]	*Min.*	0.5	1.08	0.34
	Max.	14.6	12.3	4.35
	Mean	5.0	5.1	1.2
	Stdev.	3.3	2.4	0.9
Measured runoff volume [mm]	*Min.*	0.31	0.16	0.17
	Max.	21.0	18.72	23.2
	Mean	3.3	2.7	3.4
	Stdev.	3.5	3.0	3.8

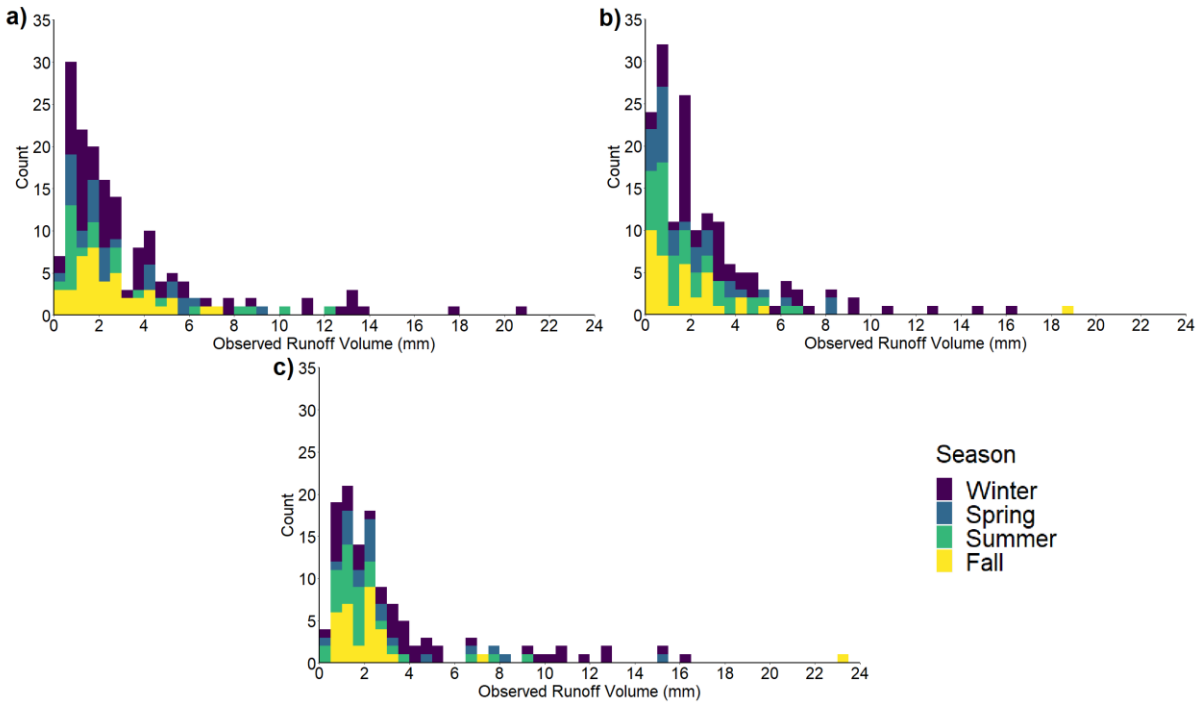

Figure 3.10. Histograms of the observed runoff volumes in the Maarkebeek (a), Bellebeek (b) and Hunselbeek (c) catchments.

3.3. Results

The simulations were run on a Dell Latitude laptop computer with an Intel Core i7 processor with 4 cores, 2.7 GHz CPU and 16 GB RAM. The average run-time of the assessed models was approximately 1 s and 3 s for respectively the Maarkebeek (48 km^2) and Bellebeek (88 km^2) catchments.

The NSE, rRMSE and NSE components *r*, α and β of the different RR-models in the three study areas are provided in resp. Table 3.5, Table 3.6, Table 3.7, Table 3.8 and Table 3.9. More models reached the adequate NSE threshold of 0.3 for the catchments of the Hunselbeek and Bellebeek than for the Maarkebeek catchment. The models performed best in the Hunselbeek catchment, with higher NSE values than the larger Bellebeek catchment. The results show that the performance of the default SCS-CN method was inadequate for all three catchments, with the rRMSE exceeding the mean of observed runoff volumes, and with negative NSE values in the Maarkebeek and Bellebeek catchments and a NSE of only 0.14 in the Hunselbeek catchment. The default SCS-CN method is also characterized by a low linear correlation *r*, especially in the Maarkebeek catchment with a value of 0.52. The values for α and β for the default SCS-CN method indicate a poor model representation of the variability and mean of the observed runoff volumes. The variability in observed runoff volume is underrepresented in the Maarkebeek catchment and is overestimated in the Bellebeek and Hunselbeek catchments, with α equal to resp. 0.80, 1.4 and 1.3. In addition, the values for β smaller than 1 indicate an underestimation of runoff volume by the default SCS-CN method in all three study areas, which is the largest underestimation in the Maarkebeek catchment (β = 0.34).

Model performance was highly influenced by the different AMC correction methods. Of the two AMC correction methods tested, the SWAT correction method (Neitsch et al., 2011) performed best. It generally performed better than equivalent models without AMC correction and outperformed the AMC correction NEMO method in the Bellebeek and Hunselbeek catchments. The NEMO method did not reach NSE of 0.3 in any model configuration and resulted in the highest RMSE values in the Bellebeek and Hunselbeek catchments, though the NEMO method generally has higher values for the linear correlation *r* than the SWAT method (Table 3.7). Compared to the models without AMC correction, values for α and β increase when implementing the NEMO method, leading to an overestimation of the runoff volume and its variability. Conversely, values for α and β are decreased by the implementation of SWAT AMC correction, resulting in values for α and β generally close to 1 in the Bellebeek and Hunselbeek catchments and leading to an underestimation (α and β < 1) in the Maarkebeek catchment.

Of the two alternative values for λ, the original 0.2 (USDA Natural Resource Conservation Service, 1986) and the alternative value 0.05 (Hawkins et al., 2001), the λ of 0.05 overall increased model performance, thereby underpinning the results of Woodward et al. (2003) that assigning λ a value of 0.05 provides a more appropriate estimation of the initial abstraction I_a in the SCS-CN method. The β values in Table 3.9 reflect a consistently higher β value for λ equal to 0.05, reflecting overall higher simulated runoff volumes.

The performance of the different re-infiltration methods were influenced by the choice in AMC correction method and λ value, though overall the Van Loo re-infiltration method outperformed the other methods, with more models having adequate to good NSE values. It is the only re-infiltration method to obtain good model performance in all three study catchments. The *P*-I_a re-infiltration method, deriving infiltration from rainfall and the SCS-CN variable I_a, only did not improve the model performance of the default SCS-CN. This method only produced adequate to good results for the Hunselbeek catchment when combined with the SWAT AMC correction. Though straightforward, with the least model parameters of the three infiltration methods, the proposed *P*-I_a method is also limited in its ability to adjust to specific conditions (e.g. overland flow velocity, seasonal variations). Overall, the Van Loo method outperformed the KSAT method, leading to higher NSE and linear correlation values. Implementing the re-infiltration of Van Loo also leads to consistently higher β values compared to the KSAT method. For both re-infiltration methods using Manning's equation, increasing the hydraulic radius R_h resulted in higher values for α and β. By incorporating the seasonality of vegetation

cover in Manning's *n* coefficients, model performance increased, as reflected by the NSE, rRMSE and linear correlation, with the increase in NSE higher for the Van Loo method. The impact of a seasonal Manning's *n* on NSE components α and β (Table 3.8 and Table 3.9) varied, however, the relative variation in these values indicate that the Van Loo re-infiltration method is more sensitive to the changes in Manning's *n* than the proposed KSAT alternative. A similar observation can be made for changes in hydraulic radius R_h, which is confirmed by the average sensitivity index $\bar{S}$ (Equation 3.17) for the changes in R_h, provided in Table 3.10. $\bar{S}$ is consistently higher for models implementing the Van Loo re-infiltration method than corresponding models implementing its KSAT variant. The Van Loo and KSAT re-infiltration methods derive infiltration by multiplying resp. I_{ori} and K_{SAT} values with the travel time over pixels. Whereas K_{SAT} values reach maxima of respectively 20.2 and 7 mm/hr in the Maarkebeek and Bellebeek catchments, I_{ORI} values can reach higher values, depending on CN parameters, rainfall amount and the incoming runoff. An equal perturbation in R_h and thus travel time will therefore result in higher runoff volume fluctuation in the Van Loo method.

Table 3.5. The NSE values of the different RR-models for the Maarkebeek, Bellebeek and Hunselbeek catchments for respectively 165, 164 and 124 rainfall events. Two AMC correction methods, NEMO and SWAT, were implemented and compared to the results obtained without AMC correction (CN_2). Two values for λ (0.2 or 0.05) were implemented in the models, as well as three different re-infiltration methods: SCS-CN parameter based re-infiltration ($P\text{-}I_a$), Van Loo (VL) and KSAT adjusted Van Loo (KSAT). For the latter two methods, three values for the hydraulic radius R_h of 1, 2 and 3 mm were tested (respectively R1, R2 and R3) and a seasonally adjusted Manning's roughness coefficient n was also implemented (VL* and KSAT*).

			Maarkebeek			Bellebeek			Hunselbeek		
			CN_2	NEMO	SWAT	CN_2	NEMO	SWAT	CN_2	NEMO	SWAT
λ=0.2	**Default**		-0.16			-0.28			0.14		
	$P\text{-}I_a$		-0.17	0.16	-0.25	-0.28	-1.08	0.25	0.14	-0.78	0.47
	VL	R1	-0.09	0.06	-0.18	-0.33	-1.32	0.20	0.04	-1.05	0.29
		R2	0.00	-0.57	0.23	-0.62	-2.43	0.31	-0.15	-2	0.46
		R3	-0.18	-1.23	0.33	-1.05	-3.45	0.24	-0.49	-2.82	0.45
	VL*	R1	0.23	0.24	0.00	-0.12	-1.37	0.35	0.18	-1.22	0.44
		R2	0.43	-0.28	0.43	-0.27	-2.30	0.53	0.01	-2.10	0.63
		R3	0.31	-0.88	0.58	-0.64	-3.18	0.51	-0.34	-2.84	0.59
	K_{SAT}	R1	-0.31	0.18	-0.31	-0.29	-0.64	0.29	0.10	-0.51	0.47
		R2	-0.27	0.18	-0.25	-0.29	-0.78	0.31	0.11	-0.60	0.49
		R3	-0.25	0.18	-0.22	-0.29	-0.84	0.32	0.12	-0.64	0.50
	K_{SAT}*	R1	-0.27	0.22	-0.29	-0.24	-0.62	0.31	0.12	-0.53	0.49
		R2	-0.24	0.21	-0.24	-0.26	-0.76	0.33	0.13	-0.61	0.50
		R3	-0.23	0.20	-0.21	-0.27	-0.82	0.34	0.13	-0.65	0.51
λ=0.05	$P\text{-}I_a$		0.09	-0.55	0.06	-0.12	-3.02	0.33	0.26	-2.15	0.56
	VL	R1	0.02	-0.55	-0.12	-0.04	-3.01	0.22	0.24	-2.25	0.26
		R2	0.14	-1.70	0.24	-0.28	-4.56	0.34	0.11	-3.50	0.47
		R3	-0.03	-2.64	0.33	-0.68	-5.87	0.30	-0.20	-4.51	0.50
	VL*	R1	0.29	-0.38	0.05	0.16	-3.06	0.36	0.38	-2.44	0.40
		R2	0.50	-1.35	0.44	0.06	-4.33	0.56	0.27	-3.54	0.64
		R3	0.41	-2.21	0.57	-0.28	-5.47	0.56	-0.04	-4.44	0.66
	K_{SAT}	R1	-0.09	-0.23	-0.15	-0.08	-2.10	0.30	0.27	-1.64	0.51
		R2	-0.04	-0.33	-0.08	-0.09	-2.39	0.32	0.27	-1.81	0.53
		R3	-0.01	-0.37	-0.05	-0.09	-2.52	0.32	0.27	-1.89	0.54
	K_{SAT}*	R1	-0.04	-0.17	-0.12	-0.03	-2.05	0.34	0.29	-1.65	0.53
		R2	0.00	-0.29	-0.06	-0.05	-2.36	0.34	0.29	-1.82	0.54
		R3	0.02	-0.34	-0.03	-0.06	-2.49	0.34	0.28	-1.89	0.55

Table 3.6. The relative RMSE (%) values of the different RR-models for the Maarkebeek, Bellebeek and Hunselbeek catchments for respectively 165, 164 and 124 rainfall events. Mean observed runoff volumes correspond to resp. 3.3, 2.7 and 3.4 mm in the Maarkebeek, Bellebeek and Hunselbeek catchments.

			Maarkebeek			Bellebeek			Hunselbeek		
			CN_2	*NEMO*	*SWAT*	CN_2	*NEMO*	*SWAT*	CN_2	*NEMO*	*SWAT*
λ=0.2	***Default***		113			124			104	0	0
	$P\text{-}I_a$		113	96	117	124	158	95	105	150	82
	VL	*R1*	110	102	114	126	167	98	110	161	95
		R2	105	131	92	139	203	91	121	195	82
		R3	114	157	86	157	231	95	137	220	84
	*VL**	*R1*	92	92	105	116	169	88	102	168	84
		R2	79	118	79	123	199	75	112	198	68
		R3	87	143	68	140	224	77	130	221	72
	K_{SAT}	*R1*	120	95	120	124	140	93	107	139	82
		R2	118	95	117	124	146	91	106	142	80
		R3	117	95	116	124	149	90	106	144	79
	K_{SAT}*	*R1*	118	92	119	122	139	91	106	139	81
		R2	117	93	116	123	145	90	105	143	79
		R3	116	94	115	123	148	89	105	144	79
λ=0.05	$P\text{-}I_a$		100	130	102	116	220	90	96	200	75
	VL	*R1*	104	130	111	111	219	97	98	203	97
		R2	97	172	91	124	258	89	106	239	82
		R3	106	200	86	142	287	91	123	264	80
	*VL**	*R1*	88	123	102	100	220	88	89	209	87
		R2	74	161	78	106	253	73	96	240	68
		R3	81	188	68	124	279	73	115	262	66
	K_{SAT}	*R1*	109	116	112	114	193	91	96	183	79
		R2	107	121	109	114	201	90	96	189	77
		R3	105	123	107	114	206	90	96	191	76
	K_{SAT}*	*R1*	107	113	111	111	191	89	95	183	77
		R2	105	119	108	112	200	89	95	189	76
		R3	104	122	106	113	205	89	95	191	76

Table 3.7. The linear correlation *r* of the different RR-models for the Maarkebeek, Bellebeek and Hunselbeek catchments for respectively 165, 164 and 124 rainfall events.

			Maarkebeek			Bellebeek			Hunselbeek		
			CN_2	*NEMO*	*SWAT*	CN_2	*NEMO*	*SWAT*	CN_2	*NEMO*	*SWAT*
λ=0.2	***Default***		0.52			0.62			0.73		
	$P\text{-}I_a$		0.52	0.70	0.58	0.62	0.82	0.70	0.73	0.88	0.80
	VL	*R1*	0.51	0.69	0.61	0.58	0.82	0.66	0.69	0.88	0.74
		R2	0.56	0.70	0.62	0.62	0.81	0.68	0.73	0.87	0.77
		R3	0.58	0.70	0.63	0.64	0.81	0.69	0.74	0.87	0.78
	*VL**	*R1*	0.70	0.75	0.82	0.65	0.84	0.74	0.75	0.89	0.82
		R2	0.71	0.75	0.80	0.70	0.84	0.79	0.79	0.88	0.85
		R3	0.70	0.74	0.78	0.72	0.84	0.79	0.80	0.88	0.85
	K_{SAT}	*R1*	0.48	0.69	0.56	0.60	0.81	0.69	0.72	0.88	0.79
		R2	0.49	0.70	0.58	0.61	0.82	0.69	0.72	0.88	0.79
		R3	0.50	0.70	0.58	0.61	0.82	0.70	0.73	0.88	0.79
	K_{SAT}*	*R1*	0.50	0.70	0.60	0.61	0.82	0.70	0.73	0.88	0.79
		R2	0.51	0.70	0.60	0.62	0.82	0.70	0.73	0.88	0.79
		R3	0.51	0.70	0.60	0.62	0.82	0.70	0.73	0.88	0.79
λ=0.05	$P\text{-}I_a$		0.57	0.70	0.61	0.65	0.80	0.70	0.74	0.87	0.79
	VL	*R1*	0.54	0.70	0.61	0.60	0.81	0.65	0.69	0.87	0.73
		R2	0.57	0.70	0.61	0.63	0.80	0.67	0.73	0.87	0.75
		R3	0.58	0.69	0.62	0.64	0.80	0.68	0.74	0.86	0.77
	*VL**	*R1*	0.74	0.75	0.80	0.67	0.83	0.74	0.76	0.88	0.81
		R2	0.73	0.74	0.79	0.72	0.83	0.78	0.80	0.88	0.84
		R3	0.72	0.74	0.77	0.73	0.83	0.79	0.80	0.87	0.85
	K_{SAT}	*R1*	0.54	0.70	0.58	0.63	0.80	0.69	0.74	0.87	0.78
		R2	0.55	0.70	0.59	0.64	0.80	0.69	0.74	0.87	0.79
		R3	0.56	0.70	0.59	0.64	0.80	0.69	0.74	0.87	0.79
	K_{SAT}*	*R1*	0.57	0.71	0.61	0.65	0.81	0.70	0.75	0.87	0.79
		R2	0.57	0.71	0.61	0.65	0.81	0.70	0.75	0.87	0.79
		R3	0.57	0.70	0.61	0.65	0.81	0.70	0.75	0.87	0.79

Table 3.8. The error in variability α of the different RR-models for the Maarkebeek, Bellebeek and Hunselbeek catchments for respectively 165, 164 and 124 rainfall events.

			Maarkebeek			Bellebeek			Hunselbeek		
			CN_2	NEMO	SWAT	CN_2	NEMO	SWAT	CN_2	NEMO	SWAT
λ=0.2	***Default***		0.80			1.41			1.34		
	$P\text{-}I_a$		0.80	1.28	0.48	1.42	2.00	1.07	1.34	1.96	1.05
	VL	R1	0.75	1.34	0.34	1.37	2.11	0.74	1.30	2.11	0.73
		R2	1.08	1.61	0.63	1.62	2.30	0.98	1.55	2.26	1.00
		R3	1.28	1.76	0.82	1.79	2.41	1.17	1.71	2.34	1.19
	VL*	R1	0.65	1.32	0.33	1.36	2.14	0.74	1.33	2.16	0.77
		R2	0.93	1.54	0.55	1.57	2.31	0.95	1.56	2.30	1.02
		R3	1.12	1.67	0.72	1.74	2.41	1.13	1.72	2.38	1.21
	K_{SAT}	R1	0.72	1.20	0.41	1.33	1.90	0.97	1.29	1.92	0.97
		R2	0.75	1.23	0.43	1.36	1.93	0.99	1.31	1.94	0.99
		R3	0.76	1.24	0.44	1.37	1.95	1.00	1.32	1.94	0.99
	K_{SAT}*	R1	0.69	1.19	0.39	1.31	1.90	0.96	1.29	1.93	0.97
		R2	0.73	1.22	0.42	1.35	1.94	0.99	1.31	1.94	0.99
		R3	0.75	1.24	0.43	1.37	1.95	1.00	1.32	1.95	0.99
λ=0.05	$P\text{-}I_a$		0.84	1.54	0.60	1.37	2.22	1.10	1.28	2.10	1.04
	VL	R1	0.65	1.62	0.36	1.18	2.38	0.66	1.11	2.29	0.62
		R2	0.98	1.86	0.62	1.44	2.54	0.88	1.38	2.41	0.87
		R3	1.18	1.99	0.81	1.62	2.64	1.07	1.55	2.47	1.06
	VL*	R1	0.58	1.59	0.35	1.18	2.41	0.66	1.15	2.34	0.65
		R2	0.84	1.78	0.55	1.40	2.54	0.86	1.39	2.45	0.89
		R3	1.03	1.90	0.70	1.57	2.63	1.03	1.56	2.51	1.08
	K_{SAT}	R1	0.77	1.49	0.52	1.30	2.16	1.02	1.25	2.08	1.00
		R2	0.80	1.52	0.55	1.33	2.19	1.05	1.27	2.09	1.01
		R3	0.81	1.53	0.56	1.34	2.20	1.06	1.27	2.10	1.02
	K_{SAT}*	R1	0.74	1.48	0.50	1.29	2.16	1.01	1.25	2.09	1.00
		R2	0.78	1.51	0.53	1.33	2.19	1.04	1.27	2.10	1.01
		R3	0.80	1.52	0.55	1.34	2.20	1.06	1.27	2.10	1.02

Table 3.9. The bias term β of the different RR-models for the Maarkebeek, Bellebeek and Hunselbeek catchments for respectively 165, 164 and 124 rainfall events.

			Maarkebeek			Bellebeek			Hunselbeek		
			CN_2	NEMO	SWAT	CN_2	NEMO	SWAT	CN_2	NEMO	SWAT
λ=0.2	**Default**		0.38			0.79			0.82		
	$P\text{-}I_a$		0.37	1.00	0.21	0.78	1.66	0.63	0.82	1.69	0.63
	VL	R1	0.43	1.01	0.28	0.73	1.62	0.47	0.71	1.62	0.43
		R2	0.82	1.49	0.59	1.09	2.04	0.73	1.08	2.03	0.69
		R3	1.11	1.80	0.83	1.40	2.36	0.97	1.39	2.33	0.94
	VL*	R1	0.47	1.07	0.31	0.76	1.66	0.50	0.77	1.69	0.48
		R2	0.83	1.50	0.60	1.08	2.02	0.74	1.11	2.04	0.74
		R3	1.11	1.79	0.83	1.36	2.30	0.96	1.40	2.31	0.97
	K_{SAT}	R1	0.27	0.78	0.19	0.62	1.39	0.63	0.67	1.49	0.63
		R2	0.30	0.85	0.22	0.66	1.48	0.68	0.71	1.56	0.67
		R3	0.31	0.88	0.23	0.68	1.52	0.71	0.73	1.59	0.69
	K_{SAT}*	R1	0.27	0.78	0.19	0.61	1.39	0.63	0.67	1.49	0.63
		R2	0.30	0.85	0.21	0.66	1.47	0.68	0.71	1.56	0.67
		R3	0.31	0.88	0.23	0.68	1.51	0.70	0.73	1.59	0.69
λ=0.05	$P\text{-}I_a$		0.58	1.59	0.41	1.08	2.42	0.96	1.07	2.31	0.91
	VL	R1	0.47	1.46	0.32	0.76	2.20	0.50	0.71	2.12	0.43
		R2	0.84	1.95	0.62	1.10	2.63	0.74	1.05	2.53	0.67
		R3	1.12	2.25	0.86	1.40	2.95	0.97	1.36	2.82	0.91
	VL*	R1	0.50	1.52	0.35	0.79	2.24	0.52	0.76	2.17	0.47
		R2	0.85	1.95	0.63	1.10	2.59	0.75	1.09	2.51	0.71
		R3	1.11	2.24	0.86	1.37	2.87	0.96	1.37	2.77	0.94
	K_{SAT}	R1	0.40	1.30	0.28	0.81	2.04	0.74	0.86	2.07	0.74
		R2	0.44	1.40	0.32	0.89	2.16	0.81	0.93	2.15	0.79
		R3	0.47	1.44	0.34	0.92	2.21	0.84	0.96	2.19	0.82
	K_{SAT}*	R1	0.39	1.30	0.28	0.80	2.03	0.74	0.86	2.06	0.74
		R2	0.44	1.40	0.32	0.88	2.15	0.80	0.92	2.15	0.79
		R3	0.47	1.44	0.34	0.91	2.20	0.83	0.95	2.18	0.81

Table 3.10. The average sensitivity index $\bar{S}$ for changes in the hydraulic radius R_h in Manning's equation, implemented in the re-infiltration methods of Van Loo (2018) (VL) and its variant using K_{SAT} (KSAT) with standard Manning's roughness coefficients n and seasonally adjusted Manning's n (VL* and K_{SAT}*).

	Maarkebeek			Bellebeek			Hunselbeek		
λ=0.2	CN_2	NEMO	SWAT	CN_2	NEMO	SWAT	CN_2	NEMO	SWAT
$\bar{S}$(VL)	0.07	0.64	0.33	0.42	0.61	0.11	0.34	1.84	0.25
$\bar{S}$(VL*)	0.12	0.54	0.36	0.41	1.84	0.26	0.43	1.69	0.27
$\bar{S}$(KSAT)	0.04	0.00	0.05	0.00	0.24	0.04	0.02	0.16	0.04
$\bar{S}$(KSAT*)	0.03	0.01	0.05	0.04	0.24	0.04	0.02	0.14	0.02
λ=0.05	CN_2	NEMO	SWAT	CN_2	NEMO	SWAT	CN_2	NEMO	SWAT
$\bar{S}$(VL)	0.07	1.10	0.29	0.32	0.50	0.11	0.35	2.38	0.33
$\bar{S}$(VL*)	0.14	0.94	0.33	0.32	2.48	0.30	0.32	2.10	0.37
$\bar{S}$(KSAT)	0.05	0.09	0.06	0.02	0.50	0.03	0.00	0.30	0.04
$\bar{S}$(KSAT*)	0.04	0.10	0.05	0.04	0.53	0.00	0.00	0.29	0.02

In Figure 3.11, the influence of the AMC correction methods and λ value, in combination with the re-infiltration method using SCS-CN parameters (P-I_a), is visualized through log-log scatterplots for the Bellebeek catchment. This figure illustrates that the NEMO AMC correction leads to an overestimation of runoff volumes, while a more conservative correction is implemented by the SWAT AMC correction method. Figure 3.11 shows an overestimation of runoff volume in two summer events, characterized by an average rainfall per pixel exceeding 70 mm. This overestimation is reduced by the SWAT AMC correction. The 0.05 λ value resulted in an increase in runoff volumes, as can be seen in Figure 3.11. The combination of a λ of 0.05 and the NEMO correction thus leads to a higher overestimation of runoff volumes, reflected in a decrease in NSE and increase in rRMSE, as reflected in Table 3.5 and Table 3.6.

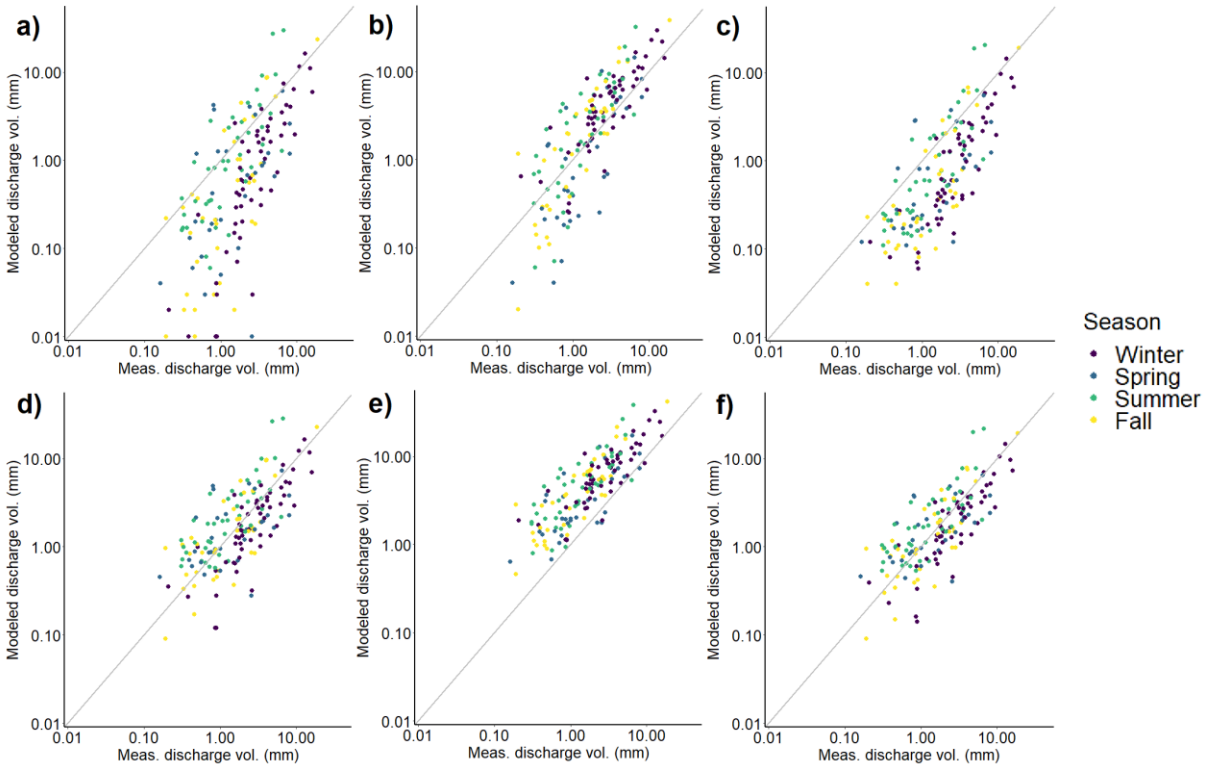

Figure 3.11. Plots of the modeled and measured (meas.) discharge volumes (vol.) in mm at the outlet of the Bellebeek catchment for the RR-models implementing the re-infiltration method using SCS-CN parameters (P-I_a) (a: λ = 0.2, no AMC correction; b: λ = 0.2, NEMO AMC correction; c: λ = 0.2, SWAT AMC correction; d: λ = 0.05, no AMC correction; e: λ = 0.05, NEMO AMC correction; f: λ = 0.05, SWAT AMC correction).

The RR-models implementing the Van Loo and KSAT re-infiltration methods are visualized for the Bellebeek catchment in resp. Figure 3.12 and Figure 3.13. The results in Table 3.5, Table 3.6 and Table 3.7 show a better model performance of RR-model configurations implementing Van Loo re-infiltration (Figure 3.12), reflected by less scattering in the plots compared to the P-I_a (Figure 3.11) and KSAT methods (Figure 3.13). Both re-infiltration methods were tested with hydraulic radius R_h values of 1 mm (Figure 3.12a/c, Figure 3.13a/c), 2 mm and 3 mm (Figure 3.12/d, Figure 3.13b/d) and a seasonally adjusted Manning's n (Figure 3.12c/d, Figure 3.13c/d). The higher sensitivity to variations in R_h of the Van Loo method (Table 3.10) is exemplified by comparing the increase in runoff volume from Figure 3.12a/c to Figure 3.12b/d and from Figure 3.13a/c to Figure 3.13b/d: the increase is higher for the Van Loo method. This is also reflected in a higher variation in α and β values in Table 3.8 and Table 3.9.

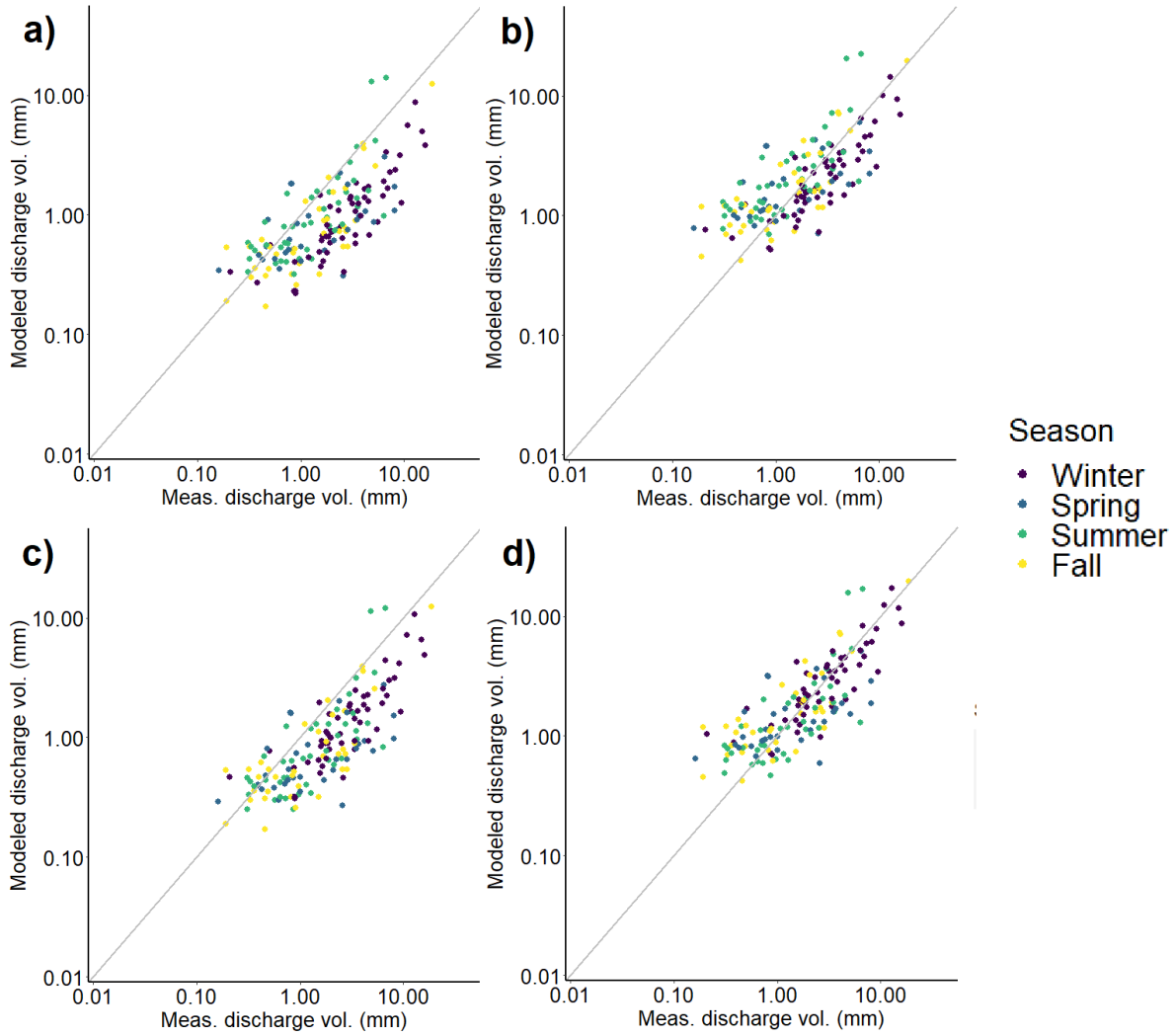

Figure 3.12. Log-log plots of the modeled and measured (meas.) discharge volumes (vol.) in mm at the outlet of the Bellebeek catchment for the RR-models implementing the re-infiltration method of Van Loo (2018) with SWAT AMC correction and a λ of 0.05 (a) R_h = 1 mm, standard Manning's *n*; b) R_h = 3 mm, constant Manning's *n*; c) R_h = 1 mm, seasonally adjusted Manning's *n*; d) R_h = 3 mm, seasonally adjusted Manning's *n*).

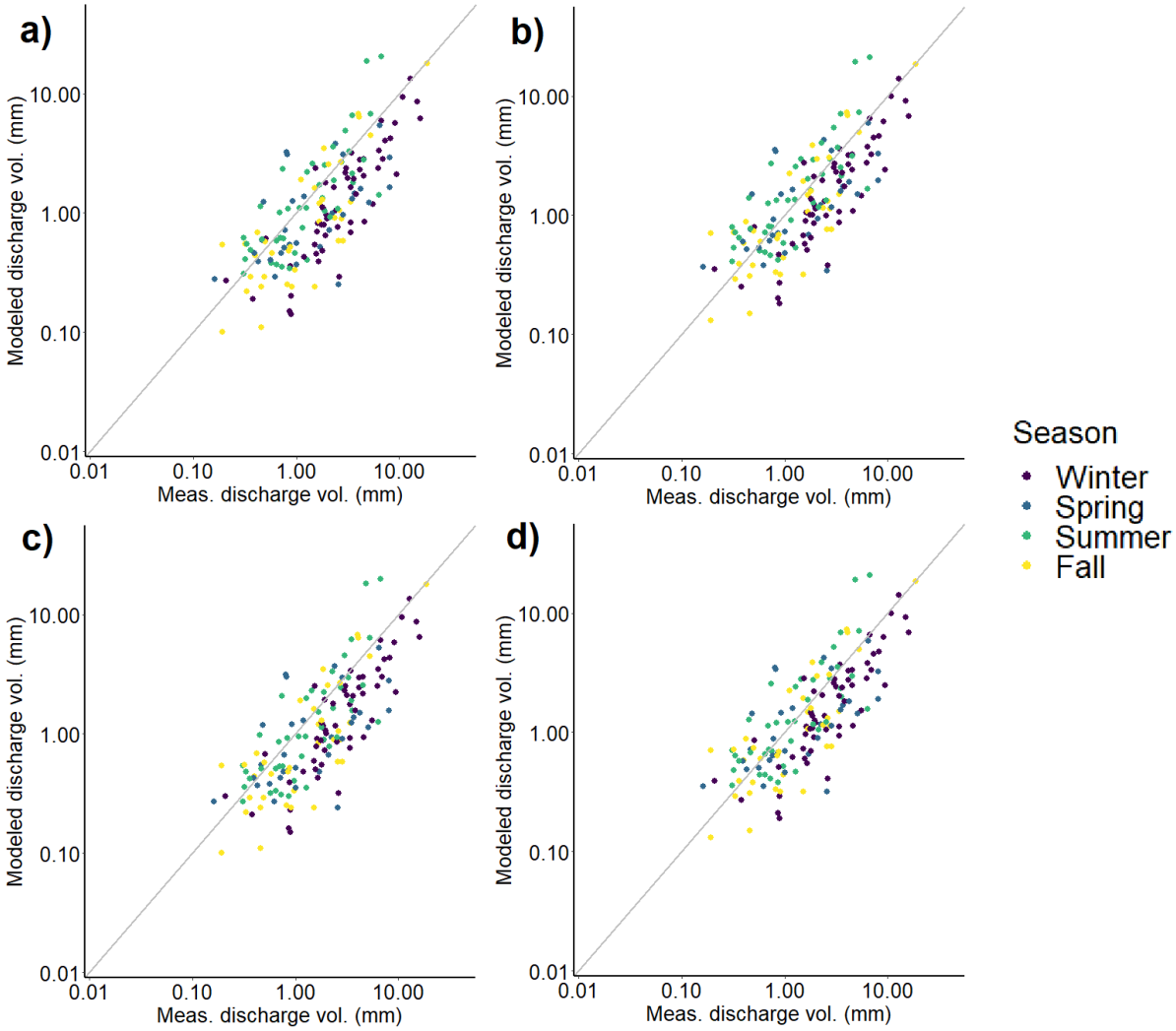

Figure 3.13. Log-log plots of the modeled and measured (meas.) discharge volumes (vol.) in mm at the outlet of the Bellebeek catchment for the RR-models implementing the re-infiltration method using the saturated hydraulic conductivity KSAT with SWAT AMC correction and a λ of 0.05 (a) R_h = 1 mm, constant Manning's n; b) R_h = 3 mm, standard Manning's n; c) R_h = 1 mm, seasonally adjusted Manning's n; d) R_h = 3 mm, seasonally adjusted Manning's n).

Consequently, the only model configurations reaching a good performance with NSE values of at least 0.5 in all three study areas were combinations of the SWAT AMC correction and Van Loo re-infiltration method, with R_h equaling 3 mm and a seasonally adjusted Manning's n. These configurations reached good model performance for both λ values, however, the λ of 0.05 resulted in higher NSE values in the Bellebeek and Hunselbeek catchments, namely NSE values of resp. 0.57, 0.56 and 0.66 with corresponding RMSE values of 2.26 mm, 1.96 mm and 2.25 mm. These RMSE values represent resp. 68%, 73% and 66% of the mean observed runoff volumes in the catchments. The scatterplots of this model configuration with a λ of 0.05 are provided for the three study catchments in Figure 3.14. These plots mainly show scattering, and errors, mainly at lower runoff volumes.

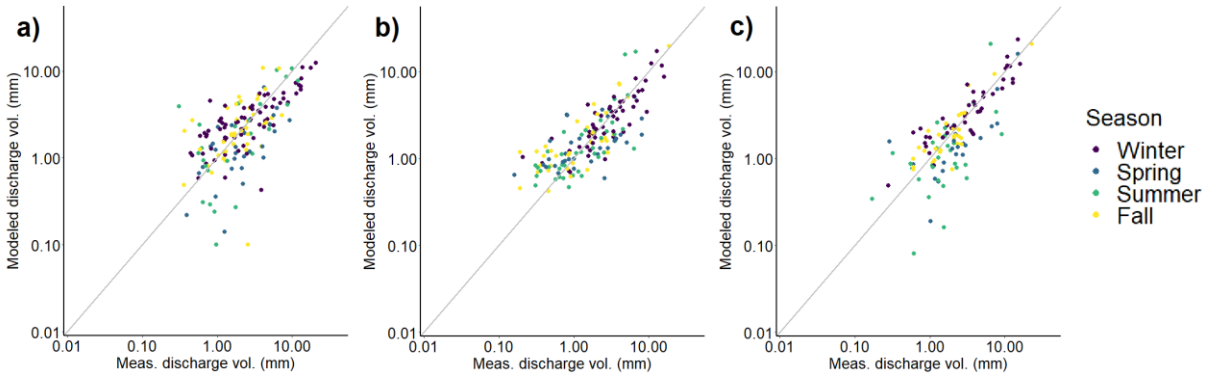

Figure 3.14. Log-log plot of modeled and measured (meas.) discharge volumes (vol.) at the outlets of the (a) Maarkebeek, (b) Bellebeek, and (c) Hunselbeek catchments for the model configuration implementing the Van Loo re-infiltration method with a hydraulic radius R_h of 3 mm and Manning's coefficient n with a seasonal adjustment, a λ of 0.05 and SWAT AMC correction (NSE of resp. 0.57, 0.56 and 0.66).

3.4. Discussion

An event-based RR-model was conceptualized based on the SCS-CN method with the objective to integrate this model in an iterative optimization procedure, evaluating the hydrological impact of land use changes in a downstream area of interest. For this purpose, eighteen RR-model configurations were evaluated in three study areas. These model configurations simulate the relationship between rainfall and runoff in a spatially explicit way, with a spatial resolution of 50 m, appropriate for assessing land use changes, and taking into account spatial interaction along the flow path using re-infiltration schemes. In addition, the RR-model configurations are each computationally efficient, thereby allowing a large number of model simulations to be performed in the context of the optimization framework.

The simulated runoff volumes from the eighteen model configurations were evaluated in the Maarkebeek, Bellebeek and Hunselbeek catchments for resp. 165, 164 and 124 rainfall events. For these rainfall events, observed runoff volumes were derived from discharge measurements at the outlets of the catchments by separating direct runoff and baseflow using the constant-slope method (McCuen, 1998). It is thereby assumed that only overland flow contributes to direct runoff, however, other inputs will also contribute to the direct runoff, including inputs from urban and agricultural drainage systems. Especially the contribution of agricultural drainage in the flat, wet terrains of the Bellebeek could provide a large contribution to the direct runoff. More sophisticated approach to separate baseflow and direct runoff may provide a better division between both types of flows, e.g. recursive digital filter approaches (Eckhardt, 2005). The choice of baseflow separation technique, and the associated uncertainty regarding the derived direct runoff, therefore also influences the model evaluations and choice of best performing model.

Two approaches were implemented in the model configurations to adjust CN values to antecedent soil moisture conditions: the method implemented in the SWAT model (Neitsch et al., 2011) and the method formulated by (Chow et al., 1988) and implemented in the BUDGET-model (Raes et al., 2006) and in ArcNEMO (Van Opstal et al., 2014). Daily soil water balance simulations from ArcNEMO were used to derive the antecedent soil moisture conditions required to adjust the CN values. However, this implies to a degree a circular reasoning as ArcNEMO was used to calculate the AMC values and the NEMO AMC method was also evaluated in the model configurations. Moreover, ArcNEMO was developed to model nutrient emissions to rivers, therefore the validation of the hydrological components of ArcNEMO was focused on the simulation of discharge into the river system rather than the simulation of the soil water balance (Van Opstal et al., 2014). For future reference, it would

therefore be preferred to implement the AMC methods using observed soil moisture conditions derived from remote sensing (Minet et al., 2010).

Model performance was evaluated using the NSE, with a NSE value of 0.5 set as a threshold to indicate a sufficiently good model performance. However, a higher threshold value, e.g. of 0.8 (Ritter & Muñoz-Carpena, 2013), is typically applied to indicate good model performance. However, given its specific application purpose in an iterative optimization approach, the emphasis is on a relative comparison of land use changes in alternative locations rather than an absolute representation of runoff volume, a lower NSE threshold was tolerated (Volk et al., 2010; Yeo & Guldmann, 2010).

The RR-model configurations leading to the highest NSE values combines the SWAT AMC method, a λ value of 0.05 and the re-infiltration method of Van Loo (2018) with a seasonally adjusted Manning's roughness coefficient *n*. This model configuration results in NSE values of resp. 0.57, 0.56 and 0.66 in the Maarkebeek, Bellebeek and Hunselbeek. However, the developed RR-model is highly empirical, not accounting for the physical soil and hydrological processes, but rather approximating these processes with model parameters CN_2 and manning's *n* derived from look-up tables. Consequently, the implementation of an alternative AMC or re-infiltration method may compensate or exacerbate inadequate representation of these parameters. The results of the SCS-CN model configurations show that a default implementation of the SCS-CN method leads to an underestimation in the three study areas, with a relatively larger underestimation in the Maarkebeek catchment. Implementing the AMC correction method of NEMO increases the simulated runoff volume, whereas the SWAT AMC correction leads to a decrease in runoff volume, which is also reflected in the comparison of both methods in Figure 3.3 and in the β values in Table 3.9. Therefore, the NEMO AMC method performs relatively better in the Maarkebeek catchment than in the Bellebeek and Hunselbeek catchments (Table 3.5). The model configurations with a λ value of 0.05 simulate an overall higher runoff volume than those configurations with a λ value of 0.2, as the assumption that λ value equals 0.05 lowers the initial abstraction in Equation 3.3. A combination of the λ value of 0.05 and the NEMO AMC correction method thus leads to an overestimation of runoff volumes (Table 3.9), whereas a combination of λ equaling 0.05 with the SWAT AMC method compensates for the latter's lowering of runoff volumes. The re-infiltration method of Van Loo (2018) can simulate higher runoff volumes than the default CN_2 method, as infiltration is assessed based on the travel time of overland flow. As such, an increase in hydraulic radius R_h decreases re-infiltration and can thus compensate for the underestimation of runoff volume in the default SCS-CN method. Conversely, the KSAT method considers re-infiltration independent from the infiltration of the SCS-CN method and thus lowers the runoff volumes from the default SCS-CN method. These findings are an indication of the issue of equifinality, where the same output can be obtained with different combinations of multiple parameter values (Beven, 2006). This issue is exacerbated by the lack of full calibration and validation of the RR-model. Consequently, it is important to note that no absolute conclusion can be drawn from this study regarding the performance of methods. Rather, the Van Loo–SWAT configuration with λ equaling 0.05 is found to perform best in the Maarkebeek, Bellebeek and Hunselbeek catchments given the initial choice of parameters. To draw more general conclusions, a more extensive calibration, validation and sensitivity analysis is required, based on more catchments.

The limited sensitivity analysis presented in Table 3.10 shows that the Van Loo re-infiltration method is sensitive to variations in the hydraulic radius R_h. To limit the RR-model complexity and maintain its efficiency, the hydraulic radius R_h was assumed constant and uniform across the catchments. Three values for R_h were assessed in the conceptualization of the RR-model, which ranged between 1 mm and 3 mm. By assuming constant values for R_h, the runoff rate determined in the Manning's equation is dependent on a pixel's soil roughness, as represented by Manning's *n,* and its slope. Increasing the

value for R_h in the RR-models will thus increase the runoff rate and, correspondingly, the simulated runoff volumes. The β values smaller than one corresponding to the RR-models implementing a value of R_h of 1 mm indicate that this value underestimates the hydraulic radius. This is also reflected by field data measurements collected by Knapen et al. (2009) of the hydraulic radius, which ranged between 4 to 15 mm for conventionally tilled field plots without vegetation residue. As the sensitivity analysis of R_h indicates that the RR-model implementing the re-infiltration scheme of Van Loo (2018) is sensitive to variations in R_h (Table 3.10), a more extensive calibration and validation is required for this model parameter, evaluating a wider range of higher values for R_h on an independent set of observations. Alternatively, the approach proposed by Liu et al. (2003), using a power relationship to relate the hydraulic radius and the upstream area of a pixel, could also be evaluated, as this approach would make the values of R_h less arbitrary.

The Van Loo re-infiltration method is also more sensitive to variations in Manning's roughness coefficient *n*, as reflected in Table 3.5–Table 3.9. This variation is illustrated per season in Figure 3.15. This figure illustrates the impact of the seasonal adjustments to Manning's *n* (Table 3.3), increasing runoff volume in winter and decreasing it in spring and summer, which improves model performance especially in winter and summer, as reflected in the NSE values. Though this is congruent with the findings of Fu et al. (2019) that Manning's *n* is affected by vegetation cover, these overall seasonal variations in runoff volume may not necessarily reflect solely variations in vegetation cover. Soil structure also influences Manning's *n* and thus seasonal agricultural practices impacting soil structure, such as tillage, will also influence runoff generation, overland flow and re-infiltration processes (Gabriel et al., 2019; Maetens et al., 2012). For instance, variations in soil structure and tillage practices can lead to preferential flow paths (Appels et al., 2011), the effect of which are not considered in the RR-model configurations. Moreover, vegetation cover in arable fields also depends on the crop type, e.g. maize stalks provide minimal cover to the soil and will contribute minimally to an increase in Manning's *n*. Correspondingly, an increase in Manning's *n* in summer in forests reflects an increase in undergrowth, however, an increase in the litter layer in fall can also justify the implementation of a higher Manning's *n* in this season. Consequently, the seasonal variations in Manning's *n* implemented in this study (Table 3.3) are too coarse to take into consideration these spatial variations. A more extensive literature review, including data from field trials, and a sensitivity analysis should be carried out to further refine these adjustments in Manning's *n* to incorporate seasonal variations in vegetation cover and soil structure.

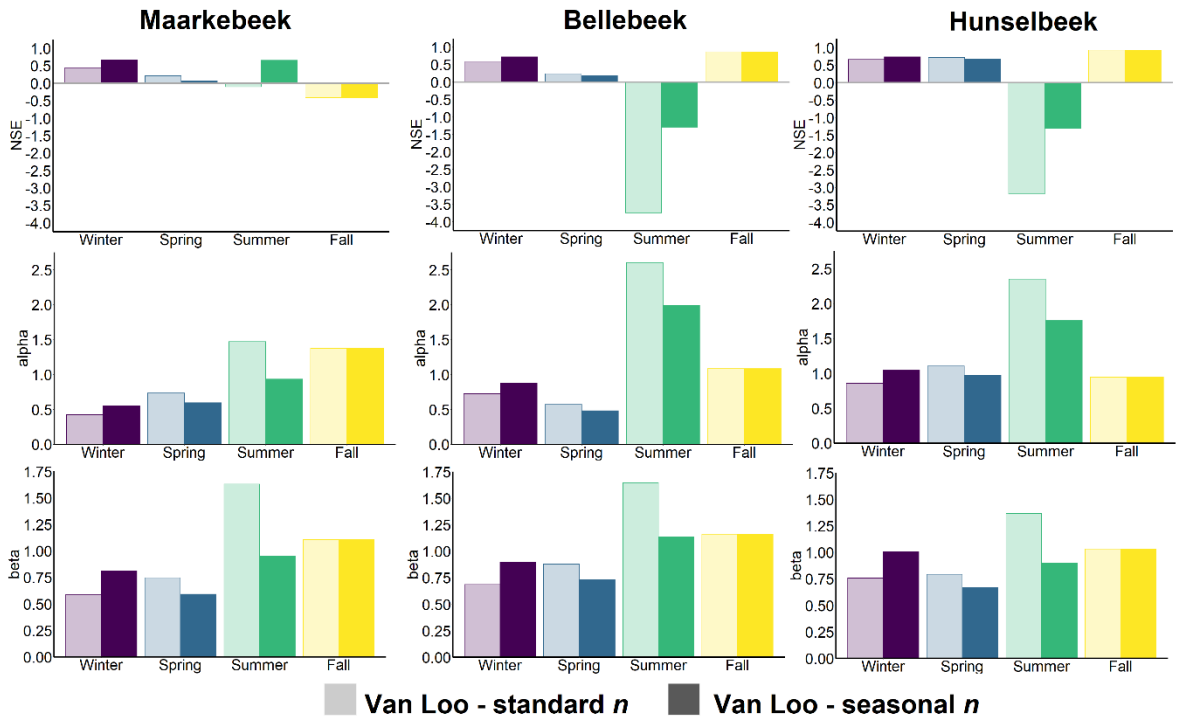

Figure 3.15. Impact of implementing a seasonally variable Manning's roughness coefficient *n* in the re-infiltration method of Van Loo (2018) on the value of NSE, and its components α (alpha) and β (beta).

Alternative to the empirical approach followed in this study, a more physics-based modeling approach could be followed. For instance, a commonly implemented physics-based approach to model infiltration into the soil is according to Green & Ampt (1911), which has been extended into several variations adding flexibility to the model (Kale & Sahoo, 2011), e.g. modeling infiltration during a temporally varying rainfall event (Chu, 1978) and accounting for soil crusting and compaction (Rawls et al., 1990). As such, the modeling of land use changes may become less arbitrary, however, such physics-based approaches are often numerically complex and thus computationally more demanding.

A number of alternative RR-models implement physical-based approaches to assess the impact of land use changes on catchment hydrology. Three interesting models are highlighted here and compared to the RR-model conceptualized in this study.

STREAM (Spatial Tools for River basins, Environment and Analysis of Management options) (Aerts et al., 1999) is a spatially distributed, raster-based RR-model used to model the impact of land use change on river basin hydrology. It has been applied from a global scale to more regional assessments, e.g. to model the sensitivity of the Meuse river discharge to climate change (Ward, Renssen, et al., 2011). STREAM provides continuous simulations of runoff, groundwater storage, and snow cover and melt based on the soil water balance model of Thornthwaite & Mather (1957). Runoff routing is modeled using a DEM, however, no spatial interaction in the form of re-infiltration is taken into account. Moreover, STREAM assesses land use changes on a larger spatial resolution, ranging from 1x1 km to 7x7 km (Aerts et al., 1999).

LISFLOOD is a spatially distributed hydrological model, developed to simulate hydrological processes in large European river catchments and to assess the impact of river regulation measures and land use changes. It is a continuous model simulating hydrological processes with a flexible time-step. As it is designed for larger river basins, its recommended spatial resolution ranges from 10–100 km (van der Knijff et al., 2010).

Another interesting physically-based modeling approach is represented by OpenLISEM, a spatially distributed hydrological model. OpenLISEM is an event-based model, designed for disaster risk management to simulate the hydrological impact of detailed land use changes and land management decisions. This model simulates infiltration, sediment dynamics and overland flow, including surface ponding and channel flooding, in catchments ranging in size from smaller than 1 km² to several 100 km². Its spatial resolution is flexible, but required to be smaller than 100 m. For instance, Bout & Jetten (2018) implemented OpenLISEM with a resolution of 40 m and 80 m to study flash floods in three study areas. As such, OpenLISEM provides an interesting physics-based alternative to the RR-model configurations presented in this study. However, its high model complexity and corresponding long run-times for simulations makes it less suitable for applications in optimization approaches.

3.5. Conclusion

The aim of this study was to develop a computationally efficient, spatially distributed RR-model, taking into account overland flow routing and re-infiltration along the flow paths, for use in applications requiring iterative optimization, e.g. for determining spatially explicit land use distributions that minimize flood hazard. Several configurations of the widely used SCS-CN-model were tested whereby the configurations differed in AMC correction method, re-infiltration algorithm, and values for λ, R_h and Manning's n. Since few re-infiltration algorithms have been proposed based on the SCS-CN method, two alternative approaches were proposed and tested in addition to the method implemented by Van Loo (Van Loo, 2018). The model configurations were used to simulate event-based runoff volumes in three catchments in Flanders, Belgium: the Maarkebeek catchment (48 km²), Bellebeek catchment (88 km²) and its subcatchment of the Hunselbeek (21.5 km²). To evaluate model performance, NSE values were calculated for respectively 165, 164 and 124 rainfall events in these catchments. The results indicated higher NSE values for a λ value of 0.05 (Woodward et al., 2003), the AMC correction method implemented in the SWAT model (Neitsch et al., 2011), and the re-infiltration method proposed by Van Loo (2018), taking into account overland flow velocity with a hydraulic radius R_h of 3 mm and Manning's roughness coefficients n adjusted to seasonal variations in vegetation cover. This SCS-CN-model configuration achieved NSE values of 0.57, 0.56 and 0.66 in the three studied catchments, which was deemed sufficiently accurate to assess and compare the hydrological impacts of land use alternatives. However, a full calibration and validation of the RR-model is lacking, and a high level of uncertainty is thus connected to the parameters implemented in the RR-model. As such, the conclusion that the RR-model configuration of Van Loo–SWAT with a λ value of 0.05 is not an absolute finding. However, the conceptualized RR-model is able to assess hydrological impacts in a computationally efficient and spatially explicit way, allowing for spatial interaction through re-infiltration. Given the current implementation of parameter values, it is deemed sufficiently accurate in its application in the Maarkebeek, Bellebeek and Hunselbeek catchments. Therefore, these abilities are assumed to make the RR-model suitable for integration in an iterative spatial optimization analysis of the study catchments, which will be presented in Chapter 4.

Chapter 4
An iterative optimization approach identifying priority locations for land use change mitigating downstream river flood hazard

Results from this chapter have been submitted for publication:
Gabriels, K., Willems, P., & Van Orshoven, J. An iterative runoff propagation approach to identify priority locations for land use change minimizing downstream river flood hazard [Manuscript submitted for publication to Landscape and Urban Planning].

4.1. Introduction

Land use types and their spatial configuration in the landscape often have strong effects on the catchment hydrology. Sealed surfaces inhibit infiltration and increase surface runoff, leading to runoff accumulation downstream and thus increased river flood frequency and intensity (Braud et al., 2013; Brown et al., 2013; Isik et al., 2013; Lin et al., 2009; Verbeiren et al., 2012; Zorrilla-Miras et al., 2014). Conversely, preservation and development of semi-natural ecosystems with high water storing and infiltration capacities have the potential to mitigate downstream flood risks (Brogna et al., 2017; Brown et al., 2013; Peel, 2009). Consequently, land use (LU) changes can be considered as intensifiers or mitigators of flood hazards in the downstream parts of watersheds. They should therefore be considered in the planning of flood resistant watersheds (Richert et al., 2011; Wu et al., 2015).

The hydrological impacts of LU changes are typically assessed by means of distributed hydrological models (Gao et al., 2015; Lin et al., 2007; Verbeiren et al., 2012; Wu et al., 2015). Due to their high computational times, these models are usually applied to assess the impact of LU changes through scenario analyses, which require only a limited number of model simulations (Jakeman & Hornberger, 1993; Kalantari et al., 2014; Lin et al., 2007; Yu et al., 2018). Spatial optimization analyses, however, aim at identifying optimal LU distributions based on one or more performance criteria (Seppelt & Voinov, 2003; Volk et al., 2010). These optimal LU distributions can then further support spatial planning, e.g. as input in collaborative stakeholder workshops (Eikelboom et al., 2015). However, these optimization analyses assess a bigger search space than scenario analyses, thus requiring more model simulations (Volk et al., 2010). Spatial optimization analyses therefore often rely on heuristic algorithms, e.g. genetic algorithms, limiting the search space and rather approximating the global optimal solution (Lin et al., 2009; Seppelt & Voinov, 2003; Yeo & Guldmann, 2010).

We present an alternative methodology and tool, aiming to support spatial planning by finding priority locations in catchments for LU changes to effectively, i.e. requiring a minimal area, minimize the impact on accumulated runoff at a downstream location of interest. Accordingly, the computationally efficient, raster-based Rainfall-Runoff (RR) model developed in Chapter 3 is integrated in an iterative spatial optimization framework. Due to the RR-model's computational efficiency, the optimization framework can structurally assess the search space based on iterative rankings of the alternatives, thus determining an optimal solution without relying on heuristic algorithms.

The RR-model calculates runoff generation based on the Soil Conservation Service Curve Number (SCS-CN) method (USDA Natural Resource Conservation Service, 1986), while runoff is routed through the catchment as lateral overland flow, considering re-infiltration along its flow paths with the re-

infiltration algorithm of Van Loo (2018). By accounting for re-infiltration, the RR-model also considers spatial interactions between raster cells in the same flow path. Hence, both on-site and off-site impacts of LU changes on runoff volume are assessed. This model is integrated in an iterative optimization framework, identifying the locations in the watershed where implementing certain types of LU changes either maximizes runoff volume reduction or minimizes runoff volume increment at a downstream point of interest. These locations are defined as the optimal locations in the catchment to implement these LU changes regarding their impact on accumulated runoff volume.

The framework was applied and tested in the Maarkebeek and Bellebeek catchments in the Flanders region of northern Belgium. To demonstrate the applicability of the combined RR-optimization tool, three types of LU change were considered for spatial optimization mitigating flood hazards at the studied watershed outlets: afforestation, sealing and the implementation of winter cover crops. Afforestation and winter cover crops are LU changes implemented to reduce runoff generation and overland flow velocity, thereby lowering runoff volume (Brown et al., 2013; Isik et al., 2013; Maetens et al., 2012), in contrast to surface sealing, which increases runoff volume by increasing runoff generation and overland flow velocity (Braud et al., 2013). Different constraints were implemented in each type of LU change. To exemplify the flexibility of the optimization framework, these LU changes were also considered during a winter and summer rainfall event, adjusting the RR-model parameters to the corresponding meteorological and seasonal conditions. The impact of LU changes and their locations in the catchment were also assessed for three uniform rainfall events with average watershed conditions.

4.2. Material and Methods

4.2.1. Rainfall-Runoff Model

The full conceptualization of the RR-model is detailed in Chapter 3. A short summary of the implemented RR-model is provided here. The RR-model is a spatially explicit, raster-based model, implemented for this study with a spatial resolution of 50 m x 50 m. A detailed description of the derivation of this model configuration and its implemented methods and equations can be found in Chapter 3. This model calculates accumulated runoff Q_{accum} [mm] from a rainfall event by routing runoff from each raster cell to the outlet, accounting for infiltration downstream. First, the model determines flow path and upstream area for every pixel by computing flow direction and flow accumulation from a DEM using the D8 algorithm of Jenson & Domingue (1988). Runoff and re-infiltration calculations are then performed, starting with the most upstream pixels.

Runoff Q [mm] is determined based on the SCS-CN method (USDA Natural Resource Conservation Service, 1986), which uses dimensionless CN values, tabulated for average watershed conditions. These CN values are assigned to each raster cell based on its LU and soil properties. From these CNs, potential maximum retention S [mm] and initial abstraction I_a [mm] are derived. Initial abstraction I_a is defined as a fraction λ of the maximum potential retention S ($\lambda * S$), set to 0.05 (Hawkins et al., 2001). This requires the CNs, tabulated for a λ of 0.2, to be conjugated to fit this assumption (Equation 3.4) (Hawkins et al., 2009). These conjugated CN values can then be adjusted to specific antecedent moisture conditions (AMC). This was done according to the Soil and Water Assessment Tool (SWAT) procedure (Equations 3.11–3.15) (Neitsch et al., 2011), increasing CN values for wet conditions with a high AMC and lowering CN values for dry conditions with low AMC. The potential maximum retention S is then derived from these conjugated CNs (Equation 3.1). Re-infiltration is calculated according to the method developed by Van Loo (2018) (see Figure 3.5), determining runoff and infiltration based on travel time of overland flow over the pixel, calculated by the Manning's equation (Equation 3.16) using the hydraulic radius R_h [m], slope s [m/m] and Manning's roughness coefficient n [s/m$^{1/3}$]. A

constant value of 3 mm is implemented for R_h. A standard roughness coefficient *n* is assigned to LU classes based on look-up tables (Arcement & Schneider, 1989; Engman & ASCE, 1986; Kalyanapu, Burian, & Mcpherson, 2009; Morgan et al., 1998; Vieux, 2016). This standard *n* can be adjusted in the RR-model for vegetated LU classes to account for an increased vegetation cover in summer and decreased cover in winter (Table 4.1).

Table 4.1. Adjustments of Manning's *n* for the vegetated LU classes to winter (high AMC) and summer conditions (low AMC) (Arcement & Schneider, 1989; Engman & ASCE, 1986; Kalyanapu et al., 2009; Morgan et al., 1998; Vieux, 2016).

	Manning's *n*		
Land use class	**Standard**	***Winter***	***Summer***
Arable	0.09	0.05	0.18
Meadows/Pasture	0.15	0.12	0.2
Forest	0.4	0.35	0.5

4.2.2. Iteration framework

The optimization framework, schematically depicted in Figure 4.1, iteratively integrates the RR-model, ranking pixels based on accumulated runoff change at a downstream point of interest (POI) for different types of LU changes. First, all pixels eligible for the LU change are selected into the candidate set. The pixels ineligible for the considered LU change, remain invariant throughout the iterations and make up the initial context set. Accumulated runoff at the downstream point of interest is then calculated by the RR-model for the initial situation without land use changes. Next, pixel rank is determined through a two-step iteration. The first iteration loops over every pixel in the candidate set. For each pixel, the RR-model calculates the accumulated runoff volume at the POI when a land use change is implemented on the pixel. An intermediate ranking is thus established for all candidate pixels based on the difference in accumulated runoff volume at the POI between the initial situation and the situation with an alternative LU type implemented for each pixel separately. Secondly, the alternative LU type of the highest ranked pixels is confirmed, and these pixels are subsequently removed from the candidate set and added to the context set as pixels with an updated LU type. Accordingly, the initial situation is updated to the implementation of the LU change in the highest ranked pixels. With the initial situation updated, the first iteration loop is then repeated for the remaining candidate pixels. These two iteration steps are repeated until all candidate pixels are processed according to their rank, i.e. until all candidate pixels are included in the context set, leaving the candidate set empty. A pixel's final rank is thus determined by the order in which they were added to the context set.

Accumulated runoff is calculated using the spatially explicit RR-model, allowing for spatial interaction between raster cells in the same flow path. A pixel's rank therefore reflects its on-site characteristics as Curve Number and Manning's *n*, as well as off-site characteristics of its upstream area and downstream flow path. Due to spatial interaction, the LU change effect of connected, equally ranked pixels is less than those pixels' combined runoff reduction. In these situations, the alternative LU type is only applied to the most downstream pixel, while the other connected pixels remain in the candidate set.

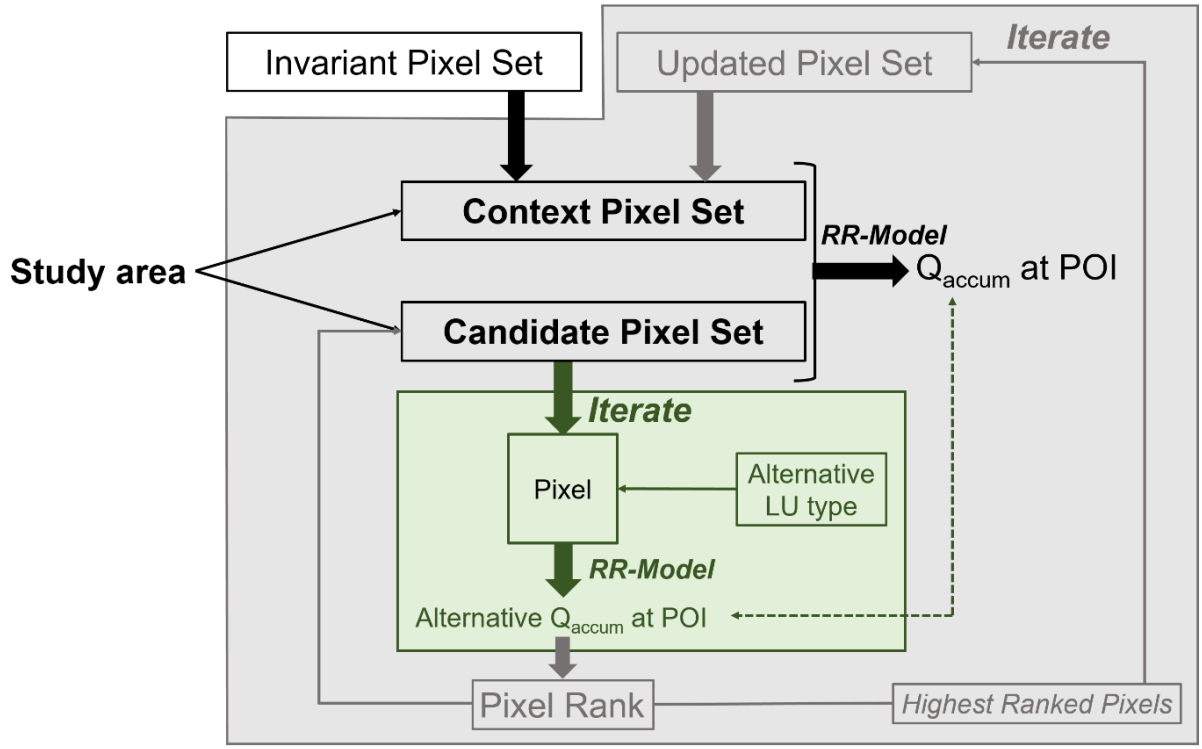

Figure 4.1. Flowchart of the iterative optimization framework, iteratively assessing pixels in the candidate set based on the change in accumulated runoff volume (Q_{accum}) at the downstream Point Of Interest (POI) resulting from a change in LU tye.

4.2.3. Study areas

The optimization method was applied to the catchments of the Maarkebeek and Bellebeek, the same study areas used in the RR-model conceptualization and assessment presented in Chapter 3. The locations of these study areas in Flanders can be found in Figure 3.7. In Chapter 3, the performance of the RR-model was evaluated in the Maarkebeek and Bellebeek catchments, and in its nested subcatchment of the Hunselbeek for respectively 165, 164 and 124 rainfall events causing a peak discharge. Based on these events, the NSE is 0.57 for the Maarkebeek catchment, 0.56 for the Bellebeek catchment and 0.66 for the Hunselbeek subcatchment.

Located in the Upper Scheldt river basin, the Maarkebeek catchment has an area of 48 km². It is a predominantly agricultural area, consisting mainly of arable land. Forest and urban areas constitute around a tenth of the Maarkebeek basin, hereby making it both the least urbanized and least afforested of the studied areas. The Bellebeek catchment (88 km²) is about twice as large as the Maarkebeek catchment. Situated in the Dender river basin, it is mainly an agricultural area, though dominated by grassland rather than arable land. A fifth of the catchment area is urbanized and around 15% is under forest (see Figure 1.8) (Agentschap Informatie Vlaanderen, 2016b). Soils in the Maarkebeek and Bellebeek watersheds have predominantly silt and silt-loam top soil textures (see Figure 1.9) (Databank Ondergrond Vlaanderen, 2017; Dondeyne et al., 2013). The Maarkebeek catchment has a more pronounced undulating terrain than the Bellebeek catchment (Figure 4.2).

Combining land use data from 2012 and soil information with look-up tables from the USDA Natural Resource Conservation Service (1986), CNs were assigned and conjugated to a λ of 0.05 (Equation 3.4) (Figure 4.2). Values for Manning's *n*, shown in Figure 4.2, were assigned based on the 2012 land use dataset (Agentschap Informatie Vlaanderen, 2016b) and look-up tables (Engman & ASCE, 1986; Kalyanapu et al., 2009; Morgan et al., 1998; Vieux, 2016), with the maximum value of 0.4 assigned to

forested areas and the lowest values (0.02 - 0.011) assigned to sealed surfaces. The Manning's *n* and slope were implemented in the Manning's equation to calculate overland flow velocity for application in the RR-model. Figure 4.3 compares the relative frequency of the pixels' conjugated CN and infiltration capacity for the Maarkebeek and Bellebeek catchments. Infiltration in the RR-model is calculated based on the re-infiltration method of Van Loo (2018), which is explained in Chapter 3 (Section 3.2.2) and illustrated in Figure 3.5. Infiltration in this method is proportional to the travel time of overland flow across a pixel, as determined by the Manning's equation (Equation 3.16). As such, the infiltration capacity in Figure 4.3 is expressed as the percentage of runoff and rainfall infiltrating during the travel time across the pixel. This figure reflects the catchments' differences in terms of land use, soil and slope configurations, highlighting relatively higher CN values and more pixels with low and high infiltration capacity in the Bellebeek watershed.

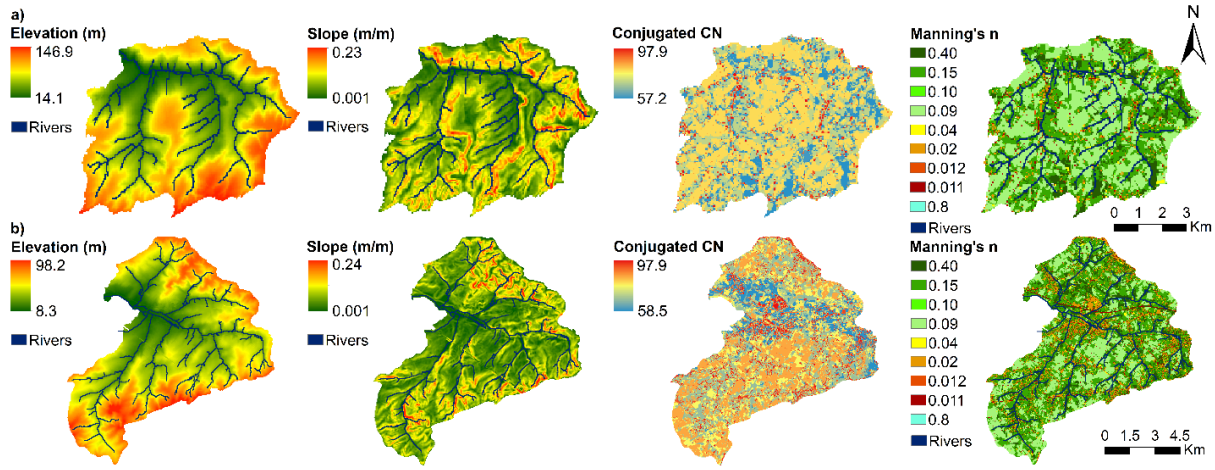

Figure 4.2. Digital Elevation Model (DEM) (Agentschap Informatie Vlaanderen et al., 2006), derived slope (m/m) map, conjugated Curve Number (CN) values (λ = 0.05) and Manning's *n* of the (a) Maarkebeek and (b) Bellebeek catchments.

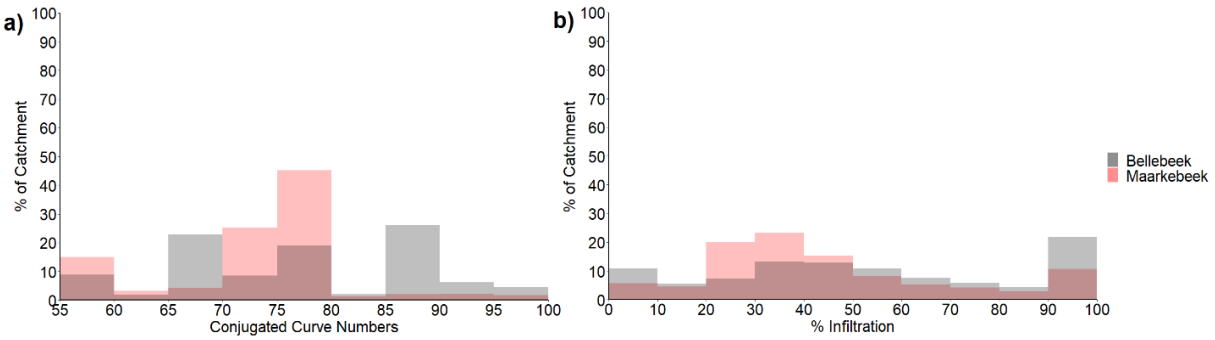

Figure 4.3. (a) Relative frequency (%) of the conjugated Curve Numbers and (b) infiltration capacity, which is proportional to the travel time of overland flow over each pixel and expressed here as the percentage of runoff and rainfall infiltrating during this travel time (%), of the Maarkebeek and Bellebeek catchments.

4.2.4. Rainfall events and types of LU changes

The goal of the iterative optimization framework is to find the optimal locations in the study areas to implement a certain change of LU type or management, i.e. locations where maximum runoff reduction or minimum runoff increment is achieved, while changing the LU type of a minimum number of pixels. As downstream points of interest, the studied catchments' outlets were selected. Three LU changes were each independently assessed in the optimization framework: afforestation, sealing and implementation of winter cover crops. These land use changes were simulated through an adjustment

in the CN value and Manning's *n* parameter in the RR-model. The LU changes of afforestation and winter cover crop illustrate a standard implementation to rank candidate pixels with differing context sets, while in the sealing scenario the candidate pixel set is dynamic, only including pixels neighboring the growing sealed area. This constraint can be considered an application of region growing.

Rainfall events

The effect of these LU changes on discharge volumes at the catchment's outlets was assessed based on two rainfall events to exemplify the pixel ranking for wet and dry antecedent soil moisture conditions. Soil moisture conditions are modelled in the RR-model based on an adjustment to the CN values according to the method presented in Neitsch et al. (2011). The corresponding AMC for one rainfall event in winter with high AMC and one summer rainfall event with low AMC were derived from daily soil water balance simulation run by means of the hydrological modules implemented in the spatially distributed nutrient-emission model ArcNEMO (Van Opstal et al., 2013). The rainfall distributions of these events were derived from rain gauge networks of the Royal Meteorological Institute (RMI) and the Flanders Environment Agency (VMM) (Figure 4.4) (Van Opstal et al., 2014). The tabulated and AMC adjusted, conjugated CN values are depicted in Figure 4.5. The AMC adjusted CN values remain mostly determined by the land use class and soil characteristics (see also Figure 1.8 and Figure 1.9). The Manning's *n* values implemented in the RR-model were also adjusted to the seasonal conditions of these events (Table 4.1).

To assess the ranking consistency of the optimization results, the LU changes were also run for three uniformly distributed rainfall events with total rainfall amounts of 30 mm, 50 mm and 100 mm. For these events, the LU changes were considered under average watershed conditions in the case of afforestation and soil sealing, implementing the conjugated, tabulated CN values and standard Manning's *n* values. In the winter cover crop scenario, the land use changes were considered based on the CN adjusted to the antecedent soil moisture conditions of the winter (high AMC) rainfall event. The Manning's *n* values in the cover crop scenario were consistently adjusted to winter conditions.

The runoff volumes at the outlets resulting from these rainfall events and their meteorological and seasonal conditions are provided in Table 4.2, averaged over the number of pixels in the catchments, i.e. 19 213 and 35 221 pixels in resp. the Maarkebeek and Bellebeek catchments. The low AMC rainfall event results in a higher accumulated runoff volume at the Maarkebeek outlet due to the much higher rainfall amounts compared to the high AMC rainfall event in this catchment. In the Bellebeek catchment, the high AMC event results in a higher runoff volume despite lower rainfall amounts, which is a reflection of the relatively higher CN values in winter due to the AMC adjustments. A distinction is made for the cover crop scenario, as this scenario is consistently assessed based on winter conditions, i.e. CN adjusted according to the high AMC values and Manning's *n* values corresponding to winter. The afforestation and sealing scenario are implemented for the uniform rainfall events with average watershed conditions, i.e. the tabulated CN_2 values and standard Manning's *n* values.

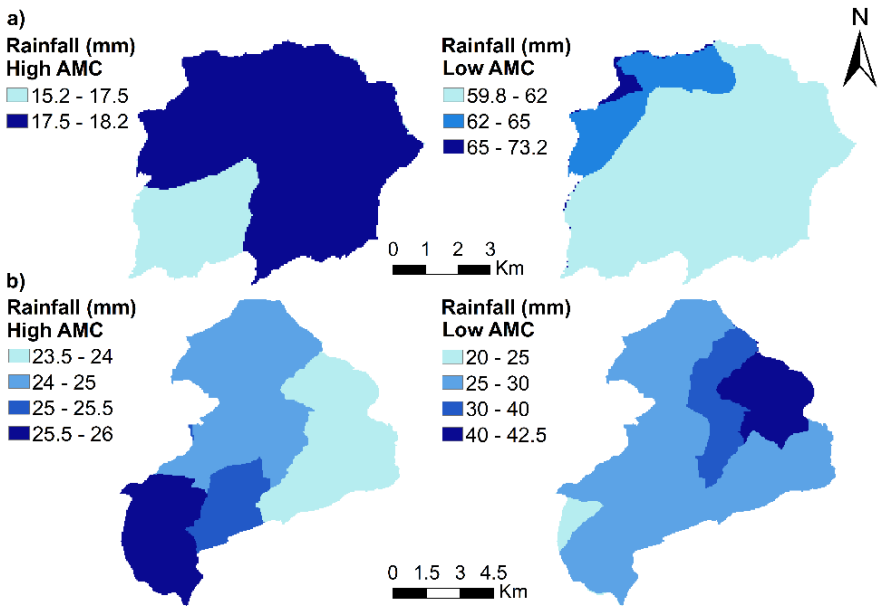

Figure 4.4. The rainfall distribution of selected winter (high AMC) and summer (low AMC) events in the Maarkebeek (a) and Bellebeek (b) catchments.

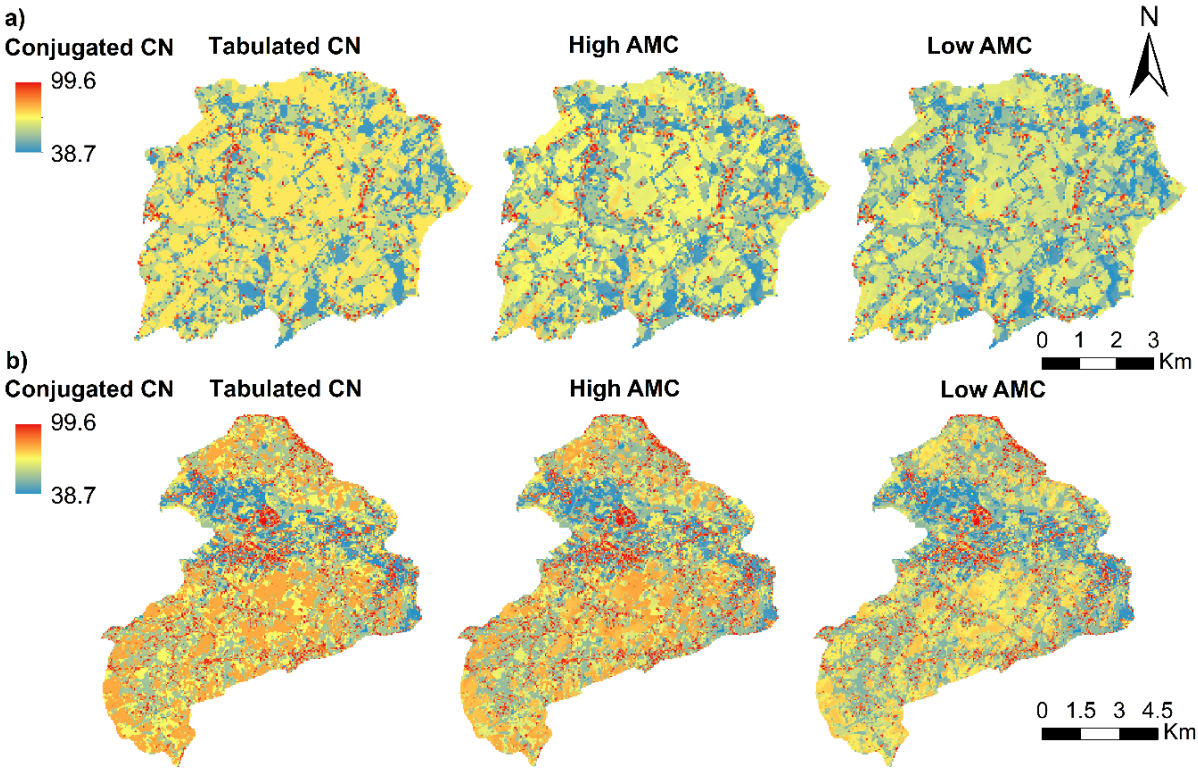

Figure 4.5. Conjugated CN values corrected for the high and low AMC events in the (a) Maarkebeek and (b) Bellebeek catchments.

Land use change scenarios

For the afforestation scenario, the optimization tool found locations in the watersheds where afforestation maximally reduced accumulated runoff at the outlet. Improbable LU changes were disregarded, therefore sealed and river pixels were excluded, as well as already afforested pixels. Urban, river and already afforested pixels therefore made up the context set. This initial context set

consisted of respectively 4643 and 12 571 pixels in the Maarkebeek and Bellebeek catchment. All other pixels made up the candidate set, comprising 14 570 pixels (76%) in the Maarkebeek catchment and 22 650 pixels (64%) in the Bellebeek catchments. Under afforestation, candidate pixels' CN values were lowered to their respective CN values under forest in good condition (USDA Natural Resource Conservation Service, 1986) (see also Table 3.1) and consequently conjugated to a λ value of 0.05. The Manning's roughness coefficient *n* was increased to 0.4 (Kalyanapu et al., 2009). For the high and low AMC events, these conjugated CNs were adjusted to specific AMC conditions and Manning's *n* was increased to 0.35 (winter) or 0.5 (summer) (Table 4.1). Decreasing a pixel's CN values and increasing its Manning's *n* decreases runoff generation and increases infiltration capacity. At each iteration, the pixel(s) with the highest accumulated runoff reduction at the outlet were selected for afforestation, labeled with its rank and moved from the candidate set to the updated context set.

In the case of soil sealing, the optimization tool determined where sealing resulted in the smallest runoff increment at the outlets. The initial candidate set consisted of 5362 pixels (28%) in the Maarkebeek catchment and 12 969 pixels (37%) in the Bellebeek catchment, while eventually respectively 15 994 pixels (83%) and 26 166 pixels (74%) were considered for sealing. Sealed pixels' conjugated CN values were increased to 98 (USDA Natural Resource Conservation Service, 1986) and Manning's *n* was decreased to 0.01 (Engman & ASCE, 1986). Since sealing pixels increases CN values and decreases Manning's *n*, additional sealed areas subsequently increase accumulated runoff. Therefore, pixels with the smallest increase in runoff were selected in each iteration to minimize the impact of sealing at the outlet. River and already urban pixels were excluded from the candidate set and made up the initial context set. As a constraint, region growing was implemented: in each iteration, only pixels neighboring sealed pixels were considered in the candidate set, taking into account the growing urban area. As a result, the candidate set in this type of LU change is dynamic, removing sealed pixels to the context set and adding these pixels' neighbors to the candidate set, whereas for the other two scenarios, pixels can only be removed from candidate sets.

The cover crop scenario specifically deals with a seasonal adjustment in land management practices, as establishing cover crops over winter avoids a fallow soil in this season (Gabriel et al., 2019; Maetens et al., 2012). Accordingly, this scenario was consistently assessed in winter conditions, and the initial situation was also adjusted to winter conditions. This LU change scenario was therefore not considered for the low AMC summer rainfall event, instead initial CN and Manning's *n* values were adjusted to the circumstances in the high AMC winter event for all rainfall events, including the uniform rainfall distributions (Table 4.2). In addition, the CN values of arable land were modified into those of bare soil (USDA Natural Resource Conservation Service, 1986) and conjugated. These CN values were then adjusted to high AMC conditions. The Manning's *n* values were decreased to the corresponding winter values of 0.05 (Table 4.1). After adjusting these initial conditions, the optimization tool was run. In implementing winter cover crops, the optimization framework indicates arable locations where cover crops were most effective in reducing accumulated runoff at the outlet. Only arable pixels were included in the candidate set, hence the initial, invariable context set was made up of pixels with all other LU types. The candidate pixel set in this analysis thus consisted of respectively 7902 arable pixels (41%) and 8636 arable pixels (25%). Under cover crop, the conjugated, AMC-corrected CN values of bare soil were modified to their respective CN values under small grained crops in straight rows with crop residue present and in good condition, which equal 60, 72, 80 and 84 for resp. HSG A (well-drained soil), B, C and D (waterlogged soil). (USDA Natural Resource Conservation Service, 1986). The arable Manning's *n* coefficient was increased from 0.05 to 0.12 to account for the increased vegetation cover (Morgan et al., 1998). These modifications have the same effect as afforestation: cover crops increase infiltration capacity and reduce runoff generation. Therefore, at

each iteration, cover crops were implemented in pixel(s) resulting in the highest runoff reduction at the outlet.

Table 4.2. Catchment-averaged runoff volumes (RO vol.; m^3) at the outlet of the Maarkebeek and Bellebeek catchments, following the different rainfall events with high AMC (winter), low AMC (summer) and 30, 50 and 100 mm uniform rainfall distributions. The uniform rainfall events (30 mm, 50 mm and 100 mm) were simulated for average watershed conditions in the afforestation and sealing scenario. For the cover crop scenario, runoff volume (RO vol. (m^3) Cover Crop) resulting from the uniform rainfall events was simulated for high AMC corresponding to winter conditions.

	Maarkebeek		**Bellebeek**	
Rainfall	**RO vol. (m^3)**	**RO vol. (m^3) Cover Crop**	**RO vol. (m^3)**	**RO vol. (m^3) Cover Crop**
High AMC rainfall event	8.7	10.2	11.1	13.3
Low AMC rainfall event	26.8		6.5	
30 mm	21	21.7	19.6	18.3
50 mm	49.9	47.2	48.9	42.6
100 mm	144.7	131.2	145.1	124.2

4.3. Results

4.3.1. Afforestation

The results of the afforestation LU change are depicted in Figure 4.6 for the high and low AMC rainfall events and in Figure 4.7 for the uniformly distributed rainfall events. These results are visualized according to each candidate pixel's reduction in accumulated runoff at the outlet. Runoff reduction of lower ranked pixels was calculated after higher ranked pixels had been afforested in previous iterations. For the high and low AMC events, the afforestation results (Figure 4.6) reflect the runoff accumulation in the watershed: the events with a higher runoff volume at the outlet, respectively the low and high AMC events in the Maarkebeek and Bellebeek, resulted in more pixels being afforested, with a higher runoff volume reduction in the pixels bordering the river system. Figure 4.7 reflects these findings as afforestation in the upstream, source areas results in runoff reduction at the outlet at higher rainfall and thus runoff amounts, even when areas surrounding the rivers have already been afforested in previous iterations. This shows a saturated infiltration capacity of the afforested pixels downstream due to the high amount of accumulated runoff.

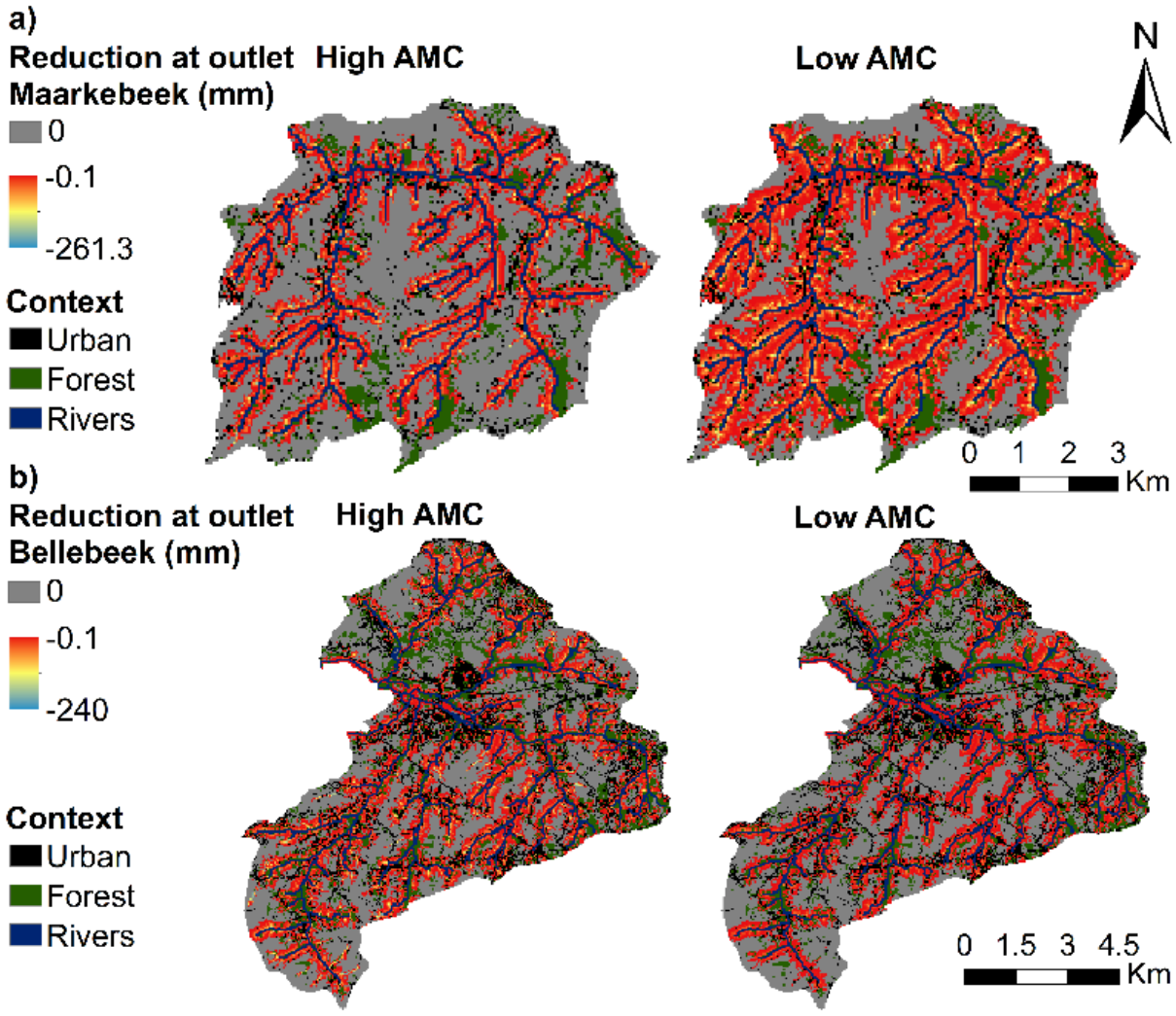

Figure 4.6. The afforestation ranking results, expressed as accumulated runoff reduction at the outlet [mm], for the (a) Maarkebeek and (b) Bellebeek catchments, for two rainfall events with high AMC and low AMC.

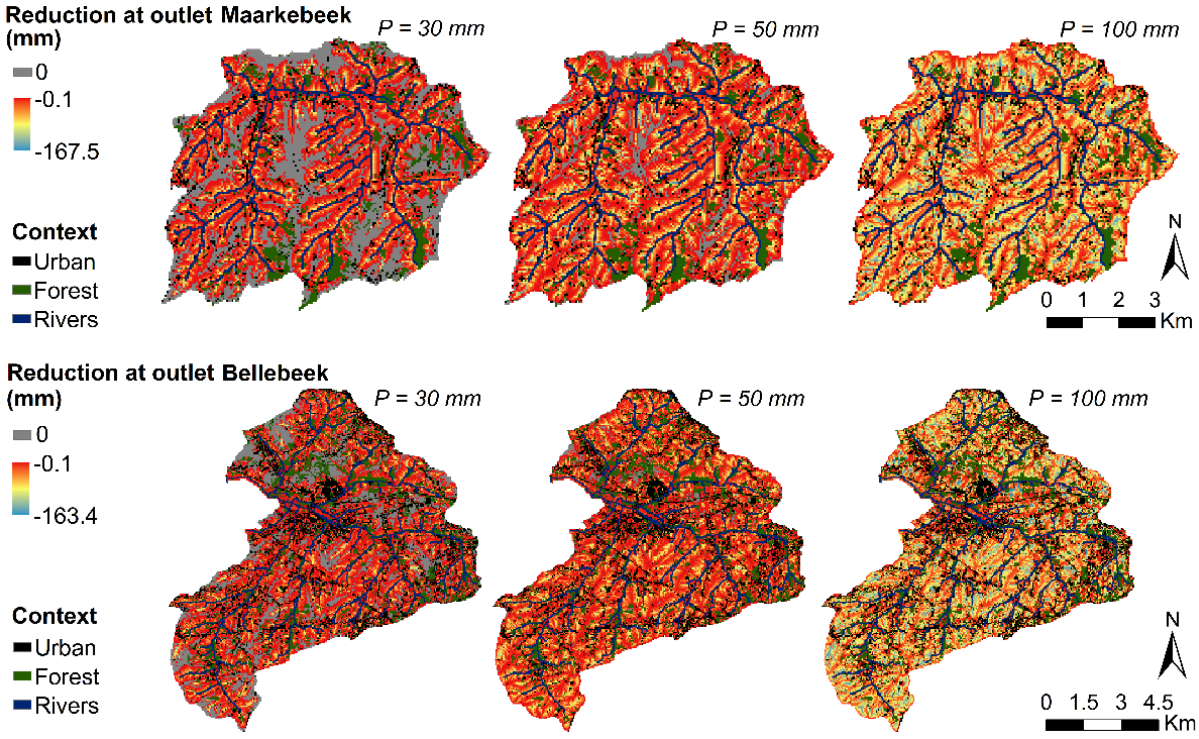

Figure 4.7. The afforestation ranking results, expressed as accumulated runoff reduction at the outlet [mm], for the (a) Maarkebeek and (b) Bellebeek catchments, under three rainfall (P) events: 30 mm, 50 mm and 100 mm.

Figure 4.11a shows the relative accumulated runoff decrease at the watersheds' outlets by afforestation. In Figure 4.11a, intervals can be observed where a larger percentage of the candidate pixel set is changed in one iteration. These intervals indicate that multiple pixels were afforested simultaneously, since these pixels had equal downstream effects and did not interact spatially with each other. After afforesting the full candidate set, the outlet's accumulated runoff at the Maarkebeek outlet decreased with approximately 84% (17.6 m^3), 79% (39.3 m^3) and 63% (90.9 m^3) for respectively 30 mm, 50 mm and 100 mm rainfall events. At the Bellebeek's outlet, accumulated runoff decreased with 67% (13.1 m^3), 60% (29.4 m^3) and 40% (58.2 m^3) for corresponding 30 mm, 50 mm and 100 mm rainfall events.

4.3.2. Soil Sealing

The results of sealing are depicted in respectively Figure 4.8 and 4.9 for the AMC and uniform rainfall events. These figures show the standardized ranking rather than runoff increment, as the latter does not unequivocally reflect pixel rank due to the region growing constraint; only pixels neighboring urban areas were considered in each iteration. Isolated pixels, bordered by rivers, were disregarded in the Bellebeek catchment. In the Maarkebeek watershed, no such pixels occur. In Figure 4.8, rank 1 corresponds to an increment of 0 mm, while the final rank corresponds to a respective increase of 344.9 mm and 400.2 mm for the high and low AMC event in the Maarkebeek catchment. In the Bellebeek catchment, rank 1 corresponds to an increment of 0 mm, while the final rank corresponds to an increase of respectively 379.9 mm and 392.1 mm for the high and low AMC events. Figure 4.8 shows more pixels in rank 1 for respectively the high and low AMC events in the Maarkebeek and Bellebeek catchments. These events correspond to the rainfall events with the lowest runoff accumulation at the outlet. Figure 4.9 shows the results of the uniform rainfall events of 30, 50 and 100 mm. For these rainfall amounts, rank 1 corresponds to an increment of respectively 0 mm, 1.6 mm and 5.8 mm, while the final rank corresponds to an increase of 181, 184.3 and 186.7 mm in the

Maarkebeek catchment. In the Bellebeek catchment, rank 1 corresponds to an increment of respectively 0 mm, 0.3 mm and 4.4 mm and the final rank corresponds to an increase of respectively 184, 185.9 and 187.4 mm for 30 mm, 50 mm and 100 mm events. The results of the uniform rainfall events (Figure 4.9) indicate that at a lower rainfall of 30 mm, mainly afforested areas are highlighted as areas to avoid urbanization. These afforested areas have lower runoff contribution and higher infiltration capacity than arable land or pastures, therefore, removing and sealing forests has a higher impact. As rainfall increases, the impact of sealing increases, while afforested pixels are still selected last, as well as pixels situated in river valleys.

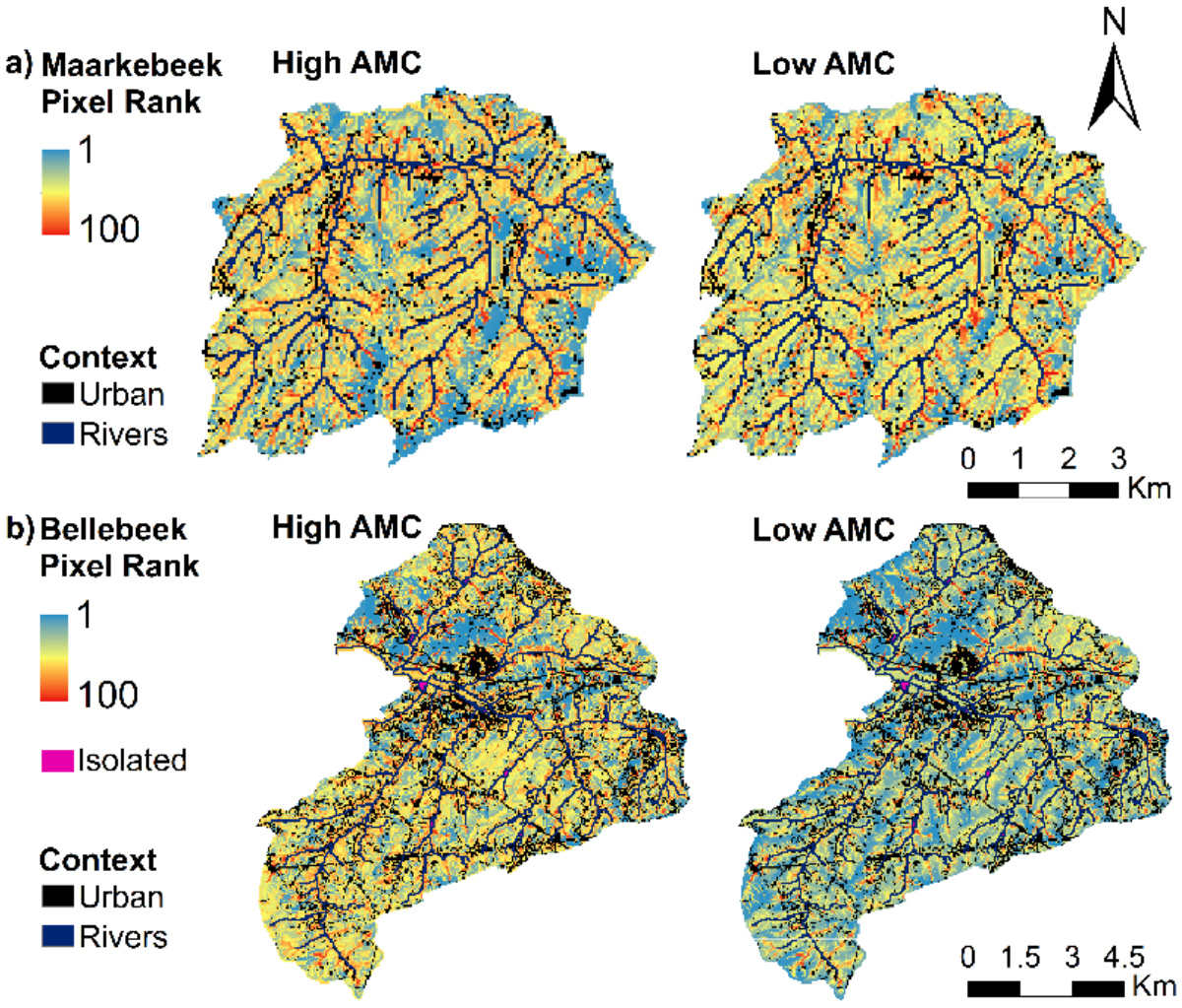

Figure 4.8. Standardized ranking of pixels considering their sealing in the (a) Maarkebeek and (b) Bellebeek catchments for the high and low AMC rainfall events. In the Bellebeek catchment, isolated patches of land, bordered by rivers, were excluded for sealing.

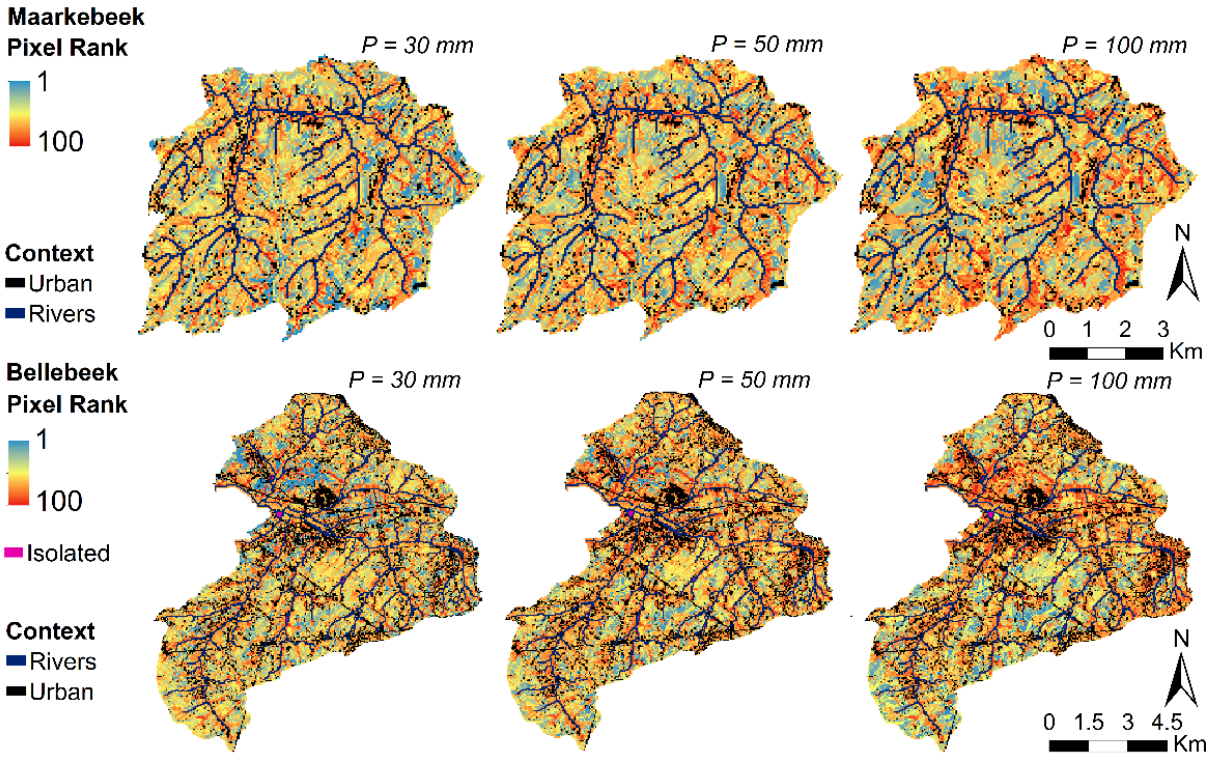

Figure 4.9. Standardized ranking of pixels considering their sealing in the (a) Maarkebeek and (b) Bellebeek catchments for three rainfall amounts (P) of 30, 50 and 100 mm. In the Bellebeek catchment, isolated patches of land, bordered by rivers, were excluded for sealing.

Figure 4.11b shows the accumulated runoff increase at the outlets due to sealing of all candidate pixels. The accumulated runoff at the Maarkebeek outlet increases approximately 201% (42.2 m^3), 120% (60.1 m^3) and 59% (85.1 m^3) after a 30 mm, 50 mm and 100 mm rainfall events, while the runoff volume at the Bellebeek outlet increases with 217% (42.5 m^3), 122% (59.7 m^3) and 58% (83.4 m^3) for corresponding rainfall amounts.

4.3.3. Winter Cover Crops

The winter cover crop implementation results for the Maarkebeek and Bellebeek watersheds are depicted in Figure 4.10 for the high AMC rainfall event and the uniform 30 mm, 50 mm and 100 mm rainfall events.

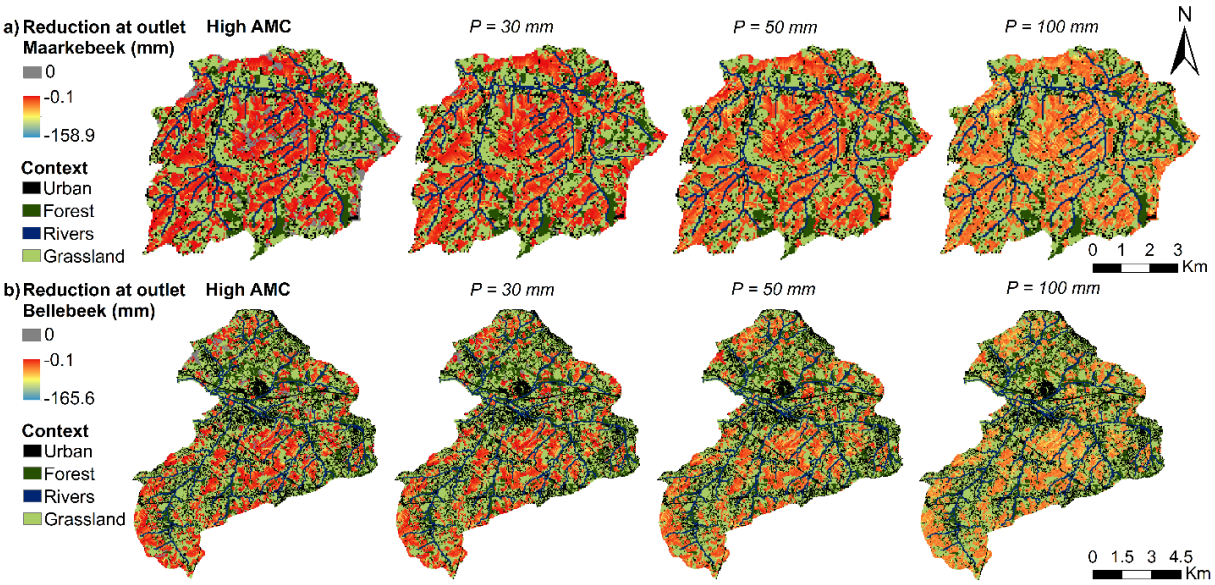

Figure 4.10. The ranking results for winter cover crop implementation, expressed as the accumulated runoff reduction [mm] at the outlet of the (a) Maarkebeek and (b) Bellebeek catchments, for the high AMC rainfall event and 30 mm, 50 mm and 100 mm rainfall (P) events.

Figure 4.11c shows the accumulated runoff decrease (%) at the catchment outlets according to the percentage of arable candidate pixels under cover crop. Though the arable area is similar in the Maarkebeek watershed (19.8 km²) and in the Bellebeek watershed (21.6 km²), arable land constitutes a bigger portion of the Maarkbeek catchment (41%) compared to the Bellebeek catchment (25%). For a rainfall event of 30 mm, 50 mm and 100 mm, accumulated runoff at the Maarkebeek outlet decreases with respectively 41.8% (9.1 m³), 37.8% (17.9 m³) and 27.6% (36.3 m³) after full implementation of cover crops, while the decrease at the Bellebeek outlet is respectively 37.3% (6.8 m³), 31.2% (13.3 m³) and 19.6% (24.4 m³).

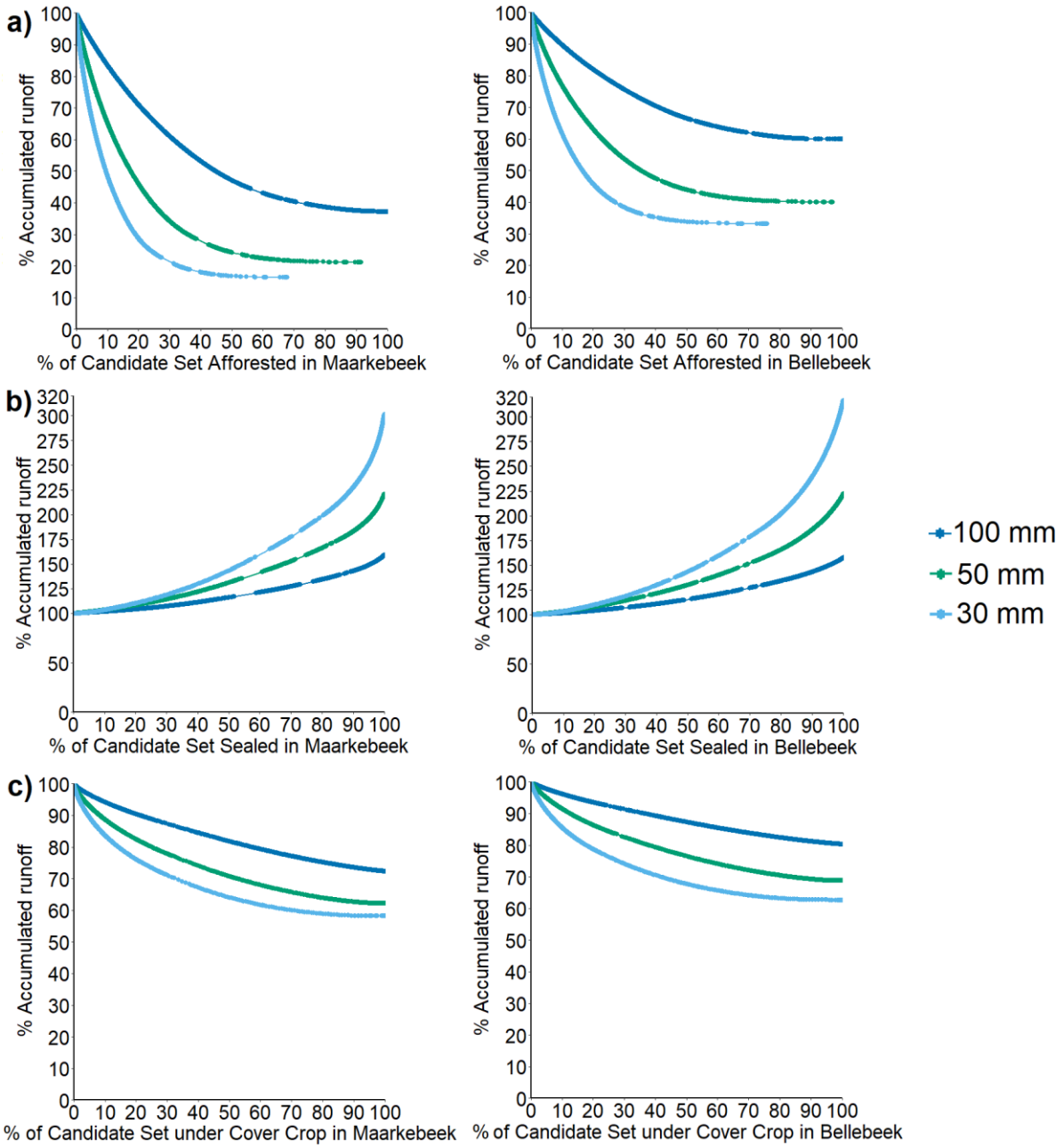

Figure 4.11. The accumulated runoff (%) at the catchment outlets after (a) afforestation, (b) sealing and (c) winter cover crop implementation for three rainfall events (30 mm, 50 mm and 100 mm).

4.4. Discussion

The proposed optimization framework was applied to identify the most effective locations in the Maarkebeek and Bellebeek watersheds for afforestation, sealing and winter cover crop implementation to maximize the runoff accumulation decrease or minimize runoff accumulation increase at the outlet.

The afforestation results illustrate that a higher runoff volume reduction is achieved by increasing downstream infiltration capacity rather than by lowering upstream runoff generation. This finding is in line with expectations as the RR-model takes into account the spatial interactions along the flow path. Consequently, pixel ranking is a reflection of both on-site characteristics, including the potential increase in infiltration capacity of the pixel, as off-site characteristics, including the upstream area and

downstream flow path of the pixel. The potential increase in infiltration capacity is fully exploited in downstream locations in the landscape with higher flow accumulation, which will therefore be selected first for afforestation by the optimization framework. The afforestation analyses (Figure 4.11a) further indicate a notable runoff volume decrease at the outlets. The sharpest decline in runoff accumulation is found after afforesting the highest ranked candidate pixels. The 20% highest ranked pixels in the candidate sets constitute respectively 2914 pixels and 4530 pixels in the Maarkebeek and Bellebeek catchments. After afforesting these pixels, the outlets' runoff volume is reduced with respectively 15 m^3 (71%), 26.9 m^3 (54%) and 41.9 m^3 (29%) in the Maarkebeek and runoff volume decreases with 10.6 m^3 (54%), 18.1 m^3 (37%) and 26.2 m^3 (18%) in the Bellebeek for 30, 50 and 100 mm rainfall events. The relative runoff volume reduction is therefore higher in the Maarkebeek catchment, while the absolute reduction is higher in the Bellebeek catchment. These differences are explained by the larger catchment size of the Bellebeek and differences in CN and infiltration capacity (Figure 4.3). The afforestation candidate set of the Maarkebeek catchment consists predominantly of arable pixels, 41% of the catchment, compared to 25% arable pixels in the Bellebeek catchment. As arable land is assigned a higher CN value and lower Manning's *n*, the decrease in CN and increase in infiltration capacity after afforestation is higher for arable land compared to grassland, resulting in less runoff generation and increased infiltration.

The sealing results show more pixels having a higher runoff increment at the outlet when the runoff accumulation in the watershed increases, with increasing rainfall in the case of the uniform rainfall events and in respectively the low and high AMC events in the Maarkebeek and Bellebeek catchments. The increment per pixel is higher in the low AMC events, explained by the initially lower CNs and higher Manning's *n* values, leading to a larger runoff increment due to a larger increase in CN and decrease in Manning's *n*. Figure 4.11b shows that full sealing of the candidate set of pixels results in a considerable accumulated runoff increase at the outlets, tripling the outlets' runoff volume for a 30 mm rainfall event and increasing runoff accumulation with more than 50% in both catchments for a 100 mm rainfall event. The steepest increase results from sealing the lowest ranked pixels. After sealing the 20% lowest ranked pixels, runoff volume at the Maarkebeek outlet increases with 21.5 m^3 (102%), 27 m^3 (54%), 35.3 m^3 (24%) after respectively 30 mm, 50 mm and 100 mm rainfall events, while runoff volume increases with 22.5 m^3 (114.6 %), 27.6 m^3 (56.5 %) and 34 m^3 (23.4%) in the Bellebeek catchment.

The winter cover crop implementation results in a similar reduction per pixel as afforestation, explained by the initially higher CN and lower Manning's *n* implemented in the cover crop scenario due to the AMC correction. However, the total reduction at the outlet (Figure 4.11c) is smaller than the afforestation scenario due to the smaller candidate set in the winter cover crop scenario. Since the cover crop scenario will be implemented on the level of agricultural parcels, the pixel ranking of this scenario can be translated to the level of agricultural parcels by considering the ranks of the pixels covered by the corresponding agricultural parcels.

Ranking consistency over the uniform rainfall events is assessed by standardizing the ranks and determining their standard deviation and average rank (Figure 4.12). These figures indicate a low standard deviation, and therefore high consistency, for pixels with low and high average ranks, which is reflected in Figure 4.13a: pixels with high (1-20) or low (80-100) average ranks are consistently ranked either high or low across the different rainfall events. Therefore, the optimization results consistently prioritize areas in the river valleys for afforestation and cover crop implementation. Afforesting these areas results in the sharpest accumulated runoff decrease at the outlet. Figure 4.13b shows that the highest ranked pixels for afforestation and cover crop implementation are located in areas with higher flow accumulation, while the lowest ranked pixels are characterized by low flow

accumulations. The reverse pattern is observed for the sealing scenario: pixels with high flow accumulation are ranked lowest for sealing. Subsequently sealing these lowest ranked pixels results in the steepest runoff volume increase (Figure 4.11b), indicating the important buffering function of these pixels. The results also indicate that the required buffer area increases when the rain storm volume increases. Higher rainfall amounts require more pixels to infiltrate the increased runoff, resulting in a higher standard deviation in the ranks of these pixels (Figure 4.12a).

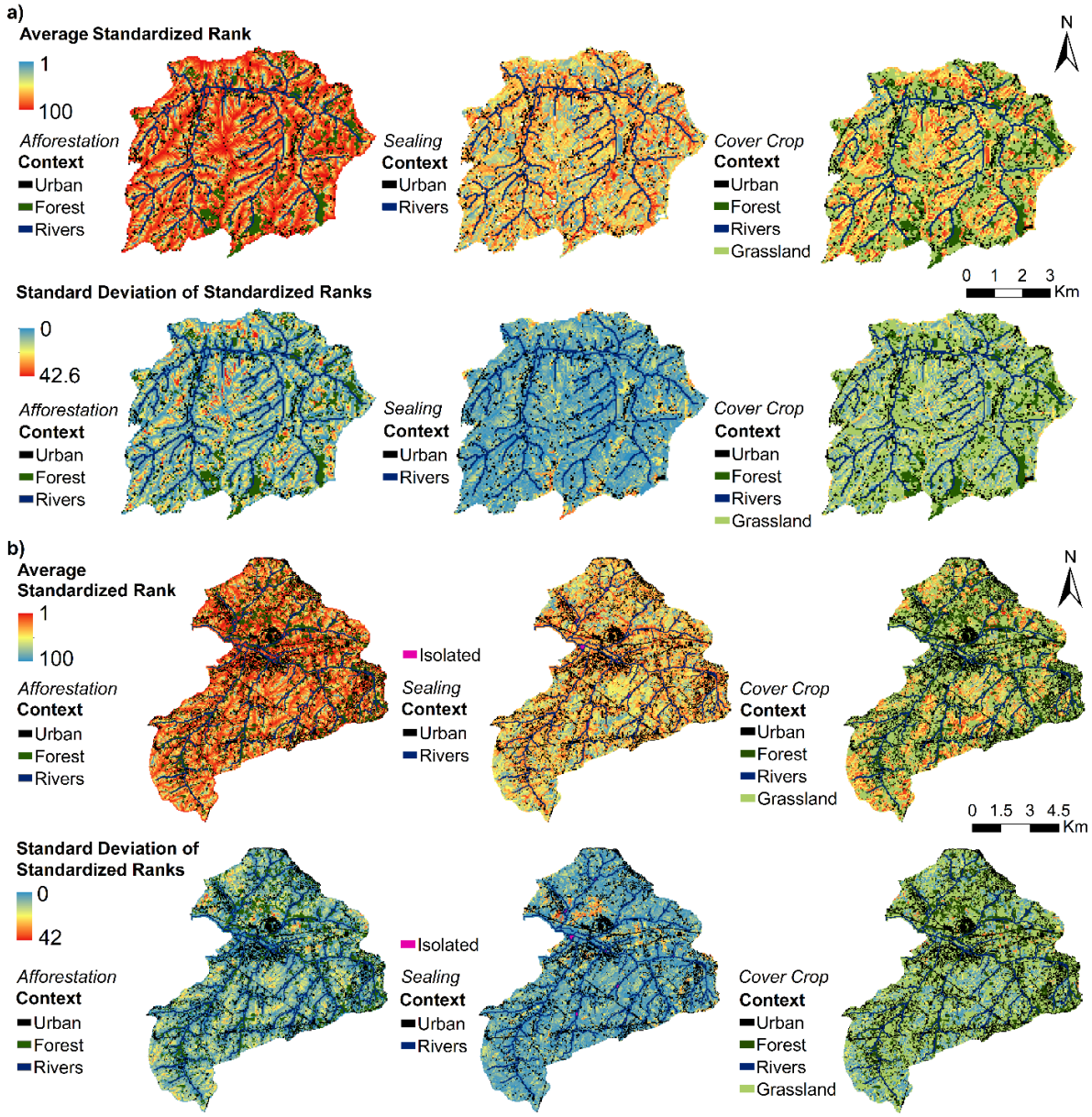

Figure 4.12. The average standardized ranks and its standard deviations for the (a) Maarkebeek and (b) Bellebeek watersheds, averaged for 30, 50 and 100 mm rainfall events and for three LU type changes.

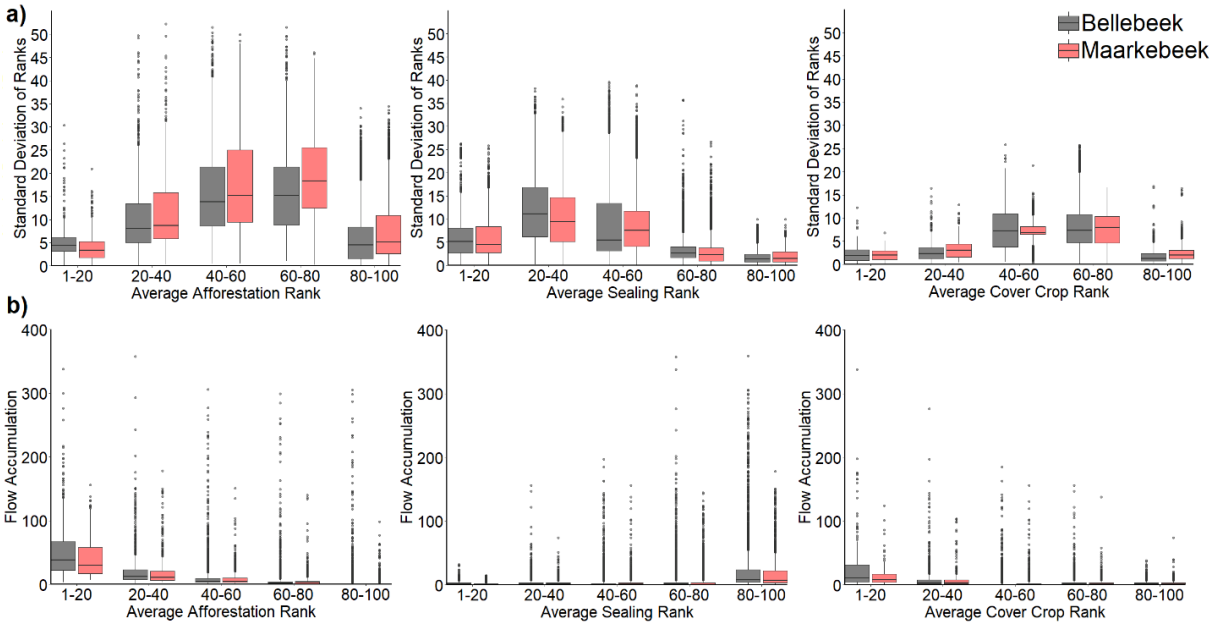

Figure 4.13. Boxplots of the standardized ranks' (a) standard deviations and (b) flow accumulation according to the average rank of afforestation, sealing and cover crop implementation in the Bellebeek and Maarkebeek catchments.

The optimization results thus show the considerable impact of the considered types of LU changes and their locations in the catchment on river discharge, thereby clearly highlighting the infiltration potential present in river valleys and its significance in mitigating overland flow accumulation. Our results thereby reflect the main findings of the land use allocation optimization presented in Yeo & Guldmann (2010), combining a heuristic algorithm with a SCS-CN based RR-model to find LU allocations minimizing peak storm runoff at the watershed outlet. Their analysis allocated urban land upstream and away from rivers, while woods and grassland were allocated along rivers, buffering urban land. These findings reflect the importance of integrated approaches using natural processes in spatial planning to mitigate flood risks. These integrated approaches are emerging as cost-effective alternatives to traditional grey infrastructure, as exemplified by the EU's Water Framework Directive (Directive 2000/60/EC, 2000) and Floods Directive (Directive 2007/60/EC, 2007), focusing on natural water retention measures such as floodplain restoration and afforestation. In addition to flood mitigation, these integrated approaches provide multiple ecosystem services (Millennium Ecosystem Assessment, 2005), including carbon storage (Ottoy et al., 2017) and a reduction in the delivery of sediment and pollutants to rivers, thus increasing water quality (Fiquepron et al., 2013; Ruangpan et al., 2020; Wheater & Evans, 2009).

The Flanders' regional planning policy also emphasizes the role of river valleys for water storage in the landscape (Departement Omgeving Vlaanderen, 2018). In the management plans for Upper Scheldt and Dender river basins, which the Maarkebeek and Bellebeek watersheds are part of, afforestation and adjustments in agricultural management are proposed as measures to increase the basins' water holding capacity (Coördinatiecommissie Integraal Waterbeleid, 2016a, 2016c). The results presented in this paper indicate where to prioritize these types of LU changes at a watershed scale in order to most effectively achieve this management goal, and as such the proposed optimization framework can be a valuable tool to integrated approaches reducing flood hazard. This optimization framework could further be extended to include budget or cost constraints (Vanegas et al., 2010) or to assess a portfolio of land use changes as opposed to the independent evaluation currently implemented (Aerts & Heuvelink, 2002). These extensions are further discussed in Section 6.2.2.

The presented optimization framework employed a computationally efficient and spatially explicit RR-model to find locations to implement LU type or land management changes to most effectively reduce runoff accumulation at a downstream point of interest. Because the optimization tool can be adjusted to specific land use conditions and changes, it is possible to bring in additional information, e.g. information on which agricultural parcels already implement cover crops, thereby assessing the effectiveness of additional measures to reduce runoff accumulation. The computational efficiency of the RR-model allowed it to be integrated in an iterative optimization approach, while being sufficiently accurate to assess the relative impact of LU changes with a NSE of 0.57 and 0.56 for respectively the Maarkebeek and Bellebeek catchment. The RR-model calculates runoff on a pixel level with a resolution of 50 m based on the popular, empirical SCS-CN method (Hawkins et al., 2009; Kalantari et al., 2014; Li et al., 2017; Sajikumar & Remya, 2015) and incorporates re-infiltration along the flow path through the algorithm of Van Loo (2018), determining infiltration based on the overland flow velocity using Manning's equation (Equation 3.16). Consequently, the RR-model allows for spatial interaction, thus incorporating off-site effects of LU changes on runoff accumulation. The spatial resolution is appropriate to assess the hydrological impact of land use changes, however, it is too coarse to asses small-scale landscape interventions which influence runoff, e.g. establishing or removing agricultural drainage ditches (Levavasseur et al., 2012).

However, the empirical approach in the RR-model does not take into account the soil physical processes or properties governing infiltration. It rather makes estimates of infiltration capacity using model parameters CN and Manning's *n* values, determined in look-up tables. Consequently, the pixel ranking in the optimization framework does not reflect soil physical properties. Additionally, though the RR-model takes into account antecedent soil moisture conditions, this event-based model also ignores temporal effects by lumping runoff generation in time, calculating accumulated runoff volume after a rainfall event. As such, the impact of land use changes on the peak discharge cannot be evaluated by the optimization framework. In addition, the land use change scenarios in the optimization framework do not incorporate a temporal dimension. Currently, the land use change scenarios assume the implementation of full-grown crops or forest, while the different forest and crop growth stages will also affect the hydrological processes differently. This temporal dimension could be modelled by combining forest growth models (Dalemans et al., 2015) or crop growth models (Raes et al., 2009) with a hydrological model (Sutmöller et al., 2011). Alternatively, the final ranking results of the optimization framework can be further analyzed and serve as input in a scenario analysis using more complex, less computationally efficient hydrological models, calculating a full physically-based soil water balance and integrating vegetation growth models, such as MIKE SHE (DHI Software, 2008; Kalantari et al., 2014), in order to assess the impact of the proposed LU changes on a finer temporal resolution, while considering temporal variations in short-duration rainfall intensity and assessing the impact of soil physical properties and vegetation growth.

The other uncertainties related to the RR-model, including the seasonal adjustment of Manning's *n* as discussed in Section 3.4, also apply for the optimization framework. Though the final pixel ranking provides a relative comparison between alternatives, these uncertainties should also be further assessed in a sensitivity analysis in the context of the optimization framework to evaluate the robustness of the final pixel ranking with regards to the choice of parameter values in the RR-model.

4.5. Conclusion

The optimization framework presented in this paper identifies locations in watersheds to implement LU type changes in order to mitigate runoff accumulation and reduce flood hazards at a downstream point of interest. The ranking results indicate how to achieve a maximum effect on runoff

accumulation with a minimum number of pixels. It thereby provides highly relevant, spatially explicit information to spatial planners and policy makers for flood hazard mitigation and sustainable landscape management. The spatially explicit RR-model calculates accumulated runoff by combining the SCS-CN method (USDA Natural Resource Conservation Service, 1986) with the re-infiltration scheme of Van Loo (2018). By combining these two methods, spatial interaction and off-site effects of LU changes are taken into account. Moreover, the RR-model parameters can be adjusted to specific meteorological and seasonal conditions. This raster-based RR-model was integrated in an optimization framework, adjusting model parameters to simulate LU changes and iteratively ranking pixels according to their downstream runoff reduction. Despite the uncertainties related to the RR-model (see Section 3.4), the RR-model is considered sufficiently accurate, with an NSE of approximately 0.5. Moreover, it is highly computationally efficient: a distributed hydrological model with a higher temporal resolution would reduce computational efficiency. The hydrological impact over time of the optimized outputs can be assessed ex-post using a more complex hydrological model. This framework can be extended to include budget and other cost constraints, thereby allowing multi-objective optimization to find the most cost-efficient pixels for LU changes. The current implementation of the optimization framework considers as alternatives the locations for a certain, fixed land use change. In the future, this framework could also be extended to consider multiple land use changes simultaneously as alternatives additional to the locations where they will be implemented.

The optimization framework was implemented for two watersheds in Flanders and for three types of LU changes: afforestation, sealing and winter cover crop implementation; each demonstrating different capabilities of the adaptable framework. In finding the most effective afforestation locations, constraints on feasible LU changes were implemented. The sealing LU change employed a region growing algorithm, only considering pixels in the candidate set neighboring already urbanized pixels. In the cover crop implementation, the RR-model parameters took account of the seasonal conditions in winter, i.e. lack of vegetation cover and higher soil moisture content. The simulation results demonstrate the considerable impact on runoff accumulation at the downstream points of interest of the LU changes and the locations where they are implemented. Afforestation reduces runoff accumulation at the Maarkebeek outlet (48 km²) with 63% of the initial volume after a rainfall event of 100 mm, while at the Bellebeek outlet (88 km²) runoff accumulation is reduced with 40% for the same event. The sealing simulations result in an increase of accumulated runoff of more than 50% at the watersheds' outlets. The results consistently highlight the importance of the infiltration capacity of areas with concentrated flow in the landscape, i.e. the river valleys: areas to prioritize afforestation and avoid sealing are located in the valleys, in the path of concentrated flow to the rivers. Afforesting and sealing these areas leads to respectively the highest decrease and increase in runoff accumulation. These findings underpin the importance of spatial policies focusing on integrated approaches, as reflected in the EU's Water Framework Directive (Directive 2000/60/EC, 2000) and Floods Directive (Directive 2007/60/EC, 2007), as well as in Flanders' new spatial planning policy. The presented optimization framework can therefore serve as valuable input for the implementation of nature- and land management based solutions in spatial planning to reduce flood hazards. This is demonstrated in Chapter 5, where the impact on flood risk of land use changes, as identified by the optimization framework, is assessed in a flood risk assessment.

Chapter 5
A comparative flood risk assessment evaluating the flood insurance value of land use changes

Results from this chapter have been submitted for publication:
Gabriels, K., Willems, P., & Van Orshoven, J. A comparative flood damage and risk impact assessment of land use [Manuscript submitted for publication to Natural Hazards and Earth System Sciences].

5.1. Introduction

River flooding is a natural process, but also poses a significant socioeconomic hazard, causing human distress and damaging properties and infrastructure. In Europe, floods caused approximately 52 billion euros overall losses and 1100 fatalities between 1998 and 2009 (EEA, 2010). Moreover, the economic losses associated with flood events have been on the increase in the past decades (since 1970), partly due to changing weather patterns (IPCC, 2014), but mainly driven by socioeconomic developments such as population growth and ongoing urbanization (Barredo, 2009; Bouwer, 2011; Koks et al., 2014). The increasing flood losses prompted a shift in flood management in Europe from a flood prevention policy to flood risk management policy (EEA, 2017), as detailed in the European Flood Directive (Directive 2007/60/EC, 2007). Flood risk management aims at minimizing flood risk, which is defined by the probability of a flood event and its potential, negative consequences or flood damages. Flood risk is thus an expression of the expected flood damages over a certain time period, i.e. the expected annual damages (Bubeck et al., 2011; de Moel et al., 2015; Grossi & Kunreuther, 2005; Merz, Kreibich, et al., 2010). The concepts related to flood hazard and risk were also detailed in Chapter 1 (Section 1.1.2) and are depicted in Figure 1.1.

Flood risk assessments follow a general approach (de Moel et al., 2015), in which flood depths are first derived from flood maps. These flood maps typically represent the flood extent and water depth of hypothetical flood events with different probabilities of occurrence. The probability of occurrence of a flood event or return period is modelled by combining frequency analysis of discharge data with hydrodynamic models (de Moel et al., 2009). Next, the corresponding flood damages are determined in flood damage models, which relate the flood hazard characteristics, established in the flood maps, to the vulnerability to flooding of the exposed ecosystems, people and property, further collectively referred to as elements. Finally, flood risk is determined by combining the flood damages of flood events with different return periods in a weighted summation, with more frequently occurring events, i.e. with a higher exceedance probability, receiving a higher weight.

A comprehensive description of the components of flood risk, including flood damage and vulnerability to flooding, is provided in Chapter 1, Section 1.1.2. The most important aspects applicable in this study are reiterated here briefly. Flood damage is defined as all negative, harmful impacts of floods on society, economy and the environment. Generally direct and indirect damages are distinguished. Direct flood damage occurs at the time of flooding through the physical contact of the exposed elements with flood waters, while indirect flood damage relates to the induced losses as a result of flooding, e.g. production losses (Merz, Kreibich, et al., 2010). A second distinction is made between tangible and intangible damages: tangible damages can easily be expressed in monetary

values, whereas intangible damages encompass damage inflicted on elements of which the financial value is more difficult to assess, including loss of life and the psychological impact of flooding. (Merz, Kreibich, et al., 2010; Messner & Meyer, 2006). Flood risk analyses often only assess tangible flood damages, as these are easier and more reliable to estimate than intangible flood damages (Merz, Kreibich, et al., 2010). The vulnerability of elements to flooding is described by damage functions, providing a link between the valuation of the elements exposed to the flood and the corresponding flood hazard characteristics, established in the flood maps. Most often, damage functions are included in flood damage models in the form of depth-damage curves, detailing the impact of water depth on the value of the exposed elements (Gerl et al., 2016).

In order to provide an estimate of tangible flood damages, an economic valuation of the elements at risk is required based on socio-economic information. Two perspectives on this economic appraisal exist, one preferring the use of depreciated values, while the other instead favors replacement values. Depreciated values reflect the value of elements at the time of flooding, i.e. the cost of a good is depreciated over time from their original value. Consequently, depreciated values provide a damage estimate in line with national accounting, thereby reflecting macro-economic risks. Replacement values, on the other hand, are suited to assess financial risk, as these values reflect the cost of replacing the damaged goods by new ones. However, the use of replacement values imply an overestimation of actual flood damage (Merz, Kreibich, et al., 2010). The estimation of macro-economic risk with depreciated values is thus more accurate, however, this type of valuation is limited by the available socio-economic data regarding the goods at risk. Replacement values, on the other hand, though simplifying and overestimating flood risk, are based on data which are easier to access and process (Kellens et al., 2013; Vanneuville et al., 2003).

The vulnerability of elements to flooding is described by damage functions, providing a link between the valuation of the elements exposed to the flood and the corresponding flood hazard characteristics, established in the flood maps. Most often, damage functions are included in flood damage models in the form of depth-damage curves, detailing the impact of water depth on the value of the exposed elements (Gerl et al., 2016). A distinction can be made between empirical functions, based on historical data from flood damage databases, and expert damage functions, based on expert knowledge (Kellens et al., 2013). Actual damage information possesses a higher accuracy than expert estimates and allows for an assessment of the variability and uncertainty of the damage estimates. However, damage surveys after flood events are rare and limited, providing a limited underlying database for damage functions. Though expert based damage functions are more subjective, they can be applied in any region, since they are not connected to a single flood event (Merz, Kreibich, et al., 2010).

Tools for flood risk analysis include the LATIS tool developed in Flanders, Belgium based on the damage model of Vanneuville et al. (2006), also described in Chapter 1, Section 1.2. The economic damage assessment in LATIS considers the direct and the internal indirect flood damages, thereby applying replacement values, adjusted to the 2015 ABEX-index, which is based on the national average construction cost of buildings (Beullens et al., 2017; Kellens et al., 2013; VMM, 2018a). The depth-damage functions implemented in LATIS are expert based, derived from enquiries conducted in the Netherlands and the United Kingdom (UK) (Vanneuville et al., 2006). In the Netherlands, flood risk frameworks were implemented by Ward, De Moel, & Aerts (2011) and de Moel, van Vliet, & Aerts (2014) based on the Damage Scanner model. This model assesses direct and indirect, both internal and external, economic flood damages, using replacement values based on the price level in 2000. The depth-damage functions implemented in the Damage Scanner are based on expert knowledge and available damage statistics. These damage functions also take into account additional damage

inflicted above a critical flow rate in the floodplain (Klijn et al., 2007). In the UK, flood risk assessments (e.g. Hall, Sayers, & Dawson, 2005) commonly implement the damage model presented in Penning-Rowsell et al. (2005). In this damage model, direct and indirect economic damages are assessed using depreciated values to represent national economic flood losses. Expert based damage functions are implemented, which assess flood damage considering both water depth and flood duration. By explicitly taking into account potential flood damages, these risk assessments identify people and assets at risk of flooding, which in turn is a basis for the determination of flood insurance premiums (Grossi & Kunreuther, 2005; Merz, Kreibich, et al., 2010) and to evaluate the effect and efficiency of flood mitigation measures (de Moel et al., 2014; Koks et al., 2014).

5.1.1. Comparative flood risk assessment of land use changes

Land use changes can reduce the runoff volume accumulation downstream and as such, these changes have the capacity to mitigate flood severity, by reducing the flooded area and the water depth in this area. Consequently, land use changes can reduce flood damages and corresponding flood risk. This reduction can be considered a flood insurance value (Chapter 1, Section 1.1.2), attributed to the allocated land use systems and provided to the benefiting flooded areas downstream. In this chapter, a spatially explicit, comparative flood risk assessment framework is proposed to evaluate land use changes as spatial mitigation measures to reduce direct economic flood damage and the associated flood risk, thus allowing for an explorative assessment of the efficiency of the proposed land use changes as flood mitigation measures by providing an estimate of their flood insurance value.

This comparative risk framework is applied on a case study in the Maarkebeek basin in Flanders, Belgium. Flood extents in Flanders have been collected and recorded in a geospatial flood archive outlining the maximum extent of flooded zones from 1988 to 2016 (Agentschap Informatie Vlaanderen & Vlaamse Milieumaatschappij, 2017; Van Orshoven, 2001). In this case study, the flood damages resulting from four flood events occurring in the Maarkebeek basin from 2000 to 2016 were assessed using a flood damage model. The overall flood risk was determined by combining the flood damages of the four events with their respective probability of occurrence. Next, two types of land use changes were considered in this case study: afforestation and soil sealing. The corresponding land use change scenarios were derived from the priority rankings as determined by the iterative raster-based optimization framework (Chapter 4). Accordingly, for a given area, the locations were identified where (i) afforestation would most effectively reduce the runoff accumulation, and (ii) where soil sealing would lead to the smallest increase in runoff accumulation, in each of the flood extents of all considered flood events. Subsequently, the corresponding impact on runoff volume accumulation of these land use change scenarios was calculated by the RR-model of Chapter 3. Based on the accumulated runoff volume after land use change, the altered flood extents and water depths were derived, and the corresponding flood damages and flood risk were calculated. Finally, flood damage and risk before and after land use changes can be compared to provide the relative impact, or flood insurance value, of the considered land use changes on the downstream flooded areas.

5.2. Material and Methods

5.2.1. Comparative flood damage and risk assessment

The framework determining the spatially explicit, relative flood damage and risk impact of land use changes is visualized in Figure 5.1. First, flood depths and volumes are derived from observed, rasterized flood extents for multiple return periods before any implementation of land use changes. Next, the impact of a land use change scenario on runoff accumulation is calculated by the spatially explicit RR-model. In this study, the optimization tool is used to determine land use change scenarios,

describing the optimal locations for land use changes with regard to their impact on the accumulated runoff volume. Consequently, an empirical relationship between observed flood volumes and the modeled runoff volume accumulation is established to determine the flood volumes after land use changes. Based on these modeled flood volumes, a DEM is progressively filled, and corresponding water depths are thus determined. The water depths before and after land use change are then combined with socio-economic information in a flood damage model to determine the corresponding flood damages. In this flood damage model, only direct, economic flood damages were taken into consideration and expressed as a monetary value with their replacement values. The difference between the flood damage datasets before and after land use change is defined as the relative flood damage impact of the land use changes. In order to evaluate the relative flood risk impact, the flood damages of several flood events with different probabilities are combined.

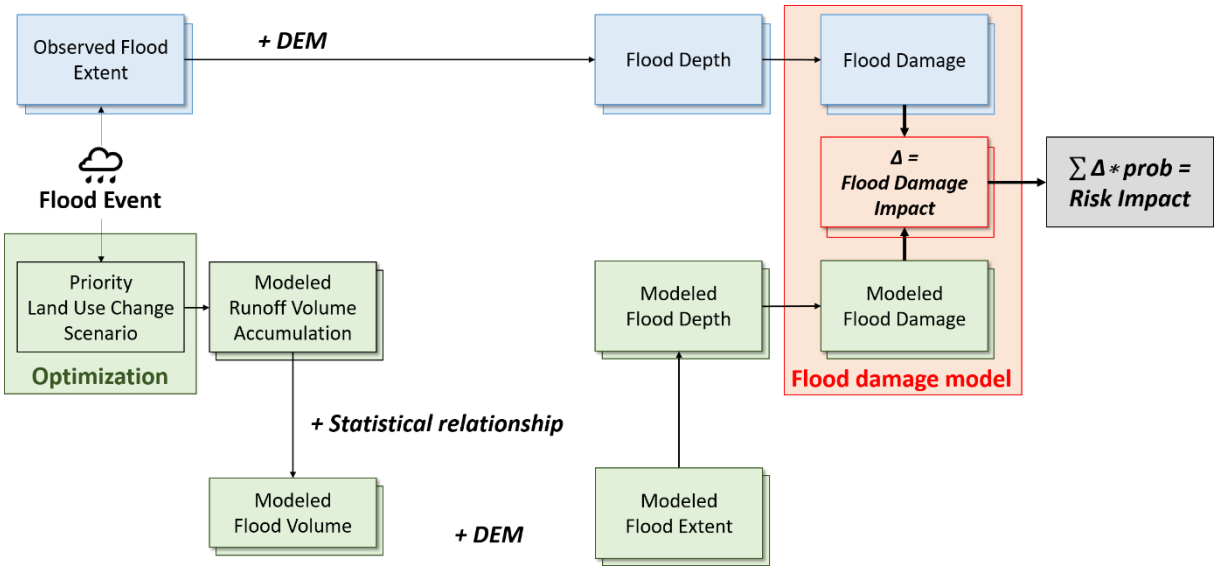

Figure 5.1. Framework determining the relative flood damage and risk impact of land use changes.

Flood depth and volume calculations before and after land use changes

Rasterized flood extents, related to a specific flood event, are first combined with a Digital Elevation Model (DEM) to derive the water depth in each of the flooded pixels. This water depth is determined by fitting a linear, least-squares plane representing the water level elevation across each flood extent based on the elevation of the pixels bordering the flood extents and the pixels representing the river banks. The water elevation trend was then corrected for each pixel, by averaging this elevation with the water level determined by a local, linear interpolation only based on the nearest flood border pixels. Finally, the water depth is calculated per pixel by subtracting the DEM from the water level. Consequently, the flooded volume in each pixel is calculated by multiplying the water depth with each pixel's area, determined by its resolution.

Next, the rainfall and AMC of each flood event together with the land use in the watershed are modeled by the RR-model to determine the runoff volume accumulated in each pixel of the basin during the flood event. This CN-based RR-model routes the runoff through the watershed, assessing downstream re-infiltration using the Manning's equation. Subsequently, the hydrological impact of land use changes is simulated using the same RR-model by adjusting the model parameters related to land use, i.e. the CN value and Manning's roughness coefficient. In this study, the land use change scenarios were first determined by the iterative optimization framework, identifying where land use changes are most effective, i.e. covering a minimal area, in reducing the runoff volume accumulation.

In order to relate the modeled runoff volume accumulation with flood volume, an empirical function is fitted through these two variables. Analogue to the relationship found by Mediero, Jiménez-Álvarez, & Garrote (2010) between flood peak discharge and flood volume, a linear relationship is determined in the log-log space between the total flood volume *Vol* in the flood extent *j* and the accumulated runoff volume *Q* at the flood extent's outlet, i.e. the most downstream pixel in each extent:

$$Vol_j = 10^a * Q_j^b \quad (5.1)$$

with *a* and *b* respectively the intercept and coefficient of the linear relationship in the log-log space. Using this correlation, the simulated accumulated runoff volume resulting from the land use change scenarios can then be expressed as a flood volume. Based on this simulated flood volume, the altered flood extent and corresponding water depth is determined by progressively filling the DEM covering the original flood extent, analogue to the simple, conceptual "bathtub" method (Teng et al., 2015).

Flood damage model

Flood damages before and after land use changes are determined for each pixel by combining the derived water depth datasets with a flood damage model. The flood damage model estimates the direct economic damages per land use class based on depth-damage curves, relating the water depth with a damage factor *α* (Koks et al., 2014). The total effective flood damage *D* in each pixel is then calculated by multiplying this damage factor *α* with the maximum possible flood damage D_{max} (€/m² or €/m for road infrastructure), summed over the different land use classes in the pixel:

$$D = \sum \alpha * D_{max} \quad (5.2)$$

The depth-damage curves implemented in the flood damage model are the expert based functions from Vanneuville et al. (2006). They are provided in Figure 5.2 for the different land use classes. The depth-damage curve of residential and open areas reaches the maximum value 1 at a water depth of 0.5 m, however, the maximum damages related to this land use class are considered limited to low-cost clean-up costs and small repairs, which occur at lower water depths.

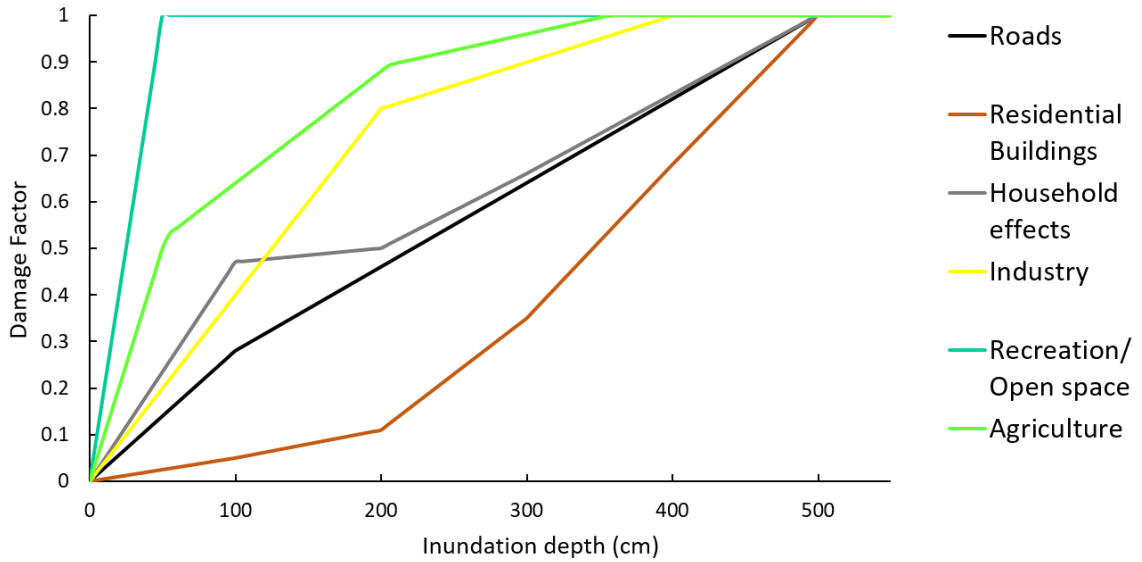

Figure 5.2. The flood damage curves depicting the relationship between the inundation depth (cm) and the damage factor (Vanneuville et al., 2006).

The maximum damage values implemented in the flood damage model are provided in Table 5.1 per land use class. These amounts were established based on the replacement values implemented in the LATIS tool (Beullens et al., 2017; Vanneuville et al., 2006) and in Koks et al. (2014); these values were not adjusted to the price level in a specific year. These maximum damage estimates were also not spatially differentiated and thus assumed valid for Flanders, with the exception of the maximum damage to residential buildings. Analogue to the method applied in LATIS, the maximum flood damage to residential buildings was derived from socio-economic data regarding the median residential housing price in a municipality divided by its average housing surface area. The maximum damage to household effects was estimated at 30% of the damage to residential buildings, while damage to residential open space, including damage to garden houses, was set at € 1/m² (Kellens et al., 2013). The maximum damage to industrial buildings was estimated at a unity price of € 700/m² (Koks et al., 2014), while maximum damage to industrial open spaces, including industrial installations and supplies, was estimated € 100/m² (Kellens et al., 2013; Vanneuville et al., 2006). Maximum damage to road infrastructure is dependent on the type of road, ranging between € 41/m for dirt roads and € 1374/m for highways, as determined by Beullens et al. (2017). The maximum damage to arable land mainly relates to losses in crop production and was set to € 0.5/m², while the maximum damage to grasslands, including pastures and meadows, was estimated at € 0.08/m². Damage to natural areas, such as forests, was set to € 0/m² (Kellens et al., 2013; Vanneuville et al., 2006).

Table 5.1. The maximum damage values as implemented in the flood damage model and derived from (Beullens et al., 2017), (Koks et al., 2014) and (Vanneuville et al., 2006).

Land use class	**Damage Function**	**Maximum damage**
Residential Buildings	Residential Buildings	*Housing price* /m²
Residential Household effects	Household effects	30% of *Housing price* /m²
Industrial Building	Industry	€ 700 /m²
Open space	Recreation/Open Space	€ 1 /m² (residential) – € 100 /m² (industrial)
Roads	Roads	€ 41–1374 /m
Arable land	Agriculture	€ 0.5 /m²
Grassland	Agriculture	€ 0.08/m²

Risk calculations

The damage datasets derived from the flood damage model for flood events with different probabilities or return periods are combined to assess the change in flood risk from the implemented land use changes. Flood risk *R* is defined as the integral of the damage-probability curve (see Figure 1.1) (Grossi & Kunreuther, 2005), which is approximated by weighted summation of flood damages *D*, thereby weighing these damages according to their corresponding exceedance probability, which equals the inverse of the return period *i*. This weighted summation takes into account the damages of events with lower return periods to avoid double counting damages of these more frequent events in the integral flood risk. This is mathematically expressed as (Kellens et al., 2013; Vanneuville et al., 2002):

$$R = \sum_{i=1}^{n} \frac{1}{i} * (D_i - D_{i-1}) \qquad (5.3)$$

Since only a limited number of return periods are assessed, a linear interpolation is performed between two return periods *x* and *p* to determine an average probability by summing the intermediate

probabilities and dividing them over the time between the two return periods, which can be expressed as (Deckers et al., 2009; Vanneuville et al., 2003):

$$R = \sum_{i=x} \left(\frac{\frac{1}{p+1} + \cdots + \frac{1}{p+(x-p)}}{x-p} \right) * \left(D_x - D_p\right) \quad (5.4)$$

Where *p* is a more frequent return period than *x*.

5.2.2. Case Study

Flood damage and risk assessment of observed flood events

The framework was implemented in a case study in the catchment of the Maarkebeek (48 km²), situated in the Upper Scheldt basin in Flanders, Belgium (see Figure 3.7) and also subject of case studies in Chapters 2, 3 and 4. This is a mostly agricultural area, dominated by arable land. Approximately 10% of the catchment is urbanized and about an equal area is afforested.

Flood damage and risk were assessed from observed flood extents derived from the geospatial flood archive. This geospatial flood archive details the maximum extent of flooded areas in Flanders for flood events between 1988 and 2016 (Agentschap Informatie Vlaanderen & Vlaamse Milieumaatschappij, 2017). Eight flood events were registered in the geospatial flood archive for the Maarkebeek catchment, namely one flood event in each of 1993, 1995, 1998, 1999, 2003 and 2010 and two flood events in 2002. Since the rainfall dataset implemented in the optimization tool ranges from 2000 to 2012 (Chapter 3), the risk assessment was performed on the four flood events observed after 2000, i.e. two flood events taking place in 2002 (19-27/02/2002 and 19-21/08/2002), one flood event in 2003 (1-3/01/2003) and one flood event in 2010 (11-15/11/2010). The extents of the flooded areas during these events are visualized in Figure 5.3: one flood extent was registered in each event in 2002, while respectively three and eight separate flood extents were observed in 2003 and 2010. Flood extents situated partially or completely outside this study area were not taken into consideration.

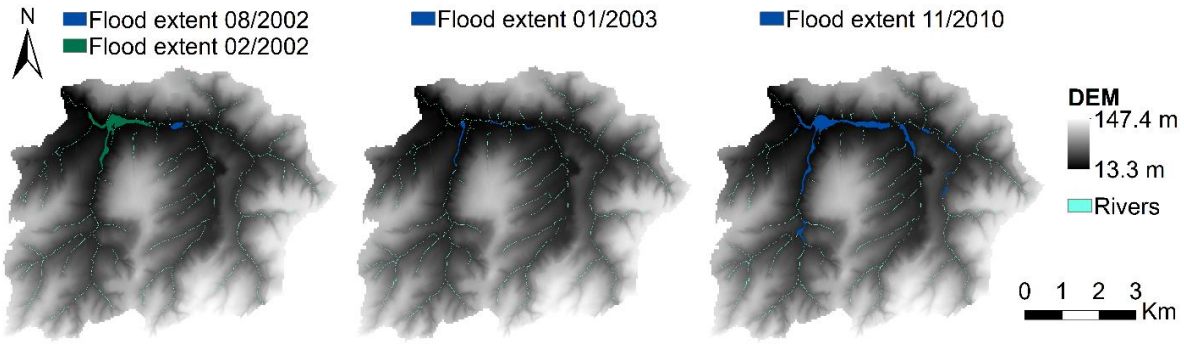

Figure 5.3. Extents of flooded areas in the Maarkebeek basin as recorded in the geospatial flood archive for the 2000–2016 period (Agentschap Informatie Vlaanderen & Vlaamse Milieumaatschappij, 2017).

For each of these flood events, the water depths in the corresponding flood extents were first determined. Consequently, the flood extents were rasterized with a resolution of 5 m and then combined with a DEM to fit a linear plane, as described above, to determine the water level and associated water depth in each pixel. Based on these water depths, the flood damages were assessed on a per-pixel basis using the flood damage model. Socio-economic information and land use datasets regarding the land use classes in Table 5.1 were collected to determine the maximum flood damage

in each pixel. The maximum damage to residential buildings was determined by combining the median residential housing price in 2002, 2003 and 2010 in the municipalities situated in the Maarkebeek subcatchment (Oudenaarde, Ronse, Brakel, Horebeke and Maarkedal) (Statbel, 2019) with the number of residences and their total surface area in the municipalities, which was derived from a high resolution dataset outlining building footprints (Agentschap Informatie Vlaanderen, 2020). These residential damages ranged from € 439/m² to € 703/m² in 2002, from € 492/m² to € 745/m² in 2003, and from € 903/m² to € 1524/m² in 2010. Road infrastructure in the catchment was derived from the road register (Agentschap Informatie Vlaanderen & Nationaal Geografisch Instituut, 2020). According to the industrial parcel dataset (Agentschap Innoveren en Ondernemen & Agentschap Informatie Vlaanderen, 2020), no industrial areas were flooded during these four events. The non-residential and non-industrial land use classes in Table 5.1, i.e. arable land, grassland and open space, were derived from the land use dataset from 2012 with a resolution of 5 m (Agentschap Informatie Vlaanderen, 2016b).

Next, the flood risk corresponding to these flood damages was determined according to Equation 5.4, for which the return period of each flood events was empirically estimated by applying the Weibull formula on an analysis of the annual maximum discharge (Chow et al., 1988), based on discharge data from 1973 to 2019 of the Maarkebeek river (Vlaamse Milieumaatschappij et al., 2020). In this analysis, 45 annual maxima were included, as data from 2016 and 2017 was incomplete. This analysis estimated the return period of the 2010 flood event at 46 years, since the highest discharge of the time series was recorded during this event. The flood event in 2003 had a return period of 3 years, while the February and August 2002 flood events had return periods of, respectively, 11 and 1 year(s). Implementing these values in Equation 5.4 results in the following formula to assess the flood risk *R* based on the damages *D* corresponding to these events:

$$R = 0.58 * D_1 + 0.27 * D_3 + 0.11 * D_{11} + 0.04 * D_{46} \quad (5.5)$$

Comparative flood damage and risk assessment

After determining the observed flood damage and corresponding flood risk over all four flood events, the relative impact of land use changes to this base-line flood damage and risk was assessed. First, the land use change scenarios were determined based on priority rankings provided the iterative optimization tool. This optimization framework was implemented for each flood event and for two types of land use changes: (i) where in the upstream area of the flooded zones afforestation maximally reduces the runoff accumulation in these zones, and (ii) where upstream soil sealing minimally increases the runoff accumulation in the flooded areas. These land use changes were implemented as described in Chapter 4. In each of the two flood events in 2002, only one flood extent was observed; the most downstream pixel in this extent, i.e. the outlet, was consequently used as point of interest (POI) in the optimization and the candidate pixels were ranked based on the change in runoff volume accumulation at this pixel. In the flood events in 2003 and 2010, respectively three and eight flood extents were observed. These extents' outlets were considered the POIs in the optimization and the candidate pixels were ranked based on the combined changes in runoff accumulation at these pixels, weighted according to the observed flood damages in each flood extent. The four optimization results, one for each of the flood events, were summed to obtain one ranking for each land use change, thereby weighting the standardized pixel ranks according to the flood hazard, i.e. as the corresponding flood damages are weighted in Equation 5.5. Based on this combined rank, the top 750 pixels, representing 187.5 ha or approximately 4% of the study area, were selected, for both the afforestation and the sealing scenario.

Next, the runoff volume accumulation *Q* of each flood event was modeled with a resolution of 50 m, based on the land use dataset from 2012 (Agentschap Informatie Vlaanderen, 2016b) and meteorological information from the Royal Meteorological Institute (RMI) and the Flanders Environment Agency (Van Opstal et al., 2014) (see Chapter 2). Subsequently, the empirical relationship, analogue to Equation 5.1, between the modeled runoff volume accumulation *Q* at the corresponding extent's outlet and the derived flood volumes *Vol* of the thirteen observed flood extents was fitted with an adjusted R^2 of 0.76:

$$Vol = 10^{-6.32} * Q^{1.9} \quad (5.6)$$

This relationship was used to determine the flood volume before and after implementing the land use change scenarios based on the corresponding modeled accumulated runoff volume. Based on these flood volumes, the DEM of the corresponding flood extents were filled to determine the water depths with a resolution of 5 m. The flood damage and risk assessment was then implemented on these water depths before and after land use changes; and based on the difference between flood damage and risk, the relative impact of these land use changes was assessed.

5.3. Results

5.3.1. Flood damage and risk assessment of observed flood events

Statistics regarding the flood events are provided in Table 5.2, which details the flooded area, volume and damage for each flood extent in each of the four flood events, as well as the modeled accumulated runoff volume at each extent's outlet and the corresponding, modeled flood volumes derived with Equation 5.6. Figure 5.4 depicts the relationship, with an adjusted R^2 of 0.76, between the observed and modeled flood volumes.

Table 5.2. Overview of the flooded area (ha), total observed flood volume (m^3), resulting flood damages (€), runoff volume accumulation at the flood extents' outlet (m^3) and total modeled flood volume (m^3) for each of the four observed flood events and their corresponding flood extents.

Event	Extent	Flood Area (ha)	Flood Vol. (m^3)	Damages (€)	Runoff Vol. Acc. (m^3)	Flood Vol. (m^3) *Modeled*
02/2002		31	153 321	566 667	1 143 815	156 840
08/2002		4.2	14 699	27 515	199 406	5667
2003	Extent 1	4.3	24 698	49 693	295 820	11 994
	Extent 2	1.0	6032	68 405	282 365	10 978
	Extent 3	0.7	4003	21 552	258 176	9260
	Total	**6**	**34 733**	**139 650**		
2010	Extent 1	43.2	243 407	827 122	1 504 926	264 226
	Extent 2	0.7	2814	60 594	136 299	2749
	Extent 3	7.2	55 990	366 219	433 442	24 794
	Extent 4	1.4	6069	4414	335 090	15 201
	Extent 5	1.4	7331	11 382	303 962	12 629
	Extent 6	0.5	2848	43 835	199 504	5672
	Extent 7	1.2	6923	100 976	188 777	5107
	Extent 8	3.7	35 724	141 813	331 361	14 881
	Total	**59.3**	**361 106**	**1 556 355**		

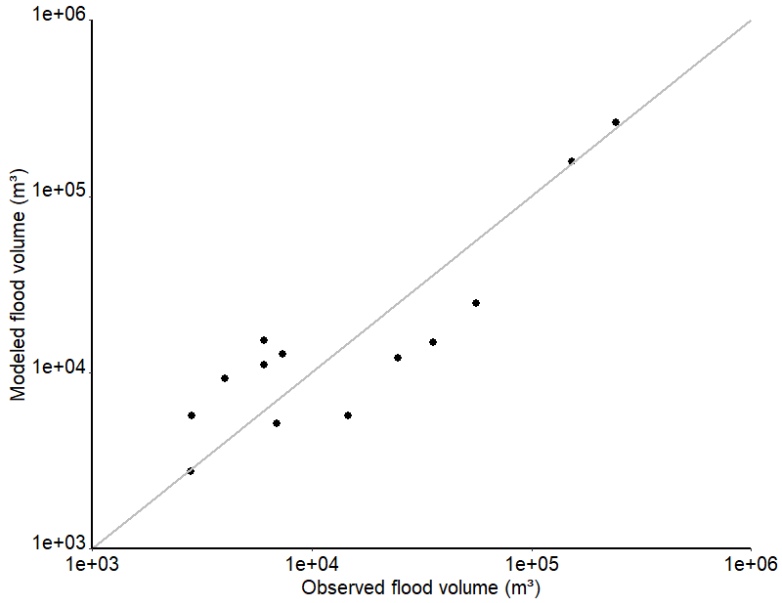

Figure 5.4. Scatterplot of the flood volumes derived from the observed flood extents (Observed flood volume, m^3) and the flood volumes as modeled by Equation 5.6 (Modeled flood volume, m^3), with an adjusted R^2 of 0.76 and a relative RMSE of 0.3.

The water depth and corresponding flood damage datasets are given on a per-pixel basis in Figure 5.5. The highest water depths were modeled in river pixels and pixels bordering the river. The flood damages are highly localized, with the highest damages inflicted in built-up pixels containing roads and residential buildings. The maximum flood damage in a pixel (25 m^2) was € 5493 or approximately € 220/m^2. The flood damage totaled respectively € 566 667, € 27 515, € 139 650 and € 1 556 355 for the flood events in February 2002, in August 2002, in January 2003 and in November 2010 (Table 5.2). During these four flood events, a total flood damage of € 2 290 187 was inflicted in the Maarkebeek catchment. The flood damage datasets were combined according to Equation 5.5 to determine flood risk or the expected annual damages in each pixel, as depicted in Figure 5.6. Analogue to flood damage, flood risk is highly localized and highest (€ 1265/year in a pixel or € 50.6/year/m^2) in repeatedly flooded, built-up pixels. The total flood risk derived from the four flood events in the Maarkebeek catchment equals € 178 252/year.

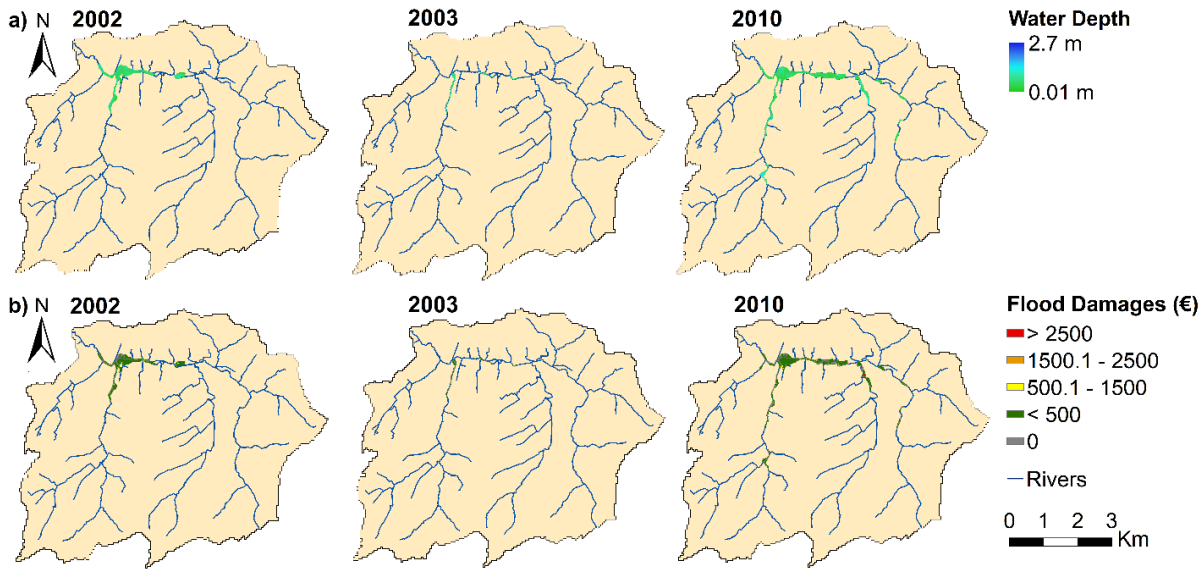

Figure 5.5. (a) The inundation depth (m) and (b) the corresponding flood damage (€) per pixel (5m X 5m resolution) derived from the flood damage model in the Maarkebeek catchment resulting from the observed flood events. The flood damage totaled respectively € 566 667, € 27 515, € 139 650 and € 1 556 355 for the flood events in February 2002, in August 2002, in January 2003 and in November 2010.

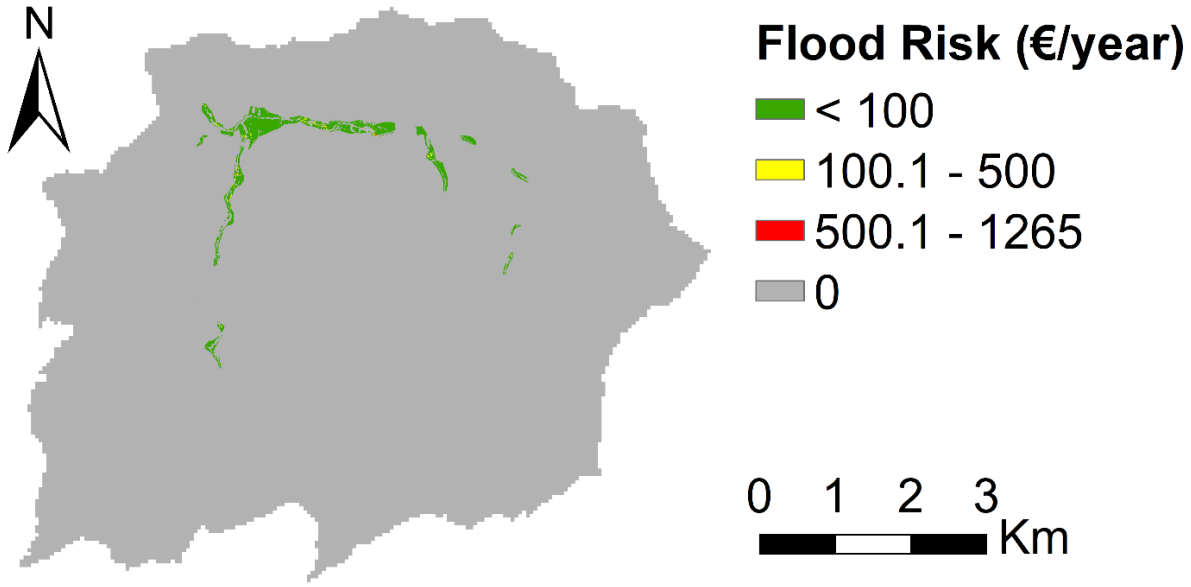

Figure 5.6. Flood risk, expressed as expected annual damages (€/year) in each pixel (5m X 5m resolution), in the Maarkebeek catchment based on the four observed flood events. Flood risk is highly localized and highest (€ 1265/year or € 50.6/year/m²) in only a few, built-up pixels which were repeatedly flooded. The total flood risk derived from the four flood events in the Maarkebeek catchment equals € 178 252/year.

5.3.2. Comparative flood damage and risk assessment

The standardized optimal rankings for the four flood events and their combined ranking are visualized in Figure 5.7 and Figure 5.8 for respectively the afforestation and soil sealing scenario, with the highest ranked pixels (rank 1) to be afforested or sealed first. The 750 highest ranked pixels or 187.5 ha, depicted in Figure 5.9, were selected in each land use change scenario. The pixels to be afforested (leading to maximal reduction of flood volume) are mostly located along the rivers, whereas pixels to

be sealed (leading to minimal increase of flood volume) are located in the more elevated parts of the catchment, away from the rivers and situated near forest patches. The selected pixels are mainly situated in the eastern part of the catchment, upstream from most flood extents: these pixels have higher ranks as land use changes in these pixels will have an impact on more flood extents. Pixels downstream from the flood extents were not taken into consideration in the soil sealing ranking, whereas in the combined ranking they were given the lowest rank (100).

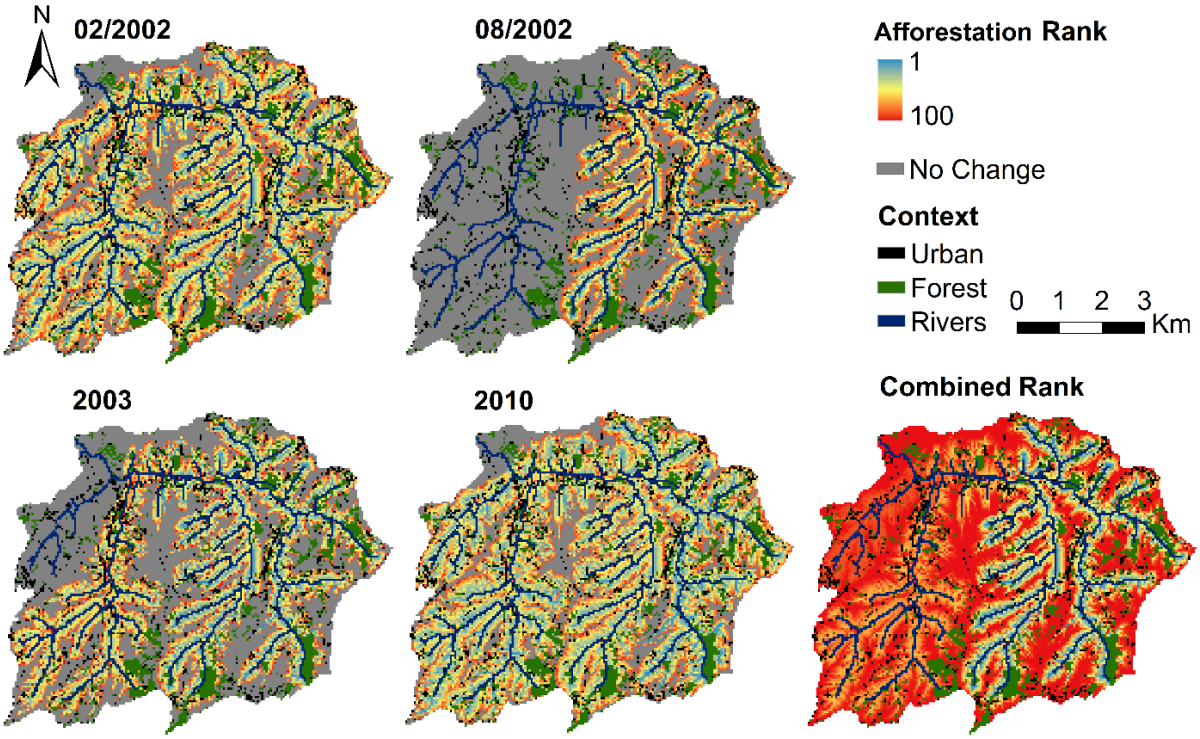

Figure 5.7. Standardized afforestation ranks of pixels in the Maarkebeek catchment for the four flood events. These standardized ranks result from a weighted summation according to the return periods of the considered flood events. The highest ranked pixels (rank 1, blue color) are to be prioritized for afforestation.

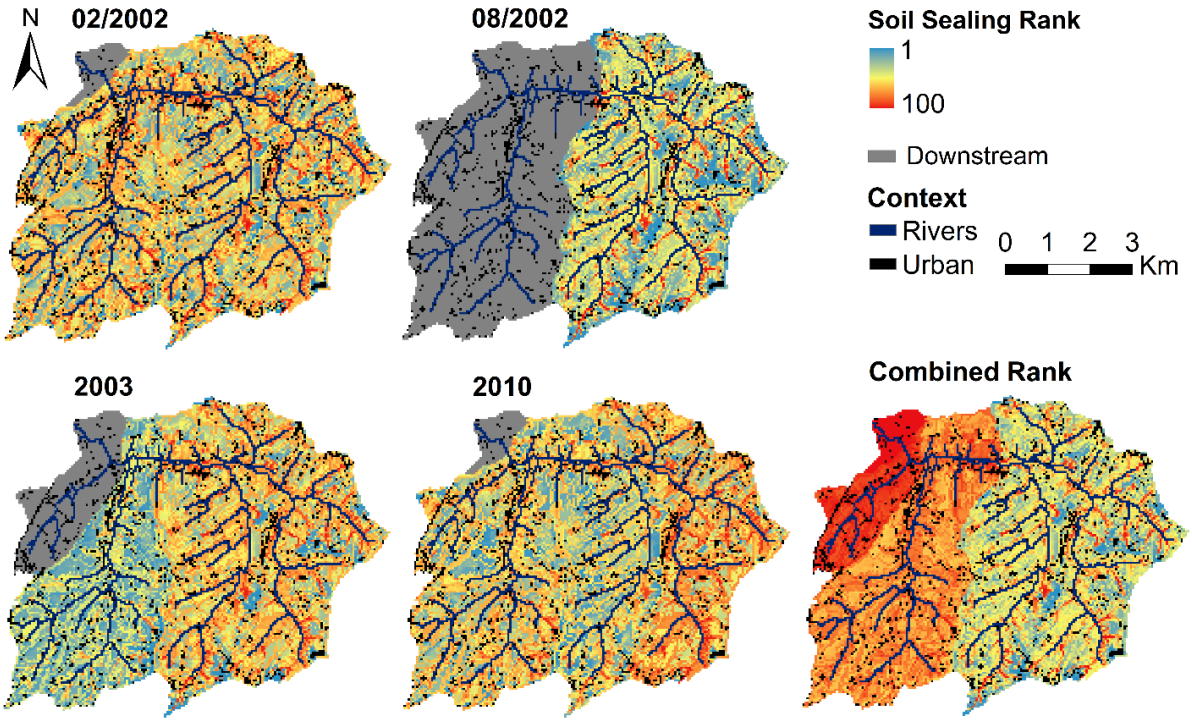

Figure 5.8. The standardized ranks for the soil sealing scenario for the four flood events in the Maarkebeek catchment. These standardized ranks result from a weighted summation according to the return periods of the considered flood events. The highest ranked pixels (rank 1, blue color) are to be prioritized for sealing.

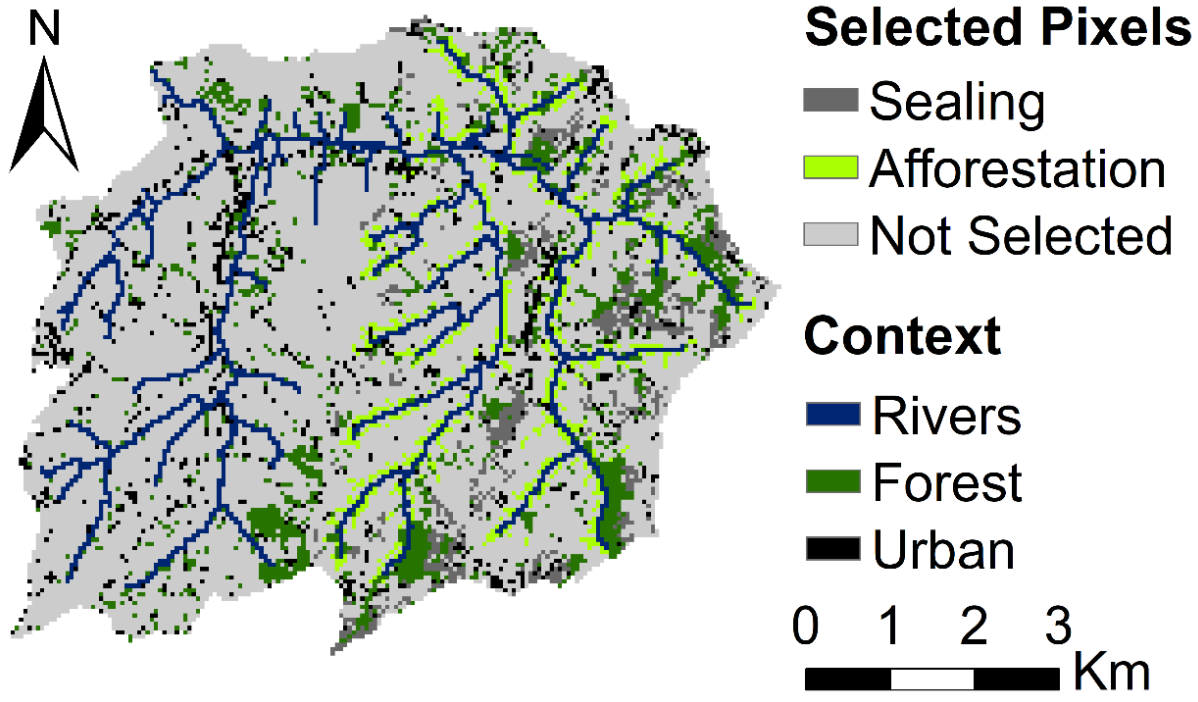

Figure 5.9. Locations of the pixels selected for land use change implementation, i.e. the 750 highest ranked pixels (187.5 ha) in the ranking combined over the four flood events, for both the afforestation and soil sealing scenarios.

Figure 5.10 depicts, for each flooded pixel, the relative decrease in flood damages after afforestation, i.e. the relative flood damage mitigation, and the relative flood damage increment after implementing the sealing scenario. This information is summarized in Table 5.3

Table 5.3for every flood extent and for each of the flood events. The relative flood damage mitigation after implementing the afforestation scheme was approximately -41.4% and -97.3% in respectively February and August 2002, -91.5% in 2003 and -39.3% in 2010. The high damage reduction in the flood event of 2003 is explained by the flood volumes in the two most upstream, smaller flood extents in this event being reduced to nearly zero (Table 5.3). The flood damage reduction is highest where the water depth is reduced in built-up urban areas. For the entire Maarkebeek catchment, the afforestation scenario reduced flood damages with 44.7%, which equals an absolute reduction of € 1 023 714. The relative damage increment after sealing the 750 least runoff incurring pixels equaled 1.1% and 2.8% in respectively February and August 2002, 0.01% in 2003 and 1.9% in 2010. The damage increase is mostly due to new pixels being flooded, however, it is limited due to the unbuilt nature of these areas, as the soil sealing took place in the uphill areas of the catchment, away from the rivers and flooded areas. Total flood damages in the Maarkebeek catchment increased with 1.5%, which resulted in an increase in total flood damage after soil sealing of € 34 353.

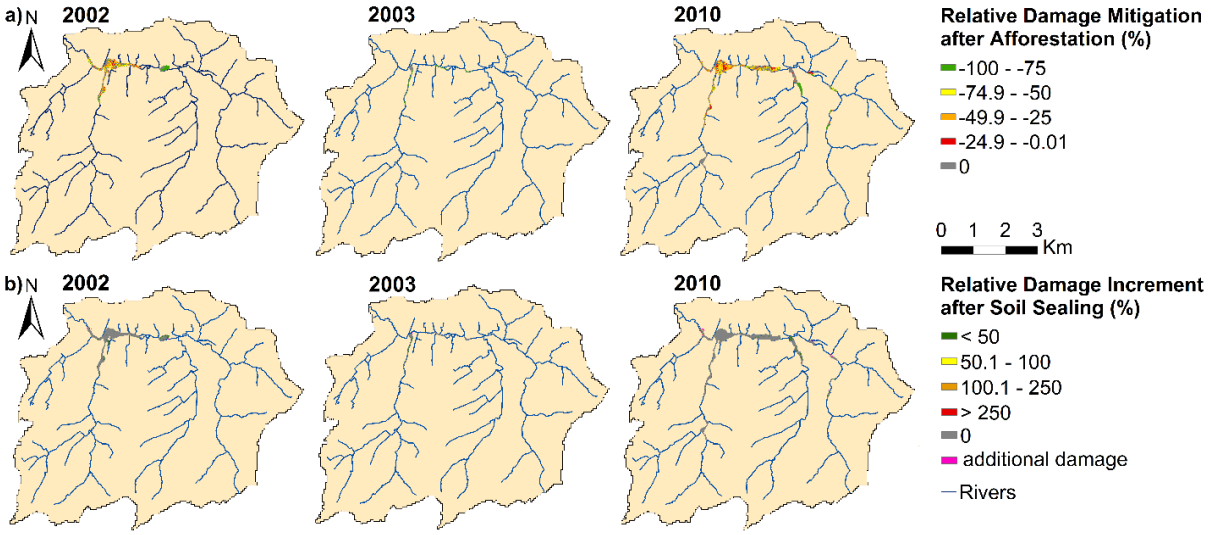

Figure 5.10. The relative impact in flood damages (%) after (a) implementing the afforestation scenario, resulting in a relative damage mitigation, and after (b) implementing the soil sealing scenario, resulting in a relative flood damage increment. New areas being flooded after soil sealing are depicted as 'additional damage', though these areas are limited to a few pixels bordering the river or existing flood extents.

Table 5.3. Relative flood damage mitigation and increment (%) after respectively afforesting and sealing the 750 highest ranked pixels in each land use change scenario.

Event	Extent	Damages (€)	Damage Mitigation (%) *Afforestation*	Damage Increment (%) *Sealed*
02/2002		566 667	-41.4	1.05
08/2002		27 515	-97.3	2.80
2003	Extent 1	49 693	-99.9	0.01
	Extent 2	68 405	-88.0	0.12
	Extent 3	21 552	-96.8	0.07
	Total	**139 650**	**-91.5**	**0.01**
2010	Extent 1	827 122	-44.3	0.77
	Extent 2	60 594	0.0	0.0
	Extent 3	366 219	-16.3	0.22
	Extent 4	4414	-67.2	0.08
	Extent 5	11 382	-74.1	74.8
	Extent 6	43 835	-86.2	3.73
	Extent 7	100 976	-22.3	0.0
	Extent 8	141 813	0.0	0.0
	Total	**1 556 355**	**-39.3**	**1.9**
Maarkebeek	**Total**	**2 290 187**	**-44.7**	**1.5**

Figure 5.11 visualizes, in a spatially explicit manner, where and how much the flood risk was relatively mitigated afforesting 187.5 ha of the most optimal locations for flood volume reduction. The total flood risk mitigation of this afforestation scenario equaled a reduction of 57% of the total flood risk (€ 178 252/year), representing an absolute value of € 101 604/year. The highest relative flood risk mitigation was achieved in areas where flood risk was highest, i.e. the built-up, urban areas, by reducing flood depth in these pixels. The relative flood risk increment after implementation of the sealing scenario (Figure 5.12) equaled 0.3%, increasing flood risk with a relatively small increment of € 535/year. Most of this increase was due to the flooding of more pixels, however, analogue to the damages, the flood risk increase is minimal since these pixels are within non-built up area.

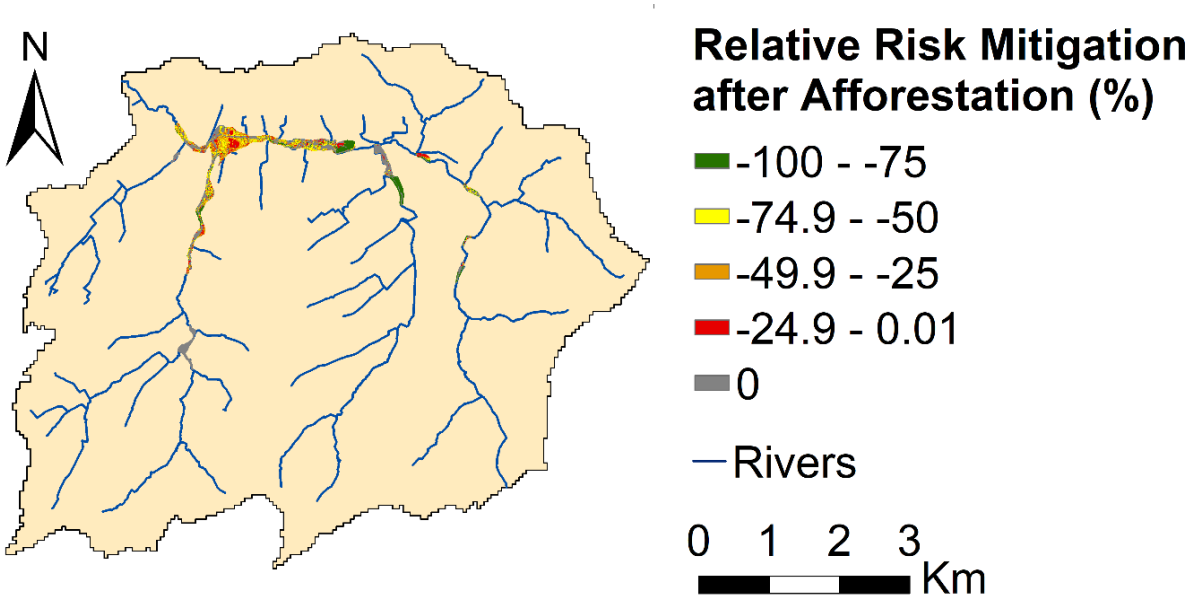

Figure 5.11. Relative flood risk mitigation (%) in the Maarkebeek catchment after afforesting the 750 highest ranked pixels in this land use change scenario.

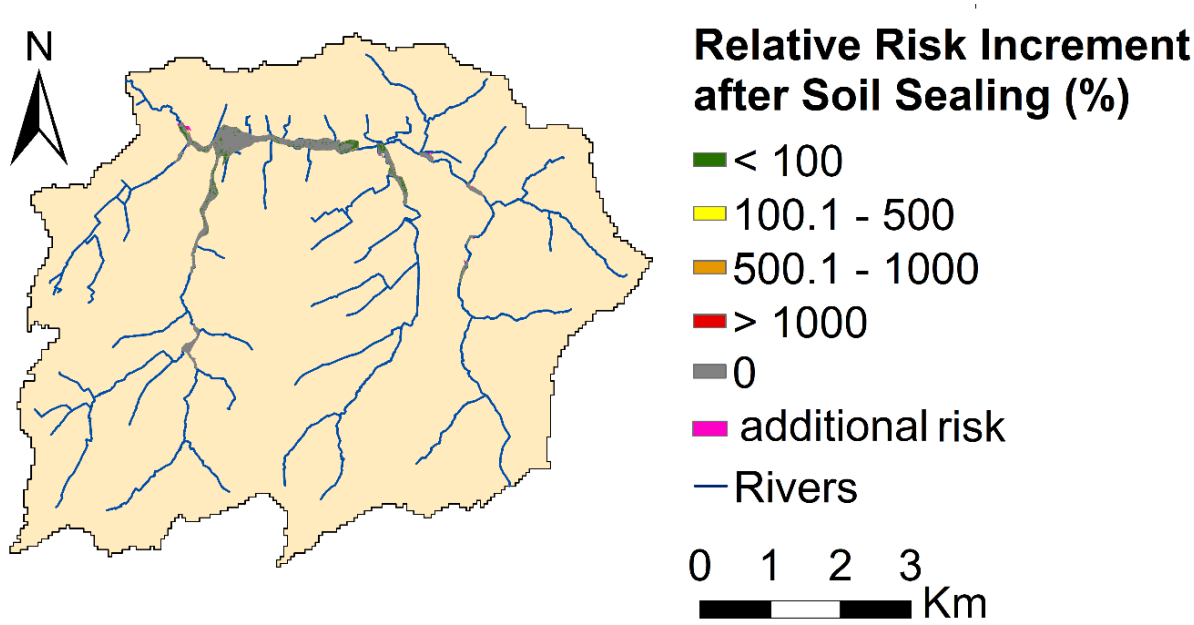

Figure 5.12. Relative flood risk increment (%) in the flooded areas in the Maarkebeek catchment after sealing the 750 highest ranked pixels in this land use change scenario. New areas being flooded after soil sealing are depicted as 'additional risk'.

5.4. Discussion

The results of the comparative flood risk assessment framework indicate the potential of identifying optimal locations in catchments for off-site flood damage and risk reduction or minimization of flood risk increment. A limited number of studies have assessed the effect of spatial adaptation measures on flood damages and flood risk, most notably Koks et al. (2014) assessed the impact of land-use zoning and compartmentalization on coastal flood risk in Belgium. This study indicated an increase in coastal flood risk without adaptation measures due to socioeconomic developments. Compartmentalization, i.e. upgrading linear elements in the landscape to serve as flood protection,

resulted in a higher risk reduction than land-use zoning, i.e. constricting urban development in flood prone areas, which decreased flood risk by 10 %. The flood risk assessment of soil sealing presented here indicates that constricting soil sealing and urbanization to higher elevations in the catchment results in an overall small relative increment in flood risk of 0.3% or € 535/year, since no additional urban areas are affected by an increase in flood volume. However, this analysis does not take into account urban floods or urban sewage systems, which also impact the hydrological response of the catchment leading to an increase in peak discharges (Poelmans et al., 2011).

The relative flood risk reduction resulting from the afforestation scenario totaled 57% in the Maarkebeek catchment, equaling € 100 856/year in absolute terms. This relative flood risk mitigation value can be considered a flood insurance value, delivered to the flooded areas downstream, i.e. each of the flood extents in the four considered events. Figure 5.12 quantitatively depicts, on a per-pixel basis, where this relative decrease in flood risk is delivered. The absolute flood risk reduction in the Maarkebeek catchment can be compared to the cost associated with the afforestation scenario, estimated based on information provided by E. Van Beek (personal communication, 3/11/2020) and from Van Den Broeck (2019). Saplings costs are approximated at € 1 – 1.5 each, resulting in a cost of € 4000 – 6000/ ha assuming a planting density of 4000 trees/ha. Labor costs are estimated at € 6000, though these costs can be reduced by working with volunteers. The highest cost in afforestation is the acquisition of land, as the price of agricultural land ranges from € 30 000 – 70 000/ha, and averages € 56 595/ha in the province of East Flanders (Federatie van het Notariaat, 2019), wherein the Maarkebeek catchment is situated. Assuming a total afforestation cost of € 67 000/ha in the Maarkebeek, the costs of afforesting 187.5 ha would amount to approximately € 12 500 000. Considering a reduction in flood risk of € 101 604/year, it would therefore take around 125 years for the risk reduction to compensate the costs of afforestation, not taking into account inflation. However, this scenario assumes the acquisition of 187.5 ha of land, constituting 85% of the cost of afforestation. The regional government in Flanders also promotes afforestation among land owners through subsidies, which can total up to € 3250/ha. Under the assumption that a governmental program would provide sufficient incentives to land owners in the Maarkebeek catchment to afforest 187.5 ha, costing at most € 8750/ha or € 1 640 625 in total, afforestation costs would be compensated by flood risk reduction after approximately 16 years. However, the afforestation scenario assumes the implementation of a full-grown forest. Consequently, the associated flood risk reduction corresponds to the risk reduction of a full-grown forest, not to a stand of saplings. Hence, afforestation costs would be compensated by the flood risk reduction approximately 16 years after the forest has reached maturity. A more detailed assessment of the risk reduction pertaining to the different development stages of a forest could be assessed by combining a forest growth model (e.g. Dalemans et al. (2015) with a hydrological model (Sutmöller et al., 2011), or by using a fully integrated hydrological model, e.g. MIKE SHE (DHI Software, 2008). In addition, one afforestation scenario, afforesting 187.5 ha of priority locations, is assessed here in terms of flood risk reduction and afforestation cost. Assessing multiple afforestation scenarios would provide the opportunity to evaluate the most performant afforestation scenario with regards to cost, i.e. afforestation cost, and benefit, i.e. flood risk reduction.

As an alternative to afforestation, cover crops can also decrease flood hazard, as assessed in Chapter 4 (Section 4.3.3), and can thus also contribute to flood risk reduction and be assigned a corresponding flood insurance value. This scenario was not assessed in this study considering its lower impact compared to afforestation. However, given the high cost associated with afforestation, cover crops may provide a more interesting alternative for risk mitigation regarding their cost-benefit. Moreover, cover cropping is easier to implement than large-scale afforestation, as it involves a shift in land management rather than a land use change.

The flood damage and risk assessment does not take into account monetary inflation; the accuracy of this assessment could therefore be increased by adjusting for inflation by using indexed prices to compare housing prices of 2002, 2003 and 2010. The flood damage assessment also only considers direct flood damages, as do most flood risk assessments (de Moel et al., 2015), as these costs are easy to quantify compared to indirect economic damages (e.g. loss of production of commercial goods for companies situated outside the flooded areas), which would require taking into account complicated economic networks (Merz, Kreibich, et al., 2010). Other risk assessments, including LATIS, also provide an indication of social and cultural impacts, together with the loss of life based on the rate of water level rise and flow velocity, however, this is beyond the scope of this assessment.

Validation of flood damage and risk assessments is generally challenging, as there is a lack of detailed and consistently updated flood damage databases. Therefore, comparisons between different risk assessments are often used as an alternative validation method (Gerl et al., 2016). Accordingly, the flood risk calculated in this study for the Maarkebeek catchment was compared to benchmark assessment of economic flood risk performed by the LATIS method, as depicted in Figure 5.13 (see also Chapter 1, Section 1.2, Figure 1.5b for the economic risk map of Flanders). This economic flood risk was determined by combining economic damages of flood events with a return period of 10, 100 and 1000 years. The overall flood risk calculated by LATIS in the Maarkebeek catchment is € 247 255/year, which is considerably higher than the flood risk of € 178 252/year calculated in this analysis. This can be explained on the one hand by the larger area at risk of flooding considered in the LATIS tool based on modeled flood events with larger return periods. Considering only the pixels at risk of flooding in the presented framework, the LATIS framework estimates flood risk at € 227 139/year. On the other hand, the maximum damage per pixel is higher in the LATIS estimate (€ 9880) than in the presented framework (€ 1265), which is the result of the more extensive economic assessment incorporated in LATIS. The LATIS framework also assesses indirect, internal economic damages, such as clean-up costs, in addition to direct economic damages, which are more comprehensive, including, for instance, damage to vehicles (VMM, 2018a). Flood damage assessments typically show a high level of uncertainty in the estimates of maximum damages and in the definition of depth-damage curves (de Moel & Aerts, 2011). Absolute estimates of flood damage therefore have a high level of uncertainty, which is less of an issue when comparing two situations relative to each other, i.e. in the comparison of land us changes, as in the relative risk assessment of the afforestation or soil sealing scenarios (de Moel & Aerts, 2011; Koks et al., 2014).

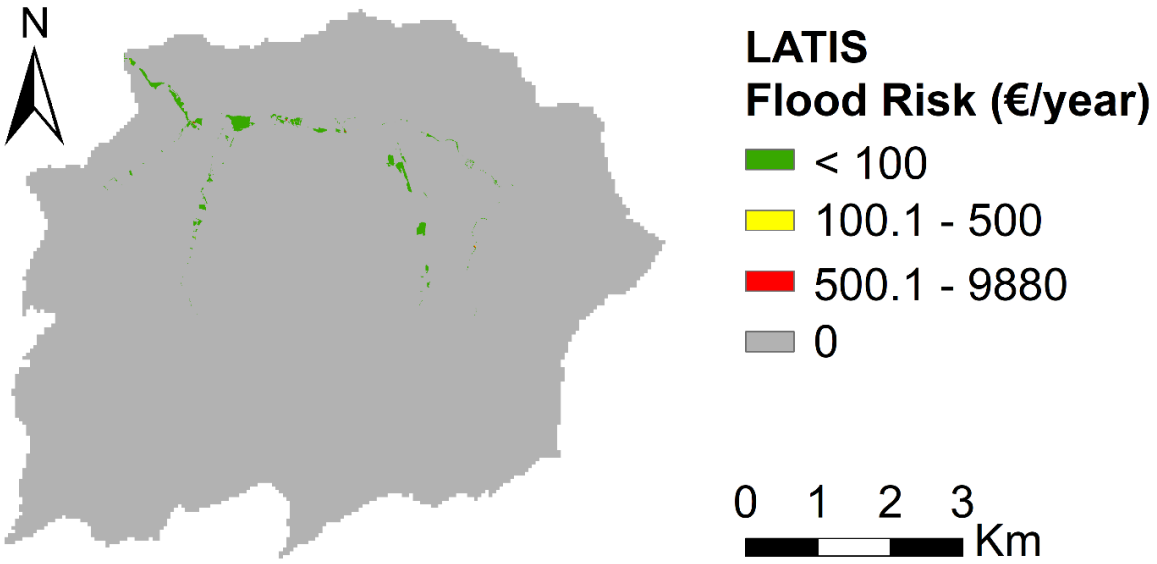

Figure 5.13. Flood risk (€/year per pixel of 25 m²) in the Maarkebeek catchment as calculated by the LATIS tool based on the flood damages determined for flood events with a return period of 10, 100 and 1000 years (adapted from (VMM, 2015b)). (source: Vlaamse Milieumaatschappij, Waterbouwkundig Laboratorium, Maritieme Dienstverlening & Kust, & De Vlaamse Waterweg nv, 2020).

The presented flood risk assessment assesses flood damage and risk reduction or increment resulting from land use changes based on an event-based rainfall-runoff model calculating runoff volume as accumulated during the event. Instead of deriving peak discharge from runoff volume using the rational method (Bingner et al., 2018; Yeo & Guldmann, 2010) and relating the flood peak discharge to flood volume analogue to Mediero et al. (2010), flood volume was directly derived from accumulated runoff through an observed statistical relationship with an adjusted R^2 of 0.76. However, a regional analysis should be performed to assess the applicability of this relationship as in Mediero et al. (2010). These peak discharges could also be related to the water level, as implemented in the Floodscanner described in Ward et al. (2011). A straightforward, conceptual 'bathtub'-model (Teng et al., 2015) was implemented to fill in the DEM based on these derived flood volumes. However, this simple method will be unable to accurately simulate inundation in more urbanized settings, where flood risk is highest. As such, more complex hydraulic models (e.g. MIKE HYDRO (DHI Software, 2020b)) need to be implemented in the framework to provide more the uncertainty in the modeled flood extents and corresponding water depth after land use changes.

Most flood risk frameworks assess risks based on hypothetical flood events with known return periods, derived from hydrodynamic models encompassing composite hydrographs, which are constructed from extreme value analyses of rainfall-runoff discharge time-series (de Moel et al., 2009, 2015; Kellens et al., 2013; Ward, de Moel, et al., 2011). The impact assessment of land use changes on these hypothetical flood events would therefore require modeling a long rainfall-runoff time series in order to assess the difference in composite hydrograph and corresponding flood extent. In the presented framework, it was therefore opted to use observed, historical flood events, of which the return periods were estimated based on an analysis of annual maximum discharges. However, the comparison between these observed flood events is restricted, since boundary conditions may have significantly altered between observations (de Moel et al., 2009). Moreover, these historical flood events are characterized by specific meteorological conditions, including rainfall distribution, which will impact the occurrence of flood extents and thus influence the pixel ranking of the optimization

framework. This is reflected in the flood event of August 2002 (Figure 5.7 and Figure 5.8), where one flood extent was recorded in the east of the Maarkebeek catchment. The historical flood events are thus not as representative to assess flood risk as the hypothetical flood events, and more flood events with a larger range in return periods are required to provide a more comprehensive assessment of flood risk (Ward, de Moel, et al., 2011).

5.5. Conclusion

The presented comparative flood risk assessment framework allows for an estimation of the relative reduction or increase in flood damages and risk due to the implementation of land use changes, thereby explicitly taking into account off-site effects of these land use changes. The comparative flood risk framework was applied in a case study in the Maarkebeek catchment, situated in Flanders, Belgium. Four historical flood events were considered in the risk assessment and their corresponding flood damages and risk were subsequently assessed using a flood damage model. Land use change scenarios were devised, based on the optimal locations in the catchment for afforestation and soil sealing over all four flood events, as identified by the iterative optimization framework, developed in Chapter 4. The 750 pixels (187.5 ha) highest ranked pixels were subsequently selected for afforestation, on the one hand, and for soil sealing, on the other hand. These pixels were situated near the rivers in the case of afforestation or at higher elevation for soil sealing. Comparing flood damages and risk before and after land use change implementation showed a large flood risk mitigation value of 57% in flood risk after afforestation, which can be interpreted as a flood insurance value delivered to the downstream flooded areas. This flood risk mitigation value or insurance value was determined in a spatially explicit manner, depicting which areas benefit the most from afforestation. A limited increase of less than 1% in flood risk after soil sealing was also observed.

However, this framework also has limitations, some inherent to flood damage estimation, such as the uncertainty in maximum damage estimates and depth-damage curves, and some specific to this assessment, as it is based on observed flood events rather than hypothetical flood events with known return periods and it derives flood volumes from runoff volume accumulation based on an empirical relationship, which should be further established using regional analyses. Despite these limitations, the framework provides the possibility for quick spatial assessments of the flood insurance value or relative risk increment associated with potential land use changes. As such, this framework can be used as an explorative tool in spatial planning processes related to flood risk management.

Chapter 6
General Discussion and Conclusions

6.1. General discussion

In Chapter 1, three research questions were put forward, in which the relationship between upstream land use configurations and downstream fluvial flood severity, expressed by its extent, water depth and water volume, is central:

1. Do upstream land use changes, particularly soil sealing, affect downstream fluvial flood severity?
2. How can upstream locations be determined where land use change has the maximal resp. minimal impact on downstream fluvial flood hazard and severity?
3. How can the mitigation or exacerbation of downstream fluvial flood hazard and severity exerted by upstream land use changes be characterized in terms of the monetary insurance value of the upstream land use system?

Figure 6.1 visualizes the workflow of this thesis, addressing these questions by (1) an empirical spatio-temporal analysis of flood extents in relation to land use configurations in Chapter 2 and the development of a computationally efficient RR-model accounting for re-infiltration along the flow paths in Chapter 3, (2) the development of an iterative framework, integrating the RR-model, for the determination of the optimal location of land use changes regarding their impact on flood hazard downstream in Chapter 4 and (3) the determination of the flood insurance value associated with these land use changes in a comparative flood risk assessment in Chapter 5. This final chapter provides an overview of the findings and discusses the main uncertainties related to each research question. A more extensive and detailed discussion was provided in each dedicated chapter of this thesis.

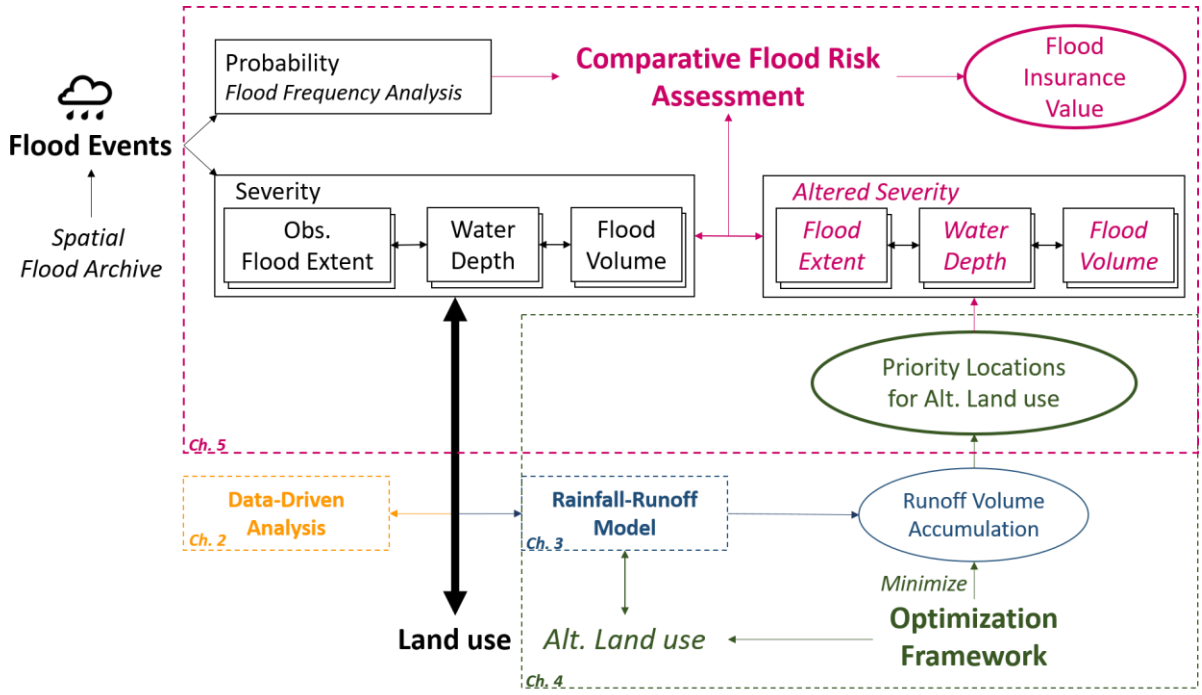

Figure 6.1. Schematic depiction of the workflow followed in this thesis, referencing the relevant chapters.

6.1.1. Upstream land use and downstream flood severity

The relationship between upstream land use and downstream flood severity is assessed in this thesis in a data-driven analysis in Chapter 2 and in the conceptualization of an empirical, computationally efficient RR-model in Chapter 3. This RR-model is subsequently implemented in an optimization framework in Chapter 4, in which three land use change scenarios were assessed, namely an afforestation, a soil sealing and a winter cover crop scenario. In Chapter 5, the RR-model is combined with a simple, conceptual "bath-tub"-approach to simulate flooding from the river based on the flood volume after implementation of a land use change scenario.

Overall, the relationship between land use and flood severity was considered in four study areas located in three primary river basins, namely the Maarkebeek catchment situated in the primary river basin of the Upper Scheldt, the Bellebeek and Hunselbeek catchment in the Dender river basin and a subcatchment of the Demer river basin, the latter being only included in Chapter 2. These four study areas constitute small to medium-sized catchments. They were chosen for this research, since it has been shown that land use, and thus land use changes, mostly impact hydrology at this spatial scale (Blöschl et al., 2007; Wheater & Evans, 2009). The RR-model of Chapter 3 assessed land use changes with a resolution of 50 by 50 m, which is also the native resolution of the ArcNEMO model used to calculate the soil moisture conditions in the catchment areas antecedent to the studied rainfall events (Van Opstal et al., 2013). This resolution is suitable to assess the impact of land use changes, while maintaining the computational efficiency. To assess the impact of smaller-scale, nature-based interventions, e.g. establishing or removing landscape elements like hedgerows, ponds and drainage ditches, a higher spatial resolution, i.e. smaller pixel size, would be required. However, this would inevitably lead to an increase of the computational burden of the RR-model in the iterative optimization framework (Chapter 4).

Soil sealing in this thesis is defined as the covering of soils with artificial, impermeable material, such as asphalt (Jones et al., 2012). In the highly urbanized Flanders region, the impact of soil sealing provides a major hydrological challenge (Pisman et al., 2018; Vlaamse Regering, 2020). However, other processes of soil degradation will also impact catchment hydrology and thus may exert an influence on flood severity. In the rural study areas of the Maarkebeek, Bellebeek and Demer catchments, soil compaction could also exacerbate downstream flood severity. Soil compaction is defined as the degradation of soil under pressure, which lowers the porosity and permeability of the soil and thus increases rapid surface runoff (Alaoui et al., 2018; Jones et al., 2012). Though a large part of Flanders is highly sensitive to soil compaction from heavy machinery (Van De Vreken et al., 2009), soil compaction was not considered as a factor in the data-driven analysis. Compaction was also not considered in the land use change scenarios in the optimization framework, though it could provide an interesting assessment to an underexposed problem in Flanders. However, the hydrological impact of soil compaction would be modelled similarly to the soil sealing scenario by increasing the CN value and decreasing the Manning's roughness coefficient *n.* As such, it can be expected that a similar conclusion could be drawn for soil compaction as for soil sealing, i.e. that compaction should be avoided first and foremost in the river valleys to prevent an increase in flood hazard. As soils in wet conditions are especially sensitive to compaction, such a conclusion would be highly relevant for policy makers, however, additional analyses are required to confirm this statement.

Flood severity is characterized in this thesis by flood extent and its corresponding water volume and water depths. In Chapters 2 and 5, flood severity was assessed based on historical, observed flood events as recorded in the geospatial flood archive maintained in Flanders since 1988 (Agentschap Informatie Vlaanderen & Vlaamse Milieumaatschappij, 2017). However, as these observed flood extents are compiled from a variety of sources, including analogue sources, the accuracy of these

observed extents is variable and not fully known. Moreover, the recorded flood extents can also be biased towards larger flood events or towards flood events causing more damage. Therefore, flood events with small extent and high return periods may be underrepresented in this archive.

In Chapters 2 and 5, flood volume and water depth were derived from the flood extents recorded in the spatial flood archive by combining the extents with a DEM with 5 m x 5 m resolution. The vertical error of 7 cm on smooth surfaces associated with this DEM (Agentschap Informatie Vlaanderen et al., 2006) is relatively small compared to the uncertainties associated with the planimetry of the recorded flood extents. The uncertainty regarding the input data of the flood volume derivation is therefore mainly associated with the uncertainty of the observed flood extents. In Chapter 2, flood volumes were derived from the flood extents, thereby assuming that the elevation of the water level equals the surface elevation of the extents' border pixels. Subsequently, the surface elevation is subtracted from the water level to derive the water depth in each pixel. In Chapter 5, flood volumes and water depths were derived by a similar approach fitting a linear trend through the same boundary vertices, as well as the vertices of the pixels bordering the river, i.e. the river banks. Next, this water elevation trend was averaged with a local derivation of the water level based only on the surface elevation of the nearest border pixels. This additional step was required to correct for negative water depths, i.e. when the trend surface was lower than the surface elevation, which mainly occurred in relatively small flood extents. The impact of the different methods was compared for the 2003 flood event in the Maarkebeek catchment, encompassing three smaller flood extents considered in both analyses. The flood volume obtained for this event in Chapter 5, i.e. around 35 000 m^3, is more than the double of the flood volume derived in Chapter 2, approx. 15 000 m^3. This points to the large influence of the method to derive water depths and associated flood volumes from the recorded flood extents, and as such to a large uncertainty on these variables. However, despite this uncertainty, it was found in Chapter 2 that the performance of the statistical models is similar when flood area or volume were considered as dependent variable. In the flood damage assessment in Chapter 5, a comparison is made between the derived water depths and corresponding water depths after implementing land use changes, which was simulated based on a statistical relationship between derived flood volume and runoff accumulation. Though a large uncertainty is associated with these water depths, flood damage assessments in general intrinsically have a high level of uncertainty, which is mainly related to the estimates of maximum damages and to the depth-damage curves (de Moel & Aerts, 2011). Moreover, this uncertainty is less of an issue when aiming at comparison (Koks et al., 2014), as in Chapter 5.

In Chapter 3, a spatially explicit and computationally efficient Rainfall-Runoff (RR-)model was conceptualized based on the empirical SCS-CN method (USDA Natural Resource Conservation Service, 1986). This model calculates the runoff volume generated during a rainfall event in each pixel, using meteorological input and parameters describing soil moisture and land use, and includes a surface runoff routing procedure to consider the spatial interactions along downstream flow paths. In the conceptualization of this model, several RR-model configurations were evaluated for three study areas, namely the Maarkebeek, Bellebeek and Hunselbeek catchments. The default SCS-CN method was compared to CN models implementing AMC correction and re-infiltration methods, thereby increasing model complexity. A comprehensive discussion of the uncertainties regarding the conceptualization RR-model was provided in Chapter 3 (Section 3.4). In this analysis, only a minimal calibration was performed i.c. the testing of a Manning's *n* adjusted to seasonal vegetation cover and the evaluation of three uniformly distributed values of hydraulic radius R_h in the Manning's equation. Though limited, the sensitivity analysis in Chapter 3 indicated that the Van Loo re-infiltration method is sensitive to variations in R_h. Given that the higher model complexity of the RR-model increases model uncertainty compared to the default SCS-CN method, a more complete uncertainty analysis of all model parameters could be performed, either with a One-At-a-Time (OAT) analysis as presented in

Chapter 2 or through a more complete Monte Carlo approach (de Moel et al., 2012), to assess this increase and the need for calibration, and quantify model uncertainty. This would also provide better insights in the uncertainty of the results of the iterative optimization procedure presented in Chapter 4 and the flood risk assessment framework presented in Chapter 5. In this regard, a sensitivity analysis with regard to the pixel rankings of the optimization framework is also of interest to evaluate the robustness of the optimization results. Despite the limited calibration, the NSE values of resp. 0.57, 0.56 and 0.66 in the Maarkebeek, Bellebeek and Hunselbeek catchments were considered sufficiently high to integrate the model configuration implementing a λ value of 0.05, the AMC method of Neitsch et al. (2011) and the re-infiltration method of Van Loo (2018) in the iterative framework and assess the hydrological impact of land use changes at alternative locations in the catchment relative to each other. However, it is important to note that the performance of this modeling framework reflects the initial parameter choice, compensating for the initial underestimation of runoff volume, thereby reflecting the issue of equifinality (Beven, 2006). It is thus not an absolute finding that this model configuration is the best performing one. Consequently, a full calibration of model parameters, including a spatially variable R_h, and independent validation on more medium-sized, nested catchments with varying land use types would provide better insights in the applicability and limitations of this RR-model, when applied to other catchment than those considered in this study.

The RR-model was developed to assess land use changes in a spatially distributed way with a low computational burden. Though the developed model is spatially distributed, it is temporally lumped, assessing the total runoff accumulated in each pixel in the course of single rainfall events of variable duration. However, land use changes also impact flood events on a temporal scale, changing the shape of the flood hydrograph, including the peak discharge, a common and important variable used in hydrological assessments of land use changes (Bronstert et al., 2002; Miller & Hess, 2017; Peel, 2009; Poelmans et al., 2011).

A common method to derive peak discharge Q_p from rainfall is the extended TR-55 procedure (Bingner et al., 2018; USDA Natural Resource Conservation Service, 1986), as implemented in Yeo & Guldmann (2010):

$$Q_p = 2.78 * 10^{-3} * P_{24} * D_a * \left[\frac{a + (c * T_c) + (e * T_c^2)}{1 + (b * T_c) + (d * T_c^2) + (f * T_c^3)}\right] \quad (6.1)$$

with Q_p the peak discharge [m³/s], D_a the total drainage area [ha], P_{24} the 24-hour effective rainfall over drainage area [mm], T_c the time of concentration [hr], and a, b, c, d, e and f representing unit peak discharge regression coefficients for I_a/P_{24} which are provided in Bingner et al. (2018). Time of concentration can be derived from the maximum travel time across all flow paths to the outlet, as determined by Manning's equation.

An alternative approach would be to derive peak discharge Q_p from flood volume V using a statistical relationship between both variables, i.e. a power law with coefficients a and b (Costelloe et al., 2013; Gaál et al., 2015; Mediero et al., 2010):

$$Q_p = b * Vol^a \quad (6.2)$$

This power law relationship was derived for the Maarkebeek, Bellebeek and Hunselbeek catchments based on the rainfall events selected in Chapter 3, resulting in an adjusted R^2 of resp. 0.77, 0.79 and 0.73 in the Maarkebeek (b=2.48, a=0.63), Bellebeek (b=0.13, a=1.69), and Hunselbeek (b=1.24, a=1.48) catchments. For the derivation of flood volume from runoff volume accumulation in Chapter 5 (see Equation 5.1), a similar power law relationship between both variables was assumed. The simulated peak discharges, derived either with the extended TR-55 or with the power law method,

could be validated in future research using the observed peak discharges corresponding to the rainfall events in Chapter 3.

The empirical approaches in Chapter 2 and Chapter 3 describing the relationship between land use and flood severity both suffer from a lack of physical context. In Chapter 2, factors describing flood regulation measures or agricultural practices influencing discharge into the river, such as the presence of drainage ditches, are not included in the linear regression or machine learning models. This is partly related to the limited sample size, which restricts the number of factors that can be included in the models with regard to their statistical power. However, not including these contextual factors contributes to the inaccuracy of the statistical models. The RR-model configurations in Chapter 3 are based on empirical methods, i.e. the SCS-CN method and Manning's equation, and as such do not model soil physical processes related to infiltration and runoff. An interesting alternative physics-based model approach is implemented in OpenLISEM, which provides methods to simulate infiltration, runoff and shallow flooding (Bout & Jetten, 2018; Jetten & De Roo, 2018). A metamodel based on OpenLISEM could possibly provide a valuable alternative to the empirical RR-model conceptualized in this thesis.

6.1.2. Where to implement land use changes? An iterative optimization framework

The computationally efficient RR-model was subsequently integrated in an iterative optimization framework in Chapter 4, which is therefore able to structurally assess the search space in a two-step iteration, which considers all eligible pixels in the basin, and finds an optimal solution, instead of relying on heuristic algorithms that more randomly limit the search space and often obtain sub-optimal solutions (Volk et al., 2010). The optimization framework identifies the priority locations for alternative land use systems, i.e. for land use changes which minimize the flood severity in downstream, flood-prone areas. As such, the runoff volume accumulation in the downstream points of interest, as calculated by the RR-model, is considered a proxy for flood severity, assuming that a higher runoff volume accumulation corresponds to a higher flood severity, by increasing the flood volume and depth.

In Chapter 4, the optimal locations were determined for afforestation, soil sealing and cover crops in the studied catchment from the perspective of flood volume minimization. The results highlight the importance of maintaining and maximizing the infiltration capacity in the river valleys. This became apparent in the afforestation case, as the potential increase in infiltration capacity after afforestation is fully exploited in downstream locations with high flow accumulation. These results reflect the findings of Yeo & Guldmann (2010).

Validation of the priority locations derived from the optimization framework is challenging, though the relative runoff volume decrease or increase, depicted in Figure 4.11, confirms the higher impact of the higher ranked pixels. However, the high level of uncertainty and empiricism related to the RR-model is propagated in the iterative optimization framework. Therefore, the resulting pixel ranking and land use change scenarios could be further assessed in an additional validation using a full spatially-distributed and integrated hydrological model, such as MIKE SHE (DHI Software, 2008). Moreover, the empirical RR-model assesses the hydrological impact of land use changes in a temporally lumped approach without taking into account soil physical subprocesses which affect infiltration and runoff. Consequently, the impact of these priority land use change scenarios could be assessed at a larger scale using other models like the continuous model STREAM (Aerts et al., 1999). Also, the event-based physical model OpenLISEM (Bout & Jetten, 2018; Jetten & De Roo, 2018) could be used to assess the land use changes with regard to soil physical properties.

Each land use change scenario was optimized and assessed independently from each other. In future research, this optimization framework could be further extended to include a portfolio of land use change types and include multiple ecosystem services. This is further elaborated in Section 6.2.2.

6.1.3. Quantitative, economic impact of land use changes: the comparative flood damage and risk assessment

In Chapter 5, a framework to compare flood damage and risk before and after the implementation of land use changes was presented. Flood damage and risk are determined in a probabilistic approach taking into account flood hazard, through its probability of occurrence, and the vulnerability of the elements exposed to the flood. This framework integrates the models and approaches formulated and evaluated in Chapter 3 and 4. Though these models are implemented with a spatial resolution of 50 m by 50 m, flood damage and risk are assessed on a finer resolution of 5 m by 5 m, corresponding to the resolution of the DEM and the land use geodataset from 2012 (Agentschap Informatie Vlaanderen, 2016b; Agentschap Informatie Vlaanderen et al., 2006).

Altered flood volumes after land use changes were derived from the runoff volume obtained with the RR-model developed in Chapter 3 using a statistical relationship. Though an analogue relationship was established between flood peak and flood volume, the reliability of this relationship should be further assessed, especially given the uncertainty related to the derived flood volumes (Section 6.1.1). This altered flood volume was translated to flood extent and related water depth based on a simple, conceptual "bath-tub" approach (Teng et al., 2015). This conceptual model does not take into consideration the complex physical context, for instance the presence of sewer systems in urbanized settings, or hydraulic flow processes, but only models water depth based on relative elevation. An alternative approach to reduce the uncertainty in the water depths and take account of physical processes would be to implement the land use change scenarios using a coupled hydrological-hydraulic model, as offered by, for instance, MIKE HYDRO (DHI Software, 2020b). However, de Moel & Aerts (2011) found the maximum damage and depth-damage curves to be the main source of uncertainty in flood risk assessments, which poses less of an issue when comparing the flood risk impact of land use changes (Koks et al., 2014), as performed in this study.

The flood damage model implemented in this assessment was used to calculate direct economic damages, thereby relying on depth-damage curves from Vanneuville et al. (2006) and data on maximum damages implemented in the LATIS tool (Beullens et al., 2017; Vanneuville et al., 2006) and retrieved from Koks et al. (2014). Flood damages and corresponding risk were assessed in the Maarkebeek catchment based on four observed flood events. Also here the presence of uncertainties regarding the uncertainties in flood extent and water depths should be mentioned (see the discussion in Section 6.1.1), since extent and depth form the basis of the flood damage calculations. Moreover, as discussed in Section 5.4, these observed flood extents are not necessarily as representative for floods of a certain return period as hypothetical, modeled flood events would be.

As the proposed flood risk assessment approach combines water depths with land use information and includes maximum damage numbers and depth-damage curves, the uncertainty in each source of information propagates through the different steps of the assessment framework into the final result (de Moel & Aerts, 2011). Moreover, validation of flood damage and risk assessment is challenging, as there is in general a lack of detailed and reliable flood loss data (Gerl et al., 2016), which also applies for Flanders. As an alternative, the outcome of the flood risk assessment in the Maarkebeek catchment was compared with results provided by LATIS, the benchmark flood risk model for Flanders. Differences in flood risk of about 30% were obtained between the benchmark LATIS flood risk (€ 247 255/year) and the reference flood risk (€ 178 252/year) calculated in Chapter 5. This could be partially

explained by the more extensive economic analysis performed in LATIS, including indirect economic damages, additional assets, e.g. vehicles, and a more comprehensive damage assessment of buildings, including also locations, which are particularly vulnerable such as underground parking lots.

6.2. General conclusion

This PhD research integrates spatial modeling and optimization with economic assessments in order to inspire policies and practices for nature-based flood risk management in Flanders. In this section we highlight the policy implications and address a selected set of issues which should be tackled in further research.

6.2.1. Policy implications

The spatial flood archive, maintained by the Flemish Environment Agency, provides a valuable source of information about the delineation and timing of effectively flooded areas in Flanders (Agentschap Informatie Vlaanderen & Vlaamse Milieumaatschappij, 2017). It is currently assembled from a variety of sources, with varying uncertainty connected to them, i.e. information provided by municipal observations and derived from aerial orthophotographs. The recorded observations in the spatial archive could be made more robust by providing a consistent benchmark for these observations, for instance through the systematic delineation of flood extents using Synthetic Aperture Radar (SAR) imagery (Benoudjit & Guida, 2019; Hostache et al., 2018).

The results presented in Chapter 4 consistently show the importance of river valleys in mitigating downstream flood hazards, as these areas are prioritized for afforestation and are to be avoided for soil sealing. The results of Chapter 5 show that, in the Maarkebeek catchment, afforesting the 187.5 ha highest ranked pixels (situated mainly in river valleys) reduced flood risk with 57%, while 187.5 hectares of extra soil sealing away from the valleys leads to a relatively small increase of less than 1% in flood risk. In Flanders, where land is scarce and costly and as such, interventions should be implemented with the highest efficiency, these results are valuable input for flood risk management and related spatial planning policy and practice, where it regards the reduction of soil sealing, the establishment of Green and Blue Infrastructures and the restoration of natural flood plains (Departement Ruimte Vlaanderen, 2017; VMM, 2019). The soil sealing results also emphasize the importance of the so-called ‘water check’ policy measure, that must inform planning and building permissions (Coördinatiecommissie Integraal Waterbeleid, 2015). The halting and even the reduction of soil sealing is a current point of discussion, centered on the so-called ‘building shift’. This policy aims to halt soil sealing in Flanders by removing the building rights on certain plots of land. However, this comes at a high cost, as the loss of these rights by the owners is to be compensated at 100% of the market value by the local authorities (Grommen, 2020). The results of this research present a procedure to most effectively allocate the efforts of this building shift by identifying the upstream areas contributing to flood risk reduction downstream, as efforts at these locations will have a higher return on investment in terms of the corresponding reduction in flood risk. The findings of this thesis with regard to afforestation (Chapter 4 and Chapter 5) thereby point to the important flood insurance value of Green and Blue Infrastructure and natural flood plains for downstream areas of interest. Efforts to establish these green networks, including cover cropping on arable land, should be prioritized in upstream catchment areas with high flow accumulation to mitigate flood risk downstream.

The optimization framework and comparative flood risk assessment were illustrated for study areas in Flanders. However, the presented frameworks are generic and can be applied in other small- to medium-sized, hilly catchments, for which sufficient input data is available. For instance, the

frameworks could be applied in catchments in other places in the world, where the establishment of nature-based flood risk management would be beneficial in support of overall flood risk management. The optimization framework and flood risk assessment provide an off-site extension to the currently available toolsets supporting sustainable flood risk management (see Chapter 1, Section 1.1.3), as those tools are mostly limited to scenario-analyses and on-site assessments.

6.2.2. Perspectives for future research

The approaches, models and frameworks presented in this thesis allow the identification of priority locations in catchment areas for land use changes with a view to mitigate downstream flood risk, and the assessment of the corresponding flood insurance values of these land use interventions. Nevertheless, as discussed in Section 6.1 and throughout the various chapters, a considerable level of uncertainty is still related to these assessments. Improvements to the currently implemented models have been proposed in Section 6.1, however, further research could also build upon and extend the overall frameworks.

Extension of optimization and flood risk framework

The presented optimization framework assesses the impact of upstream land use changes on downstream surface runoff accumulation. However, the impact of urban drainage systems were not taken into account, though these sewer systems influence and interact with the rivers (Vaes & Willems, 2007). As a significant part of rainfall on urban surfaces is drained through these sewer systems to a river overflow, it does not interact with vegetation cover as surface runoff would in overland flow paths. This secondary drainage system in catchments should therefore also be included in the model to provide a more comprehensive assessment of the impact of soil sealing and land use changes in the landscape (Braud et al., 2013). This would require the coupling of a hydrodynamic sewer model with a hydrodynamic river model, e.g. as in the integrated platforms InfoWorks ICM (Innovyze Inc., 2020) or MIKE+ (DHI Software, 2020a). Though these models provide an integrated modeling approach, they also have a high computational burden, and are therefore unsuitable to be integrated in an optimization approach, whereby as many iterations are necessary as there are pixels eligible for the land use change under consideration. An alternative conceptual sewer hydraulic modeling approach was developed by Wolfs & Willems (2017), as well as a conceptual river hydraulic modeling method (Wolfs et al., 2015). These models are more computationally efficient, and as such would provide an opportunity to integrate the impact of urban drainage systems in the optimization framework.

Furthermore, the optimization framework and risk assessment could be integrated by coupling the RR-model with a hydraulic model and flood damage model in the iterative optimization framework, which would therefore be able to identify priority locations for land use changes for flood risk mitigation as opposed to flood hazard mitigation. This would allow a direct assessment of the efficiency of land use changes in catchment areas rather than the current assessment of effectiveness followed by an evaluation of the efficiency.

Multi-objective optimization

Currently, the optimization framework is conceived to deal with the single objective to minimize downstream flood hazard, characterized by the runoff volume accumulation. In future research, the framework can be extended to simultaneously consider additional criteria, for instance optimizing the off-site delivery of flood regulation together with on-site ecosystem services, e.g. carbon storage and groundwater recharge. As such, the framework would provide a more comprehensive view on ES delivery, thus substantiating the multifunctionality of ecosystems, an important goal in sustainable flood risk management (Sayers et al., 2015). Another criterion worth considering is the cost associated with land use interventions. For instance, the costs associated with afforestation were addressed in the discussion section of Chapter 5 (Section 5.4), providing an indication of the cost efficiency of the proposed land use interventions. The cost of land use changes thus depends on the considered land use change, but also site-specific characteristics, e.g. price of land, soil type, slope and accessibility. As such, these costs are spatially variable. By integrating costs into the optimization framework, the most cost-efficient locations for a land use change could be identified in the optimization framework.

One approach to consider multiple criteria, including cost, is to combine and weight the different criteria into a single objective function. Lund (2002) formulated an integer linear programming model aimed at identifying optimal flood management measures by minimizing the sum of the costs of flood defense measures and the associated flood damages. Another approach is to define constraints in the optimization framework regarding additional criteria. For instance, Vanegas et al. (2010) incorporated a budget constraint in an integer programming formulation, thereby restricting the locations chosen for a specific land use change according to a predefined budget and the cost associated with the land use change.

Though the conversion of multiple criteria into a single objective function is straightforward, it also produces a single optimal solution, thereby failing to provide information regarding possible trade-offs between objectives. Conversely, multi-objective methods aim to provide a comprehensive overview of the solution space by considering all objectives simultaneously. A common multi-objective optimization heuristic is the Evolutionary Multi-objective Optimization (EMO) (Roberts et al., 2011). This approach identifies a set of trade-off solutions, referred to as the Pareto-optimal set (Woodward et al., 2014). A wide range of evolutionary algorithms is applied, for example the Nondominated Sorting Genetic Algorithm II (NSGAII). This algorithm has been applied by Roberts et al. (2011) in optimal landscape design and by Woodward et al. (2014) to optimize flood risk management.

The optimization framework currently compares the original land use type of each pixel, as a reference, with a single alternative land use type, for instance forest. The number of alternative solutions thus equals the number of pixels considered eligible for the land use change. Alternatively, a portfolio of land use change types could be assessed simultaneously in the optimization to provide a more comprehensive view to the most suitable land use interventions in the catchments, answering not only 'where should'-questions, but extending these questions into 'where should which intervention take place?'. A general structure of such an optimization model, evaluating the allocation of multiple land use types, is provided by Aerts & Heuvelink (2002), who propose an integer programming model assessing a number of land use types *K* for each pixel. The solution space thus increases with a factor *K*. As such, Aerts & Heuvelink (2002) apply the Simulated Annealing heuristic to solve this optimization. Alternatively, NSGAII could also be applied, thus allowing the optimization framework to be extended to a multi-objective land use allocation framework.

References

Aerts, J. C. J. H., & Heuvelink, G. B. M. (2002). Using simulated annealing for resource allocation. *Internation Journal of Geographical Information Science*, *16*(6), 571–587. https://doi.org/10.1111/j.1538-4632.2003.tb01106.x

Aerts, J. C. J. H., Kriek, M., & Schepel, M. (1999). STREAM (Spatial Tools for River basins and Environment and Analysis of Management options): "Set up and requirements." *Physics and Chemistry of the Earth, Part B: Hydrology, Oceans and Atmosphere*, *24*(6), 591–595. https://doi.org/10.1016/S1464-1909(99)00049-0

Agentschap Informatie Vlaanderen. (2002). *Bodembedekkingsbestand, opname 2001*. http://www.geopunt.be/catalogus/datasetfolder/F14B3B46-5728-4E65-8DFA-0D45D3A7A233

Agentschap Informatie Vlaanderen. (2016a). *Bodemafdekkingskaart (BAK), 5m resolutie, opname 2012*. http://www.geopunt.be/catalogus/datasetfolder/3fbc3302-7b8a-4379-92b5-d2d5f802b439

Agentschap Informatie Vlaanderen. (2016b). *Bodembedekkingskaart (BBK), 5m resolutie, opname 2012*. http://www.geopunt.be/catalogus/datasetfolder/cbd76a37-027a-48ed-a5fe-012d5f6db55b

Agentschap Informatie Vlaanderen. (2018). *Voorlopig referentiebestand gemeentegrenzen, toestand 17/08/2017 - correctie*. http://www.geopunt.be/catalogus/datasetfolder/463322e3-5041-4be4-8cb2-c495994ca217

Agentschap Informatie Vlaanderen. (2020). *Grootschalig Referentiebestand (GRBgis)*. http://www.geopunt.be/catalogus/datasetfolder/7c823055-7bbf-4d62-b55e-f85c30d53162

Agentschap Informatie Vlaanderen, & Nationaal Geografisch Instituut. (2020). *Wegenregister, 17/09/2020*. http://www.geopunt.be/catalogus/datasetfolder/b8007407-21ea-46f7-ab2c-3736e9f7fb27

Agentschap Informatie Vlaanderen, & Vlaamse Milieumaatschappij. (2017). *Recent overstroomde gebieden*. http://www.geopunt.be/catalogus/datasetfolder/6BC263EB-F4DF-4B16-963B-840CD2EFAACF

Agentschap Informatie Vlaanderen, & Vlaamse Milieumaatschappij. (2020). *Vlaamse Hydrografische Atlas - Zones, 12 maart 2020*. http://www.geopunt.be/catalogus/datasetfolder/3c22f409-ed0e-4867-a310-50cf4de853b1

Agentschap Informatie Vlaanderen, Vlaamse Milieumaatschappij, & Watlab. (2006). *DHM-Vlaanderen, raster, 5 m*. http://www.geopunt.be/catalogus/datasetfolder/B5C62D89-A0C4-4228-B359-6FCAB7020C50

Agentschap Innoveren en Ondernemen, & Agentschap Informatie Vlaanderen. (2020). *Bedrijventerreinen, Toestand 30/09/2020*.

Alaoui, A., Rogger, M., Peth, S., & Blöschl, G. (2018). Does soil compaction increase floods? A review. *Journal of Hydrology*, *557*, 631–642. https://doi.org/10.1016/j.jhydrol.2017.12.052

Alila, Y. (1999). A hierarchical approach for the regionalization of precipitation annual maxima in Canada. *Journal of Geophysical Research*, *104*(D24), 31645–31655. https://doi.org/10.1029/1999JD900764

Amatya, D. M., Williams, T. M., Bren, L., & de Jong, C. (2016). *Forest Hydrology: Processes, Management and Assessment*. CAB International.

Andréassian, V., Moine, N. Le, Perrin, C., Ramos, M. H., Oudin, L., Mathevet, T., Le Moine, N., Perrin, C., Ramos, M. H., Oudin, L., Mathevet, T., Lerat, J., & Berthet, L. (2012). All that glitters is not gold: the case of calibrating hydrological models. *Hydrological Processes*, *26*(14), 2206–2210. https://doi.org/10.1002/hyp.9264

Appels, W. M., Bogaart, P. W., & Zee, S. E. A. T. M. Van Der. (2011). Influence of spatial variations of microtopography and infiltration on surface runoff and field scale hydrological connectivity. *Advances in Water Resources*, *34*, 303–313. https://doi.org/10.1016/j.advwatres.2010.12.003

Arcement, G. J., & Schneider, V. R. (1989). *Guide for Selecting Manning's Roughness Coefficients for Natural Channels and Flood Plains*.

Assuralia. (2020). *Kerncijfers en voornaamste resultaten van de Belgische verzekeringsmarkt in 2019* (Issue 31).

Bagstad, K. J., Johnson, G. W., Voigt, B., & Villa, F. (2013). Spatial dynamics of ecosystem service flows: A comprehensive approach to quantifying actual services. *Ecosystem Services*, *4*, 117–125. https://doi.org/10.1016/j.ecoser.2012.07.012

Bales, J. D., & Wagner, C. R. (2009). Sources of uncertainty in flood inundation maps. *Journal of Flood Risk Management*, *2*(2), 139–147. https://doi.org/10.1111/j.1753-318X.2009.01029.x

Barredo, J. I. (2009). Normalised flood losses in Europe: 1970-2006. *Natural Hazards and Earth System Science*, *9*(1), 97–104. https://doi.org/10.5194/nhess-9-97-2009

Baumgärtner, S., & Strunz, S. (2014). The economic insurance value of ecosystem resilience. *Ecological Economics*, *101*, 21–32. https://doi.org/10.1016/j.ecolecon.2014.02.012

Beckers, V., Van De Vreken, P., Jacxsens, P., Van Meirvenne, M., & Van Orshoven, J. (2011). *Installatie en gebruik van de bodemdatabank Aardewerk-Vlaanderen-2010*.

Benoudjit, A., & Guida, R. (2019). A novel fully automated mapping of the flood extent on sar images using a supervised classifier. *Remote Sensing*, *11*(7). https://doi.org/10.3390/rs11070779

Berghuijs, W. R., Aalbers, E. E., Larsen, J. R., Trancoso, R., & Woods, R. A. (2017). Recent changes in extreme floods across multiple continents. *Environmental Research Letters*, *12*(11). https://doi.org/10.1088/1748-9326/aa8847

Beullens, J., Broidioi, S., De Sutter, R., De Maeyer, P., Verwaest, T., & Mostaert, F. (2017). *Ontwikkeling LATIS 4 Deelrapport bis: Actualisatie basiskaarten en schadewaarden. Versie 3.0. WL Rapporten, 13_159_7.* Universiteit Gent, Antea Group, Waterbouwkundig Laboratorium: Antwerpen.

Beven, K. J. (2006). A manifesto for the equifinality thesis. *Journal of Hydrology*, *320*, 18–36. https://doi.org/10.1016/j.jhydrol.2005.07.007

Beven, K. J., & Kirkby, M. J. (1979). A physically based, variable contributing area model of basin hydrology. *Hydrological Sciences Bulletin*, *24*(1), 43–69. https://doi.org/10.1080/02626667909491834

Bingner, R. L., Theurer, F. D., Yuan, Y., & Taguas, E. V. (2018). *AnnAGNPS Technical Process, Version 5.5*. https://www.wcc.nrcs.usda.gov/

Blöschl, G., Arcoin-Bardin, S., Bonell, M., Dorninger, M., Goodrich, D., Gutknecht, D., Matamoros, D., Merz, B., Shand, P., & Szolgay, J. (2007). At what scales do climate variability and land cover

change impact on flooding and low flows? *Hydrological Processes*, *21*, 1241–1247. https://doi.org/10.1002/hyp

Blöschl, G., Hall, J., Viglione, A., Perdigão, R. A. P., Parajka, J., Merz, B., Lun, D., Arheimer, B., Aronica, G. T., Bilibashi, A., Boháč, M., Bonacci, O., Borga, M., Čanjevac, I., Castellarin, A., Chirico, G. B., Claps, P., Frolova, N., Ganora, D., … Živković, N. (2019). Changing climate both increases and decreases European river floods. *Nature*, *573*(7772), 108–111. https://doi.org/10.1038/s41586-019-1495-6

Bout, B., & Jetten, V. G. (2018). The validity of flow approximations when simulating catchment-integrated flash floods. *Journal of Hydrology*, *556*, 674–688. https://doi.org/10.1016/j.jhydrol.2017.11.033

Bouwer, L. M. (2011). Have disaster losses increased due to anthropogenic climate change? *Bulletin of the American Meteorological Society*, *92*, 39–46. https://doi.org/10.1175/2010BAMS3092.1

Braud, I., Breil, P., Thollet, F., Lagouy, M., Branger, F., Jacqueminet, C., Kermadi, S., & Michel, K. (2013). Evidence of the impact of urbanization on the hydrological regime of a medium-sized periurban catchment in France. *Journal of Hydrology*, *485*, 5–23. https://doi.org/10.1016/j.jhydrol.2012.04.049

Breuer, L., Huisman, J. A., Willems, P., Bormann, H., Bronstert, A., Croke, B. F. W., Frede, H. G., Gräff, T., Hubrechts, L., Jakeman, A. J., Kite, G., Lanini, J., Leavesley, G., Lettenmaier, D. P., Lindström, G., Seibert, J., Sivapalan, M., & Viney, N. R. (2009). Assessing the impact of land use change on hydrology by ensemble modeling (LUCHEM). I: Model intercomparison with current land use. *Advances in Water Resources*, *32*(2), 129–146. https://doi.org/10.1016/j.advwatres.2008.10.003

Broadmeadow, S., Thomas, H., & Nisbet, T. (2014). *Opportunity mapping for woodland creation to reduce diffuse water pollution and flood risk in England and Wales* (p. 41). Forest Research.

Brogna, D., Vincke, C., Brostaux, Y., Soyeurt, H., Dufrêne, M., & Dendoncker, N. (2017). How does forest cover impact water flows and ecosystem services? Insights from “real-life” catchments in Wallonia (Belgium). *Ecological Indicators*, *72*, 675–685. https://doi.org/10.1016/j.ecolind.2016.08.011

Bronstert, A., Niehoff, D., & Bürger, G. (2002). Effects of climate and land-use change on storm runoff generation: Present knowledge and modelling capabilities. *Hydrological Processes*, *16*(2), 509–529. https://doi.org/10.1002/hyp.326

Brouwers, J., Peeters, B., Van Steertegem, M., van Lipzig, N., Wouters, H., Beullens, J., Demuzere, M., Willems, P., De Ridder, K., Maiheu, B., De Troch, R., Termonia, P., Vansteenkiste, T., Craninx, M., Maetens, W., Defloor, W., Cauwenberghs, K., & Bash, E. (2015). MIRA klimaatrapport. In *Mira*. https://doi.org/10.1017/CBO9781107415324.004

Brown, A. E., Western, A. W., Mcmahon, T. A., & Zhang, L. (2013). Impact of forest cover changes on annual streamflow and flow duration curves. *Journal of Hydrology*, *483*, 39–50. https://doi.org/10.1016/j.jhydrol.2012.12.031

Bubeck, P., de Moel, H., Bouwer, L. M., & H. Aerts, J. C. J. (2011). How reliable are projections of future flood damage? *Natural Hazards and Earth System Science*, *11*(12), 3293–3306. https://doi.org/10.5194/nhess-11-3293-2011

Carmona, A., & Nahuelhual, L. (2012). Combining land transitions and trajectories in assessing forest cover change. *Applied Geography*, *32*(2), 904–915. https://doi.org/10.1016/j.apgeog.2011.09.006

Chang, H., Franczyk, J., & Kim, C. (2009). What is responsible for increasing flood risks? The case of Gangwon Province, Korea. *Natural Hazards*, *48*(3), 339–354. https://doi.org/10.1007/s11069-008-9266-y

Chow, V. T., Maidment, D. R., & Mays, L. W. (1988). *Applied Hydrology* (B. J. Clark & J. Morriss (eds.)). McGraw-Hill.

Chu, A., Lin, Y.-C., & Chiueh, P.-T. (2017). Incorporating the effect of urbanization in measuring climate adaptive capacity. *Land Use Policy*, *68*, 28–38. https://doi.org/10.1016/j.landusepol.2017.07.019

Chu, S. T. (1978). Infiltration during an unsteady rain. *Water Resources Research*, *14*(3), 461–466.

Coördinatiecommissie Integraal Waterbeleid. (2015). *Aanpak wateroverlastproblematiek – Transitie naar meerlaagse waterveiligheid (MLWV)*.

Coördinatiecommissie Integraal Waterbeleid. (2016a). *Stroomgebiedbeheerplan voor de Schelde 2016-2021: Bekkenspecifiek deel Bovenscheldebekken* (p. 177). https://www.integraalwaterbeleid.be/nl/stroomgebiedbeheerplannen/stroomgebiedbeheerplannen-2016-2021/documenten/Bovenscheldebekken.pdf

Coördinatiecommissie Integraal Waterbeleid. (2016b). *Stroomgebiedbeheerplan voor de Schelde 2016-2021: Bekkenspecifiek deel Demerbekken*. https://www.integraalwaterbeleid.be/nl/stroomgebiedbeheerplannen/stroomgebiedbeheerplannen-2016-2021/documenten/Demerbekken.pdf

Coördinatiecommissie Integraal Waterbeleid. (2016c). *Stroomgebiedbeheerplan voor de Schelde 2016-2021: Bekkenspecifiek deel Denderbekken*. https://www.integraalwaterbeleid.be/nl/stroomgebiedbeheerplannen/stroomgebiedbeheerplannen-2016-2021/documenten/Denderbekken.pdf

Coördinatiecommissie Integraal Waterbeleid. (2018). *Decreet Integraal Waterbeleid*. https://www.integraalwaterbeleid.be/nl/regelgeving/decreet-integraal-waterbeleid

Corradini, C., Melone, F., & Smith, R. E. (2000). Modeling local infiltration for a two-layered soil under complex rainfall patterns. *Journal of Hydrology*, *237*, 58–73. https://doi.org/10.1016/S0022-1694(00)00298-5

Costelloe, J. F., Pilkington, C., & Rice, P. (2013). Can the peak discharge – total volume relationship for flow pulses be used to identify flow regime change? *20th International Congress on Modelling and Simulation*, *1-6 December*.

CRED, & UNISDR. (2018). *Economic losses, poverty & disasters 1998-2017*.

Dalemans, F., Jacxsens, P., Van Orshoven, J., Kint, V., Moonen, P., & Muys, B. (2015). Assisting sustainable forest management and forest policy planning with the sim4tree decision support system. *Forests*, *6*(4), 859–878. https://doi.org/10.3390/f6040859

Dallimer, M., Martin-ortega, J., Rendon, O., Stavros, A., Bark, R., Gordon, I. J., & Paavola, J. (2020). Taking stock of the empirical evidence on the insurance value of ecosystems. *Ecological Economics*, *167*. https://doi.org/10.1016/j.ecolecon.2019.106451

Databank Ondergrond Vlaanderen. (2017). *Digitale bodemkaart van het Vlaams Gewest: bodemtypes*. dov.vlaanderen.be/geonetwork/srv/eng/catalog.search#/metadata/a1547a01-b9fc-40fa-a2eb-009a39c02c7b

Databank Ondergrond Vlaanderen. (2021). *Kleinschalige Erosiebestrijdingsmaatregelen*. dov.vlaanderen.be/geonetwork/srv/eng/catalog.search#/metadata/692a9efb-8509-4a6f-a3be-

6887f969867d

de Moel, H., & Aerts, J. C. J. H. (2011). Effect of uncertainty in land use, damage models and inundation depth on flood damage estimates. *Natural Hazards*, *58*(1), 407–425. https://doi.org/10.1007/s11069-010-9675-6

de Moel, H., Asselman, N. E. M., & H. Aerts, J. C. J. (2012). Uncertainty and sensitivity analysis of coastal flood damage estimates in the west of the Netherlands. *Natural Hazards and Earth System Science*, *12*(4), 1045–1058. https://doi.org/10.5194/nhess-12-1045-2012

de Moel, H., Jongman, B., Kreibich, H., Merz, B., Penning-Rowsell, E., & Ward, P. J. (2015). Flood risk assessments at different spatial scales. *Mitigation and Adaptation Strategies for Global Change*, *20*(6), 865–890. https://doi.org/10.1007/s11027-015-9654-z

de Moel, H., Van Alphen, J., & Aerts, J. C. J. H. (2009). Flood maps in Europe - Methods, availability and use. *Natural Hazards and Earth System Science*, *9*(2), 289–301. https://doi.org/10.5194/nhess-9-289-2009

de Moel, H., van Vliet, M., & Aerts, J. C. J. H. (2014). Evaluating the effect of flood damage-reducing measures: A case study of the unembanked area of Rotterdam, the Netherlands. *Regional Environmental Change*, *14*(3), 895–908. https://doi.org/10.1007/s10113-013-0420-z

De Niel, J., Vermeir, A., Tran, Q. Q., Moustakas, S., & Willems, P. (2020). Efficient approach for impact analysis of land cover changes on hydrological extremes by means of a lumped conceptual model. *Journal of Hydrology: Regional Studies*, *28*, 100666. https://doi.org/10.1016/j.ejrh.2020.100666

De Vlaamse Waterweg nv, & Natuur en Bos. (2020). *Sigmaplan*. https://sigmaplan.be/nl/

Deckers, P., Kellens, W., Reyns, J., Vanneuville, W., & De Maeyer, P. (2009). A GIS for Flood Risk Management in Flanders. In P. Showalter & Y. Lu (Eds.), *Geospatial Techniques in Urban Hazard and Disaster Analysis* (pp. 51–69). https://doi.org/10.1007/978-90-481-2238-7_4

Departement Omgeving Vlaanderen. (2018). *Strategische Visie Beleidsplan Ruimte Vlaanderen*.

Departement Omgeving Vlaanderen. (2019a). *Evolutie Ruimtebeslag*. https://omgeving.vlaanderen.be/evolutie-ruimtebeslag

Departement Omgeving Vlaanderen. (2019b). *Verharding*. https://omgeving.vlaanderen.be/verharding

Departement Ruimte Vlaanderen. (2017). *Witboek Beleidsplan Ruimte Vlaanderen*.

DHI Software. (2008). *MIKE SHE - User Manual*.

DHI Software. (2020a). *MIKE+ - User Guide*.

DHI Software. (2020b). *Mike HYDRO - User Manual*.

Directive 2000/60/EC. (2000). *Establishing a framework for Community action in the field of water policy*. European Parliament, Council of the European Union. http://data.europa.eu/eli/dir/2000/60/oj

Directive 2007/60/EC. (2007). *The assessment and management of flood risks*. European Parliament, Council of the European Union. http://data.europa.eu/eli/dir/2007/60/oj

Dondeyne, S., Van Ranst, E., & Deckers, J. (2013). *The soil map of the Flemish region converted to a World Reference Base legend : the inland regions*.

Eckhardt, K. (2005). How to construct recursive digital filters for baseflow separation. *Hydrological Processes*, *19*(2), 507–515. https://doi.org/10.1002/hyp.5675

EEA. (2010). *EEA Technical report 132010: Mapping the impacts of natural hazards and technological accidents in Europe: An overview of the last decade*. European Environment Agency. https://doi.org/10.2800/62638

EEA. (2016). *EEA Report 1/2016: Flood risks and environmental vulnerability - Exploring the synergies between floodplain restoration, water policies and thematic policies.* European Environment Agency. https://doi.org/10.2800/039463

EEA. (2017). *EEA Report 15/2017: Climate change adaptation and disaster risk reduction in Europe: Enhancing coherence of the knowledge base, policies and practices*. European Environment Agency. https://doi.org/10.2800/938195

EEA. (2019). *River Floods*. Indicator Assessment; European Environment Agency, Copenhagen. https://www.eea.europa.eu/data-and-maps/indicators/river-floods-3/assessment/#_edn7

Eikelboom, T., Janssen, R., & Stewart, T. J. (2015). A spatial optimization algorithm for geodesign. *Landscape and Urban Planning*, *144*, 10–21. https://doi.org/10.1016/j.landurbplan.2015.08.011

Elith, J., Leathwick, J. R., & Hastie, T. (2008). A working guide to boosted regression trees. *Journal of Animal Ecology*, *77*(4), 802–813. https://doi.org/10.1111/j.1365-2656.2008.01390.x

Engman, E. T., & ASCE, M. (1986). Roughness Coefficients for Routing Surface Runoff. *Journal of Irrigation and Drainage Engineering*, *112*(1), 39–53.

ESRI. (2016). *ArcMap: How Trend works*. https://desktop.arcgis.com/en/arcmap/10.3/tools/spatial-analyst-toolbox/how-trend-works.htm#ESRI_SECTION1_9F35D9C4E21D4987BBDDFAD970F034BA

European Commission. (2012). *Guidelines on best practice to limit, mitigate or compensate soil sealing*. https://doi.org/10.2779/75498

Eurostat. (2020). *Countries*. https://ec.europa.eu/eurostat/web/gisco/geodata/reference-data/administrative-units-statistical-units/countries

Fang, X., Ren, L., Li, Q., Zhu, Q., Shi, P., & Zhu, Y. (2013). Hydrologic response to land use and land cover changes within the context of catchment-scale spatial information. *Journal of Hydrologic Engineering*, *18*(11), 1539–1548. https://doi.org/10.1061/(ASCE)HE.1943-5584.0000482

Federatie van het Notariaat. (2019). *Notarisbarometer: Landbouwgronden* (Vol. 1, Issue 2).

Fiquepron, J., Garcia, S., & Stenger, A. (2013). Land use impact on water quality: Valuing forest services in terms of the water supply sector. *Journal of Environmental Management*, *126*, 113–121. https://doi.org/10.1016/j.jenvman.2013.04.002

Fisher, B., Turner, R. K., & Morling, P. (2009). Defining and classifying ecosystem services for decision making. *Ecological Economics*, *68*(3), 643–653. https://doi.org/10.1016/j.ecolecon.2008.09.014

Francos, A., Elorza, F. J., Bouraoui, F., Bidoglio, G., & Galbiati, L. (2003). Sensitivity analysis of distributed environmental simulation models: Understanding the model behaviour in hydrological studies at the catchment scale. *Reliability Engineering and System Safety*, *79*(2), 205–218. https://doi.org/10.1016/S0951-8320(02)00231-4

Fu, S., Mu, H., Liu, B., Yu, X., & Liu, Y. (2019). Effect of plant basal cover on velocity of shallow overland flow. *Journal of Hydrology*, *577*, 123947.

https://doi.org/10.1016/j.jhydrol.2019.123947

Gaál, L., Szolgay, J., Kohnová, S., Hlavčová, K., Parajka, J., Viglione, A., Merz, R., & Blöschl, G. (2015). Dependence between flood peaks and volumes: a case study on climate and hydrological controls. *Hydrological Sciences Journal*, *60*(6), 968–984. https://doi.org/10.1080/02626667.2014.951361

Gabriel, J. L., Quemada, M., Martin-Lammerding, D., Vanclooster, M., Martín-Lammerding, D., & Vanclooster, M. (2019). Assessing the cover crop effect on soil hydraulic properties by inverse modelling in a 10-year field trial. *Agricultural Water Management*, *222*, 62–71. https://doi.org/10.1016/j.agwat.2019.05.034

Gao, J., Holden, J., & Kirkby, M. (2015). A distributed TOPMODEL for modelling impacts of land-cover change on river flow in upland peatland catchments. *Hydrological Processes*, *29*(13), 2867–2879. https://doi.org/10.1002/hyp.10408

Gerl, T., Kreibich, H., Franco, G., Marechal, D., & Schröter, K. (2016). A review of flood loss models as basis for harmonization and benchmarking. *PLoS ONE*, *11*(7), 1–22. https://doi.org/10.1371/journal.pone.0159791

Gizaw, M. S., & Gan, T. Y. (2016). Regional Flood Frequency Analysis using Support Vector Regression under historical and future climate. *Journal of Hydrology*, *538*, 387–398. https://doi.org/10.1016/j.jhydrol.2016.04.041

Green, R., & Ampt, G. (1911). Studies on soil physics. The flow of air and water through soils. *The Journal of Agricultural Science*, *4*(1), 1–24.

Grégoire, G. (2014). Multiple Linear Regression. *Regression Methods for Astrophysics*, *66*, 45–72. https://doi.org/10.1051/eas/1466005

Grommen, S. (2020, December 16). Akkoord over betonstop krijgt forse kritiek van oppositie en experten: "Onbetaalbaar en dus onuitvoerbaar." *VRT NWS*. https://www.vrt.be/vrtnws/nl/2020/12/16/debat-bouwshift-betonstop/

Grossi, P., & Kunreuther, H. (2005). *Catastrophe modeling: A new approach to managing risk*. Springer.

Guha-Sapir, D. (2020). *EM-DAT*. CRED/UC Louvain. www.emdat.be

Gulinck, H., Dufourmont, P., Wouters, P., & Sanders, J. (1996). *Ontwikkeling van een gebiedsdekkende informatielaag afgeleid uit satellietbeelden als basis voor monitoring en structuurkartering van het landelijk gebied in Vlaanderen* (p. 21).

Gupta, H. V., Kling, H., Yilmaz, K. K., & Martinez, G. F. (2009). Decomposition of the mean squared error and NSE performance criteria: Implications for improving hydrological modelling. *Journal of Hydrology*, *377*, 80–91. https://doi.org/10.1016/j.jhydrol.2009.08.003

Gupta, V. K., Mantilla, R., Troutman, B. M., Dawdy, D., & Krajewski, W. F. (2010). Generalizing a nonlinear geophysical flood theory to medium-sized river networks. *Geophysical Research Letters*, *37*, 1–6. https://doi.org/10.1029/2009GL041540

Guyon, I., Weston, J., Barnhill, S., & Vapnik, V. (2002). Gene selection for cancer classification. *Machine Learning*, *46*, 389–422. https://doi.org/10.1108/03321640910919020

Hall, J. W., Sayers, P. B., & Dawson, R. J. (2005). National-scale assessment of current and future flood risk in England and Wales. *Natural Hazards*, *36*, 147–164. https://doi.org/10.1007/s11069-004-4546-7

Hartmann, T., Slavíková, L., & McCarthy, S. (2019). *Nature-Based Flood Risk Management on Private Land: Disciplinary Perspectives on a Multidisciplinary Challenge*. Springer Open. https://doi.org/https://doi.org/10.1007/978-3-030-23842-1

Hawkins, R. H., Ward, T. J., Woodward, D. E., & Van Mullem, J. A. (2009). *Curve Number Hydrology: State of the Practice*. ASCE Publications.

Hawkins, R. H., Woodward, D. E., & Jiang, R. (2001). Investigation of the runoff curve number abstraction ratio. *Proceedings of the USDA-NRCS Hydraulic Engineering Workshop*, 10.

Her, Y., & Heatwole, C. (2016). Two-dimensional continuous simulation of spatiotemporally varied hydrological processes using the time-area method. *Hydrological Processes*, *30*(5), 751–770. https://doi.org/10.1002/hyp.10644

Heremans, S., & Van Orshoven, J. (2015). Machine learning methods for sub-pixel land cover classification in the spatially heterogeneous region of Flanders (Belgium): a multi-criteria comparison. *International Journal of Remote Sensing*, *36*(11), 2934–2962.

Hijmans, R. J., Phillips, S., Leathwick, J. R., & Elith, J. (2016). *Package 'dismo.'*

Hodgkins, G. A., Whitfield, P. H., Burn, D. H., Hannaford, J., Renard, B., Stahl, K., Fleig, A. K., Madsen, H., Mediero, L., Korhonen, J., Murphy, C., & Wilson, D. (2017). Climate-driven variability in the occurrence of major floods across North America and Europe. *Journal of Hydrology*, *552*, 704–717. https://doi.org/10.1016/j.jhydrol.2017.07.027

Honnay, O., Piessens, K., Van Landuyt, W., Hermy, M., & Gulinck, H. (2003). Satellite based land use and landscape complexity indices as predictors for regional plant species diversity. *Landscape and Urban Planning*, *63*(4), 241–250. https://doi.org/10.1016/S0169-2046(02)00194-9

Hosking, J. R. M., & Wallis, J. R. (1993). Some Statistics Useful in Regional Frequency Analysis. *Water Resources Research*, *29*(2), 271–281.

Hostache, R., Chini, M., Giustarini, L., Neal, J., Kavetski, D., Wood, M., Corato, G., Pelich, R. M., & Matgen, P. (2018). Near-Real-Time Assimilation of SAR-Derived Flood Maps for Improving Flood Forecasts. *Water Resources Research*, *54*(8), 5516–5535. https://doi.org/10.1029/2017WR022205

Huang, Q., Wang, J., Li, M., Fei, M., & Dong, J. (2017). Modeling the influence of urbanization on urban pluvial flooding: a scenario-based case study in Shanghai, China. *Natural Hazards*, *87*(2), 1035–1055. https://doi.org/10.1007/s11069-017-2808-4

Innovyze Inc. (2020). *InfoWorks ICM Suite*. https://www.innovyze.com/en-us/products/infoworks-icm

IPCC. (2012). *Managing the risks of extreme events and disasters to advance climate change adaptation. A Special Report of Working Groups I and II of the Intergovernmental Panel on Climate Change* (C. B. Field, V. Barros, T. F. Stocker, D. Qin, D. J. Dokken, K. L. Ebi, M. D. Mastrandrea, K. J. Mach, G.-K. Plattner, S. K. Allen, M. Tignor, & P. M. Midgley (eds.)). Cambridge University Press. https://doi.org/10.1017/CBO9781139177245.009

IPCC. (2014). *Climate Change 2014: Synthesis Report. Contribution of Working Groups I, II and III to the Fifth Assessment Report of the Intergovernmental Panel on Climate Change* (Core Writing Team, R. K. Pachauri, & L. A. Meyer (eds.)). IPCC, Geneva, Switzerland.

Isik, S., Kalin, L., Schoonover, J. E., Srivastava, P., & Lockaby, B. G. (2013). Modeling effects of changing land use/cover on daily streamflow: An Artificial Neural Network and curve number based hybrid approach. *Journal of Hydrology*, *485*, 103–112.

https://doi.org/10.1016/j.jhydrol.2012.08.032

Jakeman, A. J., & Hornberger, G. M. (1993). How much complexity is warranted in a rainfall-runoff model? *Water Resources Research*, *29*(8), 2637–2649. https://doi.org/10.1029/93WR00877

Jenson, S. K., & Domingue, J. O. (1988). Extracting Topographic Structure from Digital Elevation Data for Geographic Information System Analysis. *Photogrammetric Engineering and Remote Sensing*, *54*(11), 1593–1600.

Jetten & De Roo. (2018). *OpenLISEM Multi-Hazard Land Surface Process Model: Documentation & User Manual* (p. 255). University of Twente. https://blog.utwente.nl/lisem/download/

Jones, A., Panagos, P., Barcelo, S., Bouraoui, F., Bosco, C., Dewitte, O., Gardi, C., Erhard, M., Hervás, J., Hiederer, R., Jeffery, S., Lükewille, A., Marmo, L., Montanarella, L., Olazábal, C., Petersen, J., Penizek, V., Strassburger, T., Tóth, G., Van Den Eeckhaut, M., Van Liedekerke, M., Verheijen, F., Viestova, E., Yigini, Y. (2012). *The State of Soil in Europe: A contribution of the JRC to the EEA Environment State and Outlook Report - SOER 2010*. https://doi.org/10.2788/77361

Jordan, M. I., & Mitchell, T. M. (2015). Machine learning: Trends, perspectives, and prospects. *Science*, *349*(6245), 255–260. https://doi.org/10.1126/science.aaa8415

Kachroo, R. K., Mkhandi, S. H., & Parida, B. P. (2000). Flood frequency analysis of southern Africa: I. Delineation of homogeneous regions. *Hydrological Sciences Journal*, *45*(3), 437–447. https://doi.org/10.1080/02626660009492340

Kalantari, Z., Lyon, S. W., Folkeson, L., French, H. K., Stolte, J., Jansson, P. E., & Sassner, M. (2014). Quantifying the hydrological impact of simulated changes in land use on peak discharge in a small catchment. *Science of the Total Environment*, *466–467*, 741–754. https://doi.org/10.1016/j.scitotenv.2013.07.047

Kale, R. V., & Sahoo, B. (2011). Green-Ampt Infiltration Models for Varied Field Conditions: A Revisit. *Water Resources Management*, *25*, 3505–3536. https://doi.org/10.1007/s11269-011-9868-0

Kalyanapu, A. J., Burian, S. J., & Mcpherson, T. N. (2009). Effect of land use-based surface roughness on hydrologic model output. *Journal of Spatial Hydrology*, *9*(2), 51–71.

Kellens, W., Vanneuville, W., Verfaillie, E., Meire, E., Deckers, P., & De Maeyer, P. (2013). Flood Risk Management in Flanders: Past Developments and Future Challenges. *Water Resources Management*, *27*(10), 3585–3606. https://doi.org/10.1007/s11269-013-0366-4

Klijn, F., Baan, P., de Bruijn, K., & Kwadijk, J. (2007). *Overstromingsrisico's in Nederland in een veranderend klimaat: Verwachtingen, schattingen en berekeningen voor het project Nederland Later, Report number Q4290* (p. 165). Studie uitgevoerd door WL, Delft hydraulics in opdracht Milieu- en Natuurplanbureau.

Knapen, A., Smets, T., & Poesen, J. (2009). Flow-retarding effects of vegetation and geotextiles on soil detachment during concentrated flow. *Hydrological Processes*, *23*, 2427–2437. https://doi.org/10.1002/hyp

Knoben, W. J. M., Freer, J. E., & Woods, R. A. (2019). Technical note: Inherent benchmark or not? Comparing Nash-Sutcliffe and Kling-Gupta efficiency scores. *Hydrology and Earth System Sciences*, *23*, 4323–4331. https://doi.org/10.5194/hess-23-4323-2019

Koks, E. E., de Moel, H., Aerts, J. C. J. H., & Bouwer, L. M. (2014). Effect of spatial adaptation measures on flood risk: Study of coastal floods in Belgium. *Regional Environmental Change*, *14*, 413–425. https://doi.org/10.1007/s10113-013-0514-7

Kuhn, M. (2008). Building Predictive Models in R Using the caret Package. *Journal Of Statistical*

Software, *28*(5), 1–26. https://doi.org/10.1053/j.sodo.2009.03.002

Kundzewicz, Z. W., Pin'skwar, I., & Brakenridge, G. R. (2018). Changes in river flood hazard in Europe: A review. *Hydrology Research*, *49*(2), 294–302. https://doi.org/10.2166/nh.2017.016

Ladson, A. (2008). *Hydrology: An Australian Introduction*. Oxford University Press.

Lee, S. S., Kim, J. C., Jung, H. S., Lee, M. J., & Lee, S. S. (2017). Spatial prediction of flood susceptibility using random-forest and boosted-tree models in Seoul metropolitan city, Korea. *Geomatics, Natural Hazards and Risk*, *8*(2), 1185–1203. https://doi.org/10.1080/19475705.2017.1308971

Lee, Y., & Brody, S. D. (2018). Examining the impact of land use on flood losses in Seoul, Korea. *Land Use Policy*, *70*, 500–509. https://doi.org/10.1016/j.landusepol.2017.11.019

Levavasseur, F., Bailly, J. S., Lagacherie, P., Colin, F., & Rabotin, M. (2012). Simulating the effects of spatial configurations of agricultural ditch drainage networks on surface runoff from agricultural catchments. *Hydrological Processes*, *26*, 3393–3404. https://doi.org/10.1002/hyp.8422

Li, S., Gitau, M., Bosch, D., & Engel, B. A. (2017). Development of a soil moisture - based distributed hydrologic model for determining hydrologically based critical source areas. *Hydrological Processes*, *31*, 3543–3557. https://doi.org/10.1002/hyp.11276

Lin, Y. P., Hong, N. M., Wu, P. J., Wu, C. F., & Verburg, P. H. (2007). Impacts of land use change scenarios on hydrology and land use patterns in the Wu-Tu watershed in Northern Taiwan. *Landscape and Urban Planning*, *80*, 111–126. https://doi.org/10.1016/j.landurbplan.2006.06.007

Lin, Y. P., Verburg, P. H., Chang, C. R., Chen, H. Y., & Chen, M. H. (2009). Developing and comparing optimal and empirical land-use models for the development of an urbanized watershed forest in Taiwan. *Landscape and Urban Planning*, *92*, 242–254. https://doi.org/10.1016/j.landurbplan.2009.05.003

Liu, J., & Shi, Z. (2017). Quantifying land-use change impacts on the dynamic evolution of flood vulnerability. *Land Use Policy*, *65*, 198–210. https://doi.org/10.1016/j.landusepol.2017.04.012

Liu, X., Li, X., Shi, X., Huang, K., & Liu, Y. (2012). A multi-type ant colony optimization (MACO) method for optimal land use allocation in large areas. *Internation Journal of Geographical Information Science*, *26*(7), 1325–1343. https://doi.org/10.1080/13658816.2011.635594

Liu, Y. B., Gebremeskel, S., Smedt, F. De, Hoffmann, L., & Pfister, L. (2003). A diffusive transport approach for flow routing in GIS-based flood modeling. *Journal of Hydrology*, *283*, 91–106. https://doi.org/10.1016/S0022-1694(03)00242-7

Liu, Z., & Merwade, V. (2018). Accounting for model structure, parameter and input forcing uncertainty in flood inundation modeling using Bayesian model averaging. *Journal of Hydrology*, *565*, 138–149. https://doi.org/10.1016/j.jhydrol.2018.08.009

Lund, J. R. (2002). Floodplain Planning with Risk-Based Optimization. *Journal of Water Resources Planning and Management*, *128*(3), 202–207. https://doi.org/10.1061/(asce)0733-9496(2002)128:3(202)

Maetens, W., Poesen, J., & Vanmaercke, M. (2012). How effective are soil conservation techniques in reducing plot runoff and soil loss in Europe and the Mediterranean? *Earth-Science Reviews*, *115*, 21–36. https://doi.org/10.1016/j.earscirev.2012.08.003

McCuen, R. H. (1998). *Hydrologic Analysis and Design*. Prentice-Hall.

Mediero, L., Jiménez-Álvarez, A., & Garrote, L. (2010). Design flood hydrographs from the relationship between flood peak and volume. *Hydrology and Earth System Sciences*, *14*(12), 2495–2505. https://doi.org/10.5194/hess-14-2495-2010

Merwade, V., Olivera, F., Arabi, M., & Edleman, S. (2008). Uncertainty in Flood Inundation Mapping: Current Issues and Future Directions. *Journal of Hydrologic Engineering*, *13*(7), 608–620. https://doi.org/10.1061/(ASCE)1084-0699(2008)13

Merz, B., Hall, J., Disse, M., & Schumann, A. (2010). Fluvial flood risk management in a changing world. *Natural Hazards and Earth System Science*, *10*, 509–527.

Merz, B., Kreibich, H., & Lall, U. (2013). Multi-variate flood damage assessment: A tree-based data-mining approach. *Natural Hazards and Earth System Science*, *13*, 53–64. https://doi.org/10.5194/nhess-13-53-2013

Merz, B., Kreibich, H., Schwarze, R., & Thieken, A. (2010). Review article "assessment of economic flood damage." *Natural Hazards and Earth System Science*, *10*(8), 1697–1724. https://doi.org/10.5194/nhess-10-1697-2010

Messner, F., & Meyer, V. (2006). Flood Damage, Vulnerability and Risk Perception - Challenges for Flood Damage Research. In J. Schanze, E. Zeman, & J. Marsalek (Eds.), *Flood Risk Management: Hazards, Vulnerability and Mitigation Measures* (pp. 149–167). Springer. https://doi.org/10.1007/978-1-4020-4598-1

Meyer, V., Haase, D., & Scheuer, S. (2009). Flood risk assessment in European river basins-concept, methods, and challenges exemplified at the Mulde river. *Integrated Environmental Assessment and Management*, *5*(1), 17–26. https://doi.org/10.1897/IEAM_2008-031.1

Millennium Ecosystem Assessment. (2005). *Ecosystems and Human Well-being: Synthesis*. Island Press.

Miller, J. D., & Hess, T. (2017). Urbanisation impacts on storm runoff along a rural-urban gradient. *Journal of Hydrology*, *552*, 474–489. https://doi.org/10.1016/j.jhydrol.2017.06.025

Miller, J. D., Kim, H., Kjeldsen, T. R., Packman, J., Grebby, S., & Dearden, R. (2014). Assessing the impact of urbanization on storm runoff in a peri-urban catchment using historical change in impervious cover. *Journal of Hydrology*, *515*, 59–70. https://doi.org/10.1016/j.jhydrol.2014.04.011

Minet, J., Lambot, S., Slob, E. C., & Vanclooster, M. (2010). Soil Surface Water Content Estimation by Full-Waveform GPR Signal Inversion in the Presence of Thin Layers. *IEEE Transactions on Geoscience and Remote Sensing*, *48*(3), 1138–1150. https://doi.org/10.1109/TGRS.2009.2031907

Mishra, S. K., Jain, M. K., Suresh Babu, P., Venugopal, K., & Kaliappan, S. (2008). Comparison of AMC-dependent CN-conversion formulae. *Water Resources Management*, *22*(10), 1409–1420. https://doi.org/10.1007/s11269-007-9233-5

Mojaddadi, H., Pradhan, B., Nampak, H., Ahmad, N., & Ghazali, A. H. bin. (2017). Ensemble machine-learning-based geospatial approach for flood risk assessment using multi-sensor remote-sensing data and GIS. *Geomatics, Natural Hazards and Risk*, *8*(2), 1080–1102. https://doi.org/10.1080/19475705.2017.1294113

Morgan, R. P. C., Quinton, J. N., Smith, R. E., Govers, G., Poesen, J., Auerswald, K., Chisci, G., Torri, D., Styczen, M. E., & Folly, A. J. V. (1998). *The European Soil Erosion Model (EUROSEM): documentation and user guide*. Silsoe College, Cranfield University.

Moriasi, D., Arnold, J., Van Liew, M. W., Bingner, R. L., Harmel, R. D., & Veith, T. L. (2007). Model Evaluation Guidelines for Systematic Quantification of Accuracy in Watershed Simulations. *Transactions of the ASABE*, *50*(3), 885–900. https://doi.org/10.13031/2013.23153

Mostofi Zadeh, S., & Burn, D. H. (2019). A Super Region Approach to Improve Pooled Flood Frequency Analysis. *Canadian Water Resources Journal*, *44*(2), 146–159. https://doi.org/10.1080/07011784.2018.1548946

Munich Re. (2019). *Risks from floods, storm surges and flash floods: Underestimated natural hazards*. https://www.munichre.com/en/risks/natural-disasters-losses-are-trending-upwards/floods-and-flash-floods-underestimated-natural-hazards.html#-24989000

Nash, J. E., & Sutcliffe, J. V. (1970). River Flow Forecasting Through Conceptual Models: Part I - A discussion of principles. *Journal of Hydrology*, *10*, 282–290.

Neitsch, S. L., Arnold, J. G., Kiniry, J. R., & Williams, J. R. (2011). *Soil and Water Assessment Tool: Theoretical Documentation, Version 2009* (p. 647). Texas Water Resources Institute, College Station, Texas.

Niu, G. Y., Troch, P. A., Paniconi, C., Scott, R. L., Durcik, M., Zeng, X., Huxman, T., Goodrich, D., & Pelletier, J. (2014). An integrated modelling framework of catchment-scale ecohydrological processes: 2. The role of water subsidy by overland flow on vegetation dynamics in a semi-arid catchment. *Ecohydrology*, *7*(2), 815–827. https://doi.org/10.1002/eco.1405

Ottoy, S., Beckers, V., Jacxsens, P., Hermy, M., & Van Orshoven, J. (2015). Multi-level statistical soil profiles for assessing regional soil organic carbon stocks. *Geoderma*, *253–254*, 12–20. https://doi.org/10.1016/j.geoderma.2015.04.001

Ottoy, S., De Vos, B., Sindayihebura, A., Hermy, M., & Van Orshoven, J. (2017). Assessing soil organic carbon stocks under current and potential forest cover using digital soil mapping and spatial generalisation. *Ecological Indicators*, *77*, 139–150. https://doi.org/10.1016/j.ecolind.2017.02.010

Pappenberger, F., Beven, K. J., Hunter, N. M., Bates, P. D., Gouweleeuw, B. T., Thielen, J., & de Roo, A. P. J. (2005). Cascading model uncertainty from medium range weather forecasts (10 days) through a rainfall-runoff model to flood inundation predictions within the European Flood Forecasting System (EFFS). *Hydrology and Earth System Sciences*, *9*(4), 381–393. https://doi.org/10.5194/hess-9-381-2005

Pappenberger, F., Matgen, P., Beven, K. J., Henry, J. B., Pfister, L., & Fraipont, P. (2006). Influence of uncertain boundary conditions and model structure on flood inundation predictions. *Advances in Water Resources*, *29*(10), 1430–1449. https://doi.org/10.1016/j.advwatres.2005.11.012

Peel, M. C. (2009). Hydrology: Catchment vegetation and runoff. *Progress in Physical Geography*, *33*(6), 837–844. https://doi.org/10.1177/0309133309350122

Penning-rowsell, E., Johnson, C., Tunstall, S., Tapsell, S., Morris, J., Chatterton, J., & Green, C. (2005). *The Benefits of Flood and Coastal Risk Management: A Handbook of Assessment Techniques*. Middlesex University Press. https://doi.org/10.1596/978-0-8213-8050-5

Perrin, C., Michel, C., & Andréassian, V. (2001). Does a large number of parameters enhance model performance? Comparative assessment of common catchment model structures on 429 catchments. *Journal of Hydrology*, *242*, 275–301. https://doi.org/10.1016/S0022-1694(00)00393-0

Pianosi, F., Beven, K. J., Freer, J., Hall, J. W., Rougier, J., Stephenson, D. B., & Wagener, T. (2016). Sensitivity analysis of environmental models: A systematic review with practical workflow.

Environmental Modelling and Software, *79*, 214–232. https://doi.org/10.1016/j.envsoft.2016.02.008

Pisman, A., Vanacker, S., Willems, P., Engelen, G., & Poelmans, L. (2018). *Ruimterapport Vlaanderen (RURA). Een ruimtelijke analyse van Vlaanderen* (p. 204). Departement Omgeving.

Poelmans, L., Rompaey, A. Van, Ntegeka, V., & Willems, P. (2011). The relative impact of climate change and urban expansion on peak flows: a case study in central Belgium. *Hydrological Processes*, *25*, 2846–2858. https://doi.org/10.1002/hyp.8047

Poelmans, L., & Van Rompaey, A. (2009). Detecting and modelling spatial patterns of urban sprawl in highly fragmented areas: A case study in the Flanders-Brussels region. *Landscape and Urban Planning*, *93*(1), 10–19. https://doi.org/10.1016/j.landurbplan.2009.05.018

Powell, S. L., Cohen, W. B., Yang, Z., Pierce, J. D., & Alberti, M. (2008). Quantification of impervious surface in the Snohomish Water Resources Inventory Area of Western Washington from 1972-2006. *Remote Sensing of Environment*, *112*(4), 1895–1908. https://doi.org/10.1016/j.rse.2007.09.010

Putro, B., Kjeldsen, T. R., Hutchins, M. G., & Miller, J. (2016). An empirical investigation of climate and land-use effects on water quantity and quality in two urbanising catchments in the southern United Kingdom. *Science of the Total Environment*, *548–549*, 164–172. https://doi.org/10.1016/j.scitotenv.2015.12.132

Raes, D., Geerts, S., Kipkorir, E., Wellens, J., & Sahli, A. (2006). Simulation of yield decline as a result of water stress with a robust soil water balance model. *Agricultural Water Management*, *81*, 335–357. https://doi.org/10.1016/j.agwat.2005.04.006

Raes, D., Steduto, P., Hsiao, T. C., & Fereres, E. (2009). AquaCrop — The FAO Crop Model to Simulate Yield Response to Water: II. Main Algorithms and Software Description. *Agronomy Journal*, *101*(3), 438–447. https://doi.org/10.2134/agronj2008.0140s

Rawls, W. J., Brakensiek, D. L., Simanton, J. R., & Kohl, K. D. (1990). Development of a crust factor for a Green-Ampt model. *Transactions of the American Society of Agricultural Engineers*, *33*(4), 1224–1228. https://doi.org/10.13031/2013.31461

Richert, E., Bianchin, S., Heilmeier, H., Merta, M., & Seidler, C. (2011). A method for linking results from an evaluation of land use scenarios from the viewpoint of flood prevention and nature conservation. *Landscape and Urban Planning*, *103*(2), 118–128. https://doi.org/10.1016/j.landurbplan.2011.07.001

Ritter, A., & Muñoz-Carpena, R. (2013). Performance evaluation of hydrological models: Statistical significance for reducing subjectivity in goodness-of-fit assessments. *Journal of Hydrology*, *480*, 33–45. https://doi.org/10.1016/j.jhydrol.2012.12.004

Roberts, S. A., Hall, G. B., & Calamai, P. H. (2011). Evolutionary Multi-objective Optimization for landscape system design. *Journal of Geographical Systems*, *13*, 299–326. https://doi.org/10.1007/s10109-010-0136-2

Ruangpan, L., Vojinovic, Z., Di Sabatino, S., Sandra Leo, L., Capobianco, V., Oen, A. M. P., Mcclain, M. E., & Lopez-Gunn, E. (2020). Nature-based solutions for hydro-meteorological risk reduction: a state-of-the-art review of the research area. *Natural Hazards and Earth System Sciences*, *20*(1), 243–270. https://doi.org/10.5194/nhess-20-243-2020

Sajikumar, N., & Remya, R. S. (2015). Impact of land cover and land use change on runoff characteristics. *Journal of Environmental Management*, *161*, 460–468. https://doi.org/10.1016/j.jenvman.2014.12.041

Sayers, P., Galloway, G., Penning-rowsell, E., Yuanyuan, L., Yiwei, C., Kang, W., Quesne, T. Le, Wang, L., Guan, Y., Sayers, P., Galloway, G., Penning-rowsell, E., & Yuanyuan, L. (2015). Strategic flood management: ten 'golden rules' to guide a sound approach. *International Journal of River Basin Management*, *13*(2), 137–151. https://doi.org/10.1080/15715124.2014.902378

SEPA. (2016). *Natural Flood Management Handbook*. Scottish Environment Protection Agency, Edinburgh.

Seppelt, R., & Voinov, A. (2002). Optimization methodology for land use patterns using spatially explicit landscape models. *Ecological Modelling*, *151*, 125–142.

Seppelt, R., & Voinov, A. (2003). Optimization methodology for land use patterns — evaluation based on multiscale habitat pattern comparison. *Ecological Modelling*, *168*, 217–231. https://doi.org/10.1016/S0304-3800(03)00138-8

Sindayihebura, A., Ottoy, S., Dondeyne, S., Van Meirvenne, M., & Van Orshoven, J. (2017). Comparing digital soil mapping techniques for organic carbon and clay content: Case study in Burundi's central plateaus. *Catena*, *156*, 161–175. https://doi.org/10.1016/j.catena.2017.04.003

Sivakumar, B. (2008). Dominant processes concept, model simplification and classification framework in catchment hydrology. *Stochastic Environmental Research and Risk Assessment*, *22*, 737–748. https://doi.org/10.1007/s00477-007-0183-5

Smedema, L. K., & Rycroft, D. W. (1983). *Land drainage: planning and design of agricultural drainage systems*. Batsford Ltd., London.

Smola, A. J., & Schölkopf, B. (2004). A tutorial on support vector regression. *Statistics and Computing*, *14*, 199–222. https://doi.org/10.1023/B:STCO.0000035301.49549.88

Soto-Montes-de-Oca, G., Bark, R., & González-Arellano, S. (2020). Incorporating the insurance value of peri-urban ecosystem services into natural hazard policies and insurance products: Insights from Mexico. *Ecological Economics*, *169*, 106510. https://doi.org/10.1016/j.ecolecon.2019.106510

Srivastava, P., Hamlett, J. M., Robillard, P. D., & Day, R. L. (2002). Watershed optimization of best management practices using AnnAGNPS and a genetic algorithm. *Water Resources Research*, *38*(3), 1021. https://doi.org/10.1029/2001wr000365

Statbel. (2019). *Statistiek van de verkopen van gebouwen: aantal en verkoopprijs per datum, oppervlakte en type gebouw*. https://bestat.statbel.fgov.be/bestat/crosstable.xhtml?view=0859950c-50e4-4e39-acde-bc48f47215a5

Statbel. (2020). *Bevolkingsdichtheid*. https://statbel.fgov.be/nl/themas/bevolking/bevolkingsdichtheid#news

Strobl, C., Malley, J., & Tutz, G. (2009). An Introduction to Recursive Partitioning: Rationale, Application, and Characteristics of Classification and Regression Trees, Bagging, and Random Forests. *Psychological Methods*, *14*(4), 323–348. https://doi.org/10.1037/a0016973

Sutmöller, J., Hentschel, S., Hansen, J., & Meesenburg, H. (2011). Coupled forest growth-hydrology modelling as an instrument for the assessment of effects of forest management on hydrology in forested catchments. *Advances in Geosciences*, *27*, 149–154. https://doi.org/10.5194/adgeo-27-149-2011

Syrbe, R.-U., & Walz, U. (2012). Spatial indicators for the assessment of ecosystem services :

Providing , benefiting and connecting areas and landscape metrics. *Ecological Indicators*, *21*, 80–88. https://doi.org/10.1016/j.ecolind.2012.02.013

Tarboton, D., Bras, R., & Rodriguez-Iturbe, I. (1991). On the extraction of channel networks from digital elevation data. *Hydrological Processes*, *5*(1), 81–100. https://doi.org/10.1002/hyp.3360050107

Tehrany, M. S., Pradhan, B., & Jebur, M. N. (2014). Flood susceptibility mapping using a novel ensemble weights-of-evidence and support vector machine models in GIS. *Journal of Hydrology*, *512*, 332–343. https://doi.org/10.1016/j.jhydrol.2014.03.008

Teng, J., Jakeman, A. J., Vaze, J., Croke, B. F. W., Dutta, D., & Kim, S. (2017). Flood inundation modelling: A review of methods, recent advances and uncertainty analysis. *Environmental Modelling and Software*, *90*, 201–216. https://doi.org/10.1016/j.envsoft.2017.01.006

Teng, J., Vaze, J., Dutta, D., & Marvanek, S. (2015). Rapid Inundation Modelling in Large Floodplains Using LiDAR DEM. *Water Resources Management*, *29*, 2619–2636. https://doi.org/10.1007/s11269-015-0960-8

Thieken, A. H., Kienzler, S., Kreibich, H., Kuhlicke, C., Kunz, M., Mühr, B., Müller, M., Otto, A., Petrow, T., Pisi, S., & Schröter, K. (2016). Review of the flood risk management system in Germany after the major flood in 2013. *Ecology and Society*, *21*(2). https://doi.org/10.5751/ES-08547-210251

Thornthwaite, C. W., & Mather, J. R. (1957). *Instructions and tables for computing potential evapotranspiration and the water balance.* Laboratory of Climatology, Drexel Institute of Technology.

United Nations. (2009). *Our Waters: Joining Hands Across Borders: First Assessment of Transboundary Rivers Lakes and Groundwater*. United Nations Publications. https://books.google.be/books?id=425qzQEACAAJ

United Nations. (2019). *World Urbanization Prospects: The 2018 Revision*. United Nations, Department of Economic and Social Affairs, Population Division, New York. https://doi.org/10.4054/demres.2005.12.9

USDA Natural Resource Conservation Service. (1986). *Urban Hydrology for Small Watersheds: Technical Release 55*. https://doi.org/Technical Release 55

Vaes, G., & Willems, P. (2007). Modellering van de hydraulische interactie tussen riolen en waterlopen. *Water*, *32*, 19–23.

Van De Vreken, P., Van Holm, L., Diels, J., & Van Orshoven, J. (2009). *Bodemverdichting in Vlaanderen en afbakening van risicogebieden voor bodemverdichting: Eindrapport van een verkennende studie*. Vlaamse Overheid, Departement Leefmilieu, Natuur, Energie.

Van Den Broeck, S. (2019). Een bos aanplanten. Hoeveel moet dat kosten? *De Standaard*. https://www.gemeentevoordetoekomst.be/artikel/een-bos-aanplanten-hoeveel-moet-dat-kosten

Van Den Eeckhaut, M., Vanwalleghem, T., Poesen, J., Govers, G., Verstraeten, G., & Vandekerckhove, L. (2006). Prediction of landslide susceptibility using rare events logistic regression: A case-study in the Flemish Ardennes (Belgium). *Geomorphology*, *76*, 392–410. https://doi.org/10.1016/j.geomorph.2005.12.003

van der Knijff, J. M., Younis, J., & de Roo, A. P. J. (2010). LISFLOOD: A GIS-based distributed model for river basin scale water balance and flood simulation. *International Journal of Geographical Information Science*, *24*(2), 189–212. https://doi.org/10.1080/13658810802549154

Van Loo, M. (2018). *Human environment interactions in the past: modeling ancient crop yields in a mediterranean environment*. Doctoral dissertation, KU Leuven.

Van Opstal, M., Tits, M., Beckers, V., Elsen, A., Van Overtveld, K., Batelaan, O., Van Orshoven, J., Bries, J., Vandendriessche, H., & Diels, J. (2014). *Vernieuwde kwantificering van de verliezen van N en P vanuit de landbouw naar het oppervlaktewater. Eindrapport, mei 2014.* Studie uitgevoerd in opdracht van de Vlaamse Milieumaatschappij door het Departement Aard- en Omgevingswetenschappen (KU Leuven) en de Bodemkundige Dienst van België.

Van Opstal, M., Tits, M., Beckers, V., Van Overtveld, K., Batelaan, O., Van Orshoven, J., Elsen, A., Diels, J., D'Heygere, T., & Van Hoof, K. (2013). ArcNEMO, a new spatially distributed nutrient emission model to quantify N and P losses from agriculture to surface waters. *LUWQ2013,Land Use and Water Quality:Reducing Effects of Agriculture*.

Van Orshoven, J. (2001). Van nature overstroombare en recent overstroomde gebieden in Vlaanderen. *Proceedings of the Study Day on '"Space for Water, The Best Insurance Against Flooding,"'* 1–22.

Vanegas, P., Cattrysse, D., & Orshoven, J. Van. (2012). Allocating reforestation areas for sediment flow minimization: an integer programming formulation and a heuristic solution method. *Optimization and Engineering*, *13*, 247–269. https://doi.org/10.1007/s11081-011-9138-2

Vanegas, P., Cattrysse, D., & Van Orshoven, J. (2010). Budget constraint in reforestation meant for minimizing sediment load at a watershed outlet. *Proceedings of the International MultiConference of Engineers and Computer Scientists 2010*, *III*, 2174–2179.

Vanneuville, W., De Maeyer, P., Maeghe, K., & Mostaert, F. (2003). Model of the effects of a flood in the dender catchment, based on a risk methodology. *Bulletin of the Society of Cartographers*, *37*(2), 59–64.

Vanneuville, W., Maddens, R., Collard, C., Bogaert, P., De Maeyer, P., & Antrop, M. (2006). *Impact op mens en economie t.g.v. overstromingen bekeken in het licht van wijzigende hydraulische condities, omgevingsfactoren en klimatologische omstandigheden* (p. 120). Studie uitgevoerd in opdracht van de Vlaamse Milieumaatschappij, MIRA (MIRA/2006/02) door de Vakgroep Geografie (UGent).

Vanneuville, W., Maeghe, K., De Maeyer, P., Mostaert, F., & Bogaert, P. (2002). *Risicobenadering bij waterbeheersingplannen: Methodologie en case study Denderbekken* (p. 80). Studie uitgevoerd in opdracht van de Vlaamse Gemeenschap LIN - AWZ Afdeling Waterbouwkundig Laboratorium en hydrologisch onderzoek.

Verbeiren, B., Van De Voorde, T., Canters, F., Binard, M., Cornet, Y., & Batelaan, O. (2012). Assessing urbanisation effects on rainfall-runoff using a remote sensing supported modelling strategy. *International Journal of Applied Earth Observation and Geoinformation*, *21*(1), 92–102. https://doi.org/10.1016/j.jag.2012.08.011

Verstraeten, G., & Poesen, J. (1999). The nature of small-scale flooding, muddy floods and retention pond sedimentation in central Belgium. *Geomorphology*, *29*, 275–292. https://doi.org/10.1016/S0169-555X(99)00020-3

Vieux, B. E. (2016). *Distributed Hydrologic Modeling Using GIS*. Springer Science+Business Media.

Vlaamse Milieumaatschappij. (2015). *Riviercontract Maarkebeek: riviercontract ter vermindering van overstromingsrisico's in het stroomgebied van de Maarkebeek*.

Vlaamse Milieumaatschappij. (2020). *Riviercontract Bellebeek*. https://bellebeek.riviercontract.be/

Vlaamse Milieumaatschappij, & Agentschap Informatie Vlaanderen. (2020). *Vlaamse Hydrografische Atlas - Waterlopen, 16 november 2020*. http://www.geopunt.be/catalogus/datasetfolder/718c4c1b-0702-423c-a7d5-fe0f25084579

Vlaamse Milieumaatschappij, Waterbouwkundig Laboratorium, Maritieme Dienstverlening & Kust, & De Vlaamse Waterweg nv. (2020). *Waterinfo.be*. www.waterinfo.be

Vlaamse Regering. (2020). *Blue Deal. De strijd tegen droogte en waterschaarste*.

VMM. (2015a). *Overstromingsgevaar*. https://www.milieurapport.be/milieuthemas/waterkwantiteit/afvoer-van-neerslag-overstromingen/overstromingsgevaar

VMM. (2015b). *Overstromingsrisico*. https://www.milieurapport.be/milieuthemas/waterkwantiteit/afvoer-van-neerslag-overstromingen/overstromingsrisico/#

VMM. (2018a). *De voorlopige OverstromingsRisicoBeoordeling in Vlaanderen*. Vlaamse Milieumaatschappij, Aalst.

VMM. (2018b). *Klimaatportaal Vlaanderen: Overstromingen*. Vlaamse Milieumaatschappij, Aalst. https://klimaat.vmm.be/nl/web/guest/overstromingen

VMM. (2019). *Actieplan Droogte en Wateroverlast 2019-2021* (p. 69). Vlaamse Milieumaatschappij, Aalst.

VMM. (2020). *Milieurapport: Hydrologisch gedrag van onbevaarbare waterlopen*. Vlaamse Milieumaatschappij, Aalst. https://www.milieurapport.be/milieuthemas/waterkwantiteit/afvoer-van-neerslag-overstromingen/hydrologisch-gedrag-van-onbevaarbare-waterlopen/#

Volk, M., Lautenbach, S., & Delden, H. Van. (2010). How Can We Make Progress with Decision Support Systems in Landscape and River Basin Management? Lessons Learned from a Comparative Analysis of Four Different Decision Support Systems. *Enivronmental Management*, *46*, 834–849. https://doi.org/10.1007/s00267-009-9417-2

Wang, D., Gong, J., Chen, L., Zhang, L., Song, Y., & Yue, Y. (2012). Spatio-temporal pattern analysis of land use/cover change trajectories in Xihe watershed. *International Journal of Applied Earth Observation and Geoinformation*, *14*(1), 12–21. https://doi.org/10.1016/j.jag.2011.08.007

Ward, P. J., de Moel, H., & Aerts, J. C. J. H. (2011). How are flood risk estimates affected by the choice of return-periods? *Natural Hazards and Earth System Science*, *11*(12), 3181–3195. https://doi.org/10.5194/nhess-11-3181-2011

Ward, P. J., Renssen, H., Aerts, J. C. J. H., & Verburg, P. H. (2011). Sensitivity of discharge and flood frequency to twenty-first century and late Holocene changes in climate and land use (River Meuse, northwest Europe). *Climatic Change*, *106*(2), 179–202. https://doi.org/10.1007/s10584-010-9926-2

Weynants, M., Vereecken, H., & Javaux, M. (2009). Revisiting Vereecken Pedotransfer Functions: Introducing a Closed-Form Hydraulic Model. *Vadose Zone Journal*, *8*(1), 86–95. https://doi.org/10.2136/vzj2008.0062

Wheater, H., & Evans, E. (2009). Land use, water management and future flood risk. *Land Use Policy*, *26S*, S251–S264. https://doi.org/10.1016/j.landusepol.2009.08.019

Willems, P., Vaes, G., Popa, D., & Timbe, L. (2002). Quasi 2D river flood modelling. In D. Bousmar & Y. Zech (Eds.), *River Flow 2002* (Vol. 2, pp. 1253–1259). Swets & Zeitlinger, Lisse.

Wolfs, V., Meert, P., & Willems, P. (2015). Modular conceptual modelling approach and software for river hydraulic simulations. *Environmental Modelling and Software*, *71*, 60–77. https://doi.org/10.1016/j.envsoft.2015.05.010

Wolfs, V., & Willems, P. (2017). Modular Conceptual Modelling Approach and Software for Sewer Hydraulic Computations. *Water Resources Management*, *31*(1), 283–298. https://doi.org/10.1007/s11269-016-1524-2

Woodward, D. E., Hawkins, R. H., Jiang, R., Hjelmfelt, A. T., Van Mullem, J. A., & Quan, Q. D. (2003). Runoff curve number method: Examination of the initial abstraction ratio. *World Water and Environmental Resources Congress*, 1–10. https://doi.org/10.1061/40685(2003)308

Woodward, M., Gouldby, B., Kapelan, Z., & Hames, D. (2014). Multiobjective Optimization for Improved Management of Flood Risk. *Journal of Water Resources Planning and Management*, *140*(2), 201–215. https://doi.org/10.1061/(ASCE)WR.1943-5452.0000295

Wu, H., Bolte, J. P., Hulse, D., & Johnson, B. R. (2015). A scenario-based approach to integrating flow-ecology research with watershed development planning. *Landscape and Urban Planning*, *144*, 74–89. https://doi.org/10.1016/j.landurbplan.2015.08.012

Yan, B., Fang, N. F., Zhang, P. C., & Shi, Z. H. (2013). Impacts of land use change on watershed streamflow and sediment yield: An assessment using hydrologic modelling and partial least squares regression. *Journal of Hydrology*, *484*, 26–37. https://doi.org/10.1016/j.jhydrol.2013.01.008

Yeo, I.-Y., & Guldmann, J.-M. (2010). Global spatial optimization with hydrological systems simulation: Application to land-use allocation and peak runoff minimization. *Hydrology and Earth System Sciences*, *14*, 325–338. https://doi.org/10.5194/hess-14-325-2010

Yu, D., & Lane, S. N. (2006). Urban fluvial flood modelling using a two-dimensional diffusion-wave treatment, part 2: Development of a sub-grid-scale treatment. *Hydrological Processes*, *20*(7), 1567–1583. https://doi.org/10.1002/hyp.5936

Yu, D., Xie, P., Dong, X., Su, B., Hu, X., Wang, K., & Xu, S. (2018). The development of land use planning scenarios based on land suitability and its influences on eco-hydrological responses in the upstream of the Huaihe River basin. *Ecological Modelling*, *373*(2018), 53–67. https://doi.org/10.1016/j.ecolmodel.2018.01.010

Zorrilla-Miras, P., Palomo, I., Gómez-Baggethun, E., Martín-López, B., Lomas, P. L., & Montes, C. (2014). Effects of land-use change on wetland ecosystem services: A case study in the Doñana marshes (SW Spain). *Landscape and Urban Planning*, *122*, 160–174. https://doi.org/10.1016/j.landurbplan.2013.09.013

Curriculum Vitae

Karen Gabriels
°16/07/1992 in Malle, Belgium

Education

2010-2013 Bachelor of Science: Bioscience Engineering
University of Leuven

2013-2015 Master of Science: Bioscience Engineering 'Land and Forest Management'
University of Leuven
Graduated, June 2015, majoring in *Soil and Water*

Work experience

Researcher at KU Leuven | September, 2015 – December, 2016
Department of Earth and Environmental Sciences; Division of Forest, Nature and Landscape

- Contributed to the IWT-SBO project *ECOPLAN*, an IWT-SBO project: improving and devising calculation methods of ecosystem services related to forest (e.g. wood production, carbon sequestration in woody biomass);
- Managed and finalised the project *Feasibility study on the spatial allocation of FADN farms* for the Spatial Applications Division Leuven (SADL): using statistical class-matching techniques to allocate farms included in the Farm Accountancy Data Network (FADN);
- Contributed to *INITGeoBE* for SADL: checking the conformity of metadata to the INSPIRE standards for the National Geographic Institute of Belgium;

PhD fellow at KU Leuven | January, 2017 – December, 2020
Department of Earth and Environmental Sciences; Division of Forest, Nature and Landscape

- PhD research *Considering flood hazard and risk in spatial planning: a spatially explicit optimization approach*
- Teaching assistant in the several courses, including *Geospatial Data Infrastructure* and *Land Evaluation*

Junior Project Engineer at HydroScan | January, 2021 – Present

List of publications

Articles in internationally reviewed academic journals

Gabriels, K., Willems, P., & Van Orshoven, J. (2020). A data-driven analysis, and its limitations, of the spatial flood archive of Flanders, Belgium to assess the impact of soil sealing on flood volume and extent. *PLoS ONE*, *15*(10), 1–17. https://doi.org/10.1371/journal.pone.0239583

Vrebos, D., Staes, J., Broekx, S., De Nocker, L., Gabriels, K., Hermy, M., Liekens, I., Marsboom, C., Ottoy, S., Van Der Biest, K., Van Orshoven, J., & Meire, P. (2020). Facilitating spatially-explicit assessments of ecosystem service delivery to support land use planning. *One Ecosystem, 5*, 1–27. https://doi.org/10.3897/oneeco.5.e50540

Gabriels, K., Willems, P., & Van Orshoven, J. A distributed CN-based rainfall-runoff model for land use optimization [Manuscript submitted for publication to Journal of Hydrology].

Gabriels, K., Willems, P., & Van Orshoven, J. An iterative runoff propagation approach to identify priority locations for land use change minimizing downstream river flood hazard [Manuscript submitted for publication to Landscape and Urban Planning].

Gabriels, K., Willems, P., & Van Orshoven, J. A comparative flood damage and risk impact assessment of land use [Manuscript submitted for publication to Natural Hazards and Earth System Sciences].

Presentations (oral or poster) at international scientific conferences and symposia

Gabriels, K., Van Orshoven, J., Willems, P. (2019). Identifying upstream locations critical for downstream floods. Presented at the 10th IALE World Congress: Nature and society facing the Anthropocene, Milan, Italy, 01 Jul 2019-05 Jul 2019.

Gabriels, K., Willems, P., Van Orshoven, J. (2018). Identifying upstream locations which are critical for downstream floods. Presented at the International IUFRO conference; Landscape Management: From Data to Decision, Prague, 17 Sep 2018-19 Sep 2018.

Gabriels, K., Willems, P., Van Orshoven, J. (2018). Data driven assessment of the impact of upstream soil sealing on downstream floods in Flanders, Belgium. Presented at the International IUFRO conference; Land Management: From Data to Decision, Prague, 17 Sep 2018-19 Sep 2018.

Gabriels, K., Willems, P., Van Orshoven, J. (2017). Empirical assessment of the relationship between flood events and land use change. (Abstract No. 13). Presented at the IALE 2017 European Landscape Ecology Congress: From pattern and process to people and action, Ghent, 12 Sep 2017-15 Sep 2017.

Gabriels, K., Aerts, R., Ottoy, S., Hermy, M., Willems, P., Van Orshoven, J. (2016). The insurance value of ecosystems: concept and applicability. In: *Book of Abstracts - Poster*, (4-4). Presented at the European Ecosystem Services Conference: Helping nature to help us, Antwerp, 19 Sep 2016-23 Sep 2016.